

***Liquid Crystalline
Copper(II) Complexes of
Poly(propylene imine) Dendrimers***

Dissertation

zur Erlangung des akademischen Grades
Doktor der Naturwissenschaften (Dr. rer. nat.)
der Fakultät für Biologie, Chemie und Geowissenschaften
der Universität Bayreuth

vorgelegt von

Laura Torre Lorente

aus Calatayud (Spanien)

Bayreuth, Dezember 2007

Die vorliegende Arbeit wurde in der Zeit von September 2001 bis Dezember 2007 am Lehrstuhl für Makromolekulare Chemie I der Universität Bayreuth angefertigt.

Vollständiger Abdruck der von der Fakultät Biologie, Chemie und Geowissenschaften der Universität Bayreuth genehmigten Dissertation zur Erlangung des akademischen Grades Doktor der Naturwissenschaften (Dr. rer. nat.). Die Pflichtexemplare stimmen inhaltlich mit der Fassung überein, für die die Druckgenehmigung erteilt wurde.

Datum der Einreichung der Arbeit: 2. Januar 2008

Datum des wissenschaftlichen Kolloquiums: 13.Juni 2008

Prüfungsausschuß:

Prof. Dr. A. Fery (Vorsitzender)

Prof. Dr. H.-W. Schmidt (Erstgutachter)

Prof. Dr. H. G. Alt (Zweitgutachter)

Prof. Dr. R. Schobert

Diese Arbeit wurde von der Deutschen Forschungsgemeinschaft – Sonderforschungsbereich 481 finanziell unterstützt.

TABLE OF CONTENTS

LIST OF ABBREVIATIONS AND SYMBOLS.....	v
1 INTRODUCTION.....	1
1.1 LIQUID CRYSTALS	1
1.1.1 The Liquid Crystalline State.....	1
1.1.2 Thermotropic Mesomorphism	1
1.1.3 Mesophases.....	4
1.1.4 Lyotropic Mesomorphism.	8
1.1.5 Metallomesogens	9
1.1.6 Liquid Crystalline Polymers, LCPs	10
1.2 DENDRIMERS	12
1.2.1 Definition and Structure	12
1.2.2 Synthesis, Purity, and Polydispersity.....	12
1.2.3 Dendrimer Behaviour in Solution: Conformation	13
1.2.4 Further Properties. Comparison to Conventional Polymers.	14
1.2.5 Nitrogen containing Dendrimers: PPI, PEI, PAMAM, and PAMAMOS.....	15
1.3 DENDROMESOGENS	18
1.3.1 Shape Persistent Dendrimers	18
1.3.2 Dendromesogens with Anisometric Mesogenic Units.....	19
1.3.3 Dendromesogens with Microsegregating Structures	21
1.3.4 Supramolecular Dendrimers	22
1.3.5 Metallodendromesogens	23
1.3.6 Liquid Crystalline Nitrogen Containing Dendromesogens. PAMAM, PPI, and PEI Derivatives.....	23
1.3.7 Liquid Crystalline Metal Derivatives of PAMAM, PPI, and PEI Dendrimers.....	27
2 OBJECTIVES.....	29
2.1 MOTIVATION.....	29
2.2 WORKING PLAN	32
3 LIQUID CRYSTALLINE, DENDRIMERIC COPPER(II) COMPLEXES.....	35
3.1 SYNTHESIS	35
3.1.1 Ligands	35
3.1.2 Copper(II) Complexes. Series of Highest Copper Loading.....	35
3.1.2.1 THF-Series.....	36
3.1.2.2 γ -Butyrolactone/Chloroform Series	38
3.1.2.3 Dependence of the Highest Loading on the Generation.....	38
3.1.3 Copper (II) Complexes. Series of Lower Copper Loading. Specific Preparative Procedures	39
3.1.3.1 2 nd Generation Complexes	39
3.1.3.2 1 st Generation Complexes.....	43
3.1.4 Preparation of a Copper Complex from Copper Tetrafluoroborate.....	45
3.1.5 Conclusions	46

3.2	MOLECULAR COMPOSITION: ELEMENTAL ANALYSIS	47
3.3	MALDI-ToF-MS	53
3.3.1	MALDI-ToF-MS: Introduction	53
3.3.2	MALDI-ToF-MS of the lower Generations. Butandiamide, 1 st and 2 nd Generation Copper(II) Complexes	55
3.3.3	MALDI-ToF-MS Defect Structures, Fragments and Copper Bridged Dimers.....	58
3.3.4	MALDI-ToF-MS of the Higher Generations. 3 rd to 5 th Generation Copper(II) Complexes	64
3.3.5	Ionisation of the Copper(II) Complexes in MALDI-ToF-MS	65
3.3.6	Conclusions.....	66
3.4	TRANSMISSION ELECTRON MICROSCOPY, TEM.....	68
3.5	FTIR-INFRARED SPECTROSCOPY	73
3.5.1	FT-Infrared Spectroscopy: Introduction	73
3.5.2	FTIR-Spectrum of the Ligands	74
3.5.3	FTIR-Spectrum of the Copper(II) Complexes	76
3.5.3.1	<i>Coordinating Groups in the Ligand: Amine or Amide</i>	77
3.5.3.2	<i>Role of the Nitrate. Comparison with the Complex from Tetrafluoroborate</i>	80
3.5.3.3	<i>HNO₃: Tertiary Amine Protonation</i>	83
3.5.3.4	<i>Copper Nitrate Trihydrate and Basic Copper Nitrate</i>	85
3.5.3.5	<i>Conclusions</i>	86
3.6	UV-VIS SPECTROSCOPY	88
3.6.1	Ligand Absorption Bands in the UV-Vis Range	88
3.6.2	Copper(II) Complexes Absorption Bands in the UV-Vis Range.....	88
3.6.3	Conclusions.....	91
3.7	EPR CHARACTERISATION OF THE COPPER(II) COMPLEXES	92
3.7.1	EPR Spectroscopy: Introduction.....	92
3.7.2	Spectral Parameters of the Copper(II) Dendromesogens.....	95
3.7.2.1	<i>Signal A</i>	96
3.7.2.2	<i>Signal B</i>	97
3.7.2.3	<i>Signal C</i>	98
3.7.2.4	<i>Signals D and E</i>	99
3.7.3	Magnetic Properties of the Dendrimeric Copper(II) Complexes: Dimer Formation and Antiferromagnetism	102
3.7.3.1	<i>Blue Complexes: Dimeric Structure</i>	103
3.7.3.2	<i>Green Complexes: Nitrate Bridged Polymeric Structure</i>	104
3.7.3.3	<i>Dendrimeric Copper Complex Bridged to a Hexaaquacopper Complex</i>	105
3.7.4	Conclusions.....	107
3.8	THERMAL PROPERTIES.....	108
3.8.1	Polarising Microscopy	108
3.8.2	Thermal Analysis.....	109
3.8.2.1	<i>Series of Highest Loading: Thermal Properties</i>	111
3.8.2.2	<i>Series of Lower Copper Loading: Thermal Properties of the 2nd Generation Complexes</i>	115
3.8.2.3	<i>Series of Lower Copper Loading: Thermal Properties of the 1st Generation Complexes</i>	119
3.8.2.4	<i>Thermal Properties of the Tetrafluoroborate Copper(II) Complex</i>	112
3.8.2.5	<i>Conclusions</i>	123
3.9	X-RAY DIFFRACTOMETRY	124

3.9.1	Small-angle region.....	125
3.9.1.1	<i>Influence of the Generation on the Mesophase. Series of Highest Loading</i>	133
3.9.1.2	<i>Influence of the Copper Loading on the Mesophase. 2nd Generation Complexes of Different Loadings</i>	139
3.9.1.3	<i>X-ray Analysis of the 2nd Generation Copper(II) Complex from Tetrafluoroborate C2.21(4.0)</i>	143
3.9.2	Wide-Angle Region	145
3.9.2.1	<i>Ordered Columnar Mesophases</i>	145
3.9.2.2	<i>Possible Inorganic Impurities in the Dendrimeric Copper(II) Complexes</i>	148
3.9.2.3	<i>Conclusions</i>	153
3.10	PROPOSAL OF A MODEL FOR THE PPI COPPER(II) COMPLEXES	155
4	SUMMARY	157
5	ZUSAMMENFASSUNG	163
6	EXPERIMENTAL SECTION.....	169
6.1	MATERIALS	169
6.2	ANALYTICAL METHODS	170
6.2.1	Molecular Composition Determination: Elemental Analysis, EA.....	170
6.2.2	Molecular Weight Determination: MALDI-ToF-MS.....	170
6.2.3	Spectroscopic Methods.....	171
6.2.3.1	<i>Fourier Transform Infrared Spectroscopy, FTIR</i>	171
6.2.3.2	<i>Ultraviolet-Visible Spectroscopy, UV-Vis</i>	171
6.2.3.3	<i>Electron Paramagnetic Resonance Spectroscopy, EPR</i>	171
6.2.4	Microscopy	172
6.2.4.1	<i>Transmission Electron Microscopy, TEM</i>	172
6.2.4.2	<i>Polarized Light Microscopy, POM</i>	172
6.2.5	Thermal Analysis.....	173
6.2.5.1	<i>Thermogravimetric Analysis, TGA</i>	173
6.2.5.2	<i>Differential Scanning Calorimetry, DSC</i>	173
6.2.5.3	<i>Temperature Dependent X-Ray Diffraction</i>	173
6.3	PREPARATIVE METHODS	175
6.3.1	Procedures for Copper(II) Nitrate Trihydrate Complexation with PPI Dendrimers..	175
6.3.1.1	<i>Series of Highest Copper(II) Loading</i>	175
6.3.1.2	<i>Series of Lower Copper(II) Loading</i>	178
6.3.2	Procedure for Copper(II) Tetrafluoroborate Hydrate Complexation with PPI Dendrimers.....	179
6.4	COMPOUNDS REGISTER I: SYNTHESIS AND CHARACTERIZATION	180
6.4.1	Dendrimeric Copper(II) Complexes from Cu(NO ₃) ₂ ·3H ₂ O.....	180
6.4.1.1	<i>Copper(II) Complex of the “Zero” Generation, C0.1(n)</i>	180
6.4.1.2	<i>Copper(II) Complexes of the 1st Generation, C1.i(n)</i>	181
6.4.1.3	<i>Copper(II) Complex of the 2nd Generation, C2.i(n)</i>	183
6.4.1.4	<i>Copper(II) complex of the 3rd generation, C3.i(n)</i>	193
6.4.1.5	<i>Copper(II) Complex of the 4th Generation, C4.i(n)</i>	194
6.4.1.6	<i>Copper(II) Complex of the 5th Generation, C5.i(n)</i>	194
6.4.2	Dendrimeric Copper(II) Complex from Cu(BF ₄) ₂ ·4H ₂ O.....	195
6.5	COMPOUNDS REGISTER II: X-RAY EVALUATION OF MESOPHASES	197

6.5.1	Series of Highest Loading: CG.i(n)	199
6.5.1.1	<i>Columnar Hexagonal Mesophases</i>	199
6.5.1.2	<i>Columnar Rectangular Mesophases</i>	200
6.5.2	2 nd Generation Series: C2.i(n)	201
6.5.2.1	<i>Columnar Hexagonal Mesophases</i>	201
6.5.2.2	<i>Columnar Rectangular Mesophases</i>	202
6.5.3	1 st Generation Complexes C1.i(n).....	204
6.5.4	Complexes from Cu(BF ₄) ₂ ·4H ₂ O	205
7	REFERENCES	207

ACKNOWLEDGEMENTS

LIST OF ABBREVIATIONS AND SYMBOLS

a, b	lattice constants
amu	atomic mass unit
abbr.	abbreviated
Abs	absorption (optical density)
anneal	annealing
Ar	aromatic
as	asymmetric
ATR-FTIR	attenuated total reflection Fourier transform infrared spectroscopy
av	average
$A_x A_y A_z$	coupling constants in the x, y, z space directions (in EPR)
b	blue
B	magnetic field
Bu	butyro-
C	concentration
C	Curie-Weiss constant
c	speed of light in vacuum
c	clearing
calcd	calculated
CCD	charge-coupled device in digital imaging cameras
cf	confer, compare
Col _h	hexagonal columnar phase
Col _{h(o)}	ordered hexagonal columnar phase
Col _{ob}	oblique columnar phase
Col _r	rectangular columnar phase
Col _{r(o)}	ordered rectangular columnar phase
Col _t	tetragonal columnar phase
Cr	crystalline, crystalline state
Cub _b	bicontinuous cubic phase
Cub _s	spheroidic cubic phase
D	diameter
d	spacing or lattice distance
dec	decomposition
DSC	differential scanning calorimetry
E	energy
e.g.	for example (from Latin <i>exampli gratia</i>)
EA	elemental analysis
EELS	electron energy loss spectroscopy
EM	electromagnetic field
endo	endothermic
EPR	electron paramagnetic resonance spectroscopy
Eq.	equation
ESI-MS	electrospray ionisation mass spectrometry
ESR	electron spin resonance spectroscopy
exp.	experimental

expct.	expected
f	spring constant
FTIR	Fourier transform infrared spectroscopy
G	generation
g	glassy state
g_e	g-factor of the free electron
g_{iso}	averaging of g_x g_y g_z
gr	green
g_x g_y g_z	g-factors in the x, y and z space directions (in EPR)
H	magnetic field
h	hour(s)
h	Planck constant
hkl	Miller indices
HRTEM	high resolution transmission electron microscopy
I	isotropic melt
<i>I</i>	intensity
i.e.	that is, namely (from Latin <i>id est</i>)
ip	in plane (in FTIR)
LC	liquid crystal, liquid crystalline
LCEs	liquid crystalline elastomers
LCPs	liquid crystalline polymers
lin	linear mode (MS)
lit.	literature
M	mesophase
m	melting
M	molarity
m/z	mass/charge
MALDI-ToF-MS	matrix-assisted laser desorption ionisation time of flight mass spectrometry
MC	main chain
MCLCPs	main chain liquid crystalline polymers
meas	measured
MF	molecular formula
m_r	reduced mass
m_s	magnetic quantum number
MS	mass spectrometry
MW	molecular weight
N	nematic phase
n	director
n	copper(II) loading, i.e. the average copper(II) centres per dendrimeric ligand
n	non-bonding orbital
N_A	Avogadro's number
NHS	N-hydroxysuccinimidoyl
NMR	nuclear magnetic resonance spectroscopy
o. n.	over night
obs.	observed

PAMAM	poly(amido amine) dendrimers
PAMAMOS	poly(amido amine-organosilicon) dendrimers
PEI	poly(ethylene imine) dendrimers
PEO	poly(ethylene oxide)
PI	polarity index
POM	polarizig microscope
PPI	poly(propylene imine) dendrimers
puriss.	purissimum. (purity grade)
rec.	recrystallisation
ref.	reflector mode (MS)
R_g	radius of giration
rt	room temperature
S	order parameter
S	electron spin
s	stoichiometry
SANS	small angle neutron scattering
SC	side chain
SCLCPs	side chain liquid crystalline polymers
SEC	size exclusion chromatography
ser	series
sh	shoulder
SLWD	super - long working distance in objectives for microscopy
Sm	smectic phase
sy	symmetric
t	time
TBAB	tetrabutylammonium bromide
TEM	transmission electron microscopy
tert	tertiary
TGA	thermogravimetric analysis
THAP	2',4',6'-trihydroxyacetophenone
THF	tetrahydrofurane
UV-Vis	ultraviolet-visible spectroscopy
V, v	volume
v.s.	against (from Latin <i>versus</i>)
WAXS	wide-angle X-ray scattering
wo	washing-out
wt. %	weight percentage
α^2	covalence degree
γ	pseudotetrahedral angle
δ	deformation vibration (in FTIR)
ΔH_m	molar enthalpy variation
ΔH_w	weight enthalpy variation
ϵ	extinction coefficient
θ	diffraction angle in X-ray
θ	angle between the director and the main molecular axis in liquid crystals
θ	Curie-Weiss constant (in EPR)

λ	wavelength
μ_B	Bohr magneton
μ_o	magnetic constant
ν	frequency
ν	stretching vibration (in FTIR)
$\tilde{\nu}$	wavenumber
ρ	density
ρ	cross-correlation coefficient
χ	magnetic susceptibility
χ^2	sum of the quadratic deviations
$\langle \rangle$	arithmetic mean value

1 INTRODUCTION

1.1 LIQUID CRYSTALS

1.1.1 The Liquid Crystalline State

The liquid crystalline state, abbrev. LC state, is an intermediate phase of matter between the crystalline solid and the isotropic liquid state ^[1-3]. Molecules in this state flow and diffuse as liquids but still exhibit some degree of orientational- and often positional ordering in one or more directions, characteristic of crystals. Their properties, as a consequence of this order, are direction dependent, i.e. anisotropic. The concurrence of these two characteristics, mobility and order, allow a fast orientational response to external fields and determine the technical applications of these materials, e.g. in displays. This intermediate state, also known as “mesophase” from the Greek “mesos” middle; is limited by two transition temperatures: the melting point and the clearing point. At the melting point, the crystalline substance melts into the anisotropic liquid and at the clearing point all the positional and/or orientational order disappears, the birefringence is lost and the substance enters the isotropic, optically clear liquid state. This intermediate state can comprise several distinct phases according to the degree of ordering and the symmetry within each one. Molecules exhibiting mesophases are denoted mesogens or liquid crystals, and the phenomenon is called mesomorphism. A mesophase can be reached by either merely varying the temperature (thermotropic liquid crystals) or requires, additionally, the presence of a solvent or mixture of solvents (lyotropic liquid crystals). Molecules which exhibit both thermotropic and lyotropic mesomorphisms are called amphotropic liquid crystals.

1.1.2 Thermotropic Mesomorphism

Thermotropic mesophases occur by influence of the temperature. Mesophases appearing by both heating and cooling cycles are called enantiotropic; these phases are thermodynamically stable. Monotropic mesophases occur below the melting temperature, i.e. are observed only in the cooling process, due to a delay in the recrystallisation process (supercooling). Molecular premises for the occurrence of thermotropic mesomorphism are:

Anisometry, i.e., anisotropy in the geometry of the molecule. Most common morphologies are rods (calamitic liquid crystals) ^[4] or discs (discotic liquid crystals) ^[5]. Anisometric molecules fulfil some general structural requirements: a stiff centre (combination of several phenyl or heterocyclic units) and flexible moieties (alkyl or alkoxy chains) in the extremities of the rod-like molecule or around the core in case of discotic molecules. The rigid parts tend to arrange parallel to each other and the aliphatic chains care for space filling, leading to the formation of liquid crystalline phases. Polar groups such as nitrile, fluorine or nitro groups, are sometimes included to induce special properties. Less common but described are brick-like, (sandic mesogens) ^[6] bent-shaped (bananas) ^[7] and bowl-like (pyramidal) geometries ^[8]. Mesogens whose geometrical anisotropy is responsible for the appearance of mesophases are called anisometric or molecular mesogens, cf. Fig. 1.1

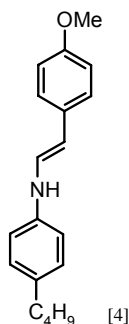
Association. The aggregation of non-anisometric units through a wide variety of interactions can lead to anisometric "supramolecular" structures, able to organise in mesophases. Possible interactions are hydrogen bridges ^[9], van der Waal forces ^[10], dipole-dipole interaction ^[11], charge transfer ^[12], π - π interactions ^[13], electrostatic forces ^[14] or coordinative bonds ^[15]. Mesogenic anisometric aggregates are referred to, as supramolecular mesogens, cf. Fig. 1.1.

Microphase segregation, i.e. a phase separation process on the molecular level. Molecules exhibiting incompatible parts such as polar/apolar ^[16, 17] hydrophilic/ lipophilic ^[18] or lipophilic/lipophobic ^[19] groups, denoted amphiphilic mesogens, segregate in microdomains separated by interfaces. The size and chemical nature of the incompatible parts determine the geometry of the interface and through this the mesophase type. The formation of mesophases of anisometric mesogens can be regarded itself as a micro-segregation of rigid and flexible parts. The segregation of different units constitutes probably the main driving force for the appearance of mesophases ^[20], cf. Fig. 1.1.

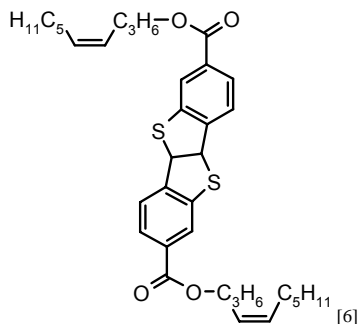
The occurrence of one of these premises can be enough to cause mesomorphism, but often several of them contribute to the appearance and stabilisation of liquid crystalline phases.

Anisometric mesogens

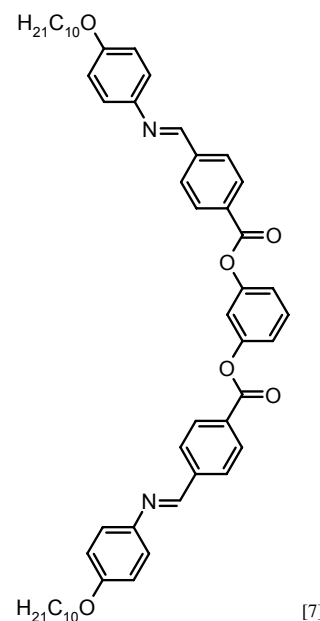
rod-like or calamitic



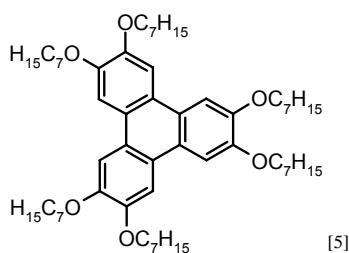
brick-like or sanidic



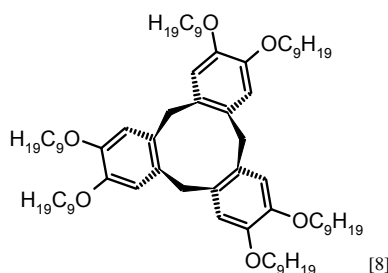
bent-core or banana



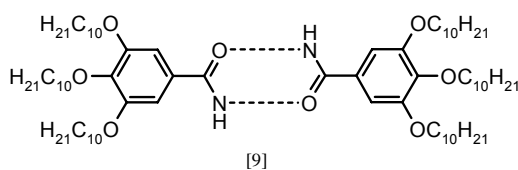
disc-like



bowl like or pyramidal

**Supramolecular mesogens**

H-bonding



metal complex formation

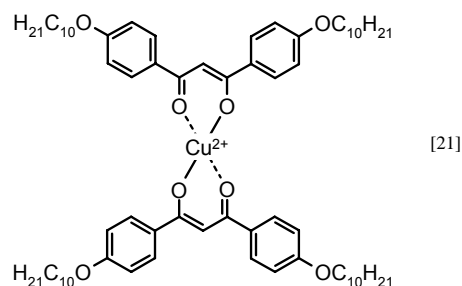
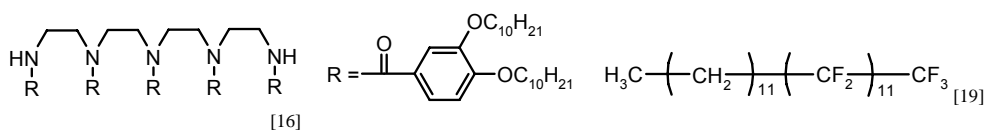
**Amphiphilic mesogens**

Fig. 1.1: Main driving forces for the appearance of liquid crystalline phases and mesogens illustrating each principle.

1.1.3 Mesophases

Different types of mesophases are described according to the degree of order and the symmetry shown by the molecular arrangements. The kind of the developed mesophase is, up to a certain degree, independent from the driving force leading to mesomorphism.

Nematic phase, N. In the nematic phase, the molecules or aggregates of molecules are in average oriented along a main direction determined by the director, \mathbf{n} , cf. Fig. 1.2. No correlation between the positions of the molecules is found, it is therefore the lowest ordered mesophase. The nematic phase exhibits, as consequence of the missing positional order, a low viscosity. This mesophase is adopted by calamitic as well as discotic molecules. The rigid anisometric shape of the individual molecules is direct responsible for the formation of nematic phases^[20].

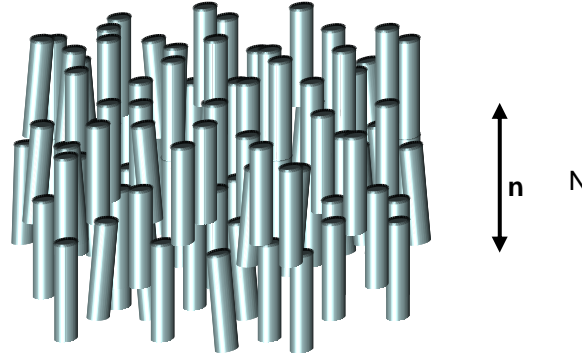


Fig. 1.2: Schematic representation of a calamitic nematic mesophase, N .

The degree of orientation is given by the order parameter S , defined^[22] as indicated in Eq. 1.1.

$$S = \frac{1}{2} \langle 3 \cos^2 \theta - 1 \rangle_x \quad \text{with } x = V, t \quad \text{Eq. 1.1}$$

θ is the angle between the director and the main molecular axis and $\langle \rangle$ indicate the average over a certain volume of molecules at a fixed time ($x = V$) or the average over time ($x = t$) for a single molecule. For perfectly ordered systems, e.g. ideal crystals, the order parameter is $S = 1$, for randomly oriented samples as isotropic liquids $S = 0$. Normally, liquid crystals exhibit intermediate values, $0.3 < S < 0.8$, because of the thermal motion of the molecules in the mesophase that avoids a perfect order. The order parameter S can be determined experimentally by e.g., Raman scattering and NMR or EPR spectroscopy^[2].

Smectic phases, Sm. ^[23] Arrangement of the mesogens into layers leads to the formation of smectic mesophases. The molecules in the smectic mesophases exhibit therefore, in addition to the orientational order, positional order at least in one direction. The molecules can lie parallel or tilted with respect to the layer normal and are free to diffuse inside and between layers. The phases are fluid. The smectic phases are denoted by Sm and a further capital letter, which specifies the particular characteristic of each phase. The most simple smectic phases, SmA and the tilted version SmC, do not exhibit an ordering within the layers, cf. Fig. 1.3. Smectic phases with short range hexagonal order inside the layers are known as SmB, SmF, or SmI phases. Additional correlation between the positions of the molecules from layer to layer, keeping rotational freedom, leads to the so-called plastic crystals or soft crystals (B, G, J). Plastic crystals fill the gap between liquid crystals and crystals.

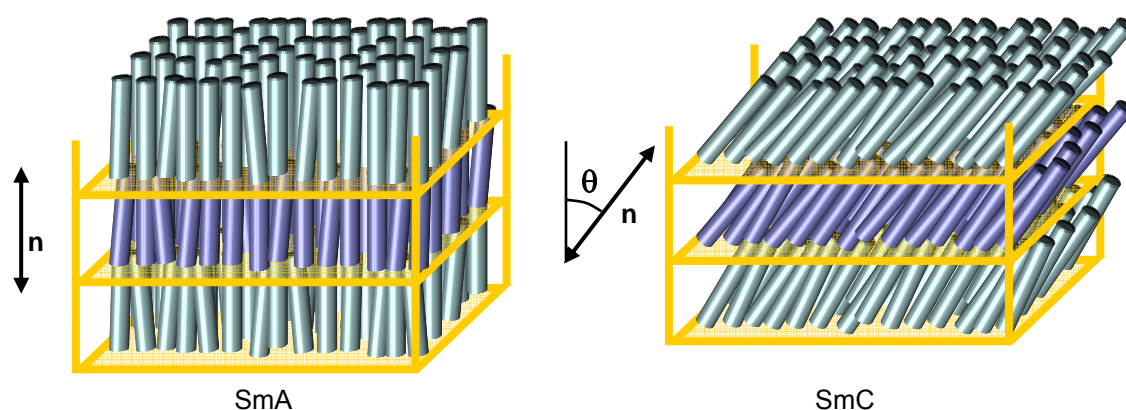


Fig. 1.3: Schematic representation of the most simple calamitic smectic phases, SmA and SmC.

Not only calamitic molecules tend to build smectic mesophases. Bent-core mesogens arrange also in a distinctive sort of smectic phases, the banana phases, with ferro- or antiferroelectric behaviour ^[7].

Molecules lacking a rigid core can also exhibit smectic mesophases, as a result of the micro-segregation of chemical incompatible parts e.g. diethylenetriamides ^[24] or myo-inositol ethers ^[25].

Columnar phases, Col. In columnar phases, the molecules are arranged in columns which self-organise in a two-dimensional lattice. Different symmetries of this lattice give rise to different columnar mesophases. Thus, hexagonal, Col_h, tetragonal, Col_t, oblique, Col_{ob}, and several rectangular columnar mesophases Col_r, have been described in the literature ^[26-39]. If the stacking of the molecules along the column is not regular, the columnar phase is referred to as a disordered one. Regular stacking of molecules in the columns leads to ordered columnar phases with a three dimensional order ^[40-42]. The subindexes “o” for ordered and “d” for disordered follow those defining the symmetry

in the notation of columnar mesophases. The absence of a subindex indicates disordered columnar phases. In that case, the molecules are free to diffuse between and within the columns and have rotational freedom. Therefore they are real fluids.

Anisometric disc-like molecules or aggregates arrange preferentially in columnar phases. The rigid cores determine the order and are embedded in a matrix made of the peripheral flexible groups. The optimal space filling is achieved in a hexagonal lattice, Col_h , where the director lies parallel to the column axis. Rectangular and oblique mesophases, Col_r , arise either from discotic molecules tilted with respect to the columnar axes, so that the column section is elliptic, breaking the high hexagonal symmetry or from sanidic mesogens^[26, 43]. Several rectangular mesophases of different symmetry have been described^[34-36]; they are denoted according to the 17 crystallographic planar groups of symmetry. Common columnar phases are depicted in Fig. 1.4. The unit cell and the characteristic parameters, lattice constants and angles are indicated.

Non-anisometric mesogens can also organise in columnar phases when the segregation of dissimilar molecule regions causes a selective starring of a part allowing thereby the arrangement in columns^[17]. Columnar polymorphism, i.e. occurrence of more than one columnar phase,^[27, 39, 44-52] mesophase is sometimes described. The usual sequence with increasing temperature is:

$$Col_{ob} \rightarrow Col_r \rightarrow Col_h$$

Further possibilities of columnar phases are the columnar nematic^[34] and the lamello-columnar mesophases. In the columnar nematic phases, the columns, made of a reduced number of stacking units, are merely oriented in a common direction as a nematic phase. Organisation of columns in layers, without correlation from layer to layer gives rise to a lamello-columnar mesophases.

Columnar mesophases

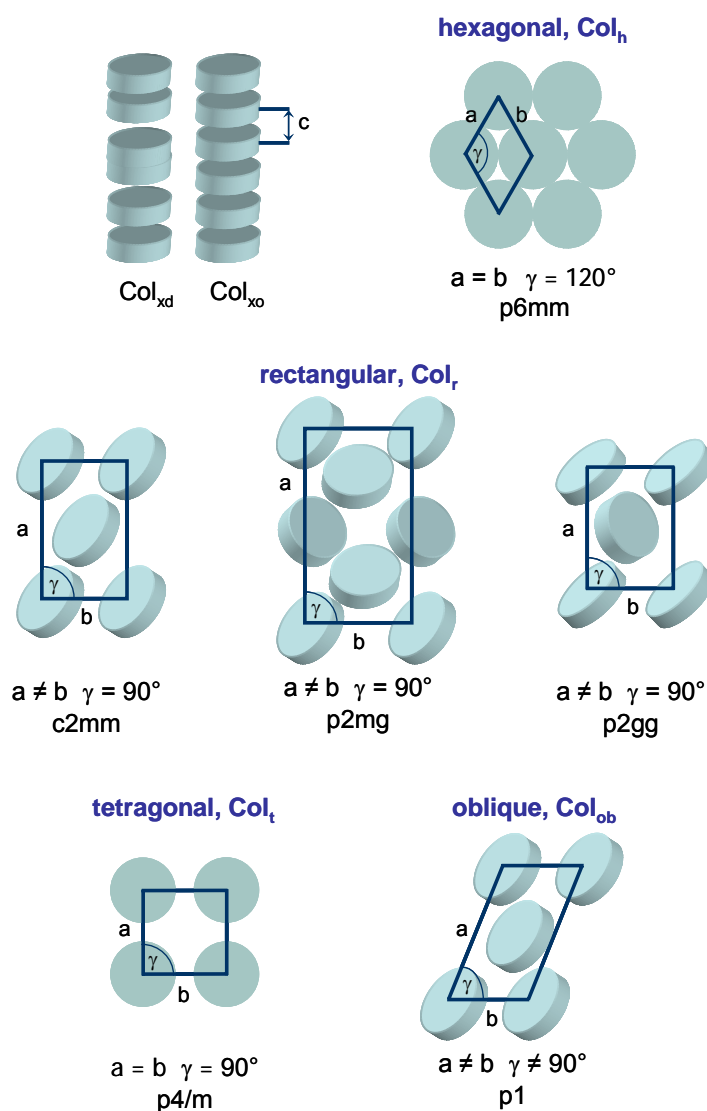


Fig. 1.4: Schematic representation of the main columnar phases, Col.

Cubic phases, Cub. In the cubic phases the mesogens are organised in lattices with cubic symmetry, i.e. they exhibit three-dimensional periodicity, cf. Fig. 1.5. This high symmetry in all space directions determines the isotropy of the physical properties of these phases. Spherical mesogens can e.g. arrange in the nodes of a cubic lattice giving rise to cubic spheroidic mesophases, Cub_s. More complex are bicontinuous cubic phases, Cub_b, consists of two interwoven but not connected, periodic, three-dimensional infinite networks with cubic symmetry ^[53]. This last phase can be considered as an intermediate stage phase in the evolution from lamellar to columnar hexagonal arrangements.

Cubic phases, Cub

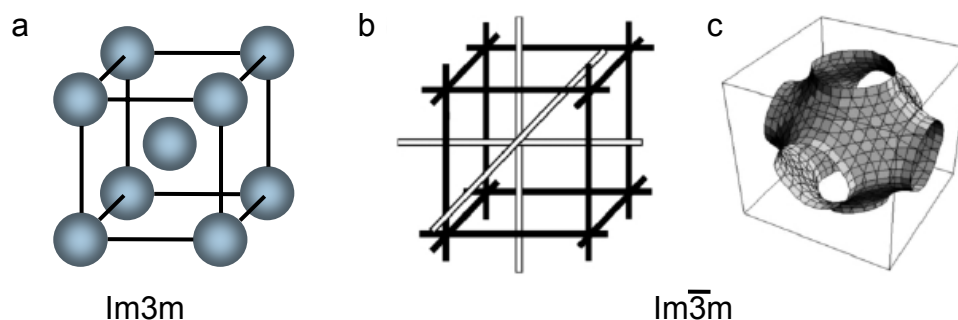


Fig. 1.5: Cubic mesophases. Exemplarily a: Cubic spheroidic phase, Cub_s with $Im\bar{3}m$ symmetry. b, c: bicontinuous cubic phase, Cub_{bic} with $Im\bar{3}m$ symmetry, b skeleton of the phase and c associated surface (images from reference [53]).

Each mesophase exhibits under optical microscope with crossed polarizer characteristic patterns, termed “textures” [54, 55]. These textures arise from distinct defects in the molecular organisation of the mesophase and from the orientation of the director in the boundaries of the different domains in which the liquid crystal is arranged. Different molecular organisations cause distinctive defects which result in characteristic patterns for. Textures frequently give hint to an identification of the mesophase, but X-ray investigations provide more accurate insight in the mesophase, e.g. distinction among different columnar, cubic or smectic phases. The transition temperatures are determined by calorimetric methods.

1.1.4 Lyotropic Mesomorphism.

Lyotropic mesophases occur in the presence of a solvent or mixture of solvents at certain concentration and in a defined temperature range. Lyotropic mesogens are usually amphiphilic (hydrophobic-hydrophilic) molecules e.g. soaps or ammonium salts. The appearance of mesophases is the consequence of the supramolecular selective association of the similar parts of the amphiphilic molecules in micelles which in turn, organise into mesophases at higher concentrations. Different morphologies are observed: spherical, disclike or cylindrical, micelles or bilayers, depending on their chemical nature and molecular shape, the solvent and the concentration. The mesophases are isostructural with those of thermotropic mesogens: nematic, smectic (here usually termed lamellar), columnar and a great variety of cubic mesophases.

1.1.5 Metallomesogens

Liquid crystalline molecules or aggregates, including one or more metal centres in their structure, are referred to as metallomesogens. With respect to pure organic mesogens, metal centres can add new interesting features, such as electron rich environments, colour or paramagnetism ^[56]. Metal incorporation, has resulted furthermore in the appearance of novel morphologies. The metal centre is in some cases directly responsible for mesomorphism. Metallomesogens comprise metal complexes of p, d, and f-groups, organometallic compounds and ionic species, cf. Fig. 1.6. Both low molecular weight compounds and polymeric metallomesogens, exhibiting thermotropic and/or lyotropic mesomorphism, have been described. The structural requirements and the mesophases observed in metal-containing liquid crystals are analogue to those of pure organic liquid crystals. Coordination to metal usually leads to higher transition temperatures.

The great majority of the thermotropic metallomesogens are anisometric coordination compounds, with calamitic ^[57] or discotic morphologies, being among the last ones porphyrine ^[32, 41, 47, 58] and phthalocyanine ^[28, 47, 50] metal complexes, extensively studied due to their possible application as unidirectional conductors. Metal coordination can favour the mesophase formation of non-mesogenic anisotropic ligands ^[59]. The metal can serve as linking group between two pro-mesogenic units giving rise to supra-molecular calamitic ^[60] or discotic metallomesogens as is the case in for instance β -diketonate copper complexes ^[61]. Rod-like metallomesogens exhibit preferentially nematic and/or smectic phases whereas, disc-like mesogenic metal complexes organise in a broad variety of columnar mesophases, hexagonal ^[28, 62], rectangular ^[62, 63], oblique, ^[63, 64] tetragonal ^[63, 65], as well as nematic columnar ^[66]. Flexible non-mesogenic ligands are also able to induce liquid crystalline phases when coordinating metal centres ^[67]. New molecular structures are thereby observed, e.g. pyramidal, conic or bowl like complexes ^[68]. The entire morphology of the metallomesogen rather than the coordination geometry is responsible for the mesophase formation ^[67].

Organometallic compounds, i.e. complexes in which the metal centre is linked to a carbon atom or a π -system, exhibiting liquid crystalline phases have also been described. Ortho-palladated ^[69] compounds are the common exponent of the former and ferrocenes ^[70] of the latter.

Metal salts of several metals like e.g. n-ammonium zinc complexes ^[71] or organic carboxylate salts ^[72] are also known to form thermotropic mesophases. The carboxylate salts display a new molecular architecture, similar to a lantern, being an example of how incorporation of a metal results in novel geometries. However, most metal salts of organic acids or the carboxylates mentioned above, organise into mesophases in the presence of a solvent, i.e. they are lyotropic mesophases ^[73, 74]. Metal complexes with a

polar head group and a hydrophobic part, imitating the classical soaps, can also give rise to lyotropic mesophases ^[75]. Furthermore several metal-containing discotic mesogens, display too lyotropic mesomorphism ^[76].

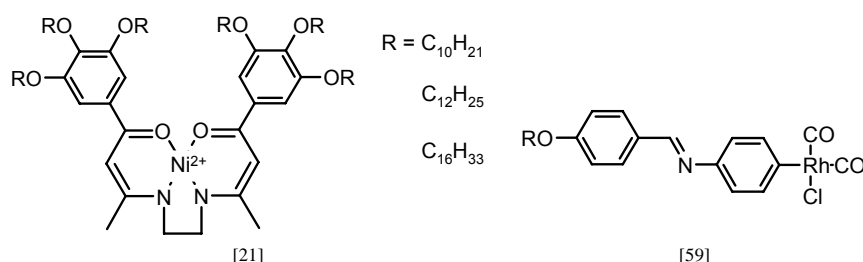


Fig. 1.6: Several examples of metallomesogens.

1.1.6 Liquid Crystalline Polymers, LCPs

Thermotropic and lyotropic mesomorphism has also been observed in polymers. The resulting mesophases are isostructural to those formed by low molecular weight mesogens. Most of the thermotropic liquid crystalline polymers include anisometric mesogenic units in their structure, which are responsible for the appearance of liquid crystalline behaviour. However, supramolecular polymers, consisting of non-mesogenic self-assembling units by means of non-covalent bonds as well as amphiphilic polymers made up of incompatible parts display liquid crystalline phases ^[1, 2, 77]. With respect to LCPs, it is attractive that many of them form glasses. This allows the conservation of the anisotropic structure of the mesophase below the glass temperature.

Conventional thermotropic LCPs incorporate anisometric units either in the polymer backbone, the so-called main chain liquid crystalline polymers (MCLCPs) or are attached to the polymer main chain as lateral groups, these ones are referred to as side chain liquid crystalline polymers (SCLCPs), cf. Fig. 1.7. Standard anisotropic units are rod- disc- or brick-like mesogens, they give rise to nematic, smectic or columnar mesophases. The anisometric units have to be separated from each other or from the main chain by a flexible spacer. In case of MCLCPs, the spacer decreases the melting temperature of the polymer and often allows the appearance of new phases. For SCLCPs, the flexible spacer plays a crucial role, since it allows the alignment of the mesogenic unit in mesophases independent from the tendency of the main chain to adopt a random coiled conformation, i.e. it allows to “decouple” the motion of the main chain ^[78]. Shorter spacers favour nematic mesophases; the longer the spacer the larger the probability to form smectic mesophases.

Cross-linked polymers, cf. Fig. 1.7, have also been described giving rise to LC-elastomers, LCEs (low degree of cross-linking), where the liquid crystalline properties can be controlled by an external mechanical field ^[79]. In LC-duromers, i.e. anisotropic net-

works the high degree of cross-linking^[80, 81] fixes the orientation of the molecules in the mesophase, preserving thereby the anisotropy, which is especially interesting for optical applications.

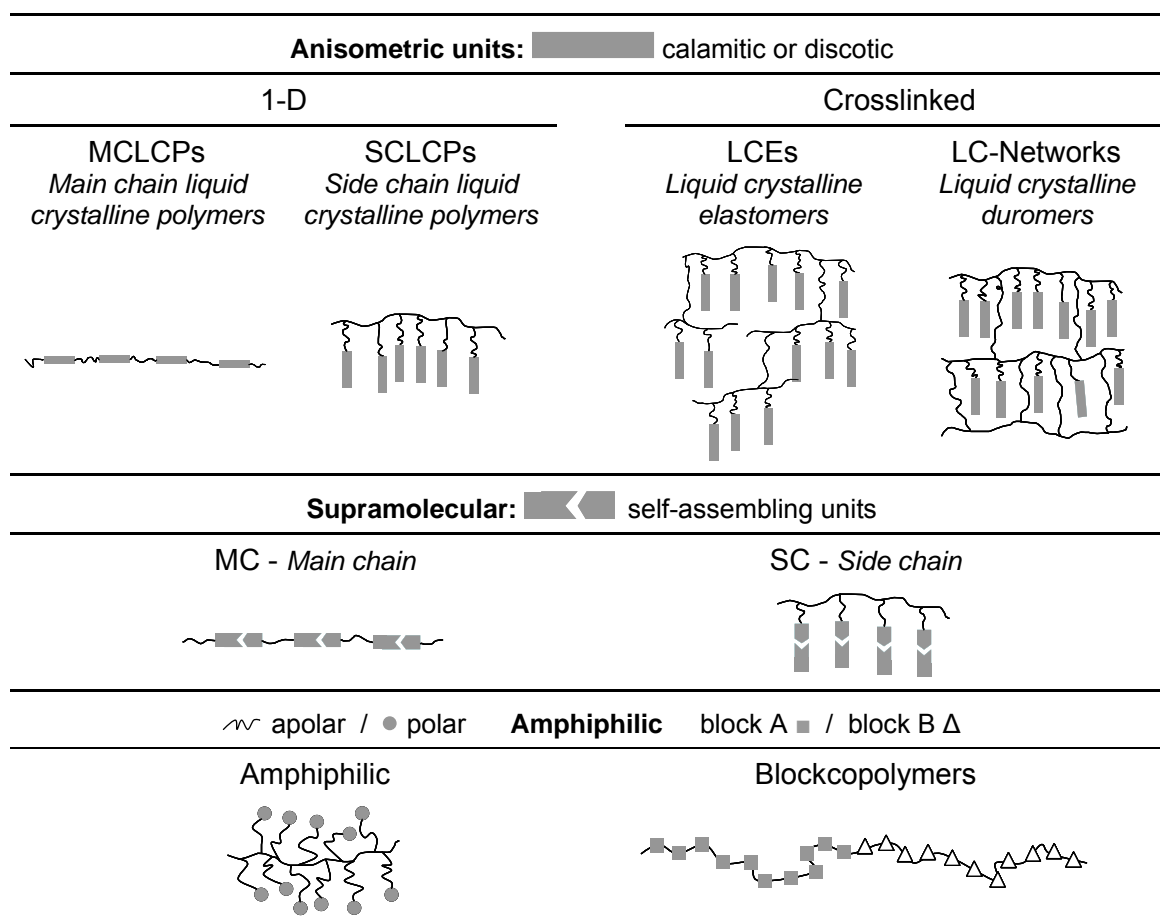


Fig. 1.7: LCPs. Diversity of morphologies and organisation principles.

The self-assembly of non mesogenic units by means of non-covalent bonding can give rise to supramolecular main and side chain liquid crystalline polymers, cf. Fig. 1.7. A common approach is the connection through hydrogen bonds^[82]. Ionic interactions and formation of coordination complexes are also known^[83, 84].

In analogy to the low molecular weight mesogens, amphiphilic polymers undergo segregation of their incompatible parts giving rise to the appearance of mesophases. Block copolymers constitute a further example of amphiphilic molecules which exhibit a great variety of morphologies analogue to LC phases by block segregation on the macroscopic scale^[85], cf. Fig. 1.7.

Some lyotropic systems are relevant for their applications as high modulus fibres. The polymer is spun from the mesophase solution where the polymer is aligned. The resulting fibres exhibit excellent tensile strength in the orientation direction, e.g. Kevlar[®].

1.2 DENDRIMERS

1.2.1 Definition and Structure

Dendrimers are molecules which, starting from a central core or focal point, are regularly and recursively branched ^[77, 86, 87]. Each level of such branching is referred to as a generation. The branching points are starting sites for a new generation, the number of branches at each branching point is denoted as connectivity. The terminal moieties of the last generation branches are called end groups. The end groups attached at the last generation branches constitute the periphery or outer shell of the dendrimer; whereas all generation branches constitute the interior or inner shell. One main branch of a dendrimer is called a dendron. A schematic two-dimensional representation of a dendrimer and associated concepts is presented in Fig. 1.8; note however that this does not describe its real conformation or space filling. The recursive architecture of the dendrimers ensures a strongly controlled topology with an in principle high symmetry and fractal geometry. The real conformation of a dendrimer however is determined by further intrinsic and extrinsic factors, cf. 1.2.3.

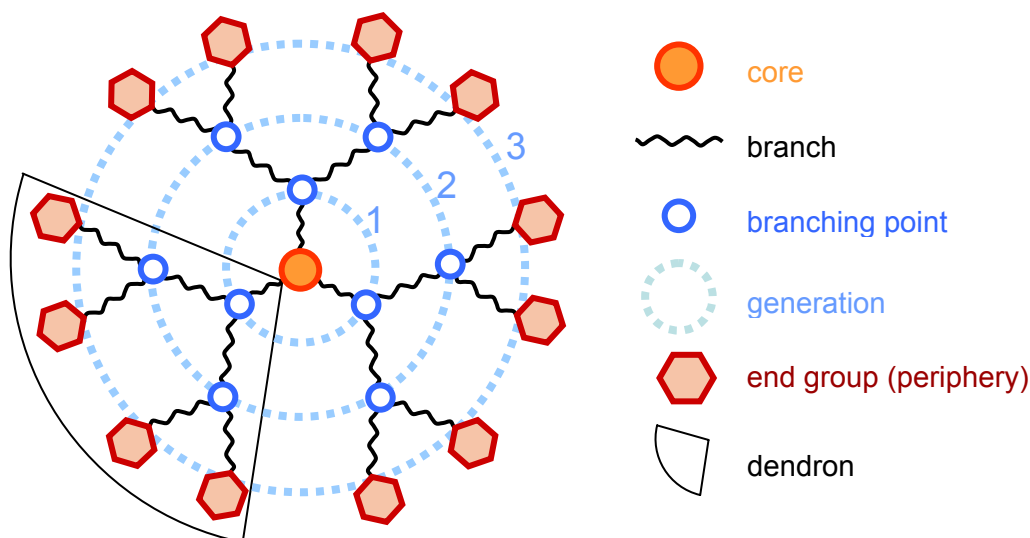


Fig. 1.8: Schematic two-dimensional representation of a dendrimer structure: core, branches, branching points, generation and end groups. One dendron is indicated with a solid line.

1.2.2 Synthesis, Purity, and Polydispersity

Dendrimers comprise low molecular weight species up to polymeric materials with increasing generation. Two opposite strategies have been developed for their synthesis: from the dendrimer core outwards (divergent approach) ^[88, 89] or from the periphery inwards (convergent approach) ^[90, 91]. Drawbacks of the divergent approach are cumber-

some purifications steps and the inevitable appearance of a certain number of statistical defects with increasing generation. Dendrimers prepared convergently exhibit less defects but the yield of the final step, consisting of the coupling of the dendrons to the core, is usually low. The dispersity, irrespective of the synthetic approach, is very low compared to that observed in conventional polymers. Defect structures have been successfully detected and identified by mass spectrometry (matrix-assisted laser desorption ionisation, MALDI and electrospray ionisation, ESI). The number of end-groups grows exponentially with the generation. As a consequence of this, dendrimers can only be prepared up to a certain limit generation, for still higher generations the accessibility to the end-groups is hindered and prevents complete functionalisation.

1.2.3 Dendrimer Behaviour in Solution: Conformation

The conformation of the dendrimers in solution is an essential issue since it determines the location of end-groups, the shape of the dendrimer and thereby some of its physico-chemical properties such as the reactivity or viscosity^[92-94]. First theoretical studies of dendrimers in solution by de Gennes and Herve^[95] assumed a fully elongated conformation of the dendrimers. Each generation of monomers fills a concentric shell of its own. Therefore, the density increases towards the periphery where all the end groups are localized. This model, known as *dense-shell* model, predicts hollow inner parts (cavities) in the dendrimer and opens the possibility of using dendrimers as unimolecular micelles for delivering small molecules, e.g. dendritic boxes^[96, 97]. Further theoretical analyses by Lesanec and Muthukumar^[98] showed however, that a flexible dendritic structure exhibits its density maximum in the centre of the molecule and decreases towards the periphery. As a consequence, the end-groups are spread over the whole volume of the dendrimer and are not confined at the periphery, i.e. branch backfolding occurs as confirmed by small angle neutron scattering, SANS, experiments^[99]. This model, the *dense-core* model, is consistent with the tendency of end-groups to maximise the entropy of the system, distributing all over the space being this tendency only modulated by the monomer-monomer^{''} excluded volume repulsive interactions. The dense-core model is supported by most of the theoretical studies, simulations and experimental investigations reported so far^[92]. Both models are depicted in Fig. 1.9. In consequence, the dendrimer solubility is not exclusively driven by the end groups and a high concentration of end-groups in a certain region of the dendrimer can not be assumed. Lower generation dendrimers adopt more open conformations and become more globular and compact with increasing generation.

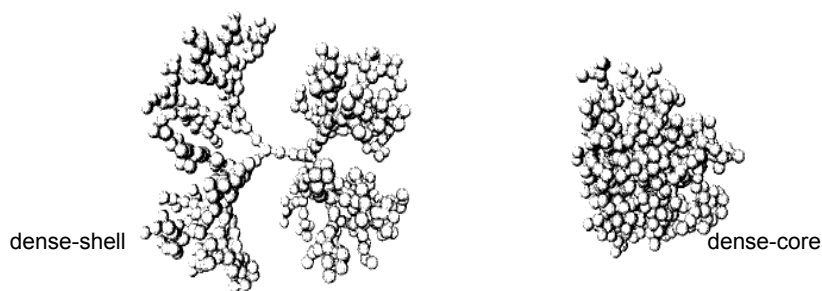


Fig. 1.9: Dense-shell / dense-core models for a dendrimer. Figure from reference [100].

The density profile can be tuned and the dense-shell conformation can be selectively achieved, if under particular conditions this conformation is made energetically the more favourable. So, Welch and Muthukumar^[100] demonstrated by Monte Carlo simulations that in media of low salt concentration or low pH this is the preferred conformation since it minimises the charge repulsions. At higher salt concentrations or higher pH values, the charges are screened, a denser packing is not hampered and the dense-core conformation is adopted. The transition from one into the other occurs by varying the electrolyte concentration and is reversible. Further interactions such as anisotropic interactions which drive the appearance of mesophases in dendrimers functionalised with mesogenic units at their periphery^[101] or segregation between dendrimer skeleton and end-groups^[102], can reduce backfolding and stabilise the dense-shell conformation.

1.2.4 Further Properties. Comparison to Conventional Polymers.

Even if dendrimers are polymers in broader sense, particular features differentiate them from common linear or branched polymers. This makes them attractive candidates for certain applications, despite the usual expensive and time consuming synthetic procedures^[86, 93]. Unlike traditional polymers, which mostly show a random coil conformation, dendrimers display predictable shapes depending on the generation. Due to their dense, cluster like shape, their hydrodynamic volume is smaller than that for linear coiled analogues. The solubility of dendrimers in a certain solvent is higher than that of linear homologous and increases with the generation, probably also caused by their dense, branched structure. Dendrimers exhibit no entanglements as conventional polymers do, in consequence they show lower viscosity. The viscosity increases with the generation up to a certain maximum, decaying after it. Dendrimers are usually amorphous materials exhibiting lower glass temperatures than linear polymers; they do not present segmental mobility but the mobility involves the whole dendrimer. The absence of interpenetration among dendrimers has been observed even for concentrated solutions of dendrimer upon worsening the solvent quality and drying after the elimination of solvent. Under those conditions they shrink^[103]. Appropriate dendrimers show an

isotropic electronic conductivity in contrast to linear polymers where the conductivity is direction dependent ^[86]. Furthermore some synergy, i.e. advantageous cooperative or amplification effects, in some physical properties is expected as result of their peculiar architecture ^[104-106].

1.2.5 Nitrogen containing Dendrimers: PPI, PEI, PAMAM, and PAMAMOS

Poly(propylene imine), PPI dendrimers are closely connected with the development of dendritic structures. Vögtle et al. described in 1978 for the first time the cascade (divergent) synthesis of low molecular weight polyamines ^[88], precursors of dendrimers. Low yields and troublesome purifications hindered the preparation of high generations. The improvement of this approach came years later from two independent groups, those of Mühlhaupt ^[107] and Meijer ^[108], being established as the industrial procedure for preparation of PPI. Poly(propylene imine) is commercially available as *Astramol*. The synthesis consists of a repetitive reaction sequence: double Michael addition of acrylonitrile to primary amines followed by reduction of the nitriles to primary amines in presence of Raney-Co or Ni, cf. Fig. 1.10.

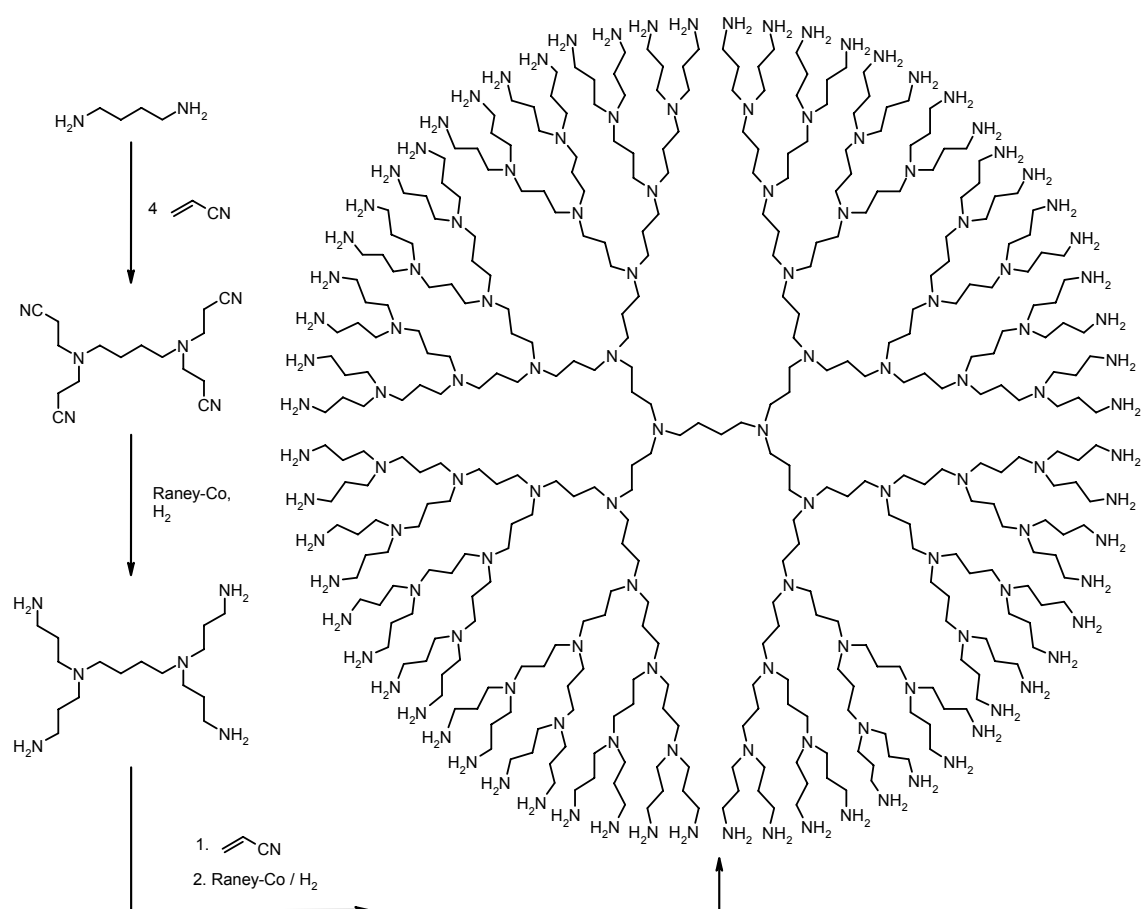


Fig. 1.10: Synthetic procedure for PPI dendrimers.

The dendrimers prepared by these means, bear a certain number of statistical defects, as observed by ESI^[109]. Usual fractions of perfect dendrimers per generation in commercial charges are indicated in Table 1.1. The polydispersity remains however low, 1.002 for the 5th generation^[110]. The PPI skeleton involves a large number of amino groups, tertiary ones at the branching points and primary ones as terminal groups of the dendrimer. Basicity is therefore one of the most characteristic features of PPI. The protonation behaviour of PPI has been studied and reveals that protonation occurs sequentially beginning from the primary amines, followed by the tertiary amines in the core and in a final step the rest of the inner tertiary amines^[111]. At room temperature PPI dendrimers are transparent or slightly yellow liquids, soluble in water, methanol and toluene^[110]. Several theoretical and experimental studies suggest a dense-core conformation of PPI in solution^[93, 110]. An estimation of the dimensions (gyration radius, R_g) of the PPI dendrimers by SANS^[112] is reproduced in Table 1.1 together with some of the properties described here. PPI dendrimers exhibit a high thermal stability, which increases with the generation. Comparison of the amine terminated PPI dendrimers with the nitrile precursors reveal that their physical properties are conditioned by the end groups and by the generation^[110].

Table 1.1: *Characteristic parameters of the PPI dendrimers in dependence on the generation.*

Generation	Number of end-groups	Number of tert. amines	M.W. /g·mol ⁻¹	Gyration radius R_g / Å ^[112]	% perfect dendrimers
1	4	2	317	4.4	100
2	8	6	773	6.9	100
3	16	14	1687	9.3	75
4	32	30	3514	11.6	50
5	64	62	7168	13.9	34

Due to their basic properties, PPI dendrimers are potential chelates for metal complexation^[113-117]. These dendrimeric metal complexes have been successfully used as catalysts^[116, 117]. Another interesting application of dendrimeric metal complexes relies on their use as templates for metal and metal oxide nanoparticle formation^[118-121]. Dendrimers exert effective control over the nanoparticle size in dependence on the generation and are able to stabilise the individual particles, preventing coagulation^[122, 123]. Metal nanoparticles prepared in this manner exhibit catalytic activity for reduction of 4-nitrophenol^[121]. An organic-inorganic semiconductor composite based on PPI-stabilised CdS nanoparticles has been also reported^[124]; in this case the periphery of the PPI has been modified with oligo(phenylene vinylene) groups. Grafting of chelating groups to the terminal branches of PPI permits the formation of new types of metal complexes and metalorganic compounds^[104, 125-128]. Gadolinium complexes have been successfully

tested as contrast agents for magnetic resonance imaging in living organisms ^[127]. Furthermore chelate-containing PPI dendrimers could find potential applications as sequestering agents for heavy metals ^[126]. Metal-organic palladium and rhodium PPI dendrimers have been tested as chiral catalysts for the asymmetric hydrogenation of diverse species whereupon a strong positive dendrimer effect has been observed ^[104, 128].

The functionalisation of the primary amine end-groups of PPI by simple amidation reactions, make possible the access to a broad variety of PPI derivatives. Modification of PPI dendrimers with apolar groups lead to the formation of amphiphilic dendrimers. They have been shown to be good extractants of anionic dyes from aqueous to organic media ^[129, 130]. Other amphiphilic PPI dendrimers have been used as templates for the preparation of mesoporous silica ^[131] or for the selective formation of different calcium carbonate modifications ^[132]. PPI dendrimers carrying photoactive units at their terminal groups have been also described ^[106, 133], among others, as systems with light harvesting properties ^[134] and efficient fluorescent sensors ^[105, 135]. Liquid crystalline PPI derivatives have received also considerable attention and are illustrated in detail in the next sections.

Close related to the PPI dendrimers are the poly(ethylene imine) (PEI), the poly(amido amine) (PAMAM) and the poly(amidoamine-organosilicon) (PAMAMOS) dendrimers. PEI dendrimers exhibit ethyl instead the propyl units between the tertiary amine branching points ^[136-138]. PAMAM dendrimers exhibit like PPI and PEI tertiary amines in their branching points and additionally an aliphatic amide moiety in each branch ^[89, 139], cf. Fig. 1.11. They are likewise hydrophilic. PAMAM dendrimers display for a given generation larger dimensions than PPI and a similar flexibility. Compared to PPI, PAMAM are thermally less stable ^[123]. PAMAMOS ^[140, 141] are amphiphilic co-dendrimers with a polar PAMAM interior substituted with diverse hydrophobic organosilicon groups at the periphery. PAMAMOS ^[140, 141] and most notably PAMAM dendrimers have been widely used as complexation agents for metals ^[142, 143] and as template for metal nanoparticle formation ^[121-123, 144-146].

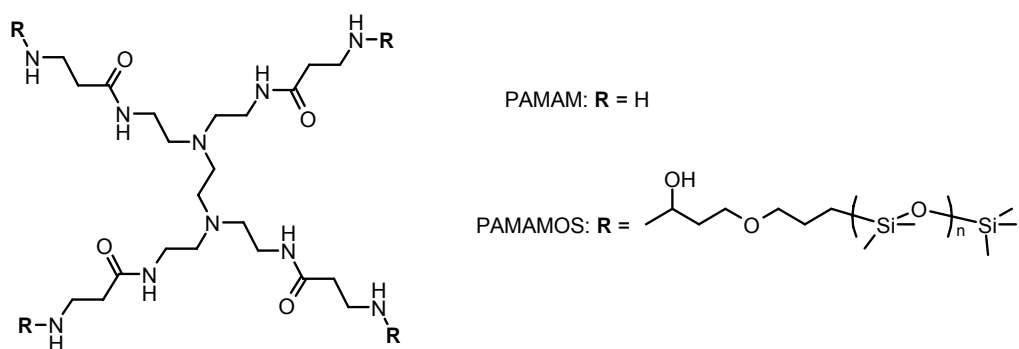


Fig. 1.11: 1st generation poly(amidoamine) PAMAM and a PAMAMOS dendrimer

1.3 DENDROMESOGENS

Dendrimers exhibit some striking features different from those of conventional polymers that make these architectures very attractive candidates for the formation of mesophases^[147, 148]. As result of their characteristic structure, they are nearly monodisperse. Therefore, their thermal properties are easily reproducible. Despite of their high branching, dendrimers exhibit neither chemical cross-linking nor entanglements. Therefore, they are less viscous than traditional polymers and they are expected to show higher mobility in the fluid phase, even at higher molecular weights. Size and shape of dendrimers can be controlled by the generation, by the connectivity of the branching points and by the chosen core; in this way, some influence can be exerted in the induction of a mesophase.

1.3.1 Shape Persistent Dendrimers

A special family of dendrimers, the *shape persistent* dendrimers, with stiff cores and long peripheral alkyl chains are intrinsically mesogenic. The Pesak's phenyl acetylene dendrimers^[149], cf. Fig. 1.12 or the stilbenoid dendrimers of Meier^[150] belong to this family. The low generations of these dendrimers exhibit, due to their chemical nature, a planar conformation, they are rigid flat discs which stack in columns arranged in hexagonal lattices. The stacking is stabilised through the π - π interactions between the aromatic rings as result, the mesophases extend over broad temperature ranges. The higher generations are not any more mesogenic, the growth lead to steric repulsions, the discs begin to twist and packing is not more possible. The high electron density conjugated all over the shape persistent dendrimer causes interesting photochemical properties with possible applications in material science.

Otherwise, the same principles observed in the mesophase formation by low molecular compounds are adopted to induce mesophases of dendritic structures, i.e. dendromesogens^[102]. Anisometric mesogenic or pro-mesogenic units are built in the dendrimer framework, branching points or branches, giving rise to the so called "main-chain" liquid crystalline dendrimers in analogy to the liquid crystalline polymers LCPs. Most commonly, the end groups of the dendrimers are functionalised with the mesogenic or pro-mesogenic moieties, the "side-chain" liquid crystalline dendrimers. Considering the geometrical growth of the endgroups with the generation, a high concentration of mesogenic groups can be achieved in this way. Dendritic effect, i.e. cooperative forces to promote or stabilise the mesophases are also expected as consequence of the peculiar structure of the dendrimers.

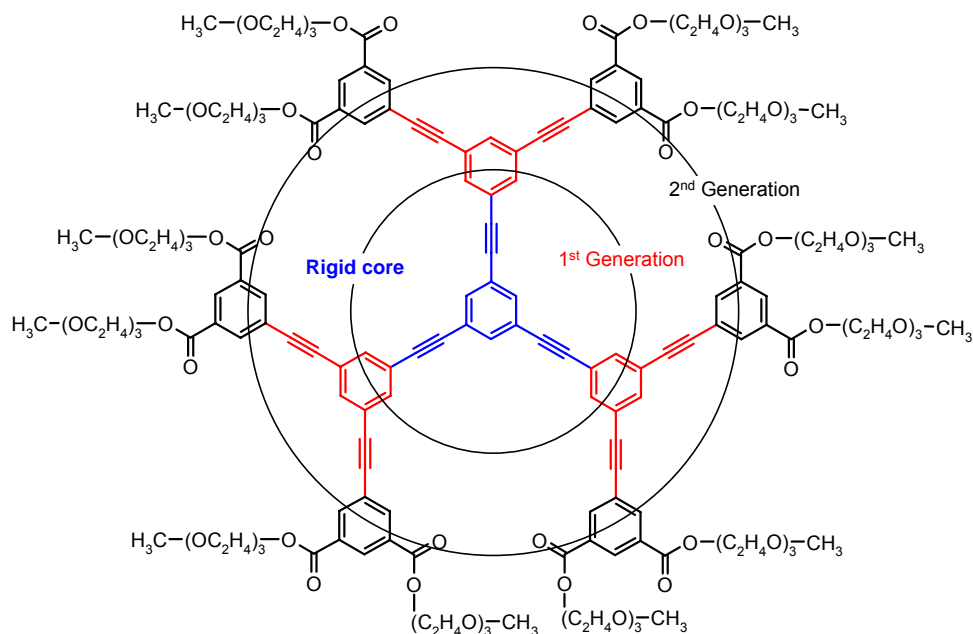


Fig. 1.12: Shape-persistent dendrimers exemplified with a 2nd generation phenyl acetylene dendrimer ^[149].

Dendrimers without anisometric units present also mesophases by micro-phase separation processes. Likewise, dendrimers resulting from the assembly of non-mesogenic dendrons, termed “supramolecular dendrimers” display also mesomorphism.

1.3.2 Dendromesogens with Anisometric Mesogenic Units

In the main chain liquid crystalline dendrimers the mesogenic units repeat through the dendritic framework. The branching points are anisometric mesogenic units themselves. *Willow* ^[151-154] and *octopus* ^[155, 156] dendrimers are examples of dendrimers exhibiting anisotropic units in their junctions: terphenylene moieties in the first case and stilbene or tolane groups in the second, cf. Fig. 1.13. The branches themselves are alkyl/alkoxy chains which bring the necessary flexibility, as spacers do in LCPs, to allow the organisation in mesophases. The mesogenic units in willow dendrimers arrange parallel to each other forcing the dendrimer to adopt an elongated shape, which organise in nematic or smectic phases. The octopus dendrimers exhibit smectic or columnar phases. The morphology of the dendrimer and in consequence the mesophase type adopted by the octopus dendrimers, does not depend from the dendrimer core ^[157], but depends on the number of terminal alkoxy chains on the end-groups. Interesting in the case of the octopus dendrimers is furthermore that the only fairly good stilbene or tolane mesogenic units result by inclusion in the dendrimeric structure in well defined mesophases, being that a proof of the expected “dendritic” effect in the enhancement of the mesogenic properties compared to the low molecular mesogens ^[147, 155, 156]. Both willow and octopus dendrimers are prepared by convergent synthesis.

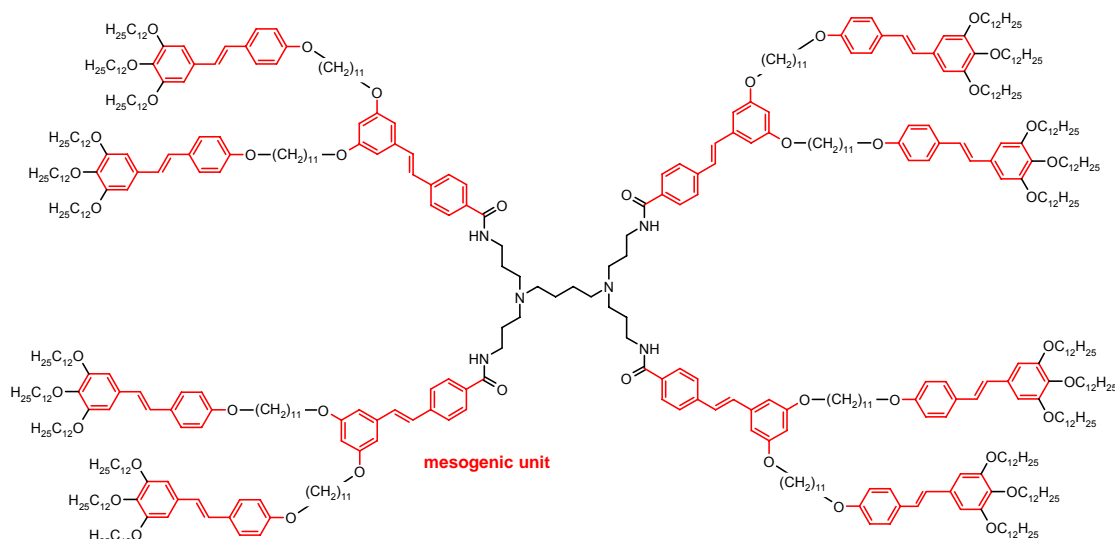


Fig. 1.13: “Main-chain” liquid crystalline dendrimer exemplified with a 1st generation octopus dendrimer. ^[155]

Dendrimers with mesogenic or pro-mesogenic units attached onto their end groups, leading as result to mesophase formation are referred to as side-chain liquid crystalline dendrimers ^[86, 147, 148]. Two opposite forces compete in the mesophase formation: the dendrimer tends to maintain its original isotropic architecture to keep the maximal entropy and the mesogenic groups tend to orient regularly to each other in mesophases with reduced entropy but an enthalpy gain. A flexible dendrimer scaffold is therefore required to “decouple” the mesogenic structures from the dendritic framework and to achieve the most stable structure for the overall molecule. In some cases, spacers are introduced between dendrimer and mesogens for further support of the decoupling. The size of each part as well as the shape of the mesogenic unit and their connectivity to the dendrimer periphery, end-on (at one extreme) or side-on (laterally), modulates the mesophase type.

As an example, carbosilane dendrimers are easily functionalised with a broad variety of mesogenic units, cf. Fig. 1.14. Depending on the mesogenic group and the generation smectic, columnar both hexagonal and rectangular phases, including examples of columnar polymorphism have been described ^[158-162]. Again, the segregation between the mesogenic units and dendrimer structure is responsible for mesophase formation and the space requirements of each part determine the mesophase type. Siloxane dendrimer with a polyhedral core and laterally attached calamitic mesogens give rise to nematic and columnar polymorphism with a transition from a rectangular to a hexagonal mesophase. End on attached mesogens exhibit SmA/C mesophases ^[163-165]. Carbosilazane dendrimers with side-on grafted mesogens result too in nematic phases formation pointing out the lateral grafting as an useful strategy to induce nematic phases ^[166, 167].

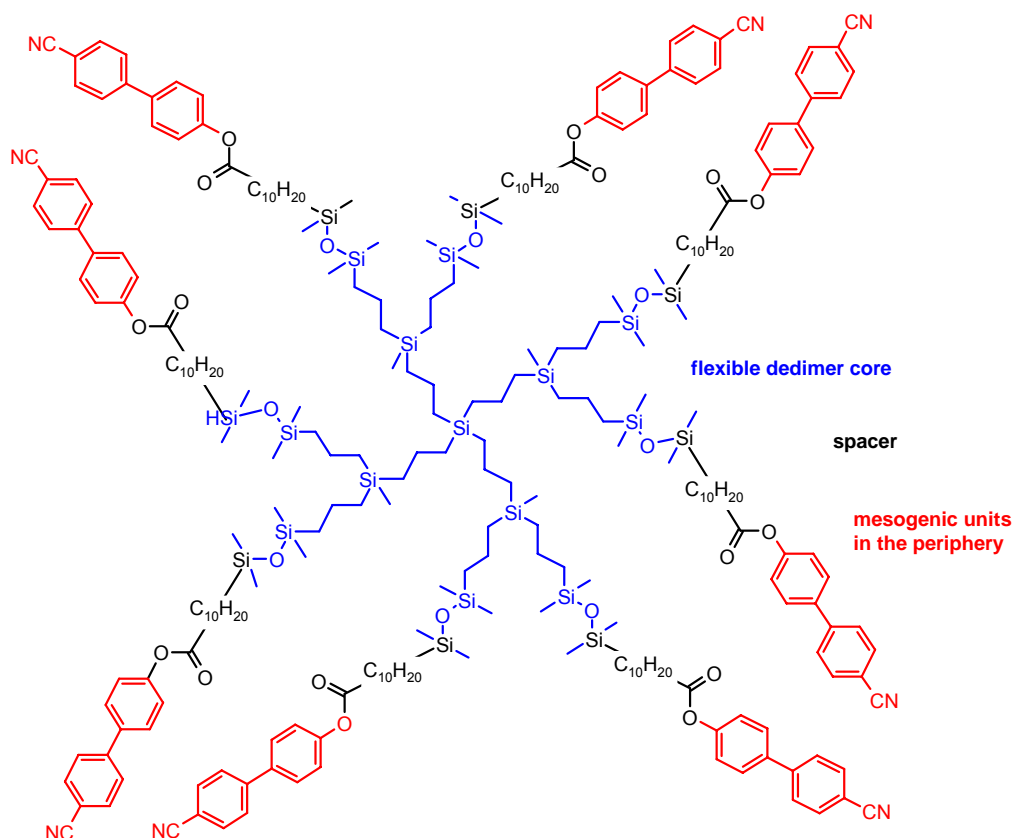


Fig. 1.14: “Side-chain” liquid crystalline dendrimer illustrated by means of a 2nd generation carbosilane dendrimer functionalised with anisometric cyanobiphenyl units at its periphery^[158].

Poly(propylene imine), PPI dendrimers and related dendrimers as poly(ethylene imine), PEI, and poly(amido amine) PAMAM dendrimers have been extensively functionalised with mesogenic units in their periphery and will be considered separately in next sections.

1.3.3 Dendromesogens with Microsegregating Structures

Diverse dendrimers display liquid crystalline behaviour with no anisometric mesogenic units in any part of their skeleton; they exhibit an incompatible core-shell structure which segregates from each other, being that the driving force for mesophase formation. An example of this type of liquid crystalline dendrimers are carboxilanes with per-fluoroalkyl chains attached at the periphery^[168]. A hybrid microsegregating structure of linear poly(ethylene oxide), PEO, connected to a polyether dendron with hydrophobic, terminal alkoxy chains has been also described^[169], cf. Fig. 1.15. Both self-assemble into lamellar and columnar mesophases.

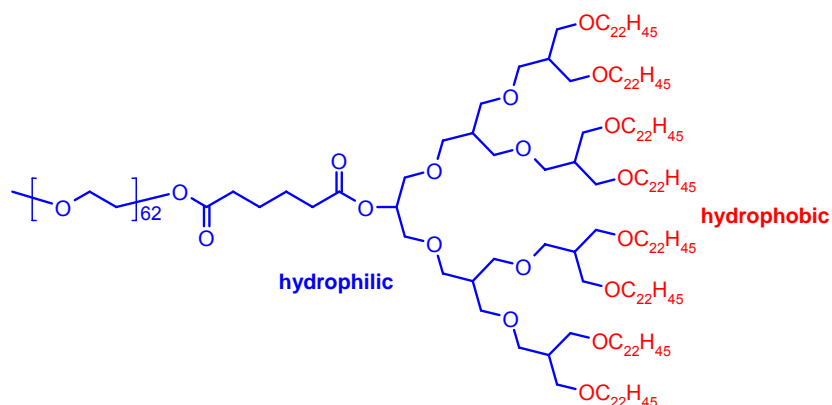


Fig. 1.15: Schematic structure of an amphiphilic dendrimer ^[169].

1.3.4 Supramolecular Dendrimers

Percec and coworkers have synthesised a wide library of poly(benzyl ether) dendrons which self-assemble into various cylindrical and pseudo-spherical dendrimers which arrange in liquid crystalline mesophases ^[170-173]. The morphology of the dendrons can be tuned varying the connectivity of the benzyl ether moiety in the dendrons, the substitution (number and position) of the peripheral groups and the functionalities in the focal point of the dendron. In this way, they have prepared flat tapered or conical dendrons that self-assemble into layers, cylinders or spheres which in turn organise into smectic, columnar and cubic phases. New symmetries, not yet described for organic compounds, have been found in this supramolecular dendrimers. Advantages of the supramolecular strategy are the simplicity of the building block, with a small demand on synthetic effort, time and materials and the consequently perfection of the dendrons. By means of this systematic combinatorial analysis, tailored morphologies and phases can be designed, cf. Fig. 1.16.

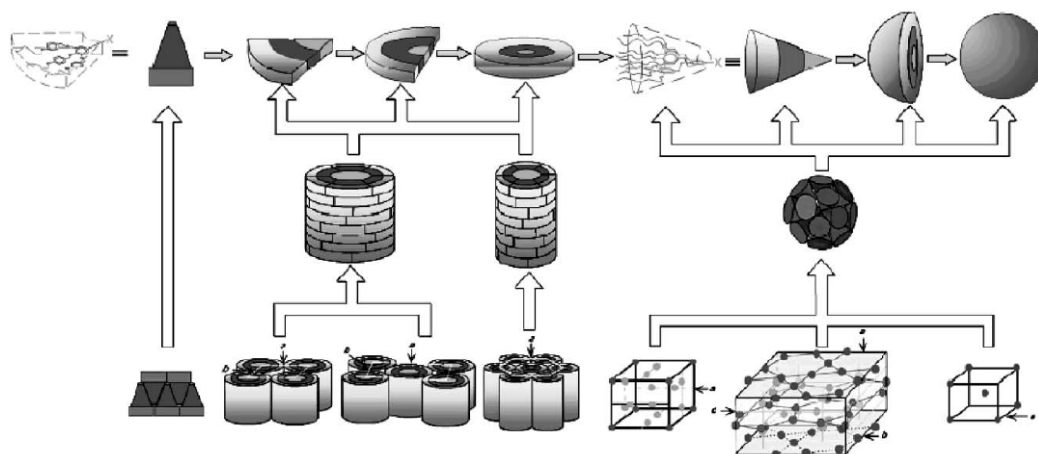


Fig. 1.16: Schematic representation of the self-assembly of flat tapered and conical dendrons into different supramolecular dendrimers and their organisation in different mesophases. Figure taken from reference ^[173].

1.3.5 Metallodendromesogens

A few examples of metal containing liquid crystalline dendrimers, “metallodendromesogens”, have been reported in the literature. Organometallic ferrocene-based dendrimers with a poly(benzyl ester) skeleton exhibiting stable smectic phases have been described ^[174]. Often is the ferrocene moiety combined with a fullerene to obtain materials with potential electron transfer. Varied liquid crystalline metallodendrimers have been prepared from PEI and PPI dendrimers. They are commented separately in the next section.

1.3.6 Liquid Crystalline Nitrogen Containing Dendromesogens. PAMAM, PPI, and PEI Derivatives

Liquid crystalline dendrimers based on pre-formed nitrogen containing dendrimers as poly(amido amine), PAMAM, dendrimers, poly(propylene imine), PPI, and to less extent poly(ethylene imine), PEI have been widely reported. Their flexible hydrophilic skeleton and the versatility of their amine endgroups have evidenced to be useful scaffolds susceptible to be modified by different strategies in order to promote mesomorphism in dendritic structures.

The widespread approach is the functionalisation of the dendrimer periphery with anisometric mesogenic or pro-mesogenic units. The mesogenic units are either directly attached to the dendrimer end-groups or are connected via a flexible spacer (several methylene units). Most of these mesogenic peripheral units are terminated with one or more alkoxy chains, which together with the topology of the connection to dendrimer, play a central role in the modulation of the displayed mesophase type.

The end-on functionalisation of PPI or PAMAM dendrimers with calamitic mesogens, exhibiting none or one terminal alkoxy chain, results in formation of nematic or smectic phases ^[49, 175-177]. An elongated conformation of the dendrimer with an overall rod-like shape is assumed. The dendrimer is deformed in two directions from the core outwards with the mesogenic units parallel to each other distributed at the extremes of the rod and the dendrimer scaffold filling the space in between, cf. Fig. 1.17a. The spacing of the smectic layers are generation independent suggesting that the dendrimer skeleton must be distorted to a high degree and must be extremely flexible to accommodate in the available room. If the mesogenic units possess two alkoxy chains in the periphery, hexagonal columnar phases are displayed ^[101, 178, 179]. Two or three terminal chains demand obviously more space than one and a cylindrical geometry provides now the required space. The mesogenic units, segregated from the dendrimer framework and pointing radially outwards are located in the outer shell of the cylinder, Fig. 1.17b. Triphenylene

functionalized PPI dendrimers organise into columnar mesophases ^[180] as expected, known the tendency of the discotic triphenylene moiety to adopt this arrangement ^[40].

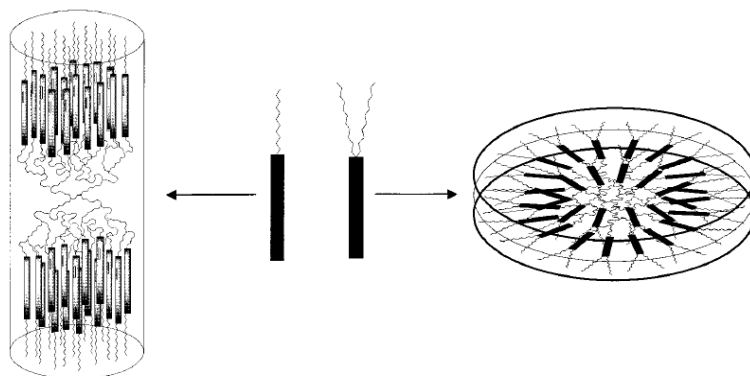


Fig. 1.17: Schematic representation of the cylindrical and discotic morphologies of end-on substituted PPI or PAMAM dendrimers with anisometric mesogenic or pro-mesogenic units wearing one or two alkoxy terminal chains. Figure from reference [101].

Rod-like mesogens laterally grafted (side-on) to dendrimers, via a flexible spacer, result give rise to nematic mesophases ^[179, 181, 182]. Combination of side-on and end-on topologies in the same dendrimer ^[183] result in the appearance of a tilted smectic C phase for compositions between the 100 % end-on (SmA) and the 100 % side-on (N). Further intriguing modifications as photo-addressable smectic PPI dendrimers ^[184] consisting of PPI scaffolds randomly substituted with azobenzene and cyanobiphenyl mesogens in variable ratios and dendrimeric nematic networks ^[185] have been also reported. No cubic mesophase has been achieved by attaching anisotropic mesogenic groups in the periphery of the PPI or PAMAM dendrimers, even by functionalisation with bulky mesogenic units ^[186].

The second approach to induce mesomorphism in these polar dendrimers is the covalent functionalisation of their peripheries with hydrophobic groups that are not mesogenic, but are nevertheless able to promote the organisation of the dendrimers in mesophases by micro-phase segregation processes. For a 1st generation poly(ethylene imine) where the terminal amine groups had been amidated with a 3,4-dialkoxy substituted benzoyl moiety, a columnar phase was achieved ^[136, 187]. The hexagonal columnar mesophase is formed by cylindrical dendritic cores that are surrounded by apolar shells of alkoxy chains. This strategy was successfully extended to poly(propylene imine) dendrimers of 1st to 5th generations ^[102, 188], cf. Fig. 1.18. The influence of the terminal chains at the benzoyl group was investigated and in addition to the 3,4- substituted, mono and tri-substituted benzoyl groups were attached to the dendrimer periphery. With increasing volume demand by the alkoxy chains, the mesophases evolve from smectic for the mono substituted benzoyl groups, via columnar hexagonal phases for the di and tri-

substituted terminal groups up into even cubic phases for high generations: monotropic cubic spherulitic phases for the 5th generation two chain derivatives, and enantiotropic cubic spherulitic phases for the 4th generation of the trisubstituted derivative. The mesomorphic behaviour of these dendrimers in different mixtures of solvents was investigated and columnar lyotropic mesophases were observed ^[189].

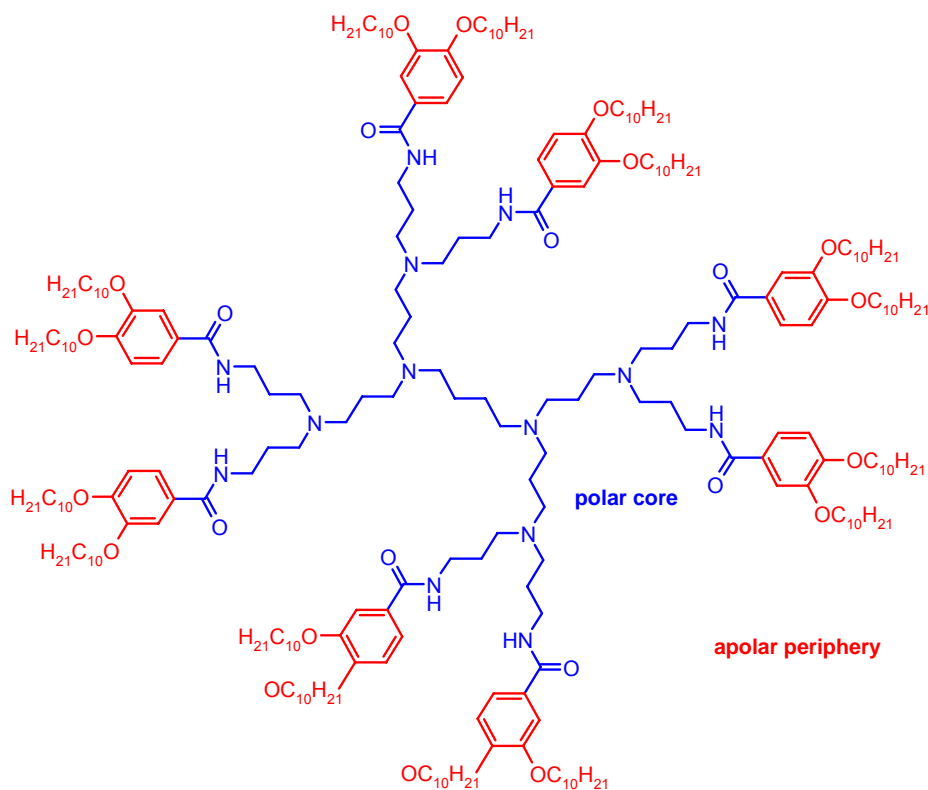


Fig. 1.18: 2nd generation PPI dendrimer substituted with non-mesogenic 3,4-didecyloxybenzoyl units ^[102].

A variation of this second approach is the “ionic functionalisation” of the periphery of the dendrimers, i.e. the supramolecular self-assembly of the dendrimers with different organic acids, forming ionic salts. Ionic amphiphiles, built up of dendrimers protonated at their terminal primary amine groups together with carboxylates of diverse fatty acids result in smectic phase formation for every PAMAM generation and smectic and columnar phases if the primary ammonium dendrimer is PPI. The columnar phases, tetragonal or hexagonal depending on the fatty acid, occur for 5th generation dendrimers ^[190]. The fluorinated homologue series have been also reported and exhibit -as the non-fluorinated- smectic and columnar phases, being these last ones broader as expected by a more pronounced micro-segregation due to the lipophobic fluorinated chains ^[191]. If the organic acids are benzoic acids ^[192] substituted with one, two or three alkoxy chains, ionic analogues of the covalent derivatives ^[102, 188] are described, cf. Fig. 1.19. One-chain ionic derivatives display as the covalent homologous smectic phases although with smaller lattice parameters than these last ones. Likewise, three-chain ionic deriva-

tives organise, as the covalent ones, into columnar rectangular and hexagonal phases with comparable lattice parameters. Two-chain ionic derivatives, on the contrary exhibit different behaviour as their covalent analogues. Ionic dendrimers display smectic phases for all generations in contrast to the covalent ones which arrange in hexagonal columnar phases. Interestingly the ionic series exhibit much broader mesophases than the covalent ones, on the one hand the crystalline phase is destabilized and on the other hand the clearing point increases.

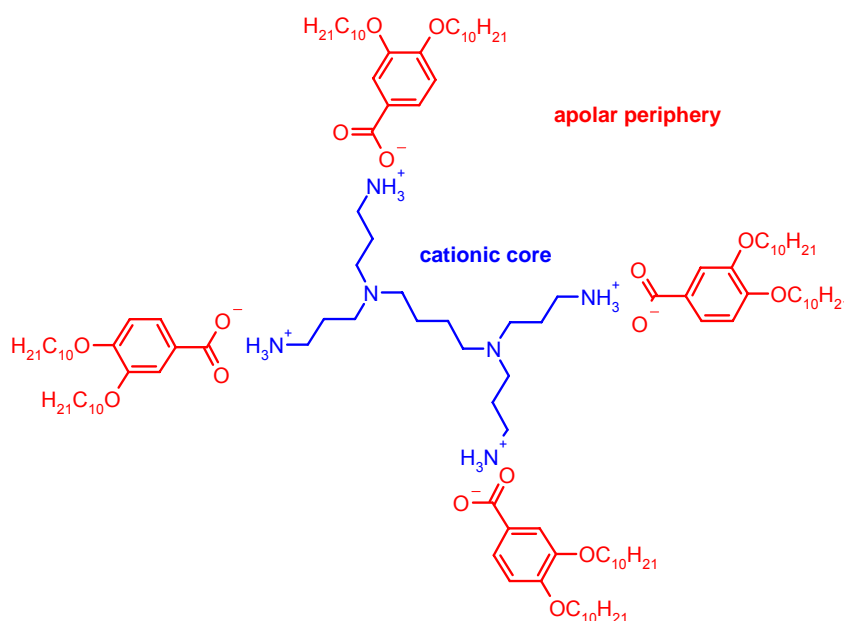


Fig. 1.19: Schematic representation of a 1st generation, ionic PPI dendrimer with disubstituted benzoic acid ^[192].

The effect of the ionic forces on the stabilisation of mesophases of polyamines have been previously studied in the zero and 1st generation of poly(ethylene imine) dendrimers ^[136]. The poly(ethylene imine) dendrimers, covalently functionalised with 3,4-didecyloxybenzoyl groups, were protonated with hydrochloric acid. The so generated quaternary ammonium salts of the zero generation are liquid crystalline while the non-protonated derivatives do not exhibit any mesophase. For the 1st generation analogues both protonated and non-protonated dendrimers present mesomorphism, although the mesophase range is substantially broader in case of the protonated species. Similar results have been observed in dodecylurea poly(propylene imine) PPI protonated and non-protonated derivatives ^[193]. In conclusion ionic forces arise to be a valuable tool for the promotion and stabilisation of mesogenic behaviour.

1.3.7 Liquid Crystalline Metal Derivatives of PAMAM, PPI, and PEI Dendrimers

PPI and PEI dendrimers incorporating metal centres in their structure with liquid crystalline properties have also been described. The tertiary amine moieties of the PEI and PPI dendrimers offer the possibility to complexation of many transition metals. Thus 3,4-didecyloxybenzoyl terminated PEI dendrimers of the zero and first generation coordinate divalent cobalt, nickel, copper and tin ^[137], and the resulting complexes exhibit columnar and lamellar mesophases. These metal complexes are the first example of metallomesogens with dendrimeric ligands. Analogue chromium(III) coordinated PPI derivatives of 2nd to 5th generation, exhibit columnar mesophases (oblique or rectangular the 2nd one and hexagonal the rest) ^[188]. The mesophase range of the chromium complexes is broader than that of the pure ligand, i.e. the presence of metal stabilize the mesophase. With increasing generation the dendrimers are able to coordinate up to eight metal centres, a N₃-coordination around chromium is assumed. Chromium(III) cations are paramagnetic and the presence of several metal centres in a single dendrimer is interesting for the possible cooperative effect in the magnetic properties. PPI derivatives have been coordinated to iron(III) ^[194, 195], the resulting polynuclear complexes exhibit columnar mesophases, oblique symmetry for the 1st generation complex and hexagonal for 2nd to 5th ones. The iron complexes have been used as starting platform for the formation of dendrimer stabilised magnetic iron oxide nanoparticles ^[196]. The coordination of metal in all the examples illustrated above, the dendrimer itself coordinates metal centres through its internal tertiary amine groups. A further location for the complexation sites, are the mesogenic groups attached at the periphery of liquid crystalline dendrimers, if they provide the necessary donor groups. In this way, salicylaldehyde functionalised PPI dendrimers of 1st and 2nd generation coordinate copper(II) centres. The resulting metallodendrimers exhibit, as the ligands do, smectic mesophases ^[197].

2. OBJECTIVES

2 OBJECTIVES

2.1 MOTIVATION

Hybrid systems consisting of organic materials and metal centres have attracted considerable attention in the last years ^[198-200]. These systems are particularly interesting since they integrate features characteristic of metals such as optical, magnetic and electronic properties with those typical of organic compounds. The addition of further features like self-assembly in ordered fluid phases and the susceptibility of orientation under external fields, typical characteristics of liquid crystals, can be of special interest, because they give rise to supramolecular ordered systems with controlled physical properties. With this purpose a large number of metallomesogens have been synthesised^[56]. Control over the number and topology of the metal centres has become an important goal in the design of these systems. Dendrimers, with their well defined structure, can enable this control, acting as dendritic chelates for metal complexation. Metal complexes are moreover suitable templates for the preparation of conducting metal nanoparticles, semiconducting or magnetic materials by further chemical modification.

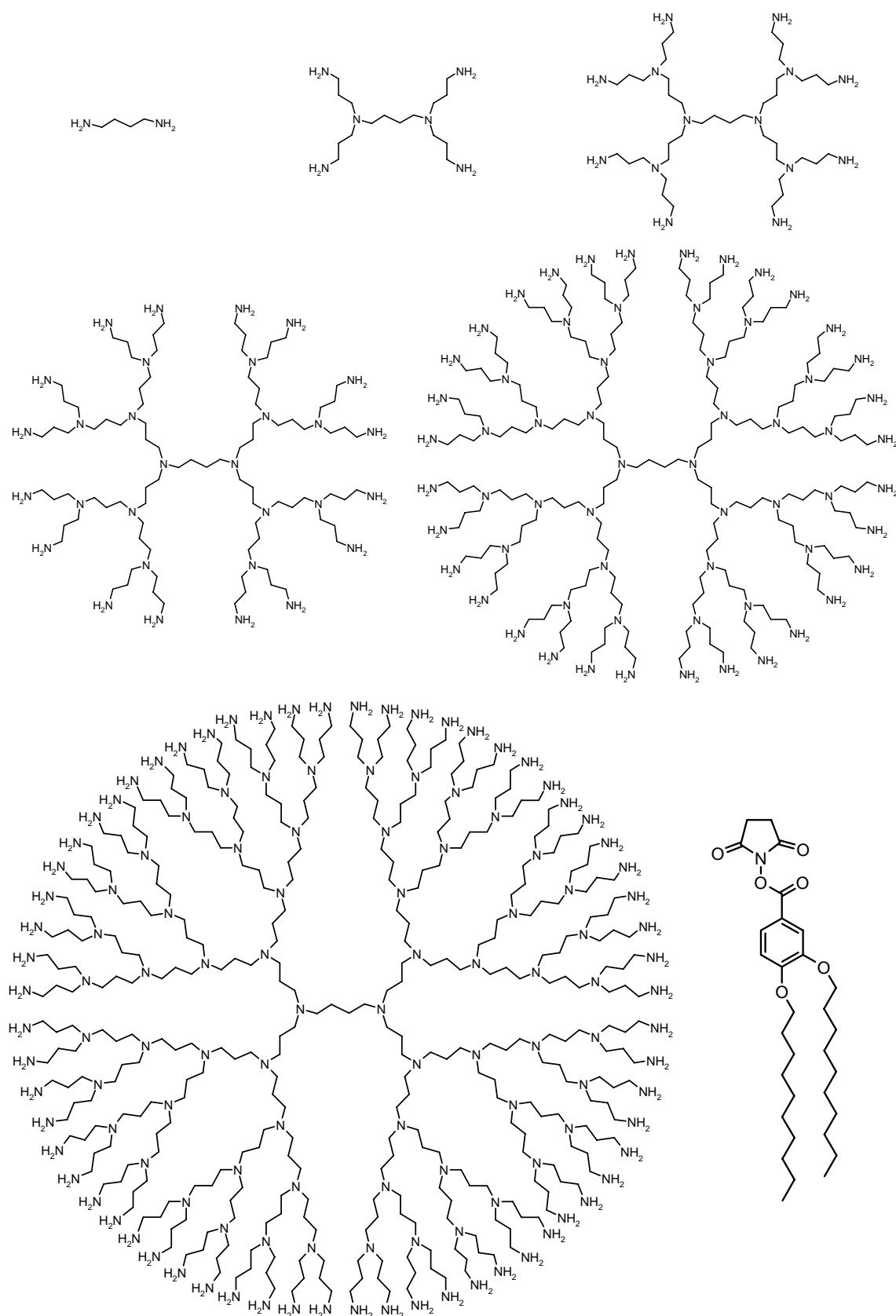
The first examples of metal containing liquid crystalline dendrimers were reported by Lattermann et al. ^[137]. First and second generation poly(ethylene imine) dendrimers complexes of divalent transition metals, Co, Ni, Cu and Zn exhibiting columnar mesophases were described. The nickel complex, presents a high spin state and is the first paramagnetic nickel complex described in the literature. The poly(ethylene imine) complexes were followed by a series of poly(propylene imine) dendrimeric chromium(III) complexes covering 1st to 5th generation ^[188]. The dendrimeric chromium complexes of generations 2nd to 5th are liquid crystalline and display columnar mesophases.

Liquid crystals containing paramagnetic metal ions are especially interesting because they can be aligned in external magnetic fields weaker than those required for diamagnetic liquid crystals. Therefore, they are interesting with respect to applications in the display and information storage technologies. Moreover cooperative magnetic properties have been described for polynuclear liquid crystalline metal complexes ^[201]. This principle could make possible the design of liquid crystalline organic magnets ^[200, 202].

With this motivation, the preparation of new liquid crystalline polynuclear dendrimeric complexes of paramagnetic metals was planned. For this purpose, the well-characterised, liquid crystalline 3,4-decyloxybenzoyl-functionalized poly(propylene imine) dendrimers as ligands and copper(II) as paramagnetic centres were chosen. Poly(propylene imine) dendrimers are amphiphilic dendrimers with a polar PPI core and apolar terminal groups, cf. Scheme 2.1. In the following, they will be abbreviated as **LG** where G stands for generation ($G = 1, 2, \dots, 5$). They show multiple donor centres for metal complexation: ($2^{G+1}-2$) tertiary amine groups (σ donor ligand) in the PPI scaffold and 2^{G+1} amide moieties (π donor ligand) in the interface between the polar core and apolar end groups. A clear advantage of the dendrimers with respect to other polymeric chelates is given by their nearly monodispersity and the clear definition of their ligand sites.

Copper(II) was chosen as metal centre, because it exhibits an electronic configuration $[\text{Ar}] 3d^9$ with one unpaired electron and is therefore paramagnetic ($S = 1/2$). Although other metal ions present more unpaired electrons or larger magnetic anisotropy ^[202, 203], copper was favoured, because it allows in principle a more simple EPR spectroscopic analysis. Copper is a border line hard acid, thus its coordination chemistry is dominated by nitrogen N and oxygen O donors, followed by chlorine and sulphur ^[204]. It covers a wide range of ligands: amine, nitrite groups, azides, cyanates and amides. Chelated groups are also common. For these reasons, it is a good candidate to be complexed by the PPI dendrimers. The vicinity of the copper centres inside a single dendrimer and the organization in mesophases is expected to contribute to a possible a spin-spin coupling leading to complexes with anti- or ferromagnetic properties.

Aim of this work is to answer basic questions concerning the structural features of the copper(II) complexes, focusing on the study of their thermal properties, especially the liquid crystalline orientation and the influence of the orientation on the magnetic properties. The findings are to be complemented with the structural information and magnetic properties provided with EPR spectroscopy ^[205, 206]. Thereby, clarification of the effect of controlled complexation of multiple metal centres in a liquid crystalline dendrimer on the magnetic properties is expected.



Scheme 2.1: Amino- terminated poly(propylene imine) dendrimers: from zero up to 5th generation and 3,4-decyloxybenzoylsuccinimide active ester for their-functionalisation. The resulting amidated ligands **L0-L5**, are used for copper(II) complexation.

2.2 WORKING PLAN

Synthesis of the ligands:

In a first step the PPI dendrimeric ligands from zero to 5th generation have to be prepared. Commercial amino-terminated PPI dendrimers (cf. Scheme 2.1) have to be acylated with decyloxy benzoyl groups, which can be synthesised following known procedures. The completeness of the acylation as well as further spectroscopic and thermal characterisation has to be performed according to the methods described in the literature ^[188].

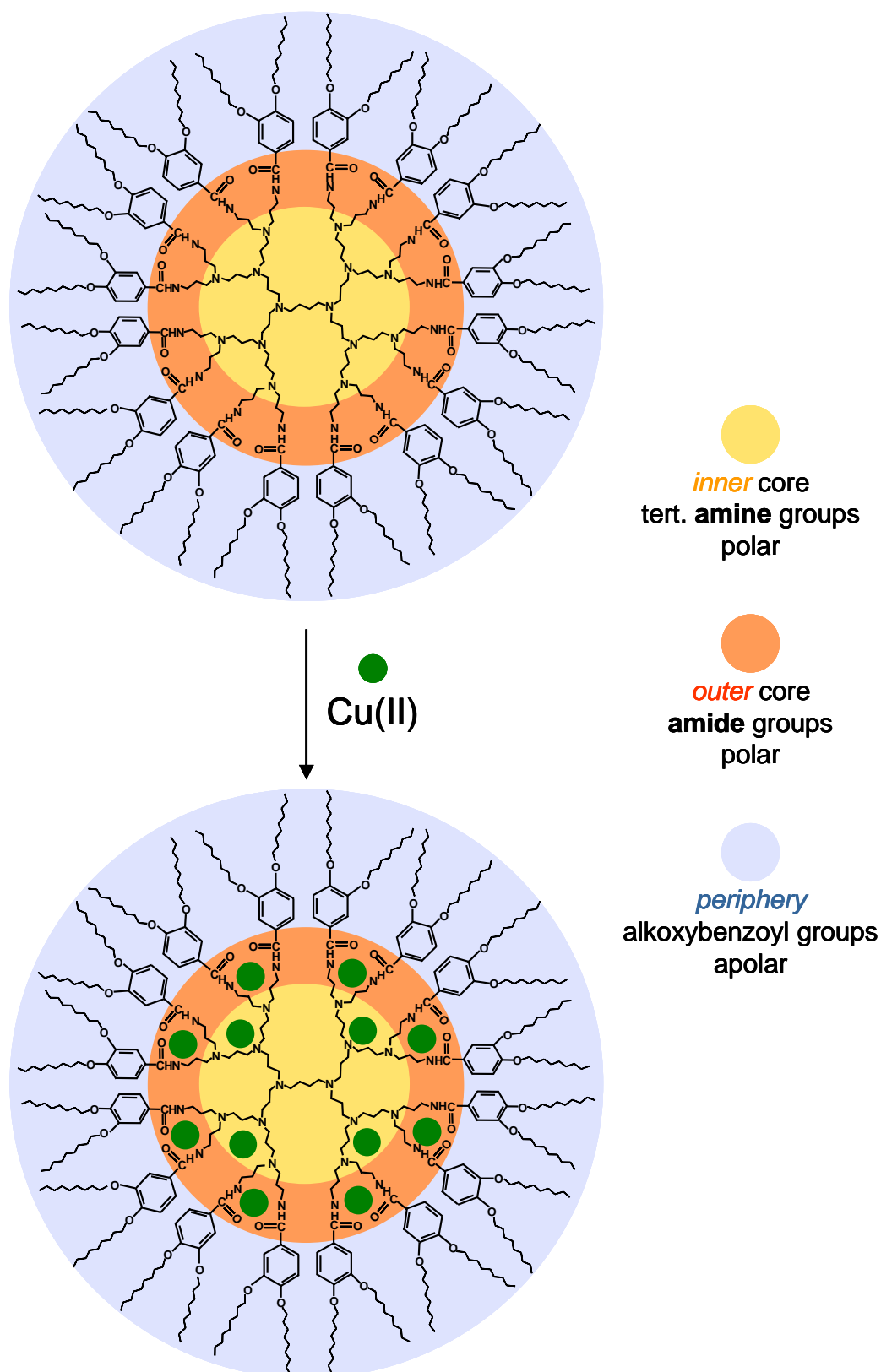
Complexation of copper(II):

These ligands are subsequently used for complexation of copper(II), cf. Scheme 2.2. In order to become insight in the influence of the copper loading on the complex properties, a series of complexes covering all range of copper loadings is necessary. This will be made exemplarily by means of the 2nd generation. Diverse strategies, such as playing with the media polarity and stoichiometry of the reaction conditions will be tested. Lower loaded complexes, with isolated copper centres are furthermore required for the investigation of the copper coordination sites by spectroscopic methods e.g. EPR.

In order to determine the maximal possible loading of copper(II) centres per dendrimer for all generations, the experimental optimisation of the copper complexation procedure and working up conditions is necessary. Therefore testing of different copper salts, reaction media and working up procedures is planned. The use of different copper salts furthermore allows to study the effect of the anion in the complex structure.

Characterisation:

The copper loading has to be determined by elemental analysis. The complex formation has to be investigated by e.g. MALDI-ToF MS spectrometry. Observation of the complexes by TEM should give information about the size of the complexes and also direct evidence of the complexation. The structure of the complex, i.e. the identification of the moieties coordinating the copper centres, amine and or amide, will be carried out by spectroscopic methods. FTIR, UV-Vis absorption and EPR spectroscopy, this last one in cooperation with the external partner Dr. N. Domracheva, Kazan Physical-Technical Institute, Russian Academy of Science, Russia. Unfortunately, no use can be made of NMR spectroscopy for structural determinations because of the paramagnetic nature of copper(II). The thermal behaviour of the complexes will be studied by thermal analysis, polarising microscopy and DSC. The identification of mesophases is to be carried out by X-ray diffractometry. The dependence of the size (generation) and copper loading on the mesomorphism will be analysed. On the basis of the obtained findings a model for the liquid crystalline dendrimeric copper(II) complexes will be proposed.



Scheme 2.2: Complexation of copper by the PPI dendrimers. In principle expected locations of copper(II): inner core (amine coordination) and outer part of the core (amide coordination).

3 LIQUID CRYSTALLINE, DENDRIMERIC COPPER(II) COMPLEXES

3.1 SYNTHESIS

3.1.1 Ligands

3,4-Decyloxybenzoyl-functionalized poly(propylene imine) dendrimers from the 1st to the 5th generation, were prepared from the homologous amino-terminated (4, 8, 16, 32 and 64 terminal groups; 1,4-diaminobutane core) commercial dendrimers and the self-synthesized *N*-hydroxysuccinimidoyl-activated ester of 3,4-decyloxybenzoic acid as described previously in the literature ^[102, 188]. On the basis of the ninhydrin-test, elemental analysis, ¹H-NMR, SEC, MALDI-ToF-MS and FTIR the substances correspond in all respects with the compounds described in Ref. [102]. The acylated dendrimers are referred to as **LG** where G stands for generation (G = 1, 2, ... 5).

3.1.2 Copper(II) Complexes. Series of Highest Copper Loading

The design of the synthesis and subsequent isolation of the dendrimeric copper(II) complexes was strongly affected by the solubility of the dendrimeric ligands. Due to their amphiphilic polar core/apolar shell structure, the ligands are only soluble in fairly polar media such as THF, chloroform, and methylene chloride, or aromatic solvents like benzene or toluene. The complexes have therefore to be prepared in a solvent in which both, dendrimeric ligand and copper salt, are soluble and must afterwards be isolated either by selective precipitation or by extraction. The solubility of the copper(II) complexes is expected to be similar to that of the ligands because of the large organic skeleton. Among the possible solvents and copper salts, two suitable combinations were found for the synthesis: copper nitrate trihydrate $\text{Cu}(\text{NO}_3)_2 \cdot 3\text{H}_2\text{O}$ or copper tetrafluoroborate hydrate $\text{Cu}(\text{BF}_4)_2 \cdot x\text{H}_2\text{O}$ (x ca. 4) and THF as solvent. The nitrate anion is a versatile σ -donor ligand, it can bind copper by either one ^[207, 208], two ^[209-211] or three ^[212, 213] oxygen atoms, acting as chelate ^[209, 211, 214] or bridge ^[210, 212, 213, 215, 216] and can be therefore present in the end product as co-ligand. Tetrafluoroborate is a non-coordinating or very weak-coordinating anion and usually does not play any other role than that of the counter ion in complexes ^[217-219]. A parallel synthesis with copper nitrate trihydrate in a binary mixture 1:1 v/v of γ -butyrolactone/chloroform was carried out to

explore the possibility of synthesis improvement, and to check an eventual participation of solvents in the coordination of copper.

The prepared complexes are abbreviated as “**CG.i(n)**”. **C** indicates a copper (II) complex, the generation of the dendrimeric ligand is given by the number **G** and **i** is a consecutive order number to identify complexes of the same generation. The loading of the complexes, i.e. the mean number of copper(II) ions per dendrimeric ligand, is denoted by **n**. A detailed description of the determination of **n** is given in section 3.2.

3.1.2.1 THF-Series

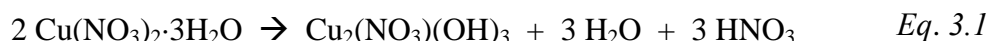
A stock solution of copper nitrate trihydrate in THF (1.13 M) was prepared for the complexation by all dendrimer generations. Analytical grade copper nitrate trihydrate yields a slightly turbid solution in dry THF. The fine, light blue precipitate was filtered off with a 200 nm Teflon filter. The resulting transparent dark blue solution, the “stock solution”, is kept under argon and remains clear over months. In order to achieve the highest copper loadings in the final product, different excesses of the copper salt per nitrogen atom in the dendrimer were tried at the beginning of the investigation, depending on the generation: 25 molar excess for the 0th and the 1st generation down to 10 for the 2nd to 5th generation. Later on, the 2nd generation synthesis was optimised and it turned out, that already an equimolar amount is enough to achieve the highest loading. Therefore, it is expected that a somewhat reduced copper salt excess would also lead to the maximal loadings for the remaining generations. The reactions were carried out at room temperature under argon atmosphere, except for the diaminobutane derivative (generation “zero”), which required heating up to 55°C to be dissolved. By addition of the ligand to the copper nitrate solution, the reaction mixture darkened or turned into green, indicating complexation. The reaction mixtures are slightly turbid, except for the 1st generation reaction, which shows strong turbidity with respect to higher generations. Once completed the reaction, the solvent was evaporated under reduced pressure and the copper complex was extracted from the residue with chloroform, in which the copper nitrate is insoluble. The precipitation of the complexes with a polar solvent such as methanol turned out to be inconvenient for isolation because, according to the results of elemental analysis, it washed out the copper coordinated to the dendrimer in the crude product. The complexes were freeze dried from benzene prior to characterisation. Light green powders were obtained. The detailed preparative procedure is described in the experimental part of this thesis, cf. 6.3.1.1.

Complexes **C0.1(0.2)**, **C1.4(1.5)**, **C2.3(6.0)**, **C3.1(12.0)**, **C4.1(24.2)** and **C5.1(45.9)** were prepared according to this procedure. 6.0, 12.0, 24.2 and 45.9 copper centres per dendrimeric ligand are the maximum copper loadings achieved for generations 2nd to 5th.

Discussion of the possible presence of inorganic impurities in the final products

Special attention was paid during the whole preparative procedure to exclude any possible inorganic impurity in the final product. Inorganic crystals would cause sharp reflection peaks in the wide angle region of the X-ray diffractograms of the complexes and could interfere in the interpretation of the mesophases. Thus, every solution in the working-up procedure was carefully filtered through a 200 nm Teflon filter. The repeated filtrations ensure the absence of particles larger than 200 nm in the end product.

As a blank test, a possible reaction of $\text{Cu}(\text{NO}_3)_2 \cdot 3\text{H}_2\text{O}$ in THF was performed in order to monitor the behaviour of copper nitrate trihydrate under the complexation conditions and to estimate up to which extent, some inorganic copper salt could have passed the filters during the working-up procedure together with the solvents. The inorganic residue of the blank reaction, a green powder, was x-rayed at rt. in WAXS ($5^\circ \leq 2\theta \leq 65^\circ$). The pattern corresponds to the diffraction peaks of a mixture of copper nitrate hemipentahydrate, $\text{Cu}(\text{NO}_3)_2 \cdot 2.5\text{H}_2\text{O}$ ^[220] (similar to the starting copper salt $\text{Cu}(\text{NO}_3)_2 \cdot 3\text{H}_2\text{O}$) and basic copper nitrate $\text{Cu}_2(\text{NO}_3)(\text{OH})_3$ ^[221, 222] cf. section 3.9.2.2., Fig. 3.56. The basic copper nitrate arises from the decomposition of the copper nitrate as indicated in Eq. 3.1.



This transformation occurs as effect of multiple factors such as temperature, vacuum, or by the presence of traces of for instance copper hydroxide in copper nitrate solutions ^[223, 224]. The preparative procedure rules out the possibility of a temperature-induced $\text{Cu}_2(\text{NO}_3)(\text{OH})_3$ formation, because the diffractograms of pure $\text{Cu}(\text{NO}_3)_2 \cdot 3\text{H}_2\text{O}$ heated up to 100°C and held at 65°C for eight hours does not exhibit any indication of decomposition. However, it was worked under reduced pressure down to 0.02 mbar, and traces of copper hydroxide may be present in the nitrate solution; both factors can have caused the transformation described in Eq. 3.1.

Consequently, the partial conversion of $\text{Cu}(\text{NO}_3)_2 \cdot 3\text{H}_2\text{O}$ into $\text{Cu}_2(\text{NO}_3)(\text{OH})_3$ and the formation of nitric acid according to Eq. 3.1 have to be considered. Quantitative analysis of the blank reaction shows however, that the fraction of the inorganic insoluble residue which is able to pass the filters, as the dendrimeric complex does, is extremely small: after the first working-up step, the extraction of the complex with CHCl_3 and filtration through 200 nm filters, maximal 1 wt. % inorganic residue of the hypothetical end product pass to the chloroform solution. Testing gravimetrically the solubility of the 1 wt. % inorganic residue in benzene, it turns out that finally at most 0.05 wt% of the end product of the complex synthesis is of inorganic nature. Under the real reaction conditions, with more components in solution, the solubility and the inorganic fraction

should be even lower. Consequently, free inorganic contaminations as copper nitrate or basic copper nitrate are very unlikely to be present in a large extent together with the dendrimeric complex. This finding is supported by the elemental analysis results. Nitric acid however passes the filter and is incorporated into the complexes as indicated by elementary analysis cf. 3.2, Table 3.2 and FTIR, cf. 3.5.3.3, this leads to interesting features in the mesogenic behaviour of the dendrimeric copper(II)-complexes, cf. 3.8, 3.9.

3.1.2.2 γ -Butyrolactone/Chloroform Series

The complexation in γ -butyrolactone/chloroform was carried out in analogy to the synthesis in THF, using an 11-12 molar fold excess of copper salt per nitrogen atom in the ligand for generations 2 to 5 and a 25 fold for the 1st one. The solution of the $\text{Cu}(\text{NO}_3)_2 \cdot 3\text{H}_2\text{O}$ in the 1:1 γ -butyrolactone/ CHCl_3 mixture is turbid and was filtered as in the THF series to prepare a clear stock solution. The concentration of the stock solution $9 \cdot 10^{-2}$ M is ten times more diluted than that in THF due to the reduced solubility of the copper nitrate in γ -butyrolactone/ CHCl_3 . The general working-up procedure was in principle similar to that of the THF series, i.e. extraction of the complex with CHCl_3 after having brought the reaction mixture to dryness, whereas the evaporation of the γ -butyrolactone required high vacuum ($3 \cdot 10^{-2}$ mbar) under mild heating (35°C). Repeated lyophilisation was required in this series to remove all traces of γ -butyrolactone from the final product, contrary to the THF series where a single run was enough to dry the samples. Careful filtration of every solution through 200 nm filter was performed.

Complexes **C2.2(6.3)**, **C3.2(7.9)**, **C4.2(7.4)** and **C5.2(44.9)** were prepared according to this procedure. The general preparative conditions lead to the highest loadings of the γ -butyrolactone/ CHCl_3 series. The 1st generation complex was prepared by a particular working up procedure (cf. 3.1.3.2).

3.1.2.3 Dependence of the Highest Loading on the Generation

The general procedure of complexation, where the dendrimeric complex is extracted from the reaction residue into chloroform yields the highest copper loadings in each series THF and γ -butyrolactone/ CHCl_3 for generations 2 to 5. In the THF series, the 1st generation complex obtained in this way, does not exhibit the maximum loading achieved in this generation, but is the highest loaded complex of this generation that presents the general coordination characteristics of the dendrimeric copper(II) complexes and is therefore brought here for comparison. The maximum loading of the 1st generation ($n = 1.9$) corresponds to complexes with a particular behaviour and was reached by an alternative working-up procedure explained later on, see 3.1.3.2, Scheme 3.1. The Cu(II) loadings reached for each generations in both series are visualized in Fig. 3.1.

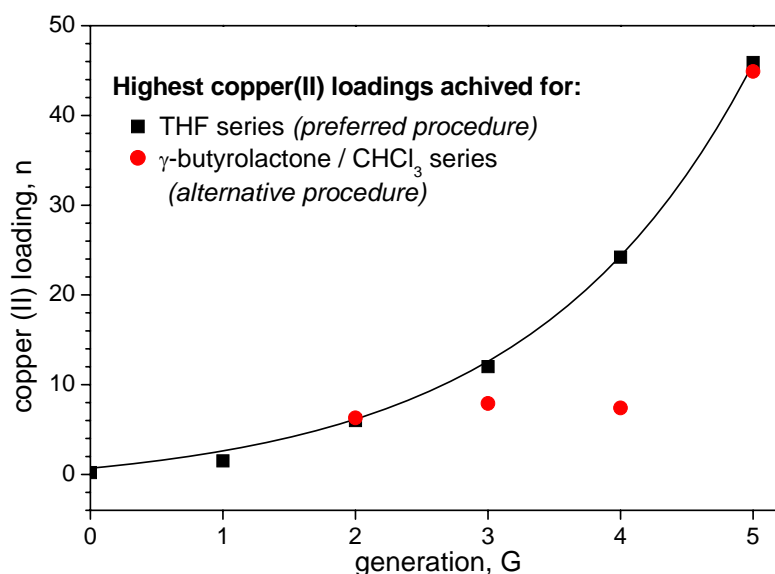


Fig. 3.1: Highest copper(II) loadings n (from elemental analysis) achieved for each generation G in both the THF and γ -butyrolactone/ CHCl_3 series. ■: complexes and — : exponential fit of the THF series, C0.1(0.2), C1.4(1.5), C2.3(6.0), C3.1(12.0), C4.1(24.2) and C5.1(45.9), ●: complexes of the γ -butyrolactone/ CHCl_3 series, C2.2(6.3), C3.2(7.9), C4.2(7.4) and C5.2(44.9).

The maximal loadings reached in the THF series exhibit an exponential increase of the copper content with the generation as also described for copper(II) complexes of PAMAM dendrimers ^[225]. They lay above the maxima of those in γ -butyrolactone/chloroform. The difficulty to remove quantitatively the γ -butyrolactone leads to complexes with virtually lower copper content for the highest generations. The higher copper loadings together with the easier preparative procedure, reveals THF as the most convenient solvent for the preparation of copper complexes of the poly(propylene imine) dendrimers.

3.1.3 Copper (II) Complexes. Series of Lower Copper Loading. Specific Preparative Procedures

3.1.3.1 2nd Generation Complexes

A set of 2nd generation copper complexes with different copper contents was synthesised to study the effect of the copper loading on the complex properties for a given generation. The 2nd generation dendrimeric ligand was chosen for this purpose, because it exhibits all the features of the dendrimeric structure and is small enough to provide insight in the copper coordination and further complex properties. A second objective was to prepare copper complexes with isolated copper centres that facilitate the EPR investigations of the direct environment of the copper in the complexes. Two strategies were developed in order to reduce the copper content:

- i. variations in the stoichiometry of the reaction,
- ii. washing out of copper from end or crude products by treatment with solvents of different polarities.

A broad set of 2nd generation complexes covering the loading range from 0.3 to 6.3 copper centres were prepared.

Variations in the stoichiometry of the reaction

A series of complexation reactions were carried out according the general preparative procedure for complexation in THF varying the Cu(NO₃)₂·3H₂O to ligand ratio. The differences in the stoichiometry are expected to lead to different copper loadings in the final products. The introduced copper salt ratios (*m*) are referred to *one nitrogen atom* per dendrimer, because nitrogen atoms, both in amide (8 groups) and amine (6 groups), are the available donors in the ligand. For the 2nd generation ligand, with 14 (8 + 6) nitrogen atoms, the ratio *m* is given by:

$$\frac{m_{Cu}}{14 \cdot m_{L2}} = m \quad \text{Eq. 3.2}$$

where m_{Cu} , and m_{L2} are respectively the number of moles of Cu(NO₃)₂·3H₂O and 2nd generation ligand L2 used for complexation.

The determined (by elemental analysis, cf. 3.2) number of Cu ions in the complex, the copper loading “*n*” (***n*:C2.i(*n*)**), is compared to the number “*m*” of Cu ions (*per nitrogen atom* in dendrimeric ligand) introduced in the reaction mixture (***14*:*m*:L2**) in Fig. 3.2. Complexation with “under - stoichiometric” amounts of copper salt ($m < 1$) yields complexes with low copper loadings. Stoichiometric ^[i] conditions ($m = 1$) lead to the maximum loading achieved for this generation, $n = 6$ in the THF series. A higher surplus of copper nitrate ($m > 1$) does not result in higher loadings, but in a gradual decrease of the copper loading.

^[i] It will be referred to stoichiometric amounts with respect to a nitrogen atom in a dendrimer even if it is not possible to establish a priori which type of nitrogen atom in the dendrimer and with which denticity the dendrimer is involved in the coordination of copper.

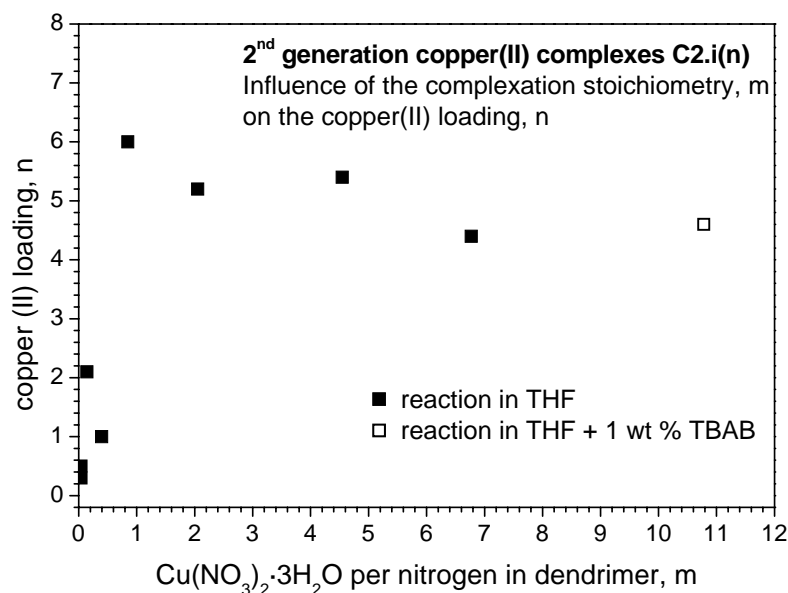


Fig. 3.2: Copper(II) loadings, *n*, i.e. number of copper(II) per dendrimeric complex (from elemental analysis) vs. number of copper(II) ions per nitrogen *m*, present in the complexation reaction. ■: reactions in THF, □: reaction in THF with 1 wt. % TBAB. Plotted complexes: **C2.17(0.3)**, **C2.19(0.5)**, **C2.16(1.0)**, **C2.12(2.1)**, **C2.8(4.4)**, **C2.7(4.6)**, **C2.6(5.2)**, **C2.5(5.4)** and **C2.3(6.0)**.

Several authors^[135, 226] have also reported that a high excess of copper salt in the complexation solutions, i.e. high ionic strength, results in incomplete coordination of the metal to poly(propylene imine) dendrimers. In Fig. 3.2, the decrease in the copper loading *n* with surplus of copper nitrate over the stoichiometric value *m* can be explained in terms of the variation of the conformation of the dendrimer sensible to variations in the ionic strength and polarity^[98, 227]. In consequence, the passage possibilities of copper through the alkyl chains in the periphery to the coordinating atoms in the dendrimer scaffold are affected. At higher concentrations of ions in the solution, the polarity increases and results in the collapse of the apolar alkyl chains around the core, which may then hinder the access of copper to the nitrogen donor atoms. Similar results have been obtained by size exclusion chromatography, SEC, analysis^[188] of the dendrimeric ligands in THF with varying fractions of tetrabutylammonium bromide, TBAB, revealing the selective solvation of the PPI core and the alkoxy chains in the periphery of the dendrimer depending on the polarity of the eluant. A maximum in the hydrodynamic volume of the dendrimeric ligands was observed at 1wt. % of TBAB according to the abovementioned SEC studies. In this state, both polar and apolar parts are expected to be acceptably solvated, i.e. the donor groups of PPI would be accessible to metal salts and would represent a good starting point for complexation of copper. However, complexation under that condition did not yield the highest loadings (cf. open symbol in Fig. 3.2) since obviously at the same time a large excess of copper salt was

used, which has the same effect on the polarity of the solution as TBAB at higher weight percentages wt. %.

Complexes **C2.5(5.4)**, **C2.6(5.2)**, **C2.7(4.6)**, **C2.8(4.4)**, **C2.12(2.1)**, **C2.16(1.0)**, **C2.17(0.3)** and **C2.19(0.5)** were prepared according to this procedure. Complexes **C2.11(2.6)**, **C2.13(2.0)** and **C2.15(1.3)** were synthesised following the general procedure for complexation in γ -butyrolactone/chloroform, using different excesses of copper than that which leads to the maximum, (“over-stoichiometric” for **C2.11(2.6)** and **C2.13(2.0)**, and “under-stoichiometric” surplus for **C2.15(1.3)**) the working-up procedure was however different, and will be explained in the next section. The modifications of the working-up procedure determine the final copper loading.

Treatment of the complex with different solvents

The treatment of crude or end products with different solvents leads likewise to copper complexes with varied copper loadings. Non-coordinating solvents as chloroform do not interfere in the complexation whereas solvents exhibiting coordinating abilities compete with the donor groups of the dendrimeric ligand (amide and amine groups) in the binding of copper. Therefore complexes treated or extracted with coordinating solvents exhibit lower copper loadings than those achieved by the general working-up procedure with chloroform. The more polar the solvent used, the stronger the “washing-out” effect on the complex. Likewise, repeated washing-out leads to a sequential loss of copper. In Table 3.1 are collected the lower loaded complexes prepared by this method, the solvents used, their polarity index *PI*, and the achieved copper content. The loading of the starting complexes, denoted n_o , is also given if known.

Table 3.1: *2nd generation copper(II) complexes, complexation behaviour in dependence on the solvent polarity*

THF			Solvent / PI	γ -butyrolactone / CHCl ₃		
C2.i(n)	n_o	n		C2.i(n)	n_o	n
C2.4(5.4)	7.3	5.4	ethyl acetate / 4.4	C2.23(4.1) ^c	6.3	4.1
C2.9(3.5)	7.3	3.5	acetone / 5.1	C2.11(2.6)	- ^{a, e}	2.6
				C2.13(2.0)	6.3	2.0 ^d
				C2.15(1.3)	- ^{a, e}	1.3
C2.10(2.7)	- ^a	2.7	γ -butyrolactone ^b			
C2.18(0.9)	- ^a	0.9	acetonitrile / 5.8			
C2.20(0.3)	- ^a	0.3	water / 10.2			

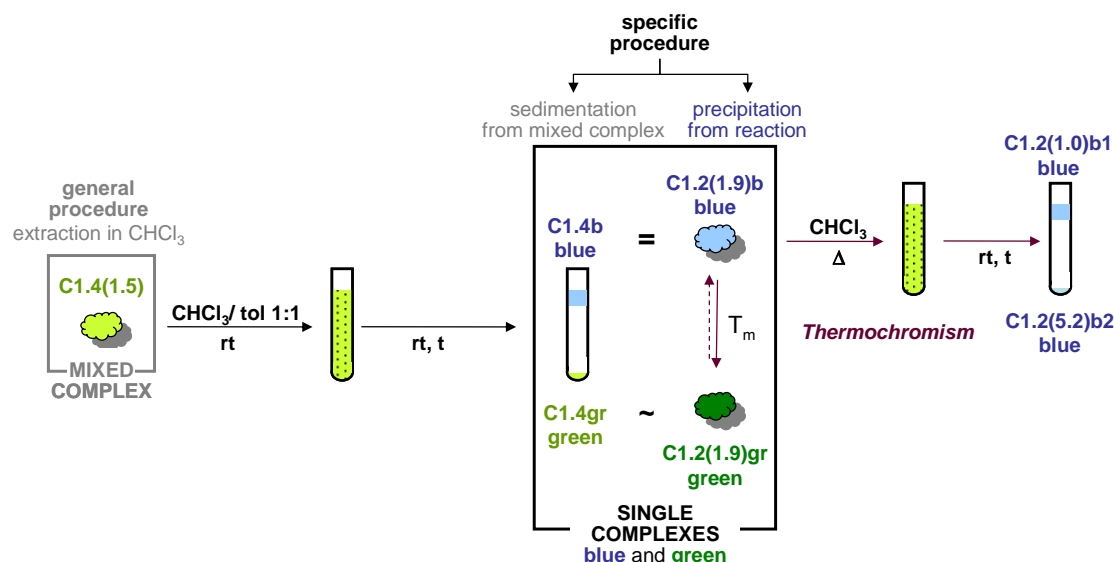
C2.i(n): 2nd generation copper complex *i*: consecutive identification index, *n*: copper(II) loading n_o : copper loading of the complex before washing, *n*: copper loading of the complex after washing, *PI*: polarity index of the solvent, a: the crude of the reaction was directly worked-up therefore no loading could be determined, b: no polarity index available, c: **C2.23(4.1)** prepared to test the washing-out abilities of ethyl acetate; no further characterisation except elemental analysis was carried out, d: repeated washing, e: outgoing complexes prepared under non-stoichiometric conditions. i.e. loadings under the maximum.

Compared to those prepared by varying the stoichiometry, the characterisation of the 2nd generation complexes prepared in this way will show that, for a similar copper loading, no essential differences are observed in the properties (copper coordination, optical, vibrational, thermal etc cf. 3.5 - 3.9) of the resulting complexes. That means, the solvents are not significantly incorporated as co-ligands in the dendrimeric copper complexes.

3.1.3.2 1st Generation Complexes

The general working up for complexation in THF under general conditions leads for the 1st generation to a green powder with a copper loading of 1.5, complex **C1.4(1.5)** as described before. Complex **C1.4(1.5)** dissolved in a 1:1 mixture of toluene and chloroform ($C = 5 \text{ mg}\cdot\text{ml}^{-1}$) separates after some days into a light blue suspension, **C1.4b**, on the top and a green precipitate **C1.4gr**, at the bottom of the test tube, cf. Scheme 3.1. Elemental analysis and mass spectrometry revealed the presence of copper and the dendritic nature of both complexes. Electron paramagnetic resonance spectroscopy, EPR, identified different environments around copper as could be expected from the different observed colours cf. 3.7.2.4. Therefore **C1.4(1.5)** is a mixture of two types of copper coordinations. In the following, the usual notation for complexes **CG.i(n)**, is maintained for the “mixed” complexes and for those exhibiting only one coordination type, the notation is followed by the characters **b** or **gr**, referred to the observed blue or green colours.

Considering this singular behaviour, a specific working-up procedure was developed for this generation. Instead of extracting the complex from the reaction residue with CHCl_3 , the turbidity in the THF solution is allowed to deposit at low temperature. A light blue powder, complex **C1.2(1.9)b**, can be isolated by filtration. Complex **C1.2(1.9)b**, exhibiting in average 1.9 copper centres per dendrimer, presents the maximum copper loading achieved for this generation. The blue powder **C1.2(1.9)b** is insoluble in all common solvents at room temperature but dissolves in warm chloroform turning the solution thereby into green. After a couple of days at room temperature, the green colour fades away, a clear colourless solution and a blue suspension on the top together with slight blue precipitate at the bottom appears, indicating the reversibility of the colour change. Likewise, the complex **C1.2(1.9)b** heated over its melting point at 127°C turns into an intense green colour, leading to complex **C1.2(1.9)gr**. The colour change seems to be reversible in the bulk only over a large time scale. EPR analysis indicates that the ligand environment of copper in **C1.2(1.9)b** is the same as in the blue suspension **C1.4b**. Likewise the complex **C1.2(1.9)gr** is very close to the green precipitate **C1.4gr**, cf. 3.7.2.4. Thus, the specific working up procedure for the 1st generation complexes, allow the isolation of this two types of complexes.



Scheme 3.1: Overview of the 1st generation complexes and relationships between the blue and green species depending on the working-up. On the left (general working-up): mixed complex **C1.4(1.5)** and its separation in solution in the blue and green single complexes **C1.4b** and **C1.4gr**. On the right (specific working-up): blue complex **C1.2(1.9)b** and its reversible thermal conversion of into the green one **C1.2(1.9)gr** neat (slow) and in solution. rt: room temperature, t: time, Δ: heating.

The coexistence of two different coordination types is also expected for the higher generations; in order to check this, similar separation experiments have been carried out with 2nd and 5th generation complexes. The experiments did not lead to a successful separation of both types of complex. The higher the generation, the larger is the number of donor atoms in the dendrimer, allowing a larger number of copper centres per dendrimer. Presumably, this causes the coexistence of both coordinations; inside a single dendrimer, overall the sample. Then all possible statistical combinations of the two coordinations will be present. The intramolecular mixture of “blue” and “green” coordination sites makes the separation of different species impossible.

The 1st generation complex of the γ -butyrolactone/ CHCl_3 series was prepared in analogy to **C2.1(1.9)b** and yields a light blue precipitate with a copper content of 1.0, complex **C1.7(1.0)b**. It exhibits the same behaviour as **C1.2(1.9)b**.

In addition to the complexes described above, a further complex with reduced copper content, complex **C1.5(1.0)**, was prepared for EPR analysis. The loading was achieved by washing out the complex **C1.4(1.5)** with acetone, as described for the second generation.

The similarities of the blue complexes **C1.4b**, **C1.2(1.9)b** and **C1.7(1.0)b**, and the green complexes **C1.4gr** and **C1.2(1.9)gr** are discussed on the basis of EPR spectroscopy, cf. 3.7. The change of the optical properties with the temperature (thermochromism) and its

dependence with the mesomorphic behaviour of the 1st generation copper (II) complexes is studied, in bulk as well as in solution, in the section devoted to thermal properties, in the last part of this chapter, cf. 3.8.2.3.

3.1.4 Preparation of a Copper Complex from Copper Tetrafluoroborate

2nd generation copper(II) complexes were prepared from copper(II) tetrafluoroborate hydrate, $\text{Cu}(\text{BF}_4)_2 \cdot x\text{H}_2\text{O}$ with $x \sim 4$. Tetrafluoroborate is a non-coordinating^[218, 228, 229] or weakly coordinating anion^[218, 219, 230-232]. The symmetrical distribution of charge of the tetrafluoroborate (tetrahedral geometry) and the electronegativity of the fluorine atoms connected to boron are responsible for the low basicity of tetrafluoroborate^[217]. As a consequence, its tendency to act as ligand for metals is small. This makes it interesting for comparison with the complexes of the coordinating nitrate, in order to study the influence of the anion in the complex properties.

The synthesis was carried out in analogy to the general procedure for complexation in THF using those stoichiometric conditions, which led to the maximum copper loading in the synthesis with copper(II) nitrate ($m = 1$, i.e. one mol of copper per nitrogen atom in the dendrimeric ligand, cf. 3.1.2.1). The complex was extracted from the light green reaction residue with benzene; the solution was filtrated and lyophilised. The complex was obtained as a light brown powder. If the benzenic solution is allowed to stay, a slight precipitate arises within few minutes; even solutions of fresh freeze-dried complexes develop turbidity very quickly. These tiny differences in the working-up times cause different copper contents in the final product. It makes difficult to define a reproducible and reliable synthetic procedure.

The change in the colour (green to brown) of the complex suggests furthermore an -at least partial- reduction of copper(II) to copper(I) as described in the literature^[228, 233]. The continuous appearance of turbidity could be connected to the instability of copper(I) which tends to disproportionate into Cu(II) and Cu(0)^[234]. It is further supported by the observed darkening of the tetrafluoroborate complexes, once isolated, in the course of time. Copper(I) is diamagnetic and is therefore not interesting for the preparation of materials with magnetic properties. The tetrafluoroborate synthesis was then given up as a standard procedure because of the lack of reproducibility and specially because of the possible reduction of copper(II) to copper(I).

The two 2nd generation complexes prepared with tetrafluoroborate, complexes **C2.21(4.0)** and **C2.22(2.9)** can however still give insight into the role of the anion in the complexation by comparison with the nitrate complexes. Therefore, they were further investigated.

3.1.5 Conclusions

Liquid crystalline polynuclear copper(II) complexes of 3,4-decyloxybenzoyl-function-alized poly(propylene imine) dendrimers from the 1st to the 5th generation have been prepared through coordination of copper(II) by the corresponding liquid crystalline dendritic ligands. On varying either the stoichiometry of the reaction or the working-up procedure, a wide range of copper loadings have been achieved. The 2nd generation was chosen to investigate these possibilities. For the complexation, the copper has been used as its nitrate trihydrate $\text{Cu}(\text{NO}_3)_2 \cdot 3\text{H}_2\text{O}$. Since the nitrate itself can coordinate copper, a further copper complex from a non-coordinating anion, the tetrafluoroborate, $\text{Cu}(\text{BF}_4)_2 \cdot 4\text{H}_2\text{O}$, has been prepared to study the influence of the anion on the complex properties. Nevertheless, the lack of reproducibility of the synthesis with the tetrafluoroborate salt and a possible reduction of copper(II) to copper(I) under the reaction conditions advises against its use for the preparation of the copper complexes. Two series of syntheses in different reaction media, namely in THF and in a binary mixture of γ -butyrolactone and chloroform, has been carried out.

3.2 MOLECULAR COMPOSITION: ELEMENTAL ANALYSIS

The copper content per dendrimer, i.e. copper loading n , and the molecular formula of the dendrimeric copper complexes were calculated from the carbon, hydrogen, nitrogen and copper contents in weight per cent, wt%, determined by elemental analysis in external laboratories. The oxygen content was not measured but calculated as the difference between 100% and the measured components.

The copper loading was calculated in reference to the number of carbon atoms in the complex (n_C). n_C is expected to be the same as in the pure dendrimeric ligand, since no further carbon-containing ligands are likely to be involved in the complexation of copper according to the preparation procedure. Nitrogen can not be taken as reliable reference, because nitrate anion of the starting copper salt can participate in the complexation both as ligand and/or as counter ion. The molecular weight of the complex $M_{complex}$ is then calculated from the experimental mass fraction of carbon $wt_C\%$:

$$wt_C\% = \frac{n_C \cdot M_C}{M_{complex}} \cdot 100 \rightarrow M_{complex} = \frac{n_C \cdot M_C}{wt_C\%} \cdot 100 \quad Eq. 3.3$$

where n_C is the number of carbon atoms in the dendrimeric ligand and M_C the carbon molar mass. The product:

$$f = \frac{n_C \cdot M_C}{wt_C\%} \quad Eq. 3.4$$

is defined as factor f and corresponds formally to 1/100 of the molar mass of the complex. Therefore the number of copper atoms per dendrimeric ligand, n , is calculated according to:

$$wt_{Cu}\% = \frac{n \cdot M_{Cu}}{f \cdot 100} \cdot 100 \rightarrow n = \frac{wt_{Cu}\%}{M_{Cu}} \cdot f \quad Eq. 3.5$$

where $wt_{Cu}\%$ stands for the mass fraction of copper, M_{Cu} represents its molar mass. For the calculations, the real number of carbon atoms in each dendrimeric ligand and not the number of atoms in a perfect-built dendrimer is considered. The commercial $-NH_2$ terminated poly(propylene imine) dendrimers, exhibit, with increasing generation, a certain number of defect sites, lacking e.g. one or more arms (propylenamine units) ^[109, 235]. Consequently the number of carbon atoms in the used ligand will be less than in the ideal ligand. A realistic number of carbons is determined to a first approximation from

the experimental carbon weight percents of the ligands measured by elementary analysis as described in Eq. 3.6:

$$n_C = n_{C_{real}} \approx \frac{wt_{C_{real}} \%}{wt_{C_{perfect-built}} \%} \cdot n_{C_{perfect-built}} \quad Eq. 3.6$$

The number describing the metal loading of a dendrimeric complex is usually not a whole number, since it is the mean value of a distribution of complexes of the same generation with different copper(II) loadings.

The molecular formula of the complexes was calculated from the experimental percentages of each element (except oxygen, calculated by difference) determined by elemental analysis. The number of carbon atoms in the real existing dendrimeric ligand with defects $wt_{C_{real}} \%$ was taken as reference. For a realistic correlation of the elemental analysis values, in addition to the dendrimeric ligand of generation G **LG**, and copper nitrate, **Cu(NO₃)₂**, we assumed the presence of compounds, resulting from the partial decomposition of the copper nitrate trihydrate according to section 3.1.2.1, i.e. basic copper nitrate, **Cu₂(NO₃)(OH)₃**, nitric acid, **HNO₃** and water:



a , b , c and d indicate respectively the number of molecules of **Cu(NO₃)₂**, **Cu₂(NO₃)(OH)₃**, **HNO₃** and **H₂O** per dendrimeric ligand.

These numbers, a - d , were calculated with the “*Solver*” optimisation tool available for *Excel* (Microsoft). It is an iterative numerical procedure by which a , b , c and d are varied until the calculated molecular formula fits the experimental elementary analysis values best. In some particular cases b , c or d can be equal to zero. The equation system, that has been set up, is over-determined, i.e. more than one solution is mathematically possible. Therefore it was necessary to impose reasonable chemical boundary conditions which confine possible solutions. The used boundary conditions are the following:

- i. the number of copper calculated with Eq. 3.5 was taken as fixed value,
- ii. the number of **HNO₃** molecules cannot overtake the number of tertiary amines in the dendrimeric ligand. This postulation is related to the most probable reaction of **HNO₃** with the tertiary amine sites in the dendrimeric core, leading to their protonation.

Under those conditions the possible solutions of the system are much more reduced and satisfactory fits can be found. The estimated composition and elemental weight percentages for each complex are given in Table 3.2.

Table 3.2: Estimated molecular weight and composition of the copper complexes.

LG + a Cu(NO₃)₂ + b Cu₂(NO₃)(OH)₃ + c HNO₃ + d H₂O									
CG.i(n)	M_{complex}	LG	a	b	c	d	χ²	wt. %_{calcd}	wt. %_{exp}
C0.1(0.2)	940	L0	0.2	0.01	0.00	4.77	2.41	C: 66.43 H: 10.53 N: 3.17 Cu: 1.12	C: 67.22 H: 10.12 N: 2.22 Cu: 1.49
C1.2 (1.9)b	2442	L1	1.88	0.01	1.48	0.00	0.02	C: 61.01 H: 8.81 N: 6.14 Cu: 4.92	C: 61.00 H: 8.81 N: 6.27 Cu: 4.90
C1.2 (1.9)gr	2317	L1	1.76	0.00	0.00	0.00	0.65	C: 63.78 H: 9.16 N: 5.36 Cu: 4.65	C: 64.28 H: 9.29 N: 4.73 Cu: 5.24
C1.4(1.5)	2499	L1	1.50	0.00	2.00	4.97	0.12	C: 59.69 H: 9.05 N: 5.86 Cu: 3.84	C: 59.59 H: 9.07 N: 6.18 Cu: 3.87
C1.5(1.0)	2370	L1	0.95	0.03	1.99	4.03	0.14	C: 65.55 H: 9.46 N: 5.37 Cu: 3.05	C: 64.93 H: 9.54 N: 7.79 Cu: 2.75
C1.7(1.0)b	2470	L1	1.00	0.00	2.00	9.18	0.69	C: 60.03 H: 9.44 N: 5.33 Cu: 2.57	C: 60.30 H: 8.83 N: 5.71 Cu: 2.59
C2.2(6.3)	6152	L2	6.30	0.00	3.71	35.70	0.84	C: 49.43 H: 8.47 N: 6.51 Cu: 6.46	C: 49.98 H: 7.95 N: 6.48 Cu: 6.53
C2.3(6.0)	6058	L2	6.00	0.00	5.13	30.95	1.20	C: 50.19 H: 8.33 N: 7.00 Cu: 6.24	C: 50.76 H: 7.63 N: 7.00 Cu: 6.26
C2.4(5.4)	5840	L2	5.40	0.00	6.00	18.81	0.32	C: 52.36 H: 8.43 N: 7.01 Cu: 5.86	C: 52.65 H: 8.06 N: 7.08 Cu: 5.90
C2.5(5.4)	5915	L2	5.40	0.00	3.45	35.54	3.37	C: 50.98 H: 8.73 N: 6.23 Cu: 5.71	C: 51.98 H: 7.51 N: 6.07 Cu: 5.76
C2.6(5.2)	5734	L2	5.20	0.00	2.54	27.98	0.82	C: 53.09 H: 8.81 N: 6.17 Cu: 5.72	C: 53.62 H: 8.27 N: 6.13 Cu: 5.77

3. LIQUID CRYSTALLINE, DENDRIMERIC COPPER(II) COMPLEXES

CG.i(n)	M _{complex}	LG	<i>a</i>	<i>b</i>	<i>c</i>	<i>d</i>	χ^2	wt. % _{calcd}		wt.% _{exp}	
C2.7(4.6)	5401	L2	4.60	0.00	0.05	25.97	0.87	C:	56.50	C:	56.93
								H:	9.06	H:	8.42
								N:	5.97	N:	5.86
								Cu:	5.15	Cu:	5.41
C2.8(4.4)	5645	L2	4.40	0.00	4.30	27.31	1.16	C:	53.87	C:	54.47
								H:	8.76	H:	8.07
								N:	6.61	N:	6.53
								Cu:	4.90	Cu:	4.91
C2.9(3.5)	5335	L2	3.50	0.00	6.00	10.27	0.27	C:	57.45	C:	57.64
								H:	8.93	H:	8.54
								N:	6.69	N:	6.89
								Cu:	4.17	Cu:	4.15
C2.10(2.7)	5046	L2	2.70	0.00	6.00	1.95	0.03	C:	60.97	C:	60.94
								H:	9.14	H:	9.07
								N:	6.66	N:	6.81
								Cu:	3.41	Cu:	3.41
C2.11(2.6)	5090	L2	2.60	0.00	0.89	25.30	1.44	C:	59.74	C:	60.41
								H:	9.78	H:	9.02
								N:	5.08	N:	5.00
								Cu:	3.22	Cu:	3.23
C2.12(2.1)	4671	L2	2.10	0.00	2.52	0.00	2.40	C:	66.17	C:	65.83
								H:	9.75	H:	9.62
								N:	5.69	N:	6.99
								Cu:	2.88	Cu:	2.80
C2.13(2.0)	4919	L2	1.97	0.01	2.84	15.39	0.18	C:	62.26	C:	62.51
								H:	9.61	H:	9.37
								N:	5.86	N:	5.85
								Cu:	2.54	Cu:	2.54
C2.14(1.3)	4587	L2	1.27	0.01	2.72	4.56	0.07	C:	66.92	C:	67.03
								H:	9.90	H:	9.69
								N:	5.73	N:	5.81
								Cu:	1.77	Cu:	1.76
C2.15(1.3)	4766	L2	1.25	0.03	2.76	12.62	0.03	C:	64.39	C:	64.51
								H:	10.04	H:	10.08
								N:	5.23	N:	5.29
								Cu:	1.67	Cu:	1.67
C2.16(1.0)	4722	L2	0.99	0.01	5.74	3.66	0.20	C:	64.88	C:	65.11
								H:	9.80	H:	9.49
								N:	6.00	N:	5.95
								Cu:	1.33	Cu:	1.33
C2.18(0.9)	4692	L2	0.90	0.00	6.00	2.07	0.71	C:	65.71	C:	65.54
								H:	9.77	H:	9.45
								N:	6.13	N:	6.87
								Cu:	1.31	Cu:	1.22
C2.19(0.5)	4295	L2	0.48	0.01	0.39	4.21	0.04	C:	71.64	C:	71.59
								H:	10.54	H:	10.56
								N:	4.83	N:	4.99
								Cu:	0.73	Cu:	0.71

CG.i(n)	M _{complex}	LG	a	b	c	d	χ^2	wt. % _{calcd}		wt. % _{exp}	
C2.20(0.3)	4417	L2	0.30	0.00	2.50	5.75	0.00	C:	69.60	C:	69.61
								H:	10.30	H:	10.25
								N:	5.39	N:	5.37
								Cu:	0.43	Cu:	0.47
C3.1(12.0)	12628	L3	11.99	0.01	14.00	59.63	0.47	C:	49.04	C:	49.46
								H:	8.19	H:	7.83
								N:	7.26	N:	7.29
								Cu:	6.04	Cu:	6.03
C3.2(7.9)	10708	L3	7.80	0.05	5.37	23.80	0.02	C:	58.27	C:	58.33
								H:	8.98	H:	9.08
								N:	6.39	N:	6.45
								Cu:	4.67	Cu:	4.67
C4.1(24.2)	24504	L4	24.20	0.00	30.00	55.47	0.11	C:	51.28	C:	51.37
								H:	8.23	H:	8.06
								N:	7.85	N:	8.08
								Cu:	6.32	Cu:	6.28
C4.2(7.4)	19838	L4	7.39	0.01	6.83	58.50	0.40	C:	63.09	C:	63.45
								H:	10.04	H:	9.65
								N:	5.63	N:	5.6
								Cu:	2.37	Cu:	2.38
C5.1(45.9)	47156	L5	45.90	0.00	18.23	198.19	3.19	C:	52.65	C:	53.59
								H:	8.49	H:	7.26
								N:	6.82	N:	6.63
								Cu:	6.16	Cu:	6.19
C5.2(44.9)	44165	L5	43.20	0.85	0.00	102.90	1.37	C:	56.55	C:	57.22
								H:	8.65	H:	8.25
								N:	6.60	N:	5.99
								Cu:	6.23	Cu:	6.46

LG: dendrimeric ligand of generation **G**; **a, b, c, d:** moles per dendrimeric ligand of: **a**, copper nitrate; **b**, basic copper nitrate; **c**, nitric acid; **d**, water **CG.i(n):** dendrimeric copper (II) complex, of the **G** generation, **i:** consecutive index, **n:** copper(II) loading of the complex. **M_{complex}:** molecular weight of the complex estimated according to Eq. 3.3. χ^2 is the sum of the quadratic deviations of the calculated mass percentages wt. %_{calcd.} of each element **i** from those estimated by elemental analysis wt. %_{exp}, χ^2 is defined by:

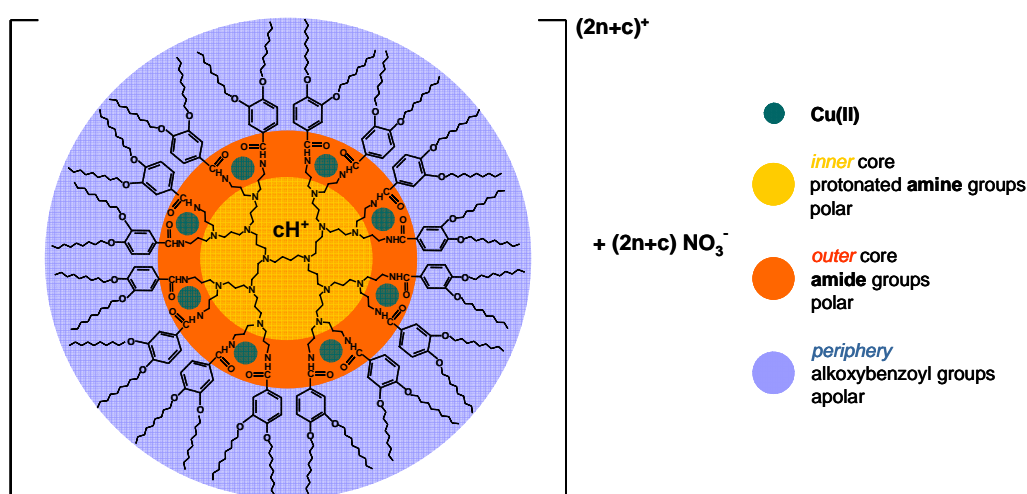
$$\chi^2 = \sum_i (\text{wt. \%}_{\text{exp},i} - \text{wt. \%}_{\text{calcd},i})^2$$

The analysis shows that, if some, only traces of Cu₂(NO₃)(OH)₃ (usually ≤ 0.01 mol per dendrimer, i.e. < 0.001 wt. %) can be present in the dendrimeric copper complex of the THF series, in accordance with the gravimetric results of the blank reaction. The 5th generation copper(II) complex of the γ -butyrolactone/CHCl₃ series exhibits some small amount of Cu₂(NO₃)(OH)₃ (0.85 mol). The longer working-up procedure in this series seems to be responsible for larger Cu₂(NO₃)(OH)₃ formation.

HNO₃ takes part in the composition of almost every complex. The protonation of the tertiary amines is assumed as consequence. This statement is supported by spectroscopic analysis, cf. 3.5.3.3. Furthermore, the quaternisation of tertiary amine groups in the

dendrimers is well known in the literature for both liquid crystalline and non-liquid crystalline poly(propylene imine)-^[111, 192, 236] and poly(ethylene imine) dendrimers^[136]. Therefore, it is to be assumed that the core of the poly(propylene imine) consists of a quaternary ammonium nitrate sites. Immediate consequence of the protonation of the tertiary amines in the dendrimer core is the exclusion of these groups with respect to the coordination of copper. In the series of highest copper loading, we can observe that the moles of nitric acid and copper are of the same order, except for the 5th generation, where the number of acid molecules is considerably smaller. Probably, the extent of decomposition of the $\text{Cu}(\text{NO}_3)_2 \cdot 3\text{H}_2\text{O}$ is not large enough to produce HNO_3 to protonate quantitatively the tertiary amines in the 5th generation. The complexes of the 2nd generation exhibit, already at low copper contents, a high protonation of the amine groups. Remarkably, the elimination of the boundary condition, concerning the protonation of the tertiary amines, yields the same nitric acid contents per dendrimer indicating that this condition does not represent a manipulation of the equations system.

In conclusion, based on these findings a preliminary model of the dendrimeric copper(II) complexes, consisting of a protonated poly(propylene imine) dendrimer core surrounded by the amide interface groups where probably takes place the complexation, is presented in Scheme 3.2.



Scheme 3.2: Preliminary model of the copper(II) complexes of quaternary poly(propylene imine) ammonium derivatives with $\text{Cu}(\text{NO}_3)_2 \cdot 3\text{H}_2\text{O}$, depicted for the 3rd generation. n : number of copper(II) per dendrimer (loading), c : number of protons per dendrimer

3.3 MALDI-ToF-MS

3.3.1 MALDI-ToF-MS: Introduction

The dendrimeric copper(II)-complexes were examined by *Matrix-Assisted Laser Desorption Ionisation Time of Flight Mass Spectrometry*, MALDI ToF-MS, which is a method for the determination of absolute molecular masses. In MALDI ^[237], gaseous ions from the analyte are generated and their mass-to-charge ratio, m/z , is measured. The ionisation of the sample does not take place directly but by means of the matrix, in which the analyte is embedded. The molecules of the matrix absorb the energy of the incident laser light and are ionised into the gas phase desorbing thereby the analyte molecules. In the gas phase, a series of charge transfer processes between matrix and analyte occur resulting in the ionisation of the analyte. The gentle ionisation technique of this spectrometric method minimizes the fragmentation of the analyte and allows therefore the detection of the molecular ion peak. The ionised analyte is exposed to a high voltage, by which it is accelerated into a field free flight tube, and finally the cations (positive ion detection mode) hit the ion-detector. The time passed from desorption until detection, the so called “time of flight” (ToF), is measured and is proportional to the square root of the ratio of the mass and the charge of the analyte, m/z , ($t \propto \sqrt{m/z}$).

Two possibilities for detection are available: linear and reflector mode. In the linear mode, the ions simply travel straight through the drift tube and are detected at its end. This mode is more sensitive and allows the detection of higher masses. However, due to the velocity dispersion of the desorbed and accelerated ions of the same m/z ratio, broad signals with low resolution are recorded. To avoid this shortcoming, in the reflector mode, ions of the same m/z ratio but different velocities are “time focused” by an electric field. Then, these ions reach the detector at the same time and consequently improve the resolution of the signal. The sensitivity of MALDI can be further improved by the incorporation of a LIFT device ^[238], a further accelerator which reduces the signal to noise ratio of the spectra.

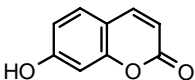
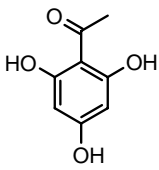
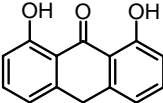
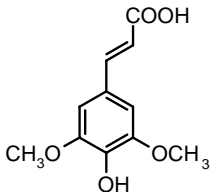
Even if the molar mass of the analyte can be directly calculated from the flight time measured by MALDI, a calibration is necessary in order to avoid inaccuracies in the determination of the flight time. Despite calibration, the measured mass (m/z) is not affected by parameters such as interactions with the solvent and morphology of the molecule as is the case in SEC. Furthermore, whereas SEC yields continuous traces, MALDI-spectra are mass-resolved and together with its high sensitivity, it allows not

only the detection but also the identification of impurities as well as possible oligomers or eventual defective dendrimeric structures present in the final product.

Because of the high isotope resolution, the copper(II) complexes were measured in the reflector mode. Positive ion mode was used for detection. Measurements in the negative ion mode did not show any signal in the molecular peak region, indicating that in the ionisation of the dendrimeric copper(II) complexes cation formation is favoured.

Umbelliferone was used as matrix for complexes of the 1st and 2nd generations and 2', 4', 6'-trihydroxyacetophenone, THAP, for the 3rd generation since they have been shown to favour the ionization of copper complexes of poly(amido amine) [225], PAMAM, dendrimers. The PAMAM dendrimers have a relatively similar core to poly(propylene imine) dendrimers. Dithranol and sinapinic acid matrices, used successfully for the measurement of the corresponding PPI dendrimeric ligands, led to poorer ionisation of the complexes than umbelliferone. The matrices are depicted in Table 3.3. The adequate laser power is also decisive for ionizing the copper complexes. Depending on the complex and generation, around 30 - 40% laser intensity is needed to ionize the analyte, lower laser powers cause lower signal-to-noise ratios and decreased sensitivity.

Table 3.3: *Matrices used for the ionisation of the dendrimeric copper(II) complexes and starting ligands.*

Umbelliferone 7-Hydroxy-2H-1-benzopyran-2-one MF: C ₉ H ₆ O ₃ ; MW: 162.15	THAP 2',4',6'-Trihydroxyacetophenone MF: C ₈ H ₈ O ₄ ; MW: 168.15
	
Dithranol 1,8-Dihydroxy-9(10H)-anthracenone MF: C ₁₄ H ₁₀ O ₃ ; MW: 226.23	Sinapinic acid 3,5-Dimethoxy-4-hydroxycinnamic acid MF: C ₁₁ H ₁₂ O ₄ ; MW: 208.22
	

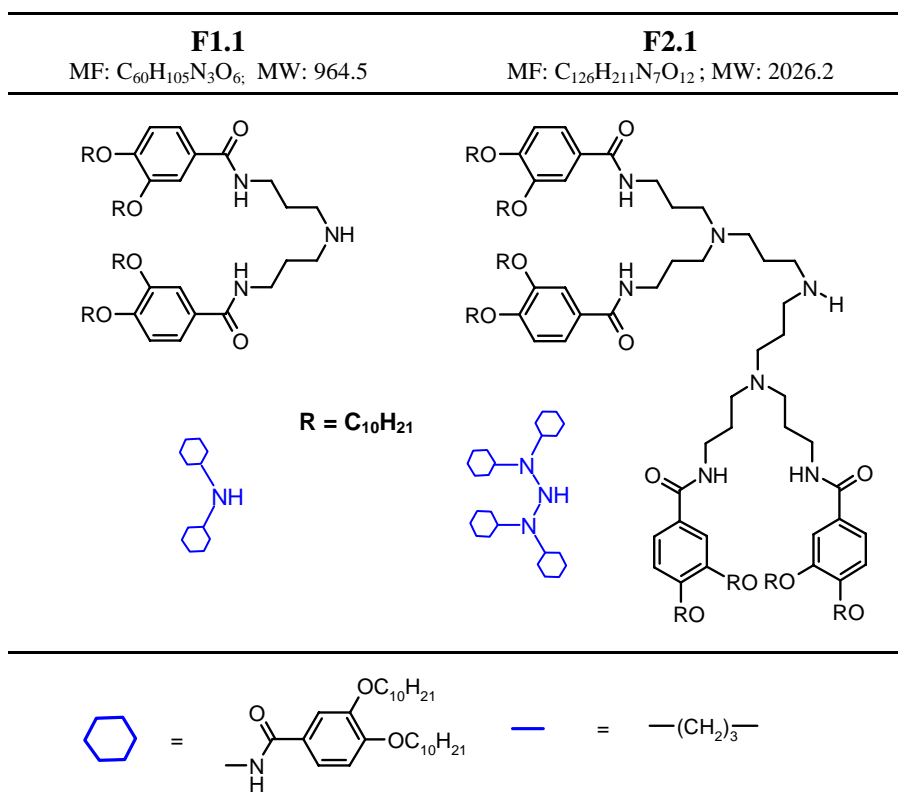
3.3.2 MALDI-ToF-MS of the lower Generations. Butandiamide, 1st and 2nd Generation Copper(II) Complexes

As an example, a mass spectrogram of complex **C2.2(6.3)** is presented in Fig. 3.3a, b to illustrate the behaviour of the dendrimeric copper-complexes of the 1st and 2nd generations under MALDI. It shows the occurrence of a series of signals of decreasing intensity with increasing m/z which can be ascribed to $L2-Cu_n\pm H$ with **L2** = 2nd generation dendrimeric ligand, $n = 0, 1, 2, \dots$, indicating the copper loading and $\pm xH$ mass differences of $\pm x$ amu, or protons incorporated/lost during the ionisation, cf. Table 3.5.

Adducts carrying sodium or potassium are also observed in the spectra giving rise to secondary weight distributions. Even if these cations were not added to the matrix/analyte mixture, sodium and potassium are always present as impurities as well in the matrix, as in reagents, solvents or glassware and play a role in the ionization of polymers^[237].

A fourth series of complexes, built up by the assembly of two equal dendrimeric fragments coordinated by copper are also observed in the spectra. The fragment, denoted **F2.1**, corresponds approximately to the half of a 2nd generation dendrimer, i.e. two dendrons bridged by a dipropyl amine unit. An homologous fragment **F1.1** appears in the spectra of the 1st generation complexes, both fragments are depicted in Table 3.4. These fragments are formed as a result of the intramolecular nucleophilic attack of one nitrogen atom of the diaminobutane core of the dendrimer to the other nitrogen atom^[235]. The nucleophilic displacement makes necessary the protonation of one of the diaminobutane nitrogen atoms. It has been shown that, as result of the synthetic procedure, formation of HNO_3 and concomitant protonation of the tertiary amine groups in the dendrimer core occur during the complexation. Therefore, we can not exclude the formation of these fragments already during the complexation preceding their possible development during the MALDI measurement.

The measurements, carried out in the reflector mode, allow isotopic resolution and the observed spacings among the peaks in the isotopic multiplets (1 amu) indicate that the masses correspond to singly charged species, i.e. to $\sim LG^+$, $LGCu^+$, $LGCu_2^+$, \dots . The simulated isotopic distribution peaks of the proposed species are furthermore in good agreement with the measured isotopic patterns, confirming the structures of the copper complexes, cf. Fig. 3.3c.

Table 3.4: Fragments **F1.1** and **F2.1** observed in the mass spectra of the copper(II) complexes of 1st and 2nd generation respectively.

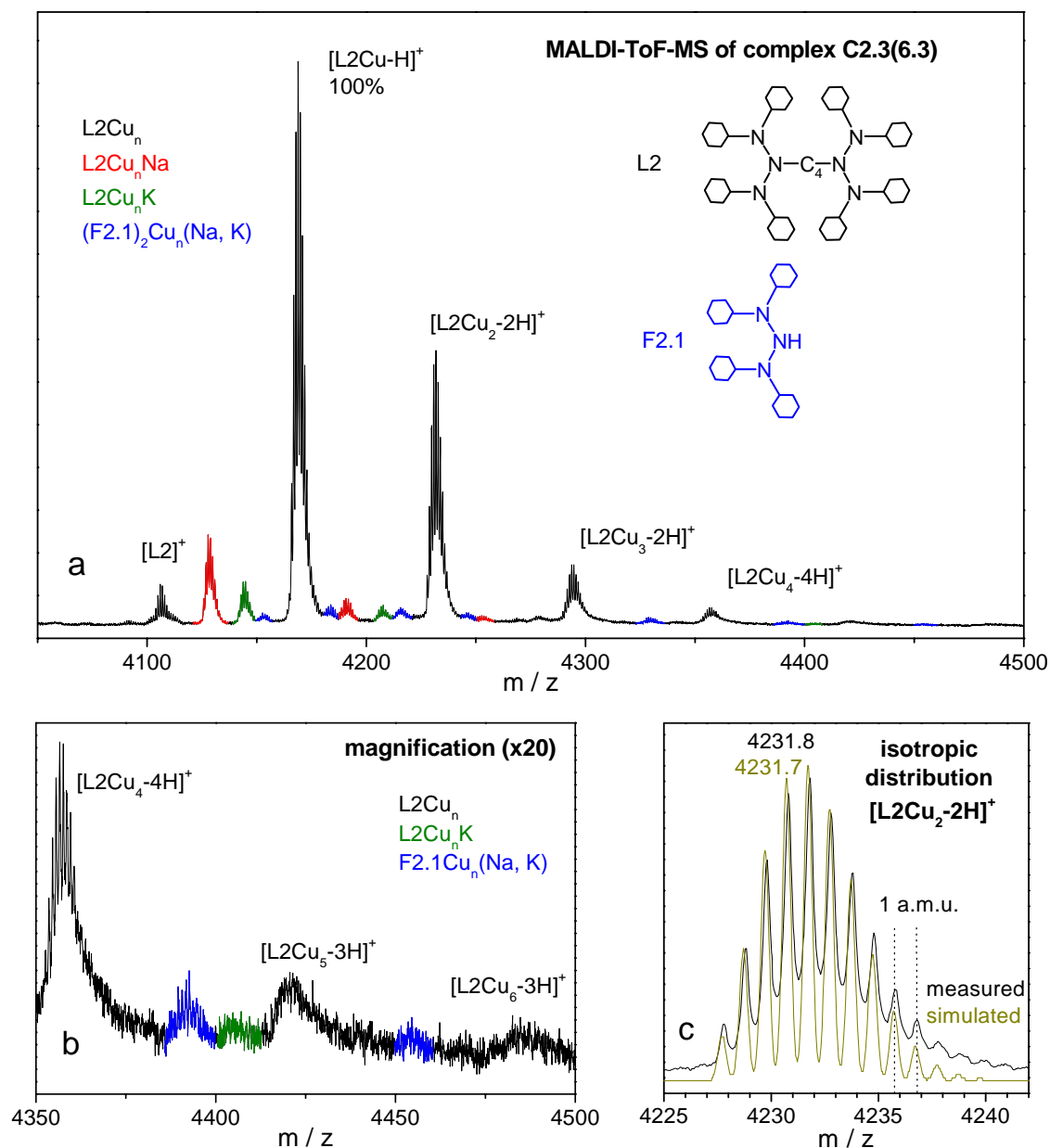


Fig. 3.3: Positive-ion MALDI ToF-MS spectrum of the 2nd generation copper(II) complex **C2.2(6.3)** measured in reflector mode, laser intensity 30 % with umbelliferone as matrix. a) m/z range from 4050 to 4500 amu, b) magnification of m/z range 4350 - 4500 ccomparison of the measured and simulated isotope distribution of the peak at $m/z = 4231$. Only the peaks of the L2Cu series are labelled, the complete assignment of peaks is presented in Table 3.5.

The mass spectra of the 1st generation reveal the existence of copper complexes exhibiting up to four copper centres per dendrimeric ligand. Secondary weight distributions of sodium and potassium adducts are also observed. As it happens for the 2nd generation complexes, it was shown that copper is able to act as bridge between the fragments. So, dimers of the fragment **F1.1**, cf. Table 3.4, [F1.1₂Cu_n±xH]⁺ are observed.

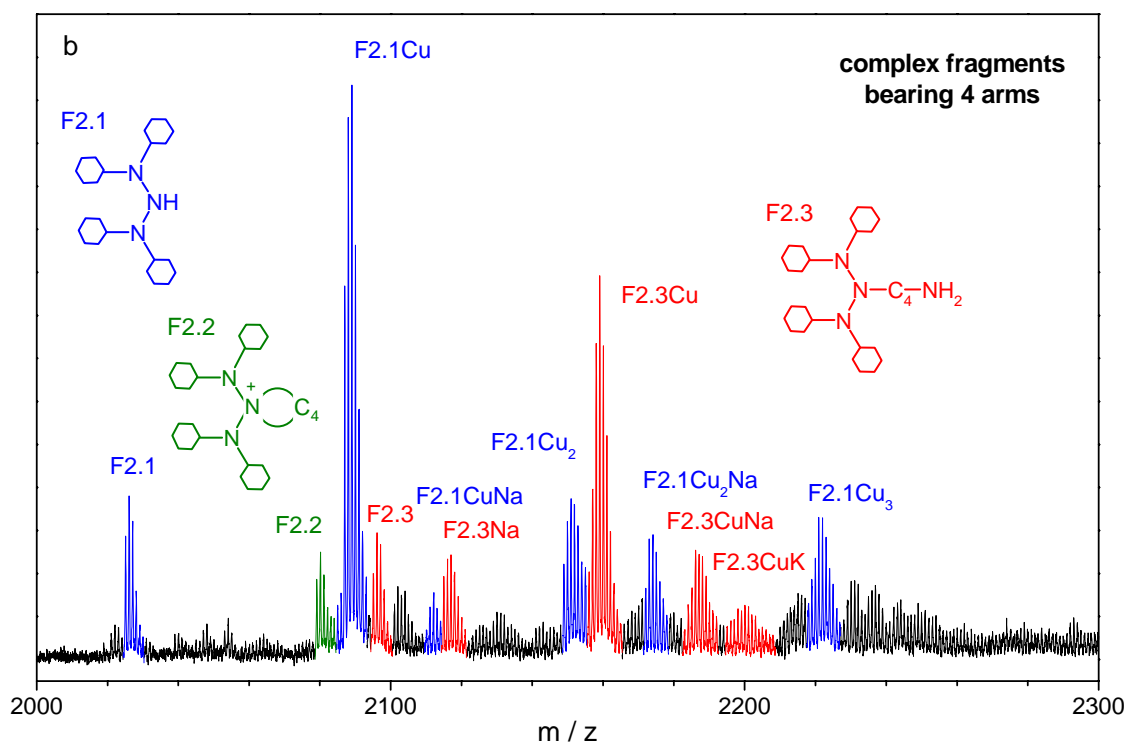
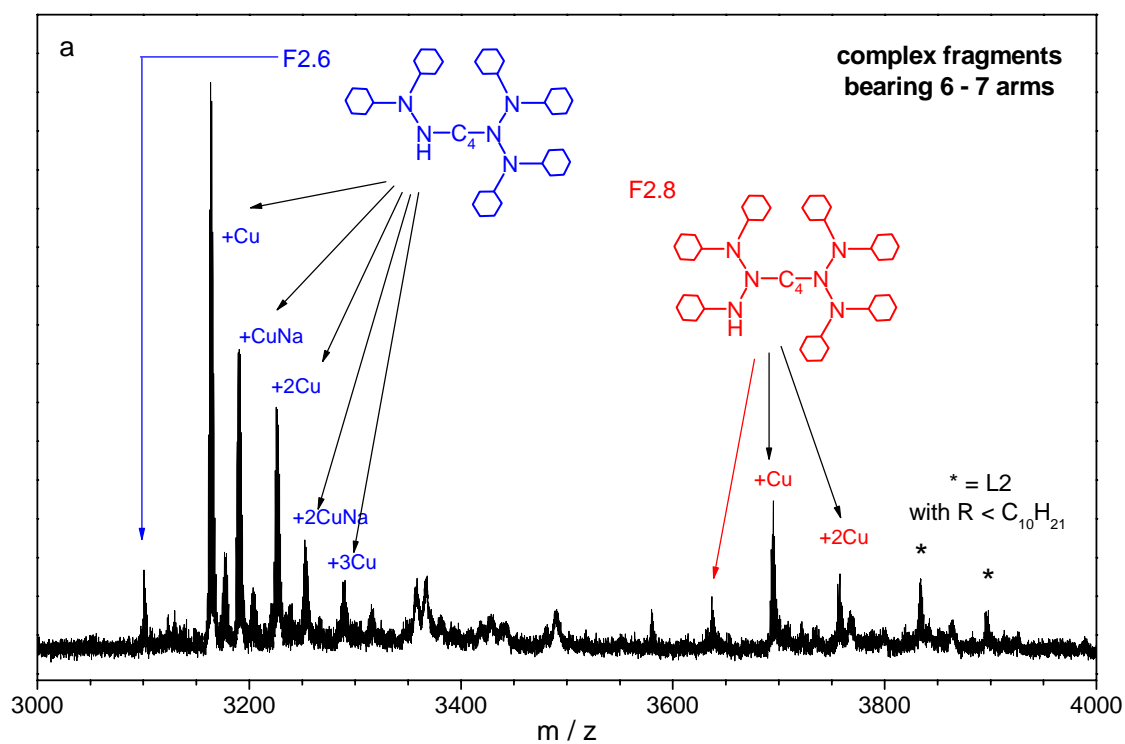
A MALDI-ToF spectrum of the model compound, the copper complex of the butandiamide derivative, was recorded too (not shown). In the mass range corresponding to the molecular peak, the predominant species is the free ligand. The peak corresponding to a complex with one copper centre is present but its intensity relative to that of the ligand is very low. It is in good agreement with the results of elemental analysis cf. 3.2 Table 3.2, which indicate that in average the butanediamide is coordinated to 0.2 copper centres, i.e. only one of five butanediamide complexes copper.

3.3.3 MALDI-ToF-MS Defect Structures, Fragments and Copper Bridged Dimers

In addition to the peaks corresponding to copper complexes of a perfect built dendrimeric ligand, the 2nd generation copper complexes exhibit a very small amount of peaks corresponding to fragments (two, four or six - seven arms) of a dendrimer. Fragments comprising six (**F2.8**, cf. Table 3.6) or seven arms (**F2.7**, cf. Table 3.6) are observed in the range of 3000 to 4000 m/z , cf. Fig. 3.4a. These structures are present in the mass spectra of the ligands and are inherent to the divergent synthetic procedure of the poly(propylene imine) core. Defect dendrimeric ligands arising from incomplete amidation of the poly(propylene imine) core and corresponding copper(II) complexes were not detected by MALDI. Defect dendrimers exhibiting alkoxy chains other than C₁₀H₂₁, hexyl or more probably in average 4 octyl chains in the peripheric groups instead of the decyl chains were also observed, cf. peaks labelled with asterisk in Fig. 3.4a.

Fragments bearing four arms are observed in the range of 2000 to 2300 m/z , cf. Fig. 3.4b. They correspond to copper(II) complexes of half 2nd generation dendrimeric ligand (**F2.1**, **F2.2** and **F2.3** in Table 3.6) with varied copper(II) loadings. The homologous consisting of two arms (**F2.4**, **F2.5** and **F2.6**, cf. Table 3.6) are observed at m/z between 950-1100 amu, cf. Fig. 3.4c.

These fragments (and sodium and potassium adducts) of the parent peak, also detected in the spectrogram of the ligands, are the result of the usual fragmentation path of the polypropylene imine dendrimers as observed by electrospray ionisation mass spectrometry ESI-MS ^[235]. Given the chemical similarity between ideal and defective dendrimer structures, both species are expected to be ionized with equal efficiency. The relative amount of these fragments in the complex as in case of the ligand varies with the laser intensity indicating that they are probably formed during the MALDI measurement whereas the fragmentation during the complexation cannot be completely excluded either as discussed before.



continued on next page

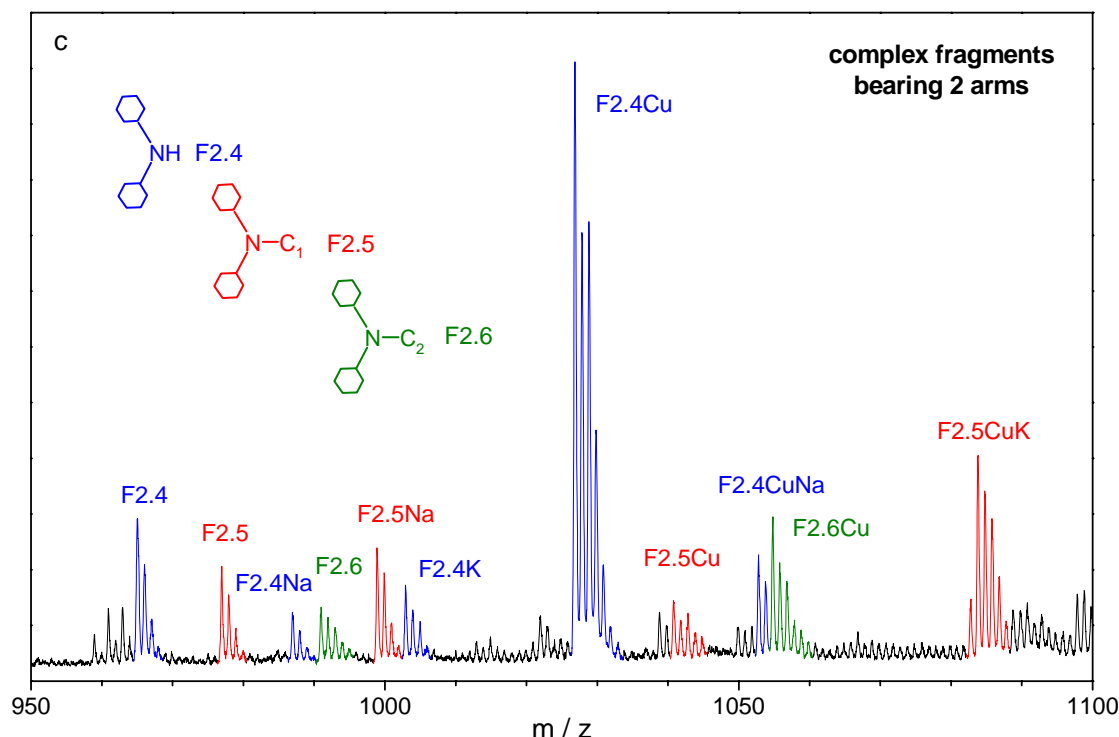


Fig. 3.4: Fragments observed in the positive-ion MALDI ToF-MS spectrum of the 2nd generation copper(II) complex C2.2 (6.3). a) m/z range of fragments corresponding to a “half” dendrimer (2000 to 2300 amu). b) fragments corresponding to one dendron, a quarter of dendrimer. Measured in reflector mode, laser intensity 30 % with umbelliferone as matrix. Denomination of the fragments are explained in Table 3.6 below.

No metal bridged adducts of perfect built dendrimers are present in the 2nd generation samples or if present they are not detected by MALDI, however two fragments **F2.1** (cf. Table 3.6), bridged by copper ion $\text{F2.1}_2\text{Cu}_n$, built a complex of the same size order of the perfect ligand, and it is observed by MALDI as already shown in Fig. 3.3 and Table 3.5.

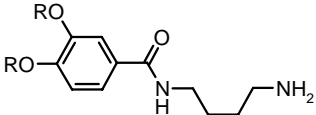
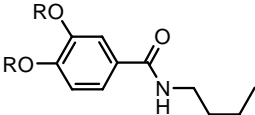
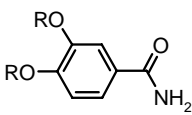
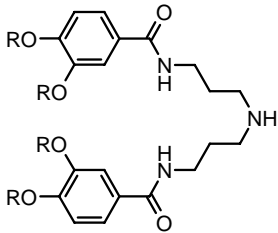
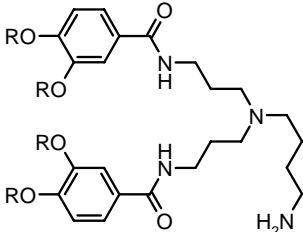
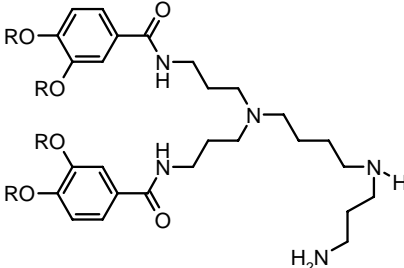
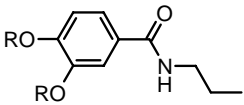
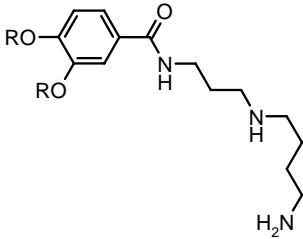
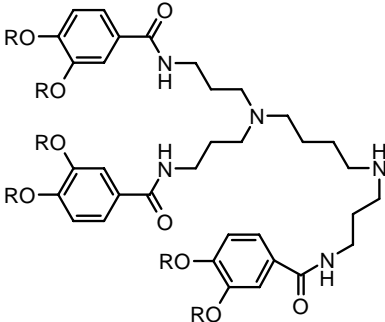
The defects and fragmentation paths of the 1st generation copper complexes are homologous with those of the 2nd generation, cf. Table 3.6. Masse signals at $m/z \sim 3/4$, $1/2$ or $1/4$ the molecular ion, corresponding to copper complexes of dendrimers lacking one, two or three amidated propylamine arms are to be observed. The intensity of these fragments, relative to the molecular ion, is higher than for the 2nd generation complexes and is independent of the laser power used in the measurement indicating that they are probably not caused by fragmentation during the ionisation procedure of MALDI but rather during the complexation reaction. The extent of fragmentation observed by MALDI is for the green complex **C1.2 (1.9)gr** rather high compared to the other 1st generation complexes. The individual peaks were identified by the comparison of the measured isotope distribution peaks with the simulated ones for the proposed structures.

The occurrence of copper bridged complexes of the most common 1st generation fragment, **F1.1** ($[\text{F1.1}_2\text{Cu}_n\pm x\text{H}]^+$) is accompanied by the appearance of complexes of other fragments ($[\text{F1.1F1.2Cu}_n\pm x\text{H}]^+$ and $[\text{F1.1F1.3Cu}_n\pm x\text{H}]^+$) corresponding to roughly two halves of the ligand and even the combination of a half-dendrimer fragment with a 3/4 - dendrimer fragment is observed ($[\text{F1.1F1.6Cu}_n\pm x\text{H}]^+$), cf. 6.4. No metal bridged oligomers of perfect built 1st generation dendrimers are detected by MALDI.

The intensity of the peaks corresponding to fragments of the butandiamide (**F0.1**, **F0.2**, **F0.3**, cf. Table 3.6) is of the same order as that of peaks corresponding to the complete molecule. The fragments are able to built copper-bridged dimeric structures ($\text{F0.1}_2\text{Cu}_n$). Mixed dimers of ligand and fragment (L0F0.1Cu) assembled by copper are observed too.

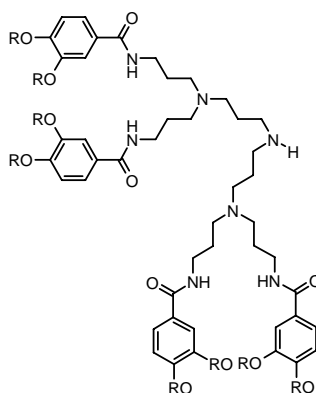
3. LIQUID CRYSTALLINE, DENDRIMERIC COPPER(II) COMPLEXES

Table 3.6: Fragments observed in the mass spectra of the copper(II) complexes of zero (**F0.i**), 1st (**F1.i**) and 2nd (**F2.i**) generation. $R = C_{10}H_{21}$

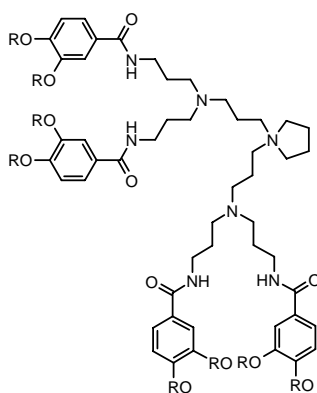
zero generation fragments		
F0.1 MF: $C_{31}H_{56}N_2O_3$ MW: 504.8	F0.2 MF: $C_{31}H_{55}NO_3$ MW: 489.8	F0.3 MF: $C_{27}H_{47}NO_3$ MW: 433.7
		
1 st generation fragments		
F1.1 MF: $C_{60}H_{105}N_3O_6$ MW: 964.5	F1.2 MF: $C_{64}H_{114}N_4O_6$ MW: 1035.7	F1.3 MF: $C_{67}H_{121}N_5O_6$ MW: 1092.7
		
F1.4 MF: $C_{30}H_{53}NO_3$ MW: 475.8	F1.5 MF: $C_{34}H_{63}N_3O_3$ MW: 561.9	F1.6 MF: $C_{94}H_{165}N_5O_9$ MW: 1509.4
		

2nd generation fragments**F2.1**

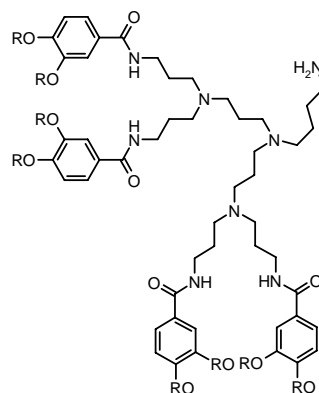
MF: C₁₂₆H₂₂₁N₇O₁₂
MW: 2026.2

**F2.2**

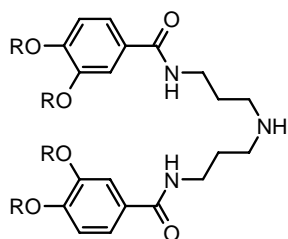
MF: C₁₃₀H₂₂₈N₇O₁₂
MW: 2081.3

**F2.3**

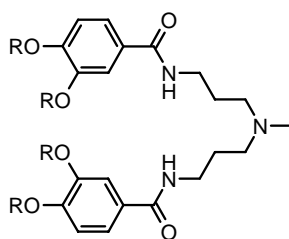
MF: C₁₃₀H₂₃₀N₈O₁₂
MW: 2097.3

**F2.4 = F1.4**

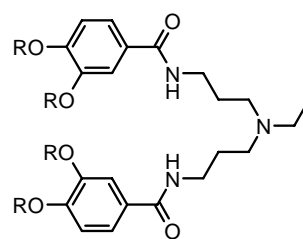
MF: C₆₀H₁₀₅N₃O₆
MW: 964.5

**F2.5**

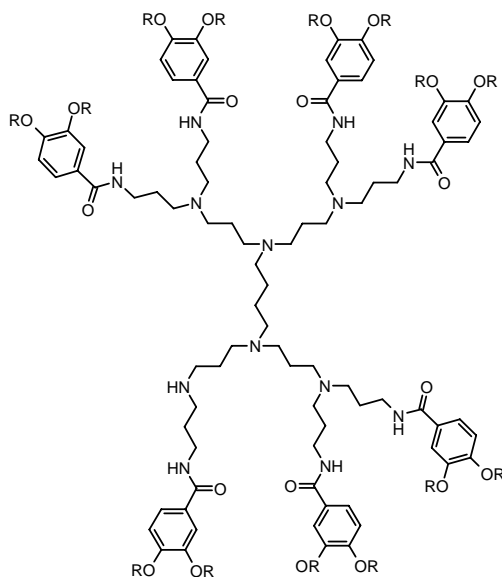
MF: C₆₁H₁₀₇N₃O₆
MW: 978.6

**F2.6**

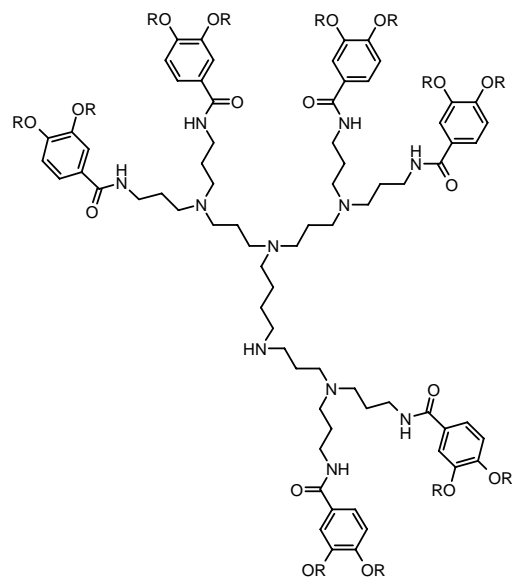
MF: C₆₂H₁₀₉N₃O₆
MW: 992.6

**F2.7**

MF: C₂₂₇H₄₀₀N₁₃O₂₁
MW: 3647.7

**F2.8**

MF: C₁₉₃H₃₄₀N₁₁O₁₈
MW: 3102.9



3.3.4 MALDI-ToF-MS of the Higher Generations. 3rd to 5th Generation Copper(II) Complexes

1st and 2nd generation copper(II) complexes were easily detected by MALDI, and all possible copper complexes (all individual copper loadings) are identified for each generation. MALDI ToF mass spectrogram of the 3rd generation, cf. Fig. 3.5, Table 3.7, reveals a broad step from low m/z up to 9000. The broad peak can not be related to the appearance of increasing defects in the dendrimer structures with increasing generation, because the spectrogram of the 3rd generation ligand exhibits discrete peaks corresponding only to a perfect built 3rd generation dendrimer and no significant peaks corresponding to defective dendrimers are observed. The broad peak arises more probably because of a fragmentation in the complex during the measurement due to the high laser power required (40%). Peaks corresponding to 3rd generation complexes with up to 9 copper centres are identified in the higher range although a copper content of 12 was determined by elemental analysis, showing again the inverse dependence of the capability with the number of copper complexed.

The molecular masses of 4th and 5th generations could not be measured by MALDI despite of variations in the experimental conditions. Similar difficulties have been found in the detection of pure organic dendrimers and metal containing dendrimers of high generations [101, 175, 197, 225].

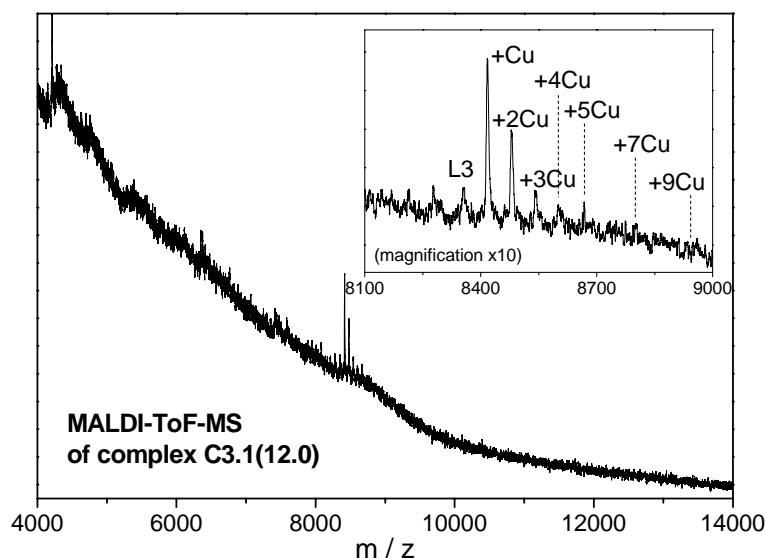


Fig. 3.5: Positive-ion MALDI ToF-MS spectrum of the 3rd generation copper(II) complex **C3.1(12.0)** measured in reflector mode, laser intensity 40 % with THAP as matrix. For clarity peaks denoted as + x Cu indicating $[L3Cu_x \pm yH]^+$. L3: 3rd generation dendrimeric ligand. Assignment of peaks presented in Table 3.7

Table 3.7: MALDI-ToF-MS of C3.1(12.0). Calculated and observed weight distributions of the 3rd generation copper(II) complex C3.1(12.0), L3: 3rd generation ligand.

$[\text{L3Cu}_n]^+_{\text{calcd}}$	m/z_{calcd}	m/z_{obs}	assignment
$[\text{L3}]^+$	8353.1	8356.4	$[\text{L3}+3\text{H}]^+$
$[\text{L3Cu}]^+$	8416.6	8417.8	$[\text{L3Cu}+1\text{H}]^+$
$[\text{L3Cu}_2]^+$	8480.1	8480.2	$[\text{L3Cu}_2-2\text{H}]^+$
$[\text{L3Cu}_3]^+$	8543.7	8540.8	$[\text{L3Cu}_3]^+$
$[\text{L3Cu}_4]^+$	8607.2	8605.1	$[\text{L3Cu}_4-3\text{H}]^+$
$[\text{L3Cu}_5]^+$	8670.8	8667.8	$[\text{L3Cu}_5-5\text{H}]^+$
$[\text{L3Cu}_7]^+$	8797.9	8801.5	$[\text{L3Cu}_7+3\text{H}]^+$
$[\text{L3Cu}_9]^+$	8925.0	8932.0	$[\text{L3Cu}_9+7\text{H}]^+$

3.3.5 Ionisation of the Copper(II) Complexes in MALDI-ToF-MS

The dendrimeric copper complexes are neutral species. The charges of the coordinated copper are equilibrated with the negative charge of the nitrates. The role of the nitrates as counterion or as charged ligand will be discussed by means of spectroscopic methods later on. Elemental analysis has revealed that the amines in the dendrimer core are to a certain extent protonated and neutralised by further nitrate groups.

No peaks with masses corresponding to $\text{LGCu}_n(\text{NO}_3)_{2n}$ are observed. This suggests that the nitrate group is either not detected as a free anion (this is known from the literature [197]) or that its function as a ligand is released by ionisation. MALDI-ToF-MS of similar dendrimeric copper(II)-complexes in the literature present examples of both anions absent and anions taking part in the molecular ion [125, 197]. No clear criterion is given and their presence or absence seems to be connected to the ionisation path followed by the dendrimer rather than to the role of the anion in the complex.

Assumed that the nitrates, if ligands, are released in the ionisation process; the presence in MALDI of exclusively single charged species being the complexes loaded with $(2n)^+$ charges from copper and $(x)^+$ from the protonated amine groups, seems to be contradictory at the first sight but it is explained through the ionisation paths observed for copper. For a mononuclear copper(II) complex of a dendrimeric ligand **LG**, there are several possibilities which lead to the observation of singly charged species:

- i. Deprotonation of the analyte: $[\text{LGCu(II)}-\text{H}^+]^+$ [225, 239, 240]
- ii. Reduction of copper(II) to copper(I): $[\text{LGCu(I)}]^+$ [225, 239-242]
- iii. Reduction of copper(II) to copper(0) and protonation or cationisation: $[\text{LGCu(0)}+\text{H}^+]^+$ $[\text{LGCu(0)}+\text{Na}^+/\text{K}^+]^+$ [239, 241-243]

The deprotonation of the complex is observed in our spectra and most likely occur at the amide groups, since they bear mobile hydrogens. It has been described that biological molecules and other polymers carrying metal ions characterized by MALDI-ToF MS, form single charged species by loosing protons to compensate the metal-ion charge [240, 244, 245]. Likewise, we observe ions which can only be explained considering the reduction of copper, e.g. peak at 4294.7 in Fig. 3.3 and Table 3.5 can be explained as $\text{L}_2\text{Cu(I)}_3\text{-2H}^+$, i.e. through the reduction of the three Cu(II) cations to Cu(I) and additional deprotonation. The reduction of copper under MALDI has been reported by several authors [239-241, 245, 246], they observe single charged species in MALDI spectra of polymers and peptides coordinated to copper, even if the introduced specie was Cu(II). A photochemical reduction of copper(II) to copper(I) through the laser ionization process is assumed to take place. *Zhang et al.* [242] demonstrated that the reduction of Cu(II) to Cu(I) occurs by a gas-phase exchange with matrix molecules and that it is furthermore a thermodynamically favoured process.

For polynuclear complexes we find analogous ionisation paths than those presented above, and with increasing copper loading combinations thereof, i.e. mixtures of different oxidation states and deprotonation sometimes with simultaneous cationisation and all possible arrangements. Since the presence of copper in the dendrimer is often accompanied by loss of protons to form the single charged ion, species with a higher copper content or larger protonation of the PPI core, are principally less favoured to be detected than those with a lower copper content. Already from this point of view, the relative intensities of the copper adducts are not quantitatively representative for the complex composition. For a given generation the occurrence of the different copper loaded species is in good agreement with the copper content determined by elemental analysis.

3.3.6 Conclusions

MALDI-ToF-MS has been shown to be a very valuable method for the characterisation of the copper complexes of the 1st to 3rd generations. It gives evidence of coordination of copper by the poly(propylene imine) dendrimers and allows the identification and structural analysis of the complexes. The detection of series of complexes with different copper loadings supports furthermore the results of elemental analysis. No differences are observed between complexes from the THF and the γ -Butyrolactone/ CHCl_3 series as

well as among the 2nd generation copper(II) complexes prepared by washing out with solvents of varied polarity and those prepared by the standard procedure; the participation of solvents in the copper complexes as co-ligands is therefore excluded. For 4th and 5th generations, improvement in the sample preparation, or the use of more sensitive techniques as MALDI LIFT-ToF/ToF-MS would be required to achieve the desired resolution.

3.4 TRANSMISSION ELECTRON MICROSCOPY, TEM

An electron microscope uses an electron beam to investigate an object, instead of visible light in optical microscopy. The resolution of a microscope is directly proportional to the wavelength. Since the wavelength of an electron λ_e is much smaller than that of visible light λ_{vis} ($\lambda_e \sim 0.03 \text{ \AA}$ at e.g. 200 kV vs. $\lambda_{vis} \geq 400 \text{ nm}$), smaller structures can be resolved with an electron microscope. Standard transmission electron microscopes, TEM, achieve resolutions up to 0.2 nm whereas high resolution transmission electron microscopes, HRTEM, achieve up to 0.05 nm at a maximum 3 MV acceleration voltage. Transmission electron microscopy is therefore a popular tool for analysis of organic and inorganic microstructures.

The principle of an electron microscope is as follows ^[247]: Electrons are emitted from an incandescent filament and are accelerated by the anode. A condenser system collimates the electron beam onto the specimen. The first focused image is provided by the objective lens and a system of further lenses (projector system) magnifies the image to its final size. The image is projected onto a fluorescent screen or recorded with a CCD camera or image plate. The lenses are tuneable electromagnets with varying current in order to focalize.

In the transmission mode, of TEM, the electron can interact with the sample in three different ways: it can be transmitted without energy loss, elastically scattered or inelastically scattered. In order to achieve contrast in the images, transmitted and elastically scattered light is separated with an aperture, so differences in electron density in the sample are enhanced. The brightness of the image is proportional to the number of unscattered electrons which pass through the aperture.

Besides imaging of specimen, the electron microscope can be used for analytic purposes. The electrons interacting with the sample give the diffraction pattern of the periodic structures available in the sample, and can provide important structural information of ordered materials.

Furthermore Electron Energy Loss Spectroscopy, EELS, is usually available in standard electron microscopes. The energy, lost by electrons which have interacted with the specimen, is detected and measured. The inner shell ionisations spectra, characteristic of each element, are useful for detecting the composition of a material.

The TEM images were taken by *Dr. M. Drechsler, Universität Bayreuth*, on a *Zeiss 922 OMEGA* microscope operating at 200 kV, and by *Dr. M. Krekhova, Universität Bayreuth*, on a *Zeiss CEM 902* operating at 80 kV. A diluted solution of the sample was

dropped onto a lacey carbon films on copper grids 200 mesh and was allowed to dry at room temperature before observation under the microscope. Fig. 3.6 shows a TEM image of the 2nd generation ligand, **L2**, on a 200 mesh copper grid coated with a non-treated lacey carbon film. The lacey carbon network (dark areas, dimensions from 0.25 up to 5 μm) is filled with the chloroform solution of the dendrimer, after evaporation of the solvent, a dendrimer film is suspended over the open areas. The light grainy areas on the image correspond thus to the dendrimer film, darker areas therein are thicker regions where more material has been accumulated, and homogeneous pale areas right and left of the image are empty holes which do not support any polymer film.

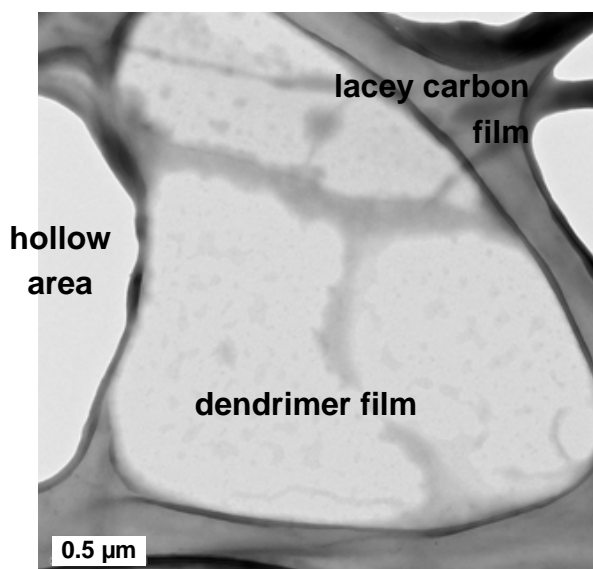


Fig. 3.6: TEM image of the 2nd generation ligand **L2**. Film from CHCl_3 solution onto lacey carbon coated copper grids.

Other substrates than lacey carbon films on copper grids resulted unsuitable for the observation of the dendrimers under TEM. An underlying support film, even ultrathin (ca. 3 nm) carbon films, diminish the contrast and incorporate some additional structure to the images which can be misleading. Furthermore lacey carbon films are more convenient for EELS since interferences of supporting film are avoided.

Only representative selected complexes of the 2nd and 5th generation were studied under transmission electron microscope; the pure dendrimeric ligand of the 2nd generation **L2** was also observed for comparison. Fig. 3.7 show typical TEM images of 2nd generation ligand **L2** (a), and complex **C2.3(6.0)** (b).

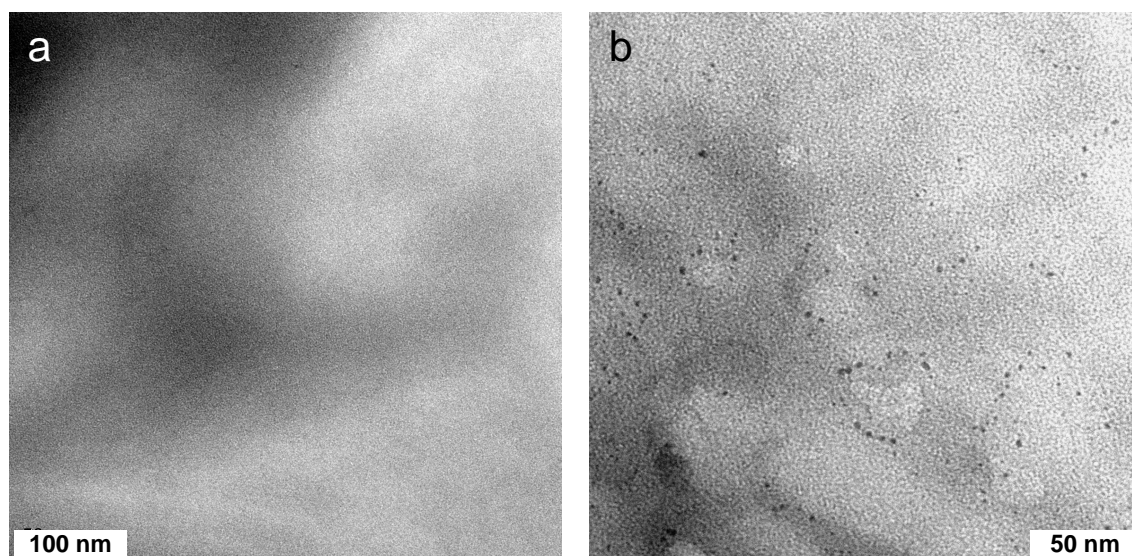


Fig. 3.7: TEM images of the 2nd generation ligand **L2** (a) and complex **C2.3(6.0)** (b). Films from CHCl_3 solution onto lacey carbon coated copper grids.

Since the differences in electron density between the atoms of the different parts (polyamine core, benzyl groups, alkyl shell of the poly(propylene imine) derivatives) are minor, no contrast in the image of **L2** is caused and no structure is observed under TEM. However, after complexation, dark spots appear in the bright field TEM images of **C2.3(6.0)**. Due to its high electron density, the coordination of copper(II) to selected parts of the dendrimer improve the contrast and allows the observation under the microscope. Together with elemental analysis and MALDI-ToF MS, this is a further direct evidence of dendrimers containing metal centres.

The size of the 2nd generation particles was determined measuring their largest diameter in the images of the complex **C2.3(6.0)**. Several images of the same magnification were evaluated in order to accumulate enough data for the statistics. Fig. 3.8a shows one sample section where the size was measured. The histogram on the right presents the distribution of particles according to their size. The particle size is rather homogeneous. The average diameter D_{av} is about 2 nm. This value is smaller than the hexagonal lattice constant of 4.38 nm, calculated from X-ray measurements for the same generation ligand **L2**, cf. 3.9.1.1, but coincides with the estimated diameter of the poly(propylene imine) core plus benzamide units: 1.86 nm^[188], cf. Fig. 3.9. It is consistent with the coordination of copper(II) to the donor atoms of the protonated poly(propylene imine) which are placed at the outer amide part of the polar core of the dendrimer, as will be shown by means of spectroscopic analysis cf. 3.5 - 3.7. The length of the apolar shell of the alkoxy benzoyl groups surrounding the core 1.26 nm is given by subtracting the diameter of the core of 1.86 nm from the hexagonal lattice constant a_h of 4.38 nm (cf. Fig. 3.9). The 5th generation complexes, cf. Fig. 3.8b, exhibit an average size of approx.

3 nm. This generation possesses an intercolumnar distance of $a_h = 5.94$ nm in the hexagonal columnar mesophase, cf. 3.9.1.1. Subtracting the apolar shell as above, the inner core shows a diameter of ca. 3.4 nm. This distance fits well with the one of about 3 nm as observed in TEM.

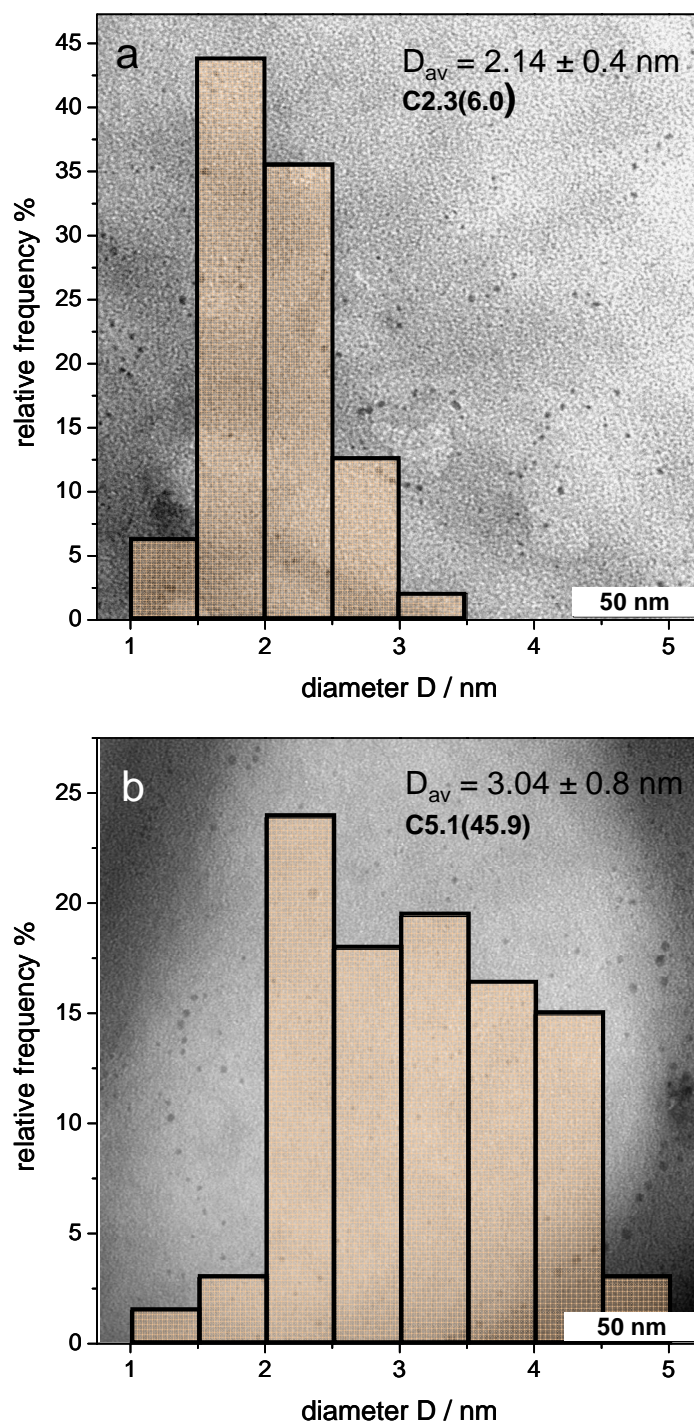


Fig. 3.8: Particle size distribution and average diameter D_{av} of the copper complexes from TEM images. a) 2nd generation complex C2.3(6.0), b) 5th generation complex C5.1(45.9).

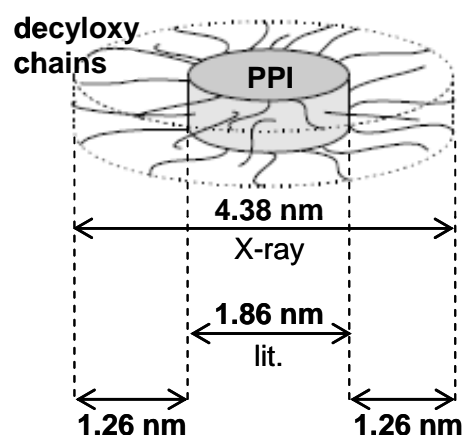


Fig. 3.9.: Schematic representation of the 2nd generation dendrimeric ligand **L2** and dimensions of the poly(propylene imine core) and decyloxy chains estimated from X-ray diffractometry^[188].

Electron energy loss spectroscopy, EELS of the samples was performed to determine the nature of the observed atoms. The $L_{2,3}$ ionisation edge of copper evidenced the presence of copper centres in the complexes. The ionisation state could not be determined by EELS. Typical EELS spectrum of copper is presented in Fig. 3.10.

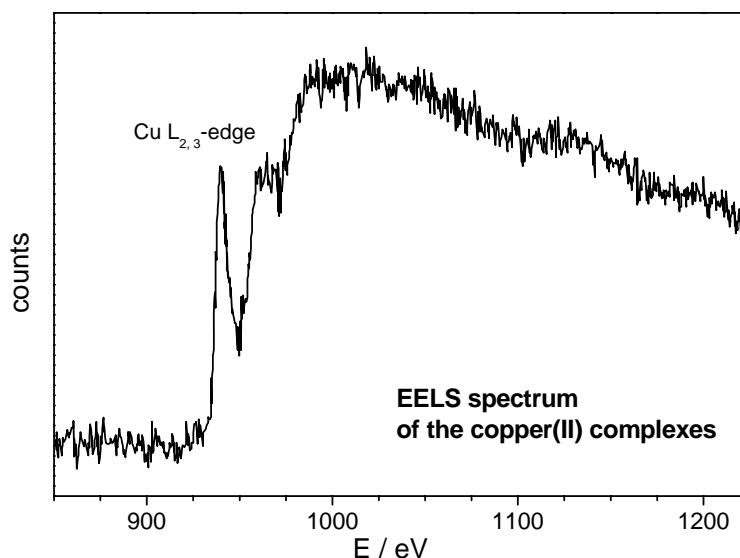


Fig. 3.10: EELS electron energy loss spectrum of the 2nd generation complex **C2.4(5.2)** showing the $L_{2,3}$ ionisation edge of copper.

In summary, TEM has been successfully used to image the dendrimeric copper(II) complexes. It has given direct information about the dendrimer shape, spherical or cylindrical, and size of their cores (2 - 3 nm diameter) depending on the generation. It has also corroborated the relatively narrow dispersity of the dendrimer sizes. Finally through EELS spectroscopy, the presence of copper in the dendrimer cores has been confirmed.

3.5 FTIR-INFRARED SPECTROSCOPY

3.5.1 FT-Infrared Spectroscopy: Introduction

Fourier transform infrared spectroscopy allows the observation of vibrational transitions of molecules. As a good approximation, these vibrations can be described with a simple harmonic oscillator model, where the bonds between atoms or group of atoms are represented by springs. The energy of the vibration is then described by the Hook law, and the wavenumber, $\tilde{\nu}$ (related to the frequency by $\tilde{\nu} = \nu / c$), of a vibration is given by Eq. 3.7:

$$\tilde{\nu} = \frac{1}{2\pi c} \sqrt{\frac{f}{m_r}} \quad \text{Eq. 3.7}$$

where c is the velocity of light in vacuum, f is the “spring constant” reflecting the bond strength and m_r is the reduced mass of the group of atoms involved in the vibration ^[248].

In order to observe a transition in the infrared spectrum, a change in the dipole moment, caused by variations in the symmetry of the charge density distribution around the considered bond, is necessary. The greater the change of the dipole moment, the stronger will be the absorption of infrared light. Therefore polar bonds show strong IR absorption.

FTIR of the copper complexes was performed with the aim of obtaining structural information of the dendrimeric copper(II)-complexes. In particular, to determine:

- i. the copper coordinating groups in the ligand: amine or amide (oxygen or nitrogen), since these are the moieties available in the dendrimer for copper complexation,
- ii. the role of nitrate, ligand or counter ion, in the complex. Comparison to the complex with tetrafluoroborate,
- iii. the presence of HNO_3 in the complex as expected because of the partial decomposition of the copper nitrate and as suggested by elemental analysis,
- iv. the presence or absence of impurities such as copper nitrate and basic copper nitrate.

3.5.2 FTIR-Spectrum of the Ligands

The main features of the ligand spectra are discussed first and constitute the basis for the analysis of the complex spectra. The bands assignment succeeds according to bibliographic data^[17, 107, 125, 175, 188, 248-253] and by comparison with spectra of precursors or fragments of the different parts, core and periphery of the dendrimeric structure. As an example, spectra of the 3rd generation 3,4-decyloxybenzoyl-functionalized poly(propylene imine) ligand **L3** are presented in Fig. 3.11 and Table 3.8.

The FTIR spectra of the ligands of every generation exhibit characteristic bands of the specific groups in the dendrimer:

- i. bands corresponding to the amide groups: a N-H stretching band at 3321 cm^{-1} of medium intensity. Amide I band corresponds to the stretching of C=O bonds at 1632 cm^{-1} and has medium intensity. Amide II and III bands correspond to a mixture of C-N stretching and N-H bending modes at 1545 and 1224 cm^{-1} and have medium intensity. A band corresponding to the stretching of amidate group $\text{O}=\text{C}-\text{N}^-$, is also observed at 1581 cm^{-1} . The position of the N-H stretching band tends to shift to higher frequencies with increasing generation, parallel to a decrease in the intensity. For the remaining generations this band was found in the range $3292 - 3321\text{ cm}^{-1}$.
- ii. stretching vibrations of the C-H bonds of propyl units and butyl core of the PPI and the decyloxy chains in the periphery, which appear as several strong bands in the range $2955\text{-}2854\text{ cm}^{-1}$.
- iii. stretching vibrations of the aromatic (Ar) rings ArC-H (3070 cm^{-1} , w) and ArC-ArC (1601 , 1510 and 1467 cm^{-1} , m, s, m respectively) bonds in the benzamide groups in the outer part of the core.
- iv. the strong absorption of the asymmetrical vibration of the aromatic (Ar) aliphatic ether bond C-O-C bond at 1272 cm^{-1} and the weak absorption of the symmetrical mode at 1068 cm^{-1}
- v. the tertiary amine exhibit several bands of medium or low intensity in the region from $1400 - 1000\text{ cm}^{-1}$ corresponding to vibrations of the C-N bonds. By comparison with the unsubstituted poly(propylene imine) probably bands at 1390 , 1379 and 1159 . These bands are not very specific and their assignment has to be taken with caution. Some further tertiary amine bands around 2817 , 2738 , 2678 and 2603 cm^{-1} are also observed.

Additionally, multiple deformation bands of lower intensity corresponding to the above-mentioned bonds are observed at lower frequencies. These bands are less specific and unambiguous assignment is not possible. The position of the bands of higher and lower generations is, unless otherwise indicated above, generation independent; differences of maximal $\pm 4 \text{ cm}^{-1}$ are observed. These variations are attributed to the limited spectral resolution of the FTIR spectrometer.

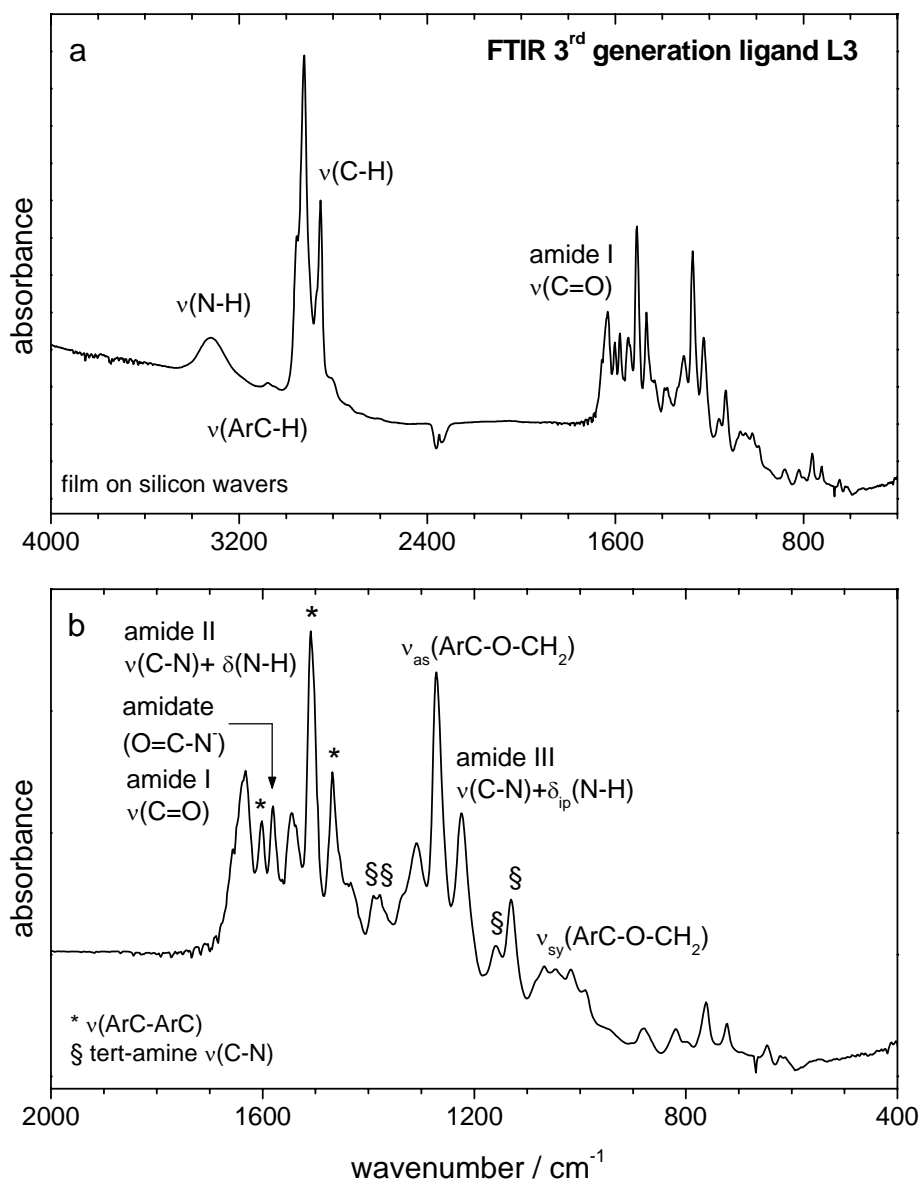


Fig. 3.11: FTIR Spectrum of the acylated 3rd generation poly(propylene imine) dendrimer, L3. a) 4000 - 400 cm^{-1} , b) magnification of the range 2000 - 400 cm^{-1} . Only bands corresponding to relevant vibrations are labelled. Film from CH_2Cl_2 on silicon wavers (double sided polished). *: $\nu(\text{ArC-ArC})$, §: tert-amine $\nu(\text{C-N})$.

Table 3.8: Main absorption bands of the 3rd generation PPI dendrimeric ligands.

moiety - vibration	band / cm ⁻¹	moiety - vibration	band / cm ⁻¹
NHC=O		Ar	
$\nu(\text{N-H})$	3321	$\nu(\text{ArC-H})$	3070
$\nu(\text{C=O})$	1632	$\nu(\text{ArC-ArC})$	1601
$\nu(\text{C=O}) + \delta(\text{N-H})$	1545		1510
$\nu(\text{C=O}) + \delta_{\text{ip}}(\text{N-H})$	1224		1467
N-C=O		ArC-O-C₁₀H₂₁	
$\nu(\text{N-C=O})$	1581	$\nu_{\text{as}}(\text{ArC-O-C})$	1272
		$\nu_{\text{sy}}(\text{ArC-O-C})$	1068 w
-CH₂-		NH⁺-C₃	
$\nu(\text{C-H})$	2955		2817
	2924		2738
	2869		2678
	2854	$\nu(\text{N-C}_3)$	2603
			1390
			1379
			1159

3.5.3 FTIR-Spectrum of the Copper(II) Complexes

Through the complexation of copper, the bands of the coordinating moieties in the ligand are expected to be affected, giving evidence of the copper location in the dendrimer. As an overview, the FTIR spectrum of the 3rd generation complex **C3.1(12.0)** is presented in Fig. 3.12. The main features are labelled and will be considered in detail in the next sections.

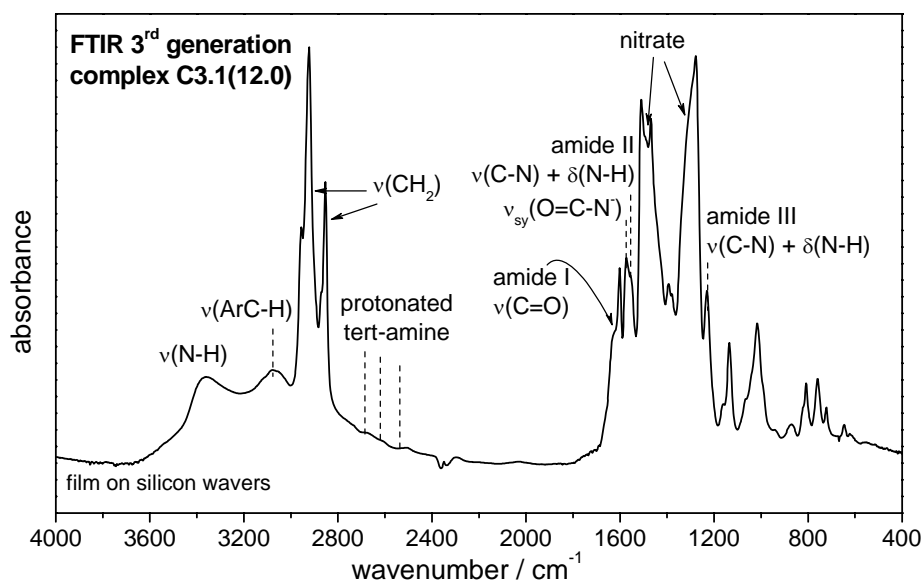


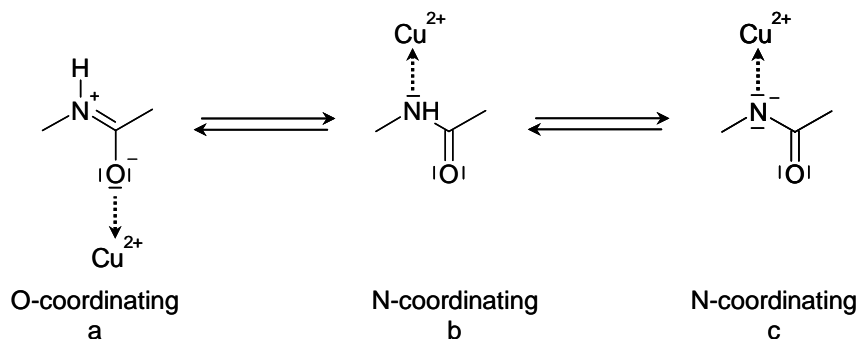
Fig. 3.12: FTIR Spectrum of the 3rd generation dendrimeric copper complex, **C3.1(12.0)**. Only bands corresponding to relevant vibrations are labelled. Film from CH₂Cl₂ on silicon wafers (double sided polished).

The copper complexed samples were prepared as films from CH_2Cl_2 solution onto double polished silicon wafers. It was not possible to disperse the complex in KBr because of displacement of the bromide by the nitrate with evolution of Br_2 as indicated by the violet colour of the pellets after preparation.

3.5.3.1 Coordinating Groups in the Ligand: Amine or Amide

The available moieties for copper(II) complexation in the benzoyl substituted poly(propylene imine) dendrimers are the tertiary amines in the inner core of the PPI and the secondary amide groups in the interphase between the polar PPI core and the apolar alkoxy shell. Amines are strong nucleophiles, in principle favoured to coordinate copper. Coordination to tertiary amine should be accompanied by the appearance of $\nu(\text{N-Cu})$ bands of medium intensity in the far infrared range of the spectra^[254-257]. FTIR spectra were recorded only down to 400 cm^{-1} , thus it is not possible to draw definitive conclusions concerning the N-Cu bands.

Although amides are not as popular copper ligands as the amines, they are also able to coordinate copper in a broad variety of compounds^[249, 256, 258-264]. The amide moiety exhibit two possible electron donating sites: nitrogen and oxygen. Their ability to coordinate copper is illustrated through the resonance structures that describe the amide bond, cf. Scheme 3.3.



Scheme 3.3: Resonance structures of the amide bond involved in the coordination of copper. a) through the oxygen, b) through the neutral nitrogen, c) through a deprotonated nitrogen.

Assumed coordination through amide oxygen (resonance structure in Scheme 3.3a, the bond $\text{C}=\text{O}$ would lose its double bond character, i.e. it would weaken by coordination of copper. In consequence the amide I band at $\sim 1632\text{ cm}^{-1}$ corresponding to the $\nu(\text{C}=\text{O})$ vibration should shift to lower wavenumbers according to Eq. 3.7. The shift is not only determined by the decrease of the bond strength (spring constant f in Eq. 3.7) but also the presence of a heavy ion, the copper(II), coordinated to the oxygen, increases the reduced mass of the system which is inversely proportional to the wavenumber, contributing as well to the shift to lower energies, i.e. to smaller $\tilde{\nu}$ -values. Simultaneously the amide II

and III bands at ~ 1545 and 1224 cm^{-1} , which are partially associated to the stretching vibrations of the C-N bond, should shift to larger energy as result of the increase of its double bond character. The N-H bond is likewise strengthened under this assumption and its absorption in the infrared spectra should be shifted to higher wavenumbers compared to the $\nu(\text{N-H})$ band in the ligand. In case of nitrogen coordination of a neutral amide, cf. Scheme 3.3b, the bands should shift in the opposite direction. A third possibility is the coordination through a deprotonated amide nitrogen, i.e. the amidate $\text{O}=\text{C}-\text{N}^-$, cf. Scheme 3.3c. Under these conditions, the N-H stretching band should disappear and a new band corresponding to the stretching of the anion $\text{O}=\text{C}-\text{N}^-$, should appear, according to the literature at around 1578 cm^{-1} [260]. All possibilities are considered in Table 3.9 on the basis of the 3rd generation copper(II) complex **C3.1(12.0)**, as example, whose spectrum is compared in Fig. 3.13 with that of the ligand **L3**.

Table 3.9: Amide O-coordination vs amide N-coordination to copper. Expected and observed shifts of the amide bands.

Vibration	Literature [248, 250, 256, 258, 260, 265, 266]	L3 / cm^{-1}	O-coordination $\bar{\nu} / \text{cm}^{-1}$		N-coordination $\bar{\nu} / \text{cm}^{-1}$			
			a		b		c	
			expct	obs	expct	obs	expct	obs
$\nu(\text{N-H})$	3330-3060	3321	↑	↑3361	↓	-	-	-
Amide I $\nu(\text{C=O})$	1640-1600	1632	↓	↓1620sh	↑	-	↓	↓1620sh
Amide II $\nu(\text{C-N}) +$ $\delta(\text{N-H})$	1570-1515	1545	↑	↑1556sh	↓	-	-	-
Amide III $\nu(\text{C-N}) +$ $\delta(\text{N-H})$	1250	1224	↑	↑1230	↓	-	-	-
$\nu_{\text{sy}}(\text{O}=\text{C}-\text{N}^-)$	1578 w	1581	-	-	-	-	↓	↓1573

a, b, c: cf. Scheme 3.3, **expct**: expected, **obs**: observed, ↑ / ↓: shift to higher- / lower wavenumbers, -: band does not occur.

Fig. 3.13 shows selected regions of the FTIR spectra of 3rd generation complex **C3.1(12.0)** and ligand **L3**. The shifts of the amide bands are consistent with amide O-coordination: The band in the ligand at 3321 cm^{-1} , corresponding to the stretching mode of the N-H bond, is shifted to a broad band at 3361 cm^{-1} after complexation. Likewise amide II and III bands appear at higher wavenumbers, 1556 and 1230 cm^{-1} , than in the ligand (1545 and 1224 cm^{-1}). The intensity of the amide I band at 1632 cm^{-1} is almost suppressed through complexation and a new band at 1620 cm^{-1} appears. Band at 1620 cm^{-1} corresponds to those C=O which are coordinated to copper [258] and the band at 1632 cm^{-1} of decreased intensity, corresponds to the fraction of carbonyl groups

which are free or not O-coordinated. The coordination of copper to oxygen should be furthermore evidenced by a $\nu(\text{O}-\text{Cu})$ band. This band appears unfortunately at $\leq 400 \text{ cm}^{-1}$ [258, 266] under the limit of detection of our device, therefore cannot provide direct support of this coordination.

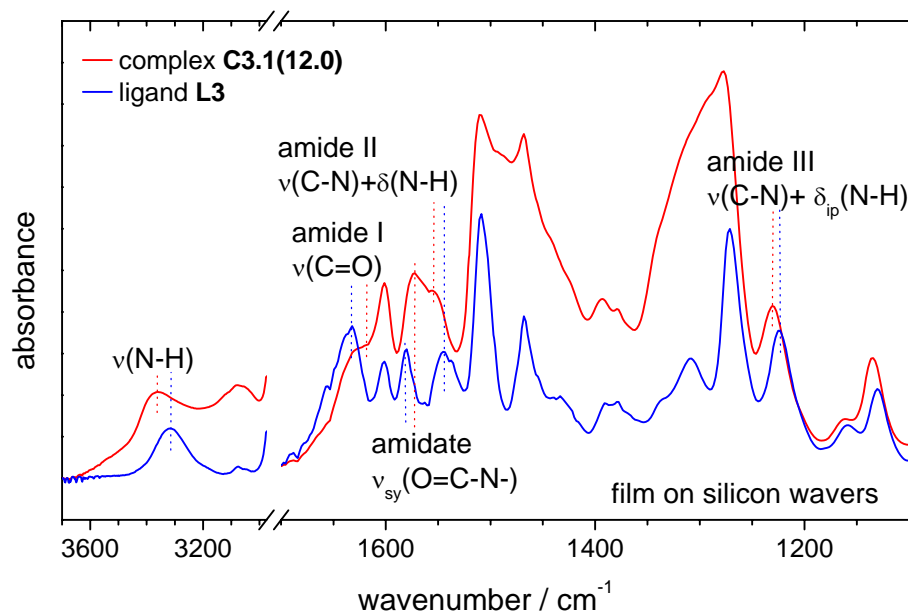


Fig. 3.13: FTIR Spectra of selected regions of the 3rd generation copper(II) complex **C3.1(12.0)** and ligand **L3**. — : **C3.1(12.0)**; — : **L3**.

The coordination of copper to neutral amide nitrogen is excluded according with the results presented in Table 3.9. The bands in the studied regions shift in the opposite direction that the expected for N coordination. However, an enhanced stretching band of the amidate is observed at 1573 cm^{-1} ; it indicates clearly the coordination of deprotonated amide nitrogen to copper. According to the literature [249, 259, 260, 267], the amide nitrogen tend to deprotonate through coordination to metal, being this resonance structure the most favoured when coordinating through the nitrogen atom.

In conclusion, FTIR analysis of the amide bands indicates thus the coexistence of both O- and N-coordination in the dendrimeric complexes. All generations belonging to the series of highest copper loading, exhibit similar qualitative behaviour. The shifts of the analysed bands are furthermore of the same order of magnitude as those described for the 3rd generation.

The evolution of the $\nu(\text{N-H})$, $\nu(\text{C=O})$ and $\nu(\text{O=C-N}^-)$ bands with increasing copper content n , for the 2nd generation is depicted in Fig. 3.14. A shift (relative to the ligand absorption, i.e. the difference in wavenumbers between the stretching bands $\nu_{\text{C2.i(n)}}$ and ν_{L2}) of the $\nu(\text{N-H})$ band to higher frequencies with increasing copper content is observed. Simultaneously, the incorporation of copper induces a shift of the $\nu(\text{C=O})$ and

$\nu(\text{O}=\text{C}-\text{N}^-)$ lines to lower wavenumbers. The shift occurs sequentially and proportional to the copper content. This indicates that the shift is due to a real bond between copper and amide and not to a perturbation of the amides by copper salt in the proximity.

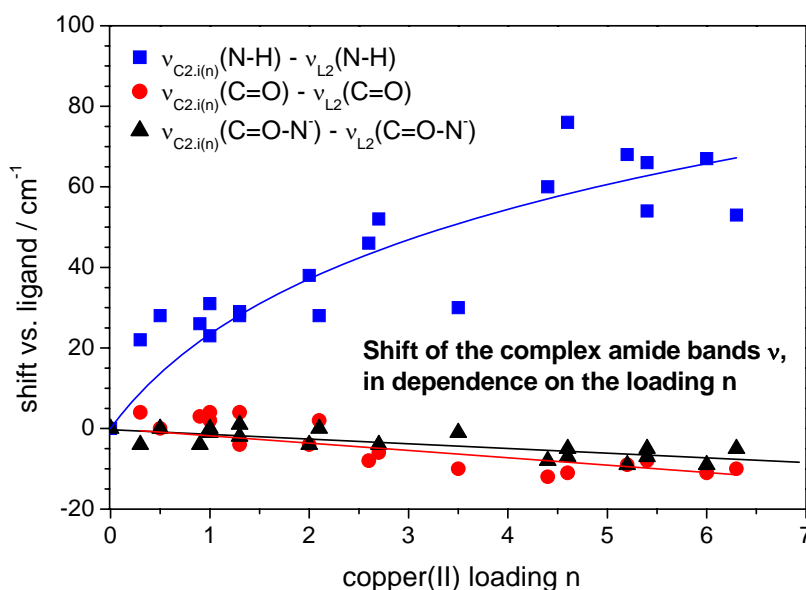
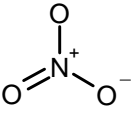
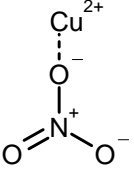
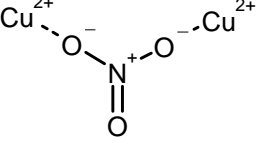
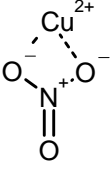


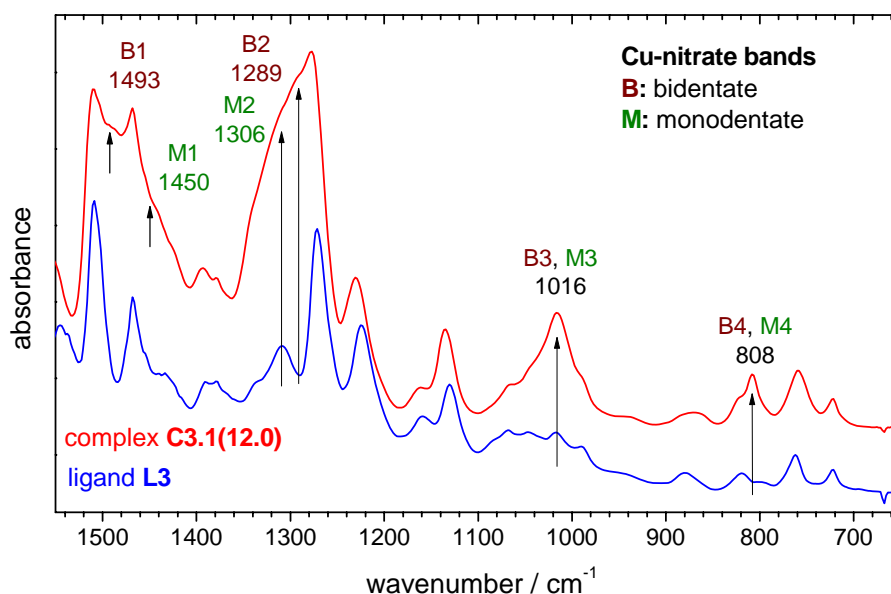
Fig. 3.14: Influence of the copper(II) loading n , on the position of the maximum of the stretching bands $\nu(\text{N-H})$, $\nu(\text{C}=\text{O})$ and $\nu(\text{O}=\text{C}-\text{N}^-)$ with respect to the corresponding bands in the ligand (copper loading zero). Fits are drawn to guide the eye.

3.5.3.2 Role of the Nitrate. Comparison with the Complex from Tetrafluoroborate

The nitrate anion is integrated into the complex because it is the counter ion of the copper salt, copper nitrate trihydrate, used for complexation. In the dendrimeric complex it can behave as counter ion as well or, since the nitrate itself is a coordinating ion, as further ligand for copper. As ligand, the nitrate exhibits multiple coordination possibilities through one or more of its oxygen atoms, being thus able to act as bridge or as chelate ^[258]. These possibilities are reflected in its FTIR by absorptions in different regions of the spectrum, which allow the elucidation of the role of nitrate in the complexes. Table 3.10 illustrates the usual absorption bands of ionic, monodentate and bidentate nitrates, according to literature data, and Fig. 3.15 displays the FTIR spectra of 3rd generation copper(II) complex **C3.1(12.0)** and ligand **L3** in the absorption range of the nitrate.

Table 3.10: FTIR bands of ionic, monodentate and bidentate NO_3^- from the literature.

Ionic [255, 268, 269]	Monodentate [215, 269, 270]	Bidentate [211, 215, 269, 271]
cm^{-1}	cm^{-1}	cm^{-1}
		
		
		bridging chelate
1365 - 1375	1406 - 1445	1505 - 1465
1022 - 1060	1298 - 1314	1280 - 1301
	1012 - 1023	1010 - 1055
	1022 - 1035	1025 - 1030
835 - 820	820 - 830	810 - 816
700 - 718	721 - 728	740 - 748
	708	695 - 702

**Fig. 3.15:** Nitrate NO_3^- FTIR bands in the 3rd generation complex **C3.1(12.0)**. **B:** bidentate, **M:** monodentate nitrate bands (cm^{-1}). For comparison the spectrum of the 3rd generation ligand **L3** is presented.

Compared to the ligand, the copper complex exhibits a new strong peak at ca. 1493 cm^{-1} (B1) overlapped by the absorptions at 1510 and 1468 cm^{-1} . A shoulder at high frequencies of the 1278 cm^{-1} peak, at ca. 1289 cm^{-1} (B2), appears in the spectrum of the complex, whereas in the dendrimeric ligand of the same generation no peak or shoulder was observed. Furthermore the peaks at 1016 cm^{-1} (B3) and 808 cm^{-1} (B4) which were only weak in the spectra of the ligand, are strongly enhanced through the complexation. The

appearance of these absorptions is in good agreement with the reported (see Table 3.10 for references) absorptions for bidentate nitrate, therefore we can assume that nitrate coordinating copper either through two of its oxygen atoms as chelate or as a bridge between two copper centres are present in the PPI copper complexes described here. Whether nitrate acts as chelate or bridge between two copper centres could not be clearly determined on the basis of infrared spectroscopy. A comparison with the absorption bands reported for bridging bidentate nitrates (1519 , 1291 and 1008 cm^{-1})^[258] suggests however the last coordination.

Less strong than the changes described above but still significant are the new shoulder at 1450 cm^{-1} (M1) and the shoulder at ca. 1306 cm^{-1} (M2). The last one is already observed in the spectrum of the ligand as a weak peak, becomes nevertheless after coordination clearly more intensive. Both absorptions can be ascribed to the occurrence of monodentate nitrate in the copper complexes. The absence of marked absorptions around 1365 - 1375 cm^{-1} excludes the presence of free anionic nitrate in the complexes. That means, all present nitrate in the complexes is coordinated to copper.

Bands corresponding to the Cu-ONO₂ bond appear according to the literature^[258, 266] at around 250 - 350 cm^{-1} , for anhydrous copper nitrate at 360 cm^{-1} ^[272], beyond the detection range of the used spectrometer therefore could not give further direct evidence of copper nitrate coordination.

The assignment of the aforementioned bands to nitrate is furthermore supported by the comparison of the infrared spectra of copper complexes from nitrate with that prepared from tetrafluoroborate. In Fig. 3.16 are depicted the FTIR spectra of the 2nd generation complexes **C2.22(2.9)** and **C2.10(2.7)**; the former is prepared from copper tetrafluoroborate hydrate and the latter from copper nitrate trihydrate, both exhibit approximately the same copper loading: 2.9 and 2.7 copper centres per dendrimeric ligand respectively. The absorption band of the tetrafluoroborate^[218, 228] is observed at 1065 cm^{-1} as a very strong and broad band, which is not present in the spectrum of the complex from copper nitrate. The spectrum of the ligand exhibits only a very weak band at 1068 cm^{-1} , attributed to the symmetrical mode of the $\nu(\text{C-O-C})$ vibration of the ether groups. In the spectrum of tetrafluoroborate no absorptions corresponding to the nitrate are observed: the band at 1493 cm^{-1} (B1) in the spectra of the nitrate-complex does not occur in the tetrafluoroborate complex and the peaks at 1510 and 1468 cm^{-1} are well resolved as is the case in the ligand. The broad shoulders on the high frequencies side of the peak at 1278 cm^{-1} , at ca. 1289 cm^{-1} (B2) and 1306 cm^{-1} (M2) which appear in the spectrum of complexes prepared from the copper nitrate trihydrate are not seen in the spectrum of the tetrafluoroborate. Since both complexes exhibit similar copper loadings and no other parameter than the anion of the starting salt is changed in one and other

complex we can conclude that the differences in the spectra can be attributed to the anion.

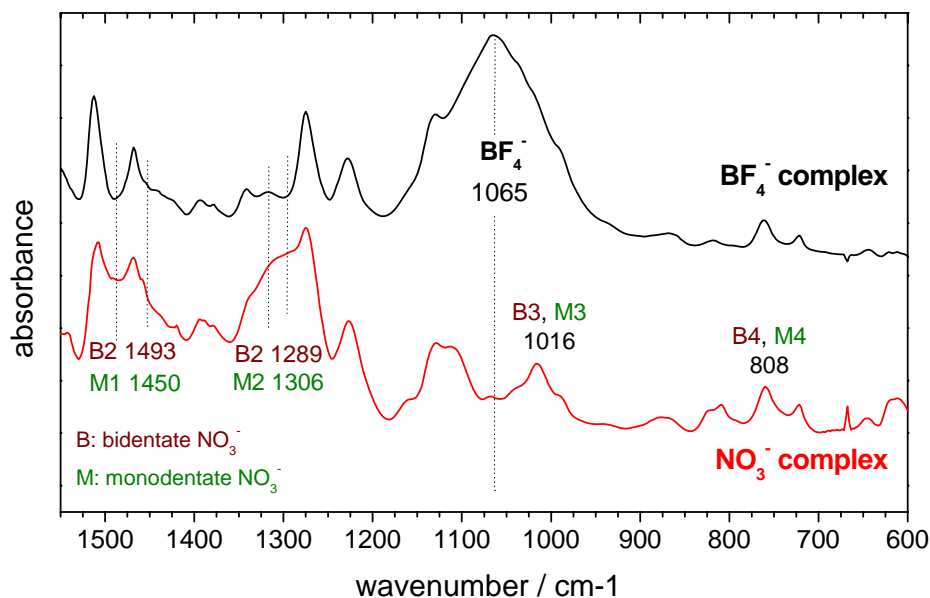


Fig. 3.16: Anion absorption bands in the 2nd generation complexes: BF_4^- vs. NO_3^- . Plotted complexes **C2.22(2.9)** (from BF_4^-) and **C2.10(2.7)** (from NO_3^-).

FTIR of the dendrimeric copper(II) complexes show, according to the literature and by comparison to the spectra of the dendrimeric ligands and tetrafluoroborate complex, that the nitrate takes part in the coordination sphere of copper. The nitrate coordinates copper partially as monodentate but mainly as bidentate through two of its oxygen atoms, probably bridging two copper centers.

3.5.3.3 HNO₃: Tertiary Amine Protonation

It has been shown (cf. 3.1.2.1) that under complexation conditions, the copper nitrate trihydrate partially decomposes into basic copper nitrate and nitric acid. Elemental analysis of the complexes reveals furthermore higher nitrogen and oxygen contents in the complexes than those required to achieve the electroneutrality of the copper ions present in the complex, cf. 3.2. The difference could be well explained assuming the presence of additional nitrate groups counterbalanced with protons. Whether these additional nitrates are present as nitric acid mixed with the dendrimeric copper complex or are intrinsic to the complex is discussed in terms of the FTIR spectra.

The literature ^[273] describes strong or very strong absorption bands for nitric acid at 3400 cm⁻¹ ($\nu(\text{O-H})$), 1675 cm⁻¹ ($\nu_{\text{as}}(\text{NO}_2)$), 1300 cm⁻¹ ($\nu_{\text{sym}}(\text{NO}_2)$), 925 cm⁻¹ ($\nu(\text{N-O})$), 680 cm⁻¹ (δ_{sym}) and 610 cm⁻¹ (δ_{as}). The bands at 3400 cm⁻¹ and the band at 1300 cm⁻¹ can be confused with the stretching band of water and the symmetric stretching band of bidentate nitrate which absorb at the same frequencies. Nevertheless the rest of the

absorptions, specially that at 1675 cm^{-1} ($\nu_{\text{as}}(\text{NO}_2)$), appear at wavenumbers where the dendrimeric complexes give no significant signal. If available, the asymmetric stretching band of the nitric acid, $\nu_{\text{as}}(\text{NO}_2)$ at 1675 cm^{-1} , should be therefore clearly observed. The absence of this signal in the spectra excludes the presence of free nitric acid in the complex, cf. Fig. 3.17.

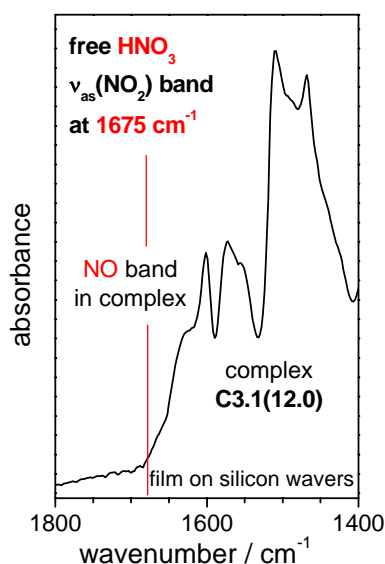


Fig. 3.17: FTIR spectrum of the complex **C3.1(12.0)** in the $1800\text{-}1400\text{ cm}^{-1}$ range.

The participation of the “additional” nitrate groups in the coordination of copper must be accompanied by a charge balance with further positive ions, i.e. protons. The natural protonation sites in the poly(propylene imine dendrimers) are the tertiary amine groups. Protonation of related poly(ethylene imine) derivatives is well known in the literature ^[136], through protonation with hydrochloric acid a new band corresponding to the tertiary ammonium salt at 2615 cm^{-1} appears in the spectrum of the poly(ethylene imine). The poly(propylene imine) dendrimeric ligand exhibit tertiary amine bands at 2817 , 2738 , 2678 and 2603 cm^{-1} . After complex formation the absorptions at 2817 and 2738 cm^{-1} smooth down, the band at 2678 cm^{-1} is shifted to 2687 and enhanced in intensity and two new broad band at 2620 and 2508 cm^{-1} appear, cf. Fig. 3.18. This behaviour is characteristic of quaternisation of tertiary amines ^[252, 253].

These observations lead to the conclusion that the “excess” of nitrate anions suggested by elemental analysis are present as further copper ligands, as already shown by the presence of bidentate and monodentate nitrate bands, and their charge is balanced with the positive charge of the tertiary ammonium salts in the inner core of the poly(propylene imine). In consequence coordination of copper by the tertiary amine groups in the dendrimer scaffold can not occur, since HNO_3 has protonated the dendrimeric core.

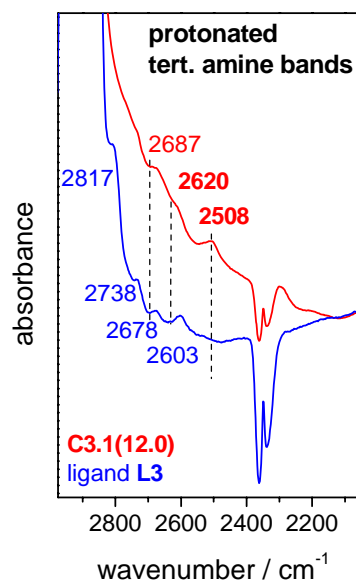


Fig. 3.18: Tertiary amine bands and tertiary ammonium salt bands of complex **C3.1(12.0)** with reference to the ligand **L3**. Ammonium bands indicated in bold.

3.5.3.4 Copper Nitrate Trihydrate and Basic Copper Nitrate

Free $\text{Cu}(\text{NO}_3)_2 \cdot 3\text{H}_2\text{O}$ has been extensively characterised by means of FTIR [272, 274]. It exhibits several absorptions of medium to strong intensity at 3542, 3497, 3320 and 3095 cm^{-1} , corresponding to the $\nu(\text{O-H})$ vibration of water and some others in the region from 1700 to 1000 cm^{-1} , corresponding to nitrate stretching modes and H_2O bend modes. In the spectra of higher loaded dendrimeric complexes, no peak broadening on the $\nu(\text{N-H})$ absorption at 3361 cm^{-1} indicating the presence of water, occurs. The described absorptions for nitrate in the copper nitrate trihydrate (1500, 1315, 1270, 1034 and 1010 cm^{-1}) coincide with absorption of aromatic rings, amide groups and ether groups already available in the ligand, therefore it is difficult to ascertain if there is a contribution of free copper nitrate to these bands. Decisive are the bands of medium intensity at 895, 580 and 460 cm^{-1} observed in the far infrared spectrum of copper nitrate trihydrate. These bands correspond respectively to the rocking and wagging vibration modes of copper-coordinated water and to the stretching of the Cu-OH_2 bond. No absorption band at 895 cm^{-1} is observed in any of the complex spectra, neither the band at 580 cm^{-1} , cf. Fig. 3.19. Occasionally, a very weak band at 560 cm^{-1} appears. This band is nevertheless present already in the ligand, no significant change in absorption frequency or intensity is observed through complexation. In some spectra an extreme weak band around 460 cm^{-1} is observed. Its appearance is nevertheless not correlated with the water content determined by elemental analysis and is therefore not significant. From the absence of the copper-water bands, we can exclude the presence of free copper nitrate trihydrate as a significant impurity in the dendrimeric copper complex.

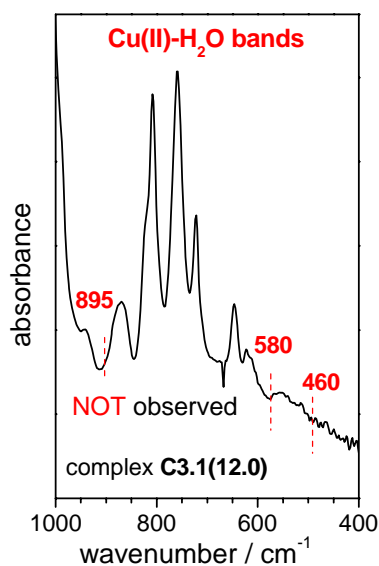


Fig. 3.19: Absence of the Cu-OH₂ bands of Cu(NO₃)₂·3H₂O in the FTIR spectrum of the 3rd generation complex **C3.1(12.0)**. Position of the missing bands indicated by dotted vertical red lines.

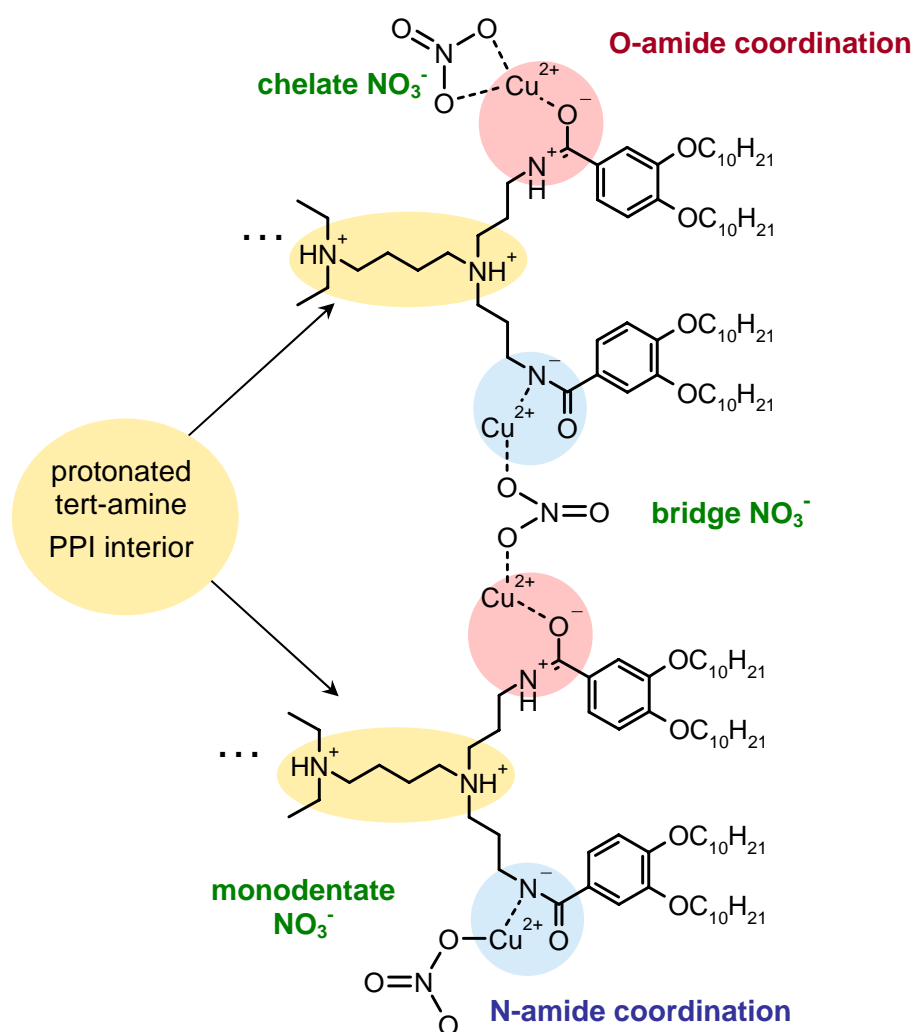
The basic copper nitrate, Cu₂(NO₃)(OH)₃, exhibit simply stretching bands from hydroxyl and nitrate groups at 3547, 3426, 1422, 1384, 1343 cm⁻¹, and a combination band at 1048 cm⁻¹. Absorptions corresponding to these vibrations are already available in the dendrimeric complex and whether the basic copper nitrate contributes to absorption or not is hard to decide due to the band overlap from one and other species.

The 1st generation complexes in their blue forms **C1.2(1.9)b** and **C1.7(1.0)b** could not be investigated with FTIR, since no film from them could be prepared. They are not soluble in common solvents at room temperature and heating - in bulk or solution - involves the conversion into their green forms **C1.2(1.9)gr** and **C1.7(1.0)gr**. Attenuated total reflection infrared spectroscopy, ATR-FTIR, is excluded as alternative for the same reasons. KBr pellets of the powder are also excluded since anion exchange occurs. Due to these practical difficulties in the sample preparation, FTIR spectroscopy was unfortunately unsuitable to study the structural changes which are supposed to take place in the transformation from the blue into the green form of these complexes.

3.5.3.5 Conclusions

In conclusion, FTIR spectroscopy of the dendrimeric copper(II) complexes, gives evidence of both amido oxygen and amido nitrogen coordination of copper by the dendrimers, i.e. coexistence of N- and O-coordinated copper centres in a dendrimer ligand occurs. The nitrate anion is as well involved in the complexation of copper acting as bidentate ligand, probably as bridge, between copper centres through two of its three oxygen atoms. Chelate nitrates can not be excluded with the data available.

Monodentate nitrate groups are also observed, however in a lower extent. All the nitrate groups are coordinated, no one is present as nitric acid or free counterion. The tertiary amines in the core of the polypropylene imine dendrimers are protonated, they are not any more available for copper coordination. No absorption bands corresponding to copper coordinated water were found. Therefore, water is excluded as further ligand in the coordination sphere of copper. No free basic copper nitrate or copper nitrate trihydrate could be detected under the given conditions. A schematic model of the dendrimeric copper(II) complexes based on the FTIR findings is presented in Scheme 3.4.



Scheme 3.4: Model of the copper(II) complexes of poly(propylene imine) according to the FTIR findings. For clarity depicted for fragments of the 1st generation

3.6 UV-VIS SPECTROSCOPY

3.6.1 Ligand Absorption Bands in the UV-Vis Range

The poly(propylene imine) dendrimeric ligands, **LG** ($G = 1, 2, \dots 5$), exhibit absorption maxima in the ultra-violet region at 254 - 258 nm and 287 - 289 nm in CHCl_3 solutions. They are nearly the same for each generation. No significant solvatochromic effect is observed in solvents of similar polarity such as THF or CH_2Cl_2 . The band at ca. 258 nm corresponds to electronic transitions between the π - π^* orbitals of the aromatic benzene rings. Its position is in good agreement with the absorption estimated by the Scott rules for the present substitution^[250]. The band at ca. 289 nm can be ascribed to n - π^* transitions of the amide carbonyl group^[248]. As an example, the absorption spectrum of the 5th generation ligand, **L5**, is presented together with those of the complex of the same generation **C5.1(45.9)** in Fig. 3.20.

3.6.2 Copper(II) Complexes Absorption Bands in the UV-Vis Range

The light green, slightly yellowish, copper(II) complexes of the poly(propylene imine) dendrimers are expected to exhibit absorption bands close to the ultraviolet, according to the complementarity principle. Spectra of the copper(II) complexes in chloroform solution exhibit absorption spectra similar to those of the ligand, slightly shifted to larger wavelengths, cf. Fig. 3.20. The bands appear now at 265 ± 3 nm and 292 ± 1 nm depending on the generation. No absorption band in the visible range, even for concentrated solutions, is observed. Only a very weak and broad absorption around 770 nm appears at highest loadings. However, a clear broadening on the low energy wing of the band at 289 nm in the near violet is to be seen. The broadening observed in solution becomes a clearly defined shoulder in the film spectra of the complexes in Fig. 3.20, the shoulder observed in the complex spectra at $\lambda = 325 - 450$ nm is in good agreement with the expected values. The absorption in solution is basically the same as in the film, indicating that no significant change in the coordination sphere or geometry takes place by dissolving the complex. This is confirmed by EPR measurements, cf. 3.7. The starting copper salt, copper nitrate trihydrate, is not soluble in chloroform. Therefore, no spectrum could be obtained in that solvent. However, dissolved in THF, a broad band or shoulder (ca. 85 nm width at half maximum) at 290 nm is observed, cf. Fig. 3.20. This band appears between 260 - 375 nm, where the broadening or shoulder is observed in the spectra of the complexes in CHCl_3 . Since free copper nitrate trihydrate is not present in chloroform solution, the observed broadening or shoulder correspond to new transitions induced by the presence of nitrate coordinated to copper, cf. Scheme 3.4, 3.5.3.5.

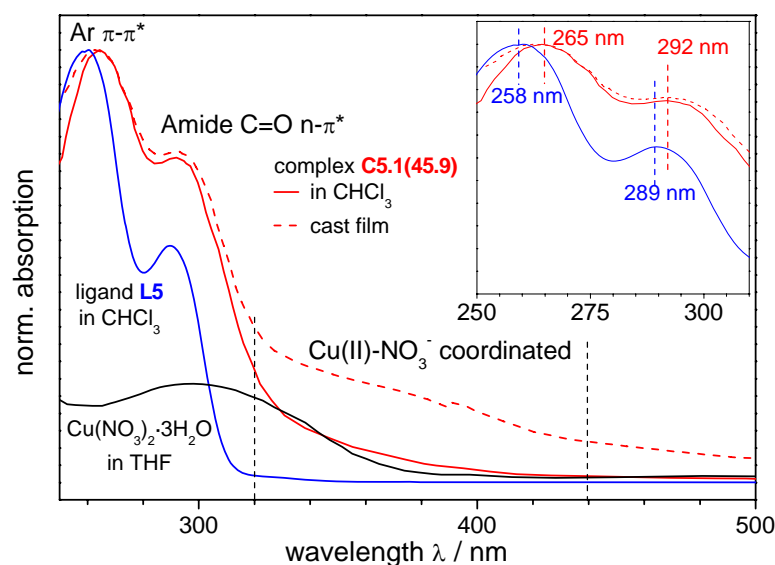


Fig. 3.20: Absorption spectra of the 5th generation complex **C5.1(45.9)** compared to that of the ligand **L5** and free copper nitrate. **C5.1(45.9)** film from toluene solution. Absorption normalised to the absorption of the benzene rings. The vertical dashed lines at $\lambda = 325$ nm and $\lambda = 450$ nm indicate the spectral region where the Cu(II)-NO_3^- coordinated absorption appears.

The spectra of representative 2nd generation complexes **C2.i(n)** (n = copper(II) loading) are plotted in Fig. 3.21. The absorptions are normalized to the absorption of the $\pi\text{-}\pi^*$ band, since the number of benzene rings does not change through complexation and no significant change in the absorption of this band is therefore expected.

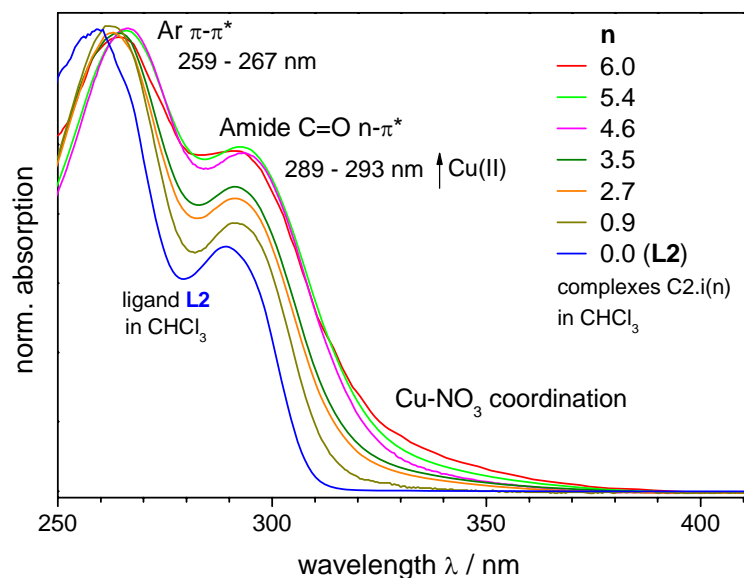


Fig.3.21: Absorption spectra of selected 2nd generation complexes **C2.i(n)** in CHCl_3 solution compared to the ligand **L2**. Plotted **L2** ($n=0$) and **C2.18(0.9)**, **C2.10(2.7)**, **C2.9(3.5)**, **C2.7(4.6)**, **C2.4(5.4)** and **C2.3(6.0)**. Absorptions normalised to the absorption of the benzene rings.

The $n\text{-}\pi^*$ band of the ligand (at 289 nm) corresponding to the carbonyl moiety, becomes stronger and shifts to lower wavelengths with increasing copper loadings (n), indicating that the number of amide moieties involved in the coordination grows with the copper content. Absorption in this spectral region is reported for copper(II) amido complexes with a N_2O_2 coordination^[275]. N_2O_2 coordination is one of the two coordinations determined by ESR spectroscopy for the poly(propylene imine) copper(II) complexes, cf. next section 3.7.2. An enhancement of the slope of the basis line in the region 325–400 nm with increasing copper loading is observed in the absorption spectra of different loaded complexes of the 2nd generation. This increase suggests the gradual participation of further nitrate groups in the coordination of copper as indicated by FTIR spectroscopy. In the literature, these bands are attributed to ligand-to-metal charge transfer transitions^[145, 275–278]. Additionally; only weak absorptions in the visible are reported for amido complexes with N_2O_2 coordination.

The observed thermochromic behaviour of the 1st generation complex **C1.2(1.9)b** could not be studied by means of its absorption spectra. The blue form of the complex is not soluble in usual solvents at room temperature. On heating, it can be dissolved (cf. Scheme 3.1, 3.1.3.2), but its solution is light green, indicating a change in the geometry and/or in the coordination sphere. Likewise it is not possible to obtain a film of it, since the films are also prepared from solutions where the blue form has turned into green.

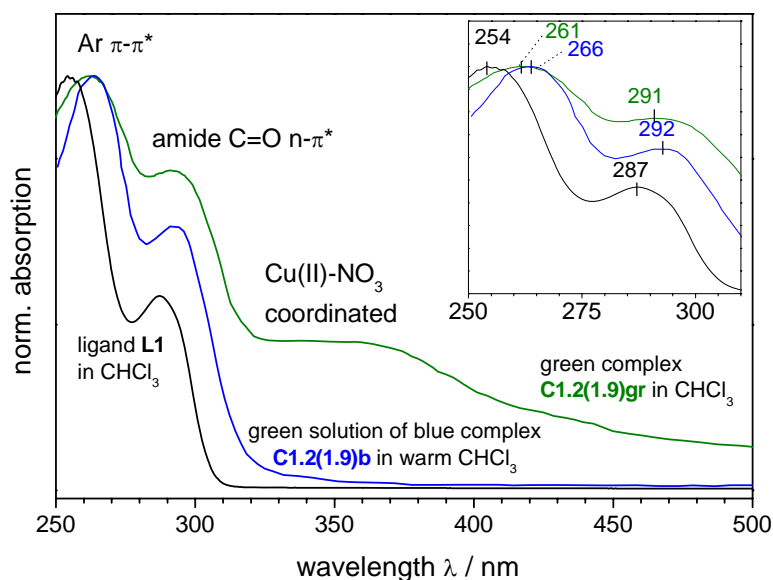


Fig. 3.22: Absorption spectra of the 1st generation complexes **C1.i(n)** compared to the ligand **L1** ($n=0$). Absorptions normalised to the absorption of the benzene rings.

The spectrum of a heated, green solution of **C1.2(1.9)b** in chloroform and the spectrum of a solution of the green complex **C1.2(1.9)gr** (after heating **C1.2(1.9)b** in the solid

state over the melting point, $T_m = 127^\circ\text{C}$) are plotted in Fig. 3.22. The green solution of the **C1.2(1.9)b** in warm chloroform exhibits the same features as the spectra of green complexes of this and higher generations in solution. The spectrum of the green complex **C1.2(1.9)gr**, with a much more pronounced absorption at ca. 360 nm, resembles the film spectra of the higher generations, cf. Fig. 3.20.

3.6.3 Conclusions

The absorption spectra of the copper complexes are red shifted compared to those of the ligands. The relative intensity of the absorption band of the amide (at ca. 287 - 289 nm) grows with increasing copper loading, suggesting that the amide moiety is involved in the copper coordination. A new broad band (or shoulder) corresponding to nitrate coordinated to copper is observed at ca. 325 - 450 nm in the spectra of the copper(II) complexes.

3.7 EPR CHARACTERISATION OF THE COPPER(II) COMPLEXES

EPR, electron paramagnetic resonance spectroscopy of the dendrimeric copper(II)-complexes was carried out by Dr. N. E. Domracheva, Kazan Physical-Technical Institute, Russian Academy of Science in a common cooperation project with Prof. Dr. M. Schwoerer, and Dr. A. Mirea, Experimentalphysik II at the Universität Bayreuth. The results have been published until now in two articles: Domracheva, N.; Mirea, A.; Schwoerer, M.; Torre-Lorente, L.; Lattermann, G.; EPR Characterisation of Cu^{II} Complexes of Poly(propylene imine) Dendromesogens: Using the Orienting Effect of a Magnetic Field. ChemPhysChem., 2005, 6, 1, p. 110-119. and Domracheva, N.; Mirea, A.; Schwoerer, M.; Torre-Lorente, L.; Lattermann, G.; Magnetic Properties of Poly(propylene imine)-Copper Dendromersogenic Complexes: An EPR Study. ChemPhysChem., 2006, 7, 12, p. 2567-2577.

3.7.1 EPR Spectroscopy: Introduction

EPR, electron paramagnetic resonance spectroscopy (also known as electron spin resonance, ESR) is a spectroscopic technique, sensitive to transitions between different electronic spin states in the presence of a magnetic field ^[279-281]. Paramagnetic molecules or atoms, such as radicals and some transition metals with unpaired electrons and systems with quasi-free electrons as conduction electrons in semiconductors are therefore appropriate to be studied by EPR.

Under the application of an external magnetic field, \vec{B} , the degenerated spin states of a free electron split into two different energy states as indicated in Fig. 3.23 left. Two orientations are now possible for the electron spin: parallel to the field \vec{B} (upper energy level) with $m_s = +1/2$ or antiparallel to the direction of the magnetic field (lower energy level) with the magnetic quantum number $m_s = -1/2$. The energy splitting ΔE is proportional to the magnitude, B , of the applied magnetic field, so that $\Delta E = g_e \mu_B B$, where g_e is the g-factor of the free electron and μ_B the Bohr magneton. In the presence of an electromagnetic field with frequency ν , absorption of energy occurs if the resonance condition $\Delta E = h\nu = g_e \mu_B B$ (h is the Planck constant) is fulfilled and transitions between both electronic levels are possible.

In practice, one usually works with a fixed frequency ν_{EM} of the electromagnetic field and the magnetic field is swept until the resonance frequency of the sample ν is equal to that of the electromagnetic field ν_{EM} . Thus, a spectrum is obtained in which the absorp-

tion of energy is plotted as a function of magnetic field strength. Typical frequencies of the electromagnetic field are 34 GHz (Q-band) and 9.7 GHz (X-band). Due to the detection technique the first derivative of the absorption line is recorded, cf. Fig. 3.23 right, spectrum b.

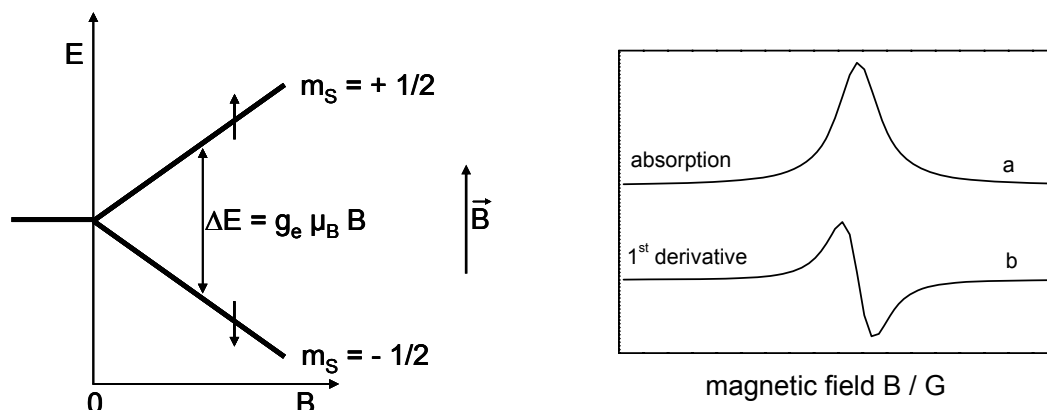


Fig. 3.23: Energy levels for a free electron in the presence of a magnetic field \vec{B} (left) and corresponding spectra recorded by EPR (right). a: absorption spectrum of a free electron, b: usual representation of the absorption as its first derivative. g_e : g-factor of the free electron, μ_B : Bohr magneton, m_s : magnetic quantum number.

A free electron gives rise to only one absorption line. In the presence of atoms, as usually is the case, the value of g deviates from that of the free electron. The deviation is correlated with the nature of the atoms in its vicinity. Furthermore, coupling of the electron spin with the nuclear spin of the atoms in the neighbourhood causes a splitting of the absorption line. This splitting is referred to as hyperfine structure, cf. Fig. 3.24. The coupling constant is denoted by A . The hyperfine splitting provides important structural information about the atoms and geometry in the direct environment of the considered electron. The g -factor and hyperfine coupling may also change depending on the orientation of the molecule in an external magnetic field. So, different values for the g -factor g and the coupling constant A are defined in the space directions x , y and z . This anisotropy yields further information about the surroundings of the unpaired electron.

EPR can provide information about the magnetic properties of the analyte as well, i.e. its antiferromagnetic or ferromagnetic character. The Curie-Weiss law, cf. Eq. 3.8, is given by:

$$I = \frac{C}{T - \theta} \quad \text{Eq. 3.8}$$

where I stands for the integrated intensity, C is the Curie constant, T is the measuring temperature and θ is the Curie-Weiss constant. If the integrated intensity of the temperature dependent EPR-spectrum of the sample follows the Curie-Weiss law, the sample is ferromagnetic for $\theta > 0$ and antiferromagnetic for $\theta < 0$. The intensity, I , is proportional to the magnetic susceptibility χ .

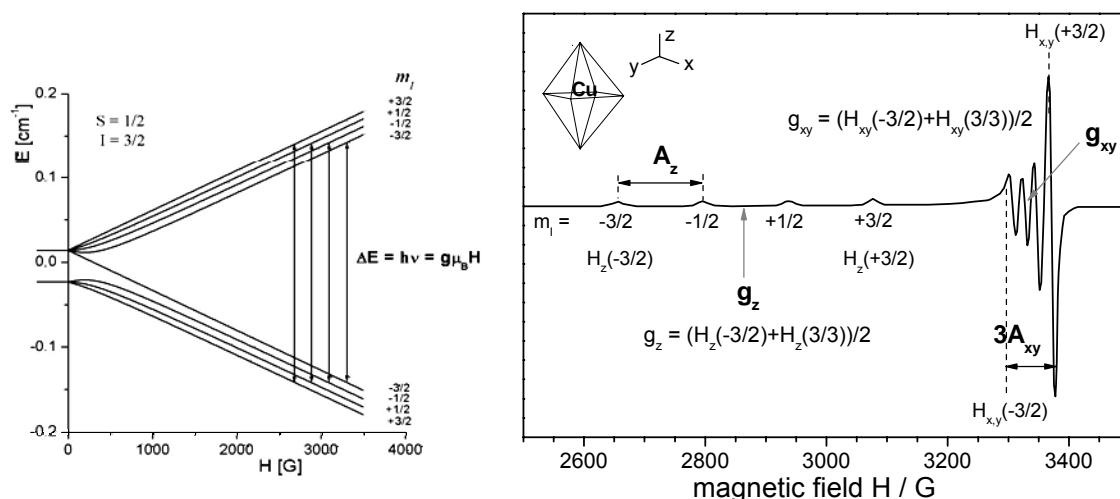


Fig. 3.24: Energy levels for the electron of a copper(II) complex (electron spin $S = 1/2$) in an octahedral environment interacting with an atom with nuclear spin $I = 3/2$ in the presence of a magnetic field \vec{H} , ($\vec{B} = \mu_0 \cdot \vec{H}$ with μ_0 the magnetic constant) and corresponding spectra recorded by EPR^[282] on the right.

Copper(II) ion possesses the electronic configuration $[\text{Ar}] 3d^9$. It is paramagnetic and therefore EPR investigations are possible. The high loaded dendrimeric copper(II) complexes with a high density of unpaired electrons whose spins (magnetic moments) eventually could couple to lead to ferromagnetic or antiferromagnetic behaviour, should be quite interesting with respect to the magnetic properties. However complexes with few isolated copper centres are required to understand the structure of the complex, coordinating groups and geometry. For EPR experiments, complementary to the strategies described in the discussion of the synthesis, i.e. variation in the stoichiometry and washing out of high loaded complexes, two further techniques were developed to reduce the copper content per dendrimer: dilution of the copper(II) content by mixing a “high loaded” complex with pure ligand in solution at room temperature as well as preparation of Zn(II) - Cu(II) mixed complexes. The bivalent zinc exhibits similar coordinating behaviour as copper and can therefore bond the same donor groups in the dendrimer. Contrary to the copper(II), zinc(II) has no unpaired electrons, i.e. it is diamagnetic and does not disturb the EPR investigations. The simplicity of the first procedure and the possibility to achieve tailored copper loadings made it preferred for the preparation of paramagnetic diluted samples.

3.7.2 Spectral Parameters of the Copper(II) Dendromesogens

For each generation of poly(propylene imine) copper(II) complexes, three different EPR spectra, characterized by their corresponding magnetic parameters, i.e. the g -factors and the coupling constants A are observed at room temperature. They are denoted as signal A, B and C respectively. As an example, the EPR spectra of selected 2nd generation complexes at room temperature are plotted in Fig. 3.25, the magnetic parameters are summarised on the right. The appearance of the different signals is copper loading dependent. For the 2nd generation, the anisotropic spectrum denoted as signal A, occurs at loadings $n \sim 0.3$, the anisotropic signal B at $0.3 < n < 2$ and additionally to B an isotropic signal denoted C emerges at loadings $n \geq 2$. At the highest loadings only signal C is observed. The occurrence of this series of signals is generation independent, the copper content limits at which they appear, are however different for each generation.

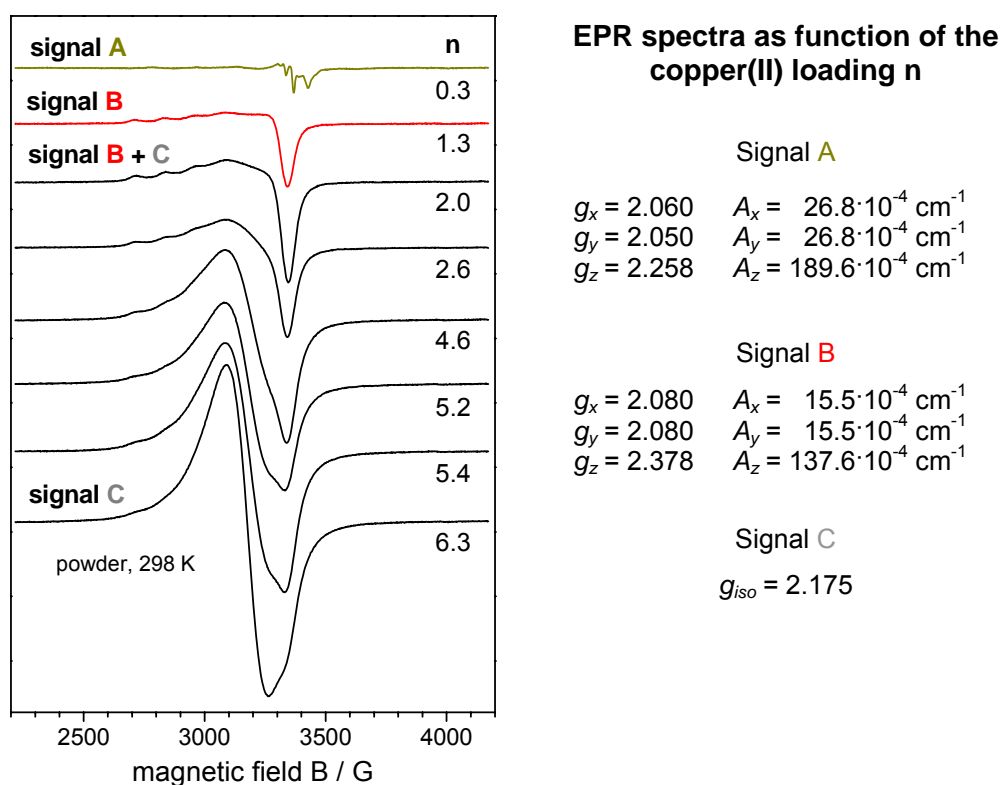


Fig. 3.25: Sequence of the powder EPR spectra observed for the 2nd generation copper(II) complexes at room temperature. Spectra denoted as signal A, B and C and the magnetic parameters characterising these spectra: g -factor (g_x, y, z) and coupling constant (A_x, y, z) in the different space directions x, y, z .

3.7.2.1 Signal A

Signal A corresponds to an anisotropic (orientation dependent) spectrum resolved in both its parallel and perpendicular components. The spectrum parameters, measured in complex **C2.20(0.3)**, $g_x = 2.060$, $g_y = 2.050$, $g_z = 2.258$, with the coupling constants $A_x = A_y = 26.8 \cdot 10^{-4} \text{ cm}^{-1}$ and $A_z = 189.6 \cdot 10^{-4} \text{ cm}^{-1}$ suggest, according to the literature [197, 283-285], a N_2O_2 coordination for copper in a square planar environment (pseudotetrahedral angle $\gamma = 40^\circ$), cf. Fig. 3.26. The powder sample, oriented in an external high magnetic field ($B_0 = 8000 \text{ G}$) and slowly cooled, permitted the observation of the super-hyperfine structure in the parallel components. This super-hyperfine structure is caused by coupling between the unpaired electron spin of copper with the nuclear spins of two nitrogens ($I_N = 1$), the coupling constant a_N amounts $36.8 \cdot 10^{-4} \text{ cm}^{-1}$. The estimated covalence degree, α^2 , for this kind of copper coordination is 0.86 ($\alpha^2 = 1$ for pure ionic compound, $\alpha^2 = 0.5$ for pure covalent compound).

In order to determine which atoms of the dendrimer are involved in the coordination, EPR spectra of the zero generation **C0.1(0.2)** were recorded for comparison. The measured magnetic parameters $g_x = g_y = 2.075$, $g_z = 2.280$ and $A_x = A_y = 14.5 \cdot 10^{-4} \text{ cm}^{-1}$, $A_z = 175 \cdot 10^{-4} \text{ cm}^{-1}$ are very close to those of the 2nd generation complex **C2.20(0.3)** exhibiting signal A. Since in the butane diamide derivative, only amide nitrogen are available, we can conclude that also in higher generations copper is coordinated to amide nitrogen.

The magnetic parameters of signal A are indicative of isolated copper centres. Furthermore, the powder spectra of complex **C2.20(0.3)**, exhibiting signal A does not change by cooling, i.e. no further interactions with other electronic spins were detected, supporting the isolated (monomeric) character of the copper centres. The conformation of the complex is rather fixed as the spectra in solution and powder are the same, i.e. no averaging of the lines to give an isotropic spectrum is observed.

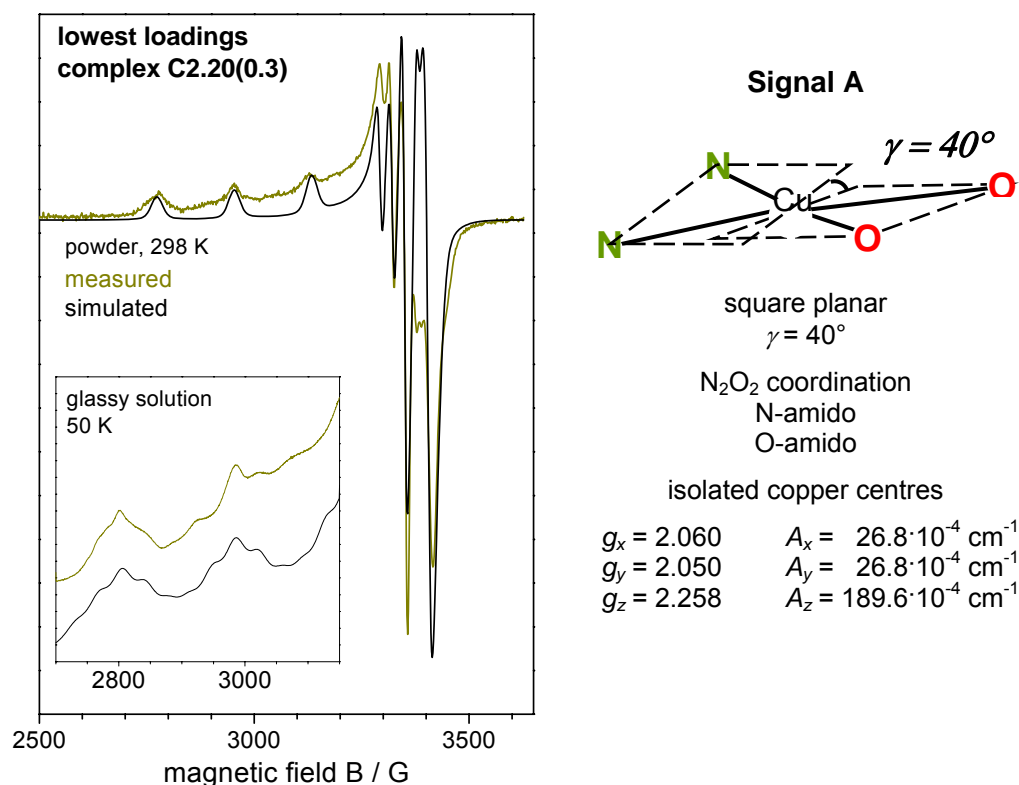


Fig. 3.26: EPR spectra and magnetic parameters corresponding to signal A. On the left EPR powder spectra recorded for the 2nd generation complex **C2.20(0.3)** at room temperature. Inset: solution spectra in toluene/CHCl₃ cooled down to 50 K in the presence of an external magnetic field ($B_o = 8000 \text{ G}$). On the right: magnetic parameters (g -factor (g_x, y, z) and coupling constant (A_x, y, z) in the different space directions x, y, z), coordination sphere of copper, geometry and magnetic properties of the copper centres giving rise to this signal on the right.

A solution of complex **C2.20(0.3)**, sharply cooled into the glassy state at 50 K, exhibits a new spectrum characterised by $g_x = 2.120$, $g_y = 2.070$, $g_z = 2.340$ and $A_x = 39.6 \cdot 10^{-4} \text{ cm}^{-1}$, $A_y = 19.3 \cdot 10^{-4} \text{ cm}^{-1}$, $A_z = 147.4 \cdot 10^{-4} \text{ cm}^{-1}$. Since no other change than the temperature happens in the transformation, the coordinating groups have to be necessarily the same, i.e. N₂O₂. The change in the magnetic parameters can be ascribed to the deformation of the coordination sphere of copper from square planar to pseudotetrahedral (pseudotetrahedral angle $\gamma = 56^\circ$)^[286-293]. The spectrum defined by these parameters is denoted as signal D and is discussed later on.

3.7.2.2 Signal B

The powder spectra of higher loaded complexes, e.g. **C2.15(1.3)** in the 2nd generation or **C1.5(1.0)** in the 1st generation, is an anisotropic spectrum, referred as signal B and characterised by the parameters $g_x = g_y = 2.080$, $g_z = 2.378$ and $A_x = A_y = 15.5 \cdot 10^{-4} \text{ cm}^{-1}$,

$A_z = 137.6 \cdot 10^{-4} \text{ cm}^{-1}$. This spectrum is presented in Fig. 3.27. The differences in the magnetic parameters compared to the spectrum of signal A indicate either differences in the coordinating groups, or different geometries of the same groups or a combination of both factors. Signal B is a linear combination of two further signals, D and E, as discussed below.

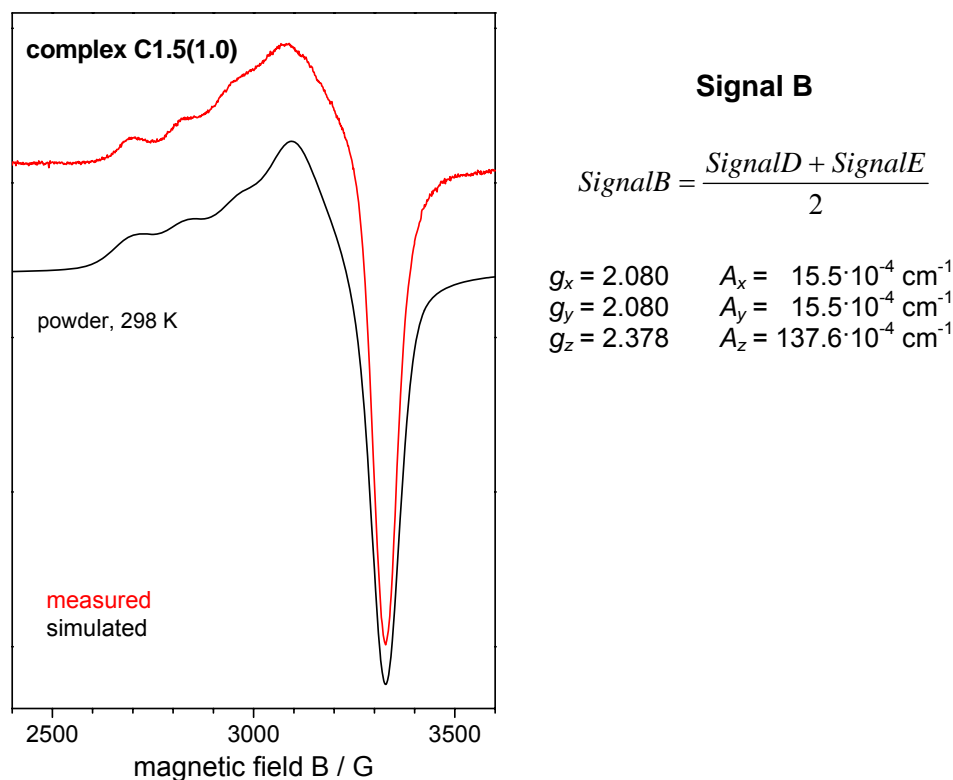


Fig. 3.27: EPR spectra and magnetic parameters corresponding to signal B. On the left: EPR powder spectrum recorded for the 1st generation complex **C1.5(1.0)** at room temperature. On the right: magnetic parameters (g_x, y, z) and coupling constant (A_x, y, z) in the different space directions x, y, z) of the copper centres giving rise to this signal.

3.7.2.3 Signal C

Signal C is a symmetrical line which appears together with signal B with increasing copper content; at the highest copper contents only signal C is observed. It can be isolated by a mathematical procedure in the 1st generation, subtracting the spectra of complex **C1.5(1.0)**, i.e. signal B, from the spectra of **C1.4(1.5)**, i.e. signal B + C, cf. Fig. 3.28, (powder spectra, 298K). A symmetrical line results, whose $g_{iso} = 2.175$ coincides with the averaging of the g_x, g_y, g_z parameters of signal B ($g_x = g_y = 2.080, g_z = 2.378$). This signal arises from the interaction of copper centres which are close together. The signal is significant for a weak interaction, i.e. interaction of their dipole moments but no interaction of spins^[294-296]. This means, no ferro or antiferromagnetic

coupling occurs at room temperature. The weak character of the interaction is further supported by the fact that the line does not narrow with increasing copper loadings.

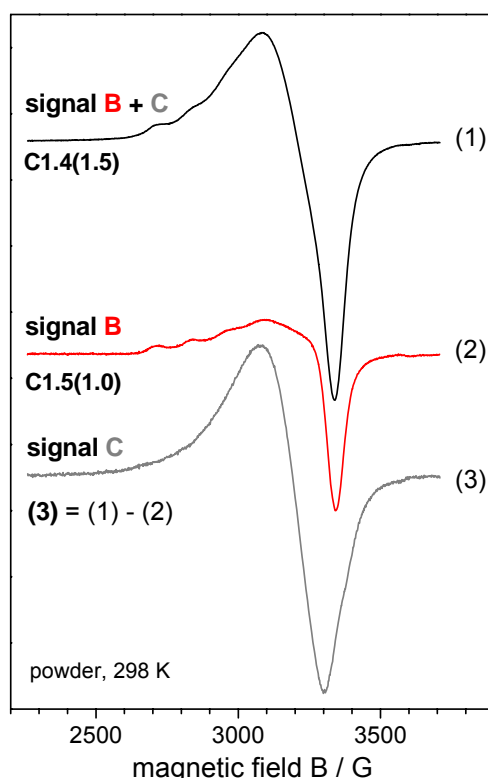


Fig. 3.28: EPR powder spectra corresponding to signals B, B+C and C. Mathematic procedure to isolate signal C: subtraction of (2) from (1).

3.7.2.4 Signals D and E

A solution of complex **C1.4(1.5)** in toluene/ CHCl_3 1:1 develops after some time ageing into a blue precipitate on top of the EPR tube, i.e. complex **C1.4b**, and a light green precipitate on the bottom, i.e. complex **C1.4gr**, cf. Scheme 3.1, 3.1.3.2. Each precipitate was isolated, dried and analysed separately.

The blue precipitate **C1.4b**, exhibits a powder spectrum at room temperature, cf. Fig. 3.29, close to the spectra of the glassy complex **C2.20(0.3)**: $g_x = g_y = 2.070$, $g_z = 2.337$, and $A_x = 38.6 \cdot 10^{-4} \text{ cm}^{-1}$, $A_y = 19.3 \cdot 10^{-4} \text{ cm}^{-1}$, $A_z = 152.6 \cdot 10^{-4} \text{ cm}^{-1}$, i.e. signal D. The orientation of the blue precipitate in a magnetic field (degree of orientation ^[65, 297, 298], $S = 0.37$) leads to observation of the super-hyperfine SHF, structure. The SHF structure gives evidence of the coupling of the electron spin of copper with two amide nitrogen atoms, coupling constants $a_{N_z} = 35.9 \cdot 10^{-4} \text{ cm}^{-1}$, $a_{N_x} = a_{N_y} = 9.6 \cdot 10^{-4} \text{ cm}^{-1}$. The remaining donors in the coordination sphere of copper are carbonyl oxygen atoms. This is in accordance with the observations in the 2nd generation complex **C2.20(0.3)** and in agreement with the magnetic parameters described in the

literature for carbonyl groups^[299, 300]. The detected coordination at room temperature for the blue complex is thus a pseudotetrahedral N₂O₂ coordination.

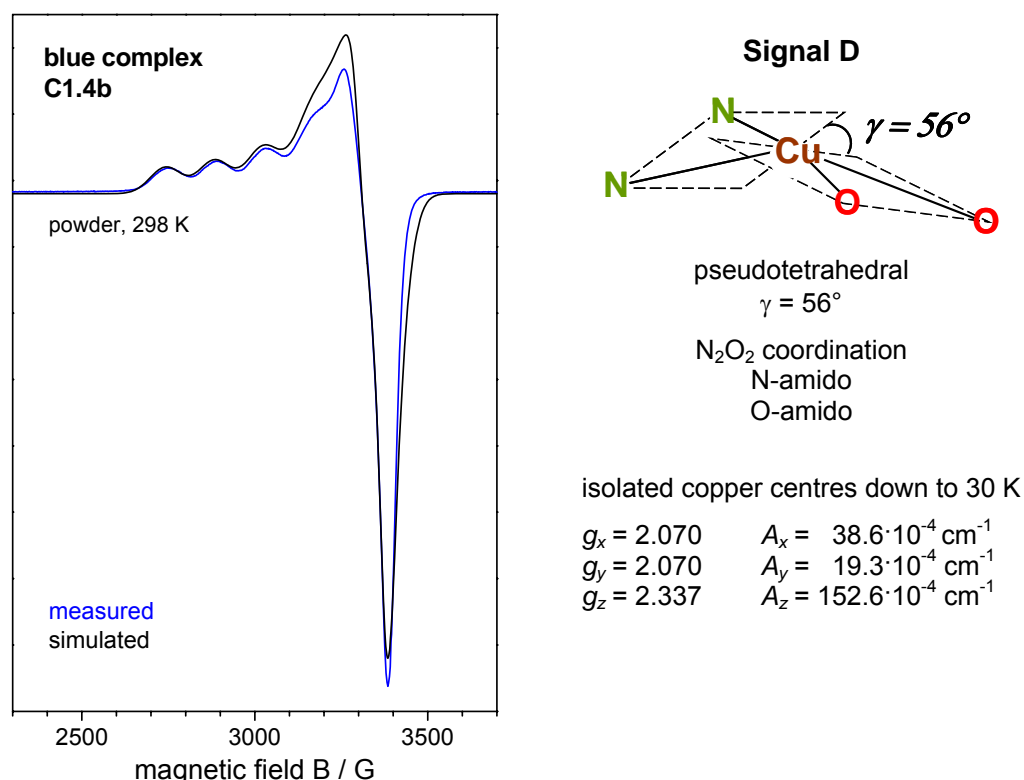


Fig. 3.29: EPR spectra and magnetic parameters corresponding to signal D. On the left: EPR powder spectra recorded for the 1st generation complex **C1.4b** at room temperature. On the right: magnetic parameters (g_x, y, z) and coupling constant (A_x, y, z) in the different space directions x, y, z), coordination sphere of copper, geometry and magnetic properties of the copper centres giving rise to this signal.

The blue precipitate can also be selectively obtained from the reaction mixture of the 1st generation, complex **C1.2(1.9)b** (Scheme 3.1, 3.1.3.2), and exhibits the same EPR features as complex **C1.4b**, $g_x = 2.060$, $g_y = 2.065$, $g_z = 2.336$, and $A_x = 38.4 \cdot 10^{-4} \text{ cm}^{-1}$, $A_y = 19.3 \cdot 10^{-4} \text{ cm}^{-1}$, $A_z = 168.0 \cdot 10^{-4} \text{ cm}^{-1}$, i.e. its EPR spectrum is of type D. The spectrum of the blue precipitate **C1.2(1.9)b**, measured at different temperatures corresponds to that of an isolated copper^[301-304] complex down to 30 K. At lower temperatures a different spectrum is detected and a dimeric structure is proven, as explained later on, cf. 3.7.3.1. The 1st generation complex of the γ -butyrolactone/CHCl₃ series, blue complex **C1.7(1.0)b**, shows similar behaviour as **C1.2(1.9)b**.

The green precipitate **C1.4gr**, exhibits a new anisotropic spectrum characterised by $g_x = g_y = 2.084$, $g_z = 2.405$ and $A_x = A_y = 10 \cdot 10^{-4} \text{ cm}^{-1}$, $A_z = 128 \cdot 10^{-4} \text{ cm}^{-1}$ (powder) or $g_x = g_y = 2.075$, $g_z = 2.395$ and $A_x = A_y = 10 \cdot 10^{-4} \text{ cm}^{-1}$, $A_z = 128 \cdot 10^{-4} \text{ cm}^{-1}$ (glassy solution) and is denoted as signal E, cf. Fig. 3.30. The blue complex **C1.2(1.9)b** heated

over 130°C leads to the green complex **C1.2(1.9)gr**, cf. Scheme 3.1, 3.1.3.2, which shows a close spectra to complex **C1.4gr** in the glassy state: $g_x = g_y = 2.065$, $g_z = 2.363$ and $A_x = A_y = 9 \cdot 10^{-4} \text{ cm}^{-1}$, $A_z = 164.5 \cdot 10^{-4} \text{ cm}^{-1}$. The interpretation of the signal E is carried out using this last complex **C1.2(1.9)gr**. Oriented in a magnetic field at 50 K, the SHF structure is resolved and evidences the coupling of copper with the nuclear spin of *one only* amido nitrogen (cf. signal A, D) and a with a hydrogen nucleus. The observed coupling constants are $a_{N_z} = a_{H_z} = 36 \cdot 10^{-4} \text{ cm}^{-1}$ and $a_{N_x} = a_{N_y} = a_{H_x} = a_{H_y} = 9 \cdot 10^{-4} \text{ cm}^{-1}$. The evolution of the magnetic parameters compared to those of the signal D indicates the coordination of one amido carbonyl oxygen and two further oxygen atoms^[305-307] probably from nitrate (according to elemental analysis, c.f. 3.2). Signal E comes therefore from copper centres with a NO₃ coordination at room temperature. Down to 20 K, the same spectrum, which corresponds to a monomeric structure (isolated copper(II) centres), is recorded. At temperatures of 20 K or lower, a spin exchange between the copper(II) centres in the green complex occurs and a new spectrum is observed, as explained in the next section cf. 3.7.3.2.

It is shown that **C1.4(1.5)** is a mixture of the complexes **C1.4b** and **C1.4gr** exhibiting signals D and E respectively. The EPR spectrum of **C1.4(1.5)** corresponds to signal B + C. The presence of signal C provides no structural information and indicates only that the dipole moments of copper centres close together are interacting. These copper centres exhibit signal B, therefore their magnetic parameters, are the result of an exchange averaging of the anisotropic spectral parameters obtained for signals D and E. In other words, complexes exhibiting signal B are a mixture of copper centres with different coordinations giving rise to signals D and E at room temperature. As shown here, 1st generation complexes exhibiting only one coordination type, can be isolated. For higher generations, a physical separation of the pure complexes type D or type E was not possible. With increasing generation the number of donor atoms, and thus the number of coordinated copper centres, increases. The probability that all copper centres coordinate in only one fashion inside a single dendrimeric ligand decreases, a distribution with all possible combinations of coordination type D and E arises, which precludes physical separation.

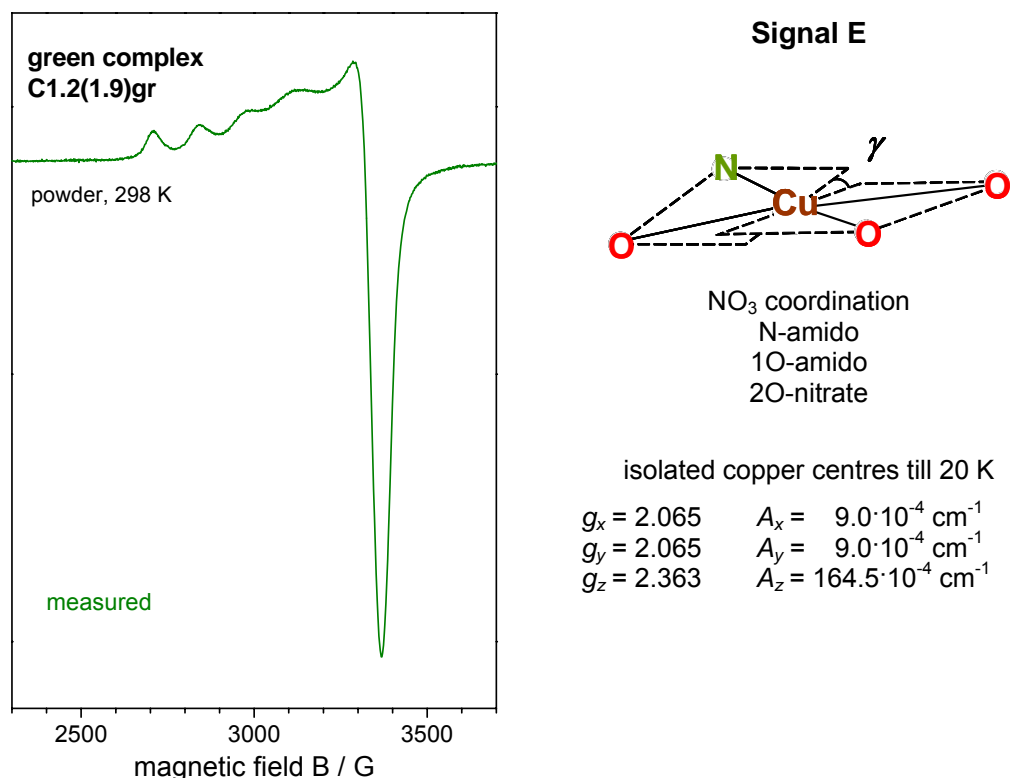


Fig. 3.30: EPR spectrum and magnetic parameters corresponding to signal E. On the left: EPR powder spectra recorded for the 1st generation complex **C1.2(1.9)gr** at room temperature. On the right: magnetic parameters (g -factor (g_x, y, z) and coupling constant (A_x, y, z) in the different space directions x, y, z), coordination sphere of copper, geometry and magnetic properties of the copper centres giving rise to this signal.

3.7.3 Magnetic Properties of the Dendrimeric Copper(II) Complexes: Dimer Formation and Antiferromagnetism

Complexes with a low copper loading, characterized by the magnetic parameters of signal A, exhibit the same kind of spectra at any temperature, no further interaction has been detected. This indicates that the copper centres are isolated, i.e. they are “monomeric” copper centres and no spin coupling takes place. However, the spectra of the blue and green complexes exhibit a temperature dependent behaviour. At room temperature they are characterised by signals D and E respectively as shown before cf. 3.7.2.4. At low temperatures, antiferromagnetic coupling is observed and new spectra are recorded. The low temperature spectra reveal further interesting points reported in the following paragraphs.

3.7.3.1 Blue Complexes: Dimeric Structure

The blue complex **C1.2(1.9)b**, exhibits the spectrum denoted as signal D down to 30 K. This spectrum indicates a N_2O_2 coordination for the copper(II) centres. Below 30 K, the spectrum of the blue complex splits in two lines: a sharp symmetrical line ($g_o = 2.025$) and a new anisotropic spectrum characterised by $g_x = g_y = 2.15$, $g_z = 2.342$ and $A_z = 162 \cdot 10^{-4} \text{ cm}^{-1}$. According to the literature ^[308], the symmetrical line corresponds to a nitrate radical. The integrated intensity of the temperature dependent EPR-spectra follows the Curie-Weiss law. The calculated Curie-Weiss constant θ , ($\theta = -11.4 \text{ K}$) is negative, indicating that the blue complex **C1.2(1.9)b** exhibits antiferromagnetic behaviour below 30 K. The electron spin coupling of the copper centres can be explained by the presence of a super-exchange interaction through the nitrate bridge ^[309] connecting the two copper centres. A schematic representation of the dimer can be found in Fig. 3.31. The copper to copper distance in the dimeric structure, estimated from distances and angles described in the literature for nitrate and copper, is 6.918 \AA ^[310, 311]. The coordination of nitrate in this fashion ($\mu\text{-}1, 3$) ^[210] or close related to it ($\eta^3:\mu_3$) ^[212, 213] has been also described for other copper(II) complexes. This is further supported by FTIR analysis, which gives evidence of the presence of bidentate nitrate and further features characteristic of bridging nitrates, cf. 3.5.3.2. Therefore, measurements below 30K reveal that the copper(II) in the blue complexes exhibits a N_2O_3 coordination. N_2O_3 consist of copper centres in a pseudotetrahedral N_2O_2 environment (as revealed at room temperature, signal D) and an additional oxygen atom belonging to a nitrate group. The nitrate group bridges two similar copper centres, leading to dimer formation. Note that above 30 K, the high thermal motion prevents the antiferromagnetic coupling and the detection of the 3rd oxygen but the nitrate bridge must still be present.

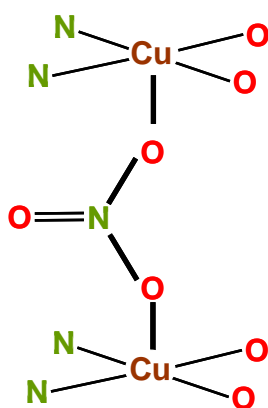


Fig. 3.31: Dimeric structure proposed for the 1st generation blue complex **C1.2(1.9)b**. Blue complexes exhibit a NO_3 coordination: N_2O_2 amido nitrogen and oxygen belonging to dendrimer, third oxygen belonging to the nitrate bridge. Antiferromagnetic coupling at $T < 30 \text{ K}$ ($\theta = -11.4 \text{ K}$).

3.7.3.2 Green Complexes: Nitrate Bridged Polymeric Structure

The EPR spectra of complex **C1.2(1.9)gr** at room temperature are those corresponding to signal E, i.e. a NO_3 coordination for copper(II) is detected. The analysis of the temperature dependence of the intensity of its EPR signal indicates antiferromagnetic behaviour at low temperatures ($T \leq 50$ K) with a Curie-Weiss constant, $\theta = -11.9$ K. Therefore it is possible to speak of a dimeric structure, i.e. copper centres exchanging electron spins. The spin exchange is further supported by the observation of the signal corresponding to a forbidden transition in EPR. The dimeric structure is assumed to be analogous to that of the complexes exhibiting signal D, i.e. the copper centres are connected through μ -1,3 nitrate bridges. The coordination of copper(II) centres in the green complexes is thus a NO_4 one.

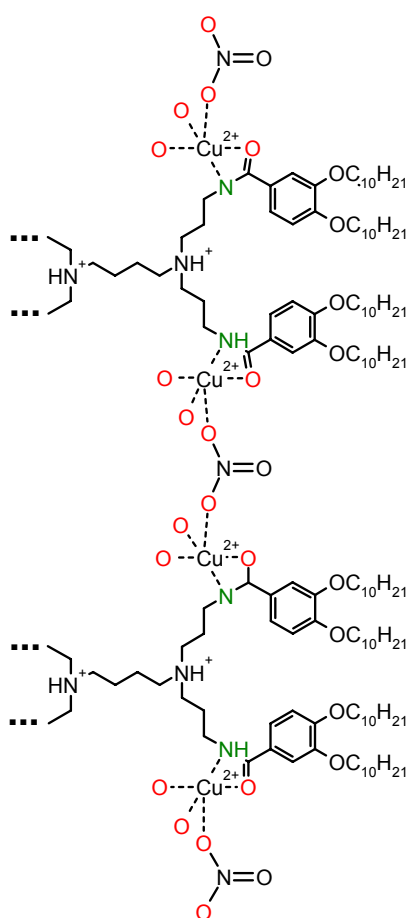


Fig. 3.32: Simplified schematic model for the polymeric structure proposed for the 1st generation green complex **C1.2(1.9)gr**. Green complexes exhibit a NO_4 coordination: amido nitrogen and oxygen belonging to dendrimer, two further oxygens belonging to nitrate and a last oxygen belonging to the nitrate bridge. Antiferromagnetic coupling at $T \leq 230$ K ($\theta = -11.9$ K).

The degree of orientation of the molecular z axis, S_z , of the dendrimeric copper(II) complexes along a magnetic field is rather high with $S_z = 0.76$ for a magnetic field $B_o = 8000$ G at 50 K ($S = 1$ corresponds to completely aligned systems). The high orientation is even observed in solution at room temperature ($B_o = 3000$ G) when the thermal motion of the molecules should prevent the orientation. Therefore, only an ordering in solution together with a coupling of the copper centres could give rise to such a pronounced orienting effect. Because the dendrimeric ligands form lyotropic rectangular columnar mesophases ^[189] in several binary mixtures of solvents, a similar ordering can be therefore easily assumed for the copper complexes. Therefore the structure of **C1.2(1).gr** must go beyond a dimer and a polymeric structure of copper centres, bridged through nitrate groups in a μ -1,3 mode, is proposed. A schematic model is depicted in Fig. 3.32.

The estimated copper to copper distance is 6.92 Å, as in case of the dimeric structure of the complex **C1.2(1.9)b**. This distance coincides well with the spacing (6.9 Å) indicated by a reflection observed in the wide angle region of the diffractograms of the columnar mesophases of the copper complexes. This distance can be interpreted as the intra-columnar distance in the columnar mesophases of the complex as discussed later on cf. 3.9.2.1.

3.7.3.3 Dendrimeric Copper Complex Bridged to a Hexaaquacopper Complex

The 2nd generation complex **C2.1(7.3)**, both the dry sample and the sample after exposure to water saturated atmosphere for 6 days, were studied by EPR, cf. Fig. 3.33. The dry complex exhibits the symmetrical line signal C ($g_{iso} = 2.170$) characteristic of the weak interaction of many copper centres close together, interchanging their dipoles in the whole range of temperature. At room temperature, the spectrum of the sample exposed to water also shows a symmetrical line, although narrower and shifted to higher field ($g_{iso} = 2.190$). At temperatures lower than 208 K, the spectrum of the sample exposed to water splits into two signals: a symmetrical line coincident with that of the dry sample and an anisotropic spectrum ($g_x = g_y = 2.085$, $g_z = 2.40$ and $A_z = 140 \cdot 10^{-4} \text{ cm}^{-1}$) which corresponds to an inorganic hexaaquacopper complex, $\text{Cu}(\text{H}_2\text{O})_6^{2+}$ ^[312-314]. The formation of the inorganic hexaaquacopper(II) dinitrate complex in the presence of ligands with nitrogen donor groups has been proven by Zibaseresht *et al.* ^[315]. Likewise, coexistence of hexaaquacopper(II) complex together with poly(amido amine), PAMAM, dendrimeric complexes in aqueous media has been described by several authors ^[143, 145, 316]. It was observed that the $g_{iso} = 2.190$ coincides with the averaging of the g_x , g_y and g_z factors of the inorganic hexaaquacopper complex. The integration of the intensities of the signal corresponding to the dry sample and to the hexaaquacopper complex reveals

that both species are present, within a 10% error, in a 2:3 ratio in the sample exposed to water.

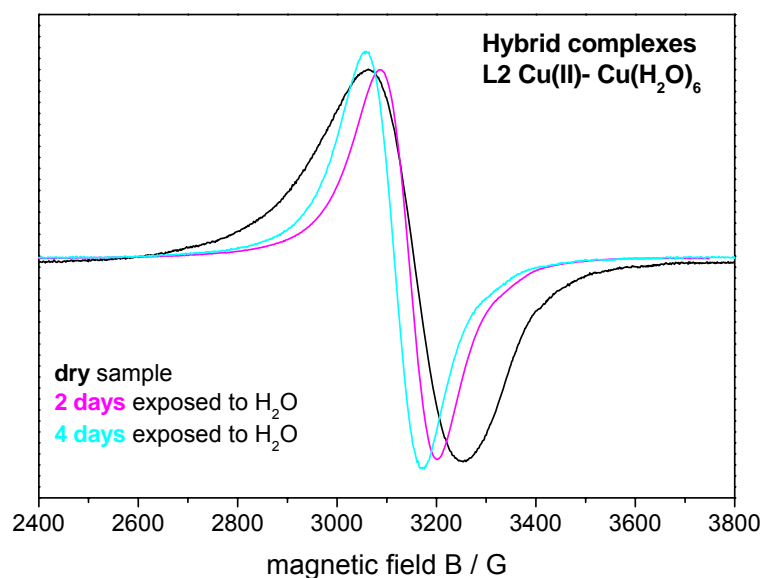


Fig. 3.33: EPR powder spectra of complex **C2.1(7.3)** with different water contents. Sample exposed to a water saturated atmosphere.

The dendrimeric complex exposed to water shows a relatively high Curie-Weiss constant, $\theta = -20.2$ K, which is much higher than that of the dry dendrimeric complex ($\theta = -0.59$ K) or that of the inorganic hexaaquacopper complex alone (coupling constant ~ 0.045 cm⁻¹ [317]). It points the presence of dissimilar interacting copper centres, i.e. the inorganic hexaaquacopper complex and the dendrimeric copper complex must be somehow connected. Simulated spectra, assuming interaction of dissimilar coppers agree well with the experimental magnetic parameters. A copper-copper distance of 4.5 Å is calculated with this model. The comparison with similar situations in the literature [309] suggests a super exchange pathway in which an O donor anion and a molecule of water connect the two copper atoms. A dimer, in which a nitrate anion bridges both a copper atom belonging to the dendrimeric copper complex and a water molecule of the hexaaquacopper complex is therefore proposed, cf. Fig. 3.34.

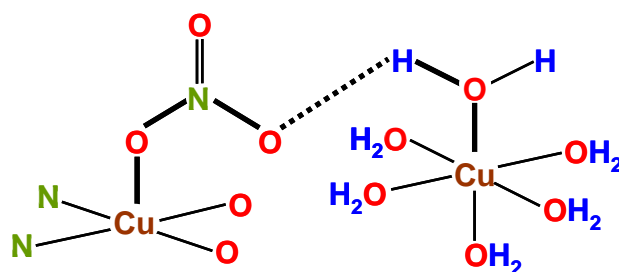


Fig. 3.34: Dimeric structure proposed for the 2nd generation complex **C2.1(7.3)** after exposure to water saturated atmosphere for 6 days. Copper(II) coordinated to the PPI dendrimer through two amido oxygen and nitrogen atoms and bridged to a $\text{Cu}(\text{H}_2\text{O})_6^{2+}$ through a nitrate bridge.

This nitrate bridge supports further the bridges proposed for the dimeric and polymeric structures at low temperature of the blue and green complexes. A similar bridge is observable in the starting copper nitrate trihydrate salt ^[318, 319]. However, the presence of rests of this salt can be completely excluded, since they give rise to a signal completely different to all observed in the dendrimeric copper complexes.

3.7.4 Conclusions

EPR, electron paramagnetic resonance, spectroscopy of the dendrimeric copper(II)-complexes has allowed the determination of the structure and geometry of the different copper(II) coordination sites in the dendrimers. Low loaded copper complexes exhibit isolated (monomeric) copper centres with an N_2O_2 coordination of both carbonyl oxygen and amido nitrogen atoms in an approximately square planar environment (signal A). In higher loaded complexes, a mixture (signal B) of two coordinations (signal D and signal E) is present. Isolation of complexes exhibiting exclusively a single coordination is only possible for the 1st generation (“blue” and “green” complexes). Thus, for the 1st generation “blue” complexes a pseudotetrahedral N_2O_2 coordination (amido nitrogen and amido carbonyl) is detected at room temperature (signal D). For the 1st generation “green” complexes a NO_3 coordination (amido nitrogen, one amido oxygen and two further oxygen atoms probably from nitrate) is observed (signal E). Increasing the copper loading leads to a dipole-dipole interaction without spin exchange at room temperature (signal C).

At low temperatures an antiferromagnetic exchange has been observed ($\theta = -11.4$ K for the “blue” complex and $\theta = -11.9$ K for the “green” complex). A nitrate group bridging two copper centres in a μ -1,3- bridging mode is responsible for this exchange. The estimated nitrate bridged copper to copper distance is 6.92 Å. The nitrate bridge gives rise to highly ordered dimeric (for “blue” complexes) or polymeric (for “green” complexes) structures. The copper(II) in the blue complexes exhibit a N_2O_3 coordination. It consists of a pseudotetrahedral N_2O_2 environment with an additional oxygen atom from the nitrate bridge in apical position. The copper(II) in the green complexes exhibit a NO_4 coordination: one nitrogen and one oxygen atom, belonging to amido moieties, and three nitrato oxygens, one of them belonging to the nitrato bridge. These structures are already present at room temperature as indicated by the unusual high degree of order of the “green” complex observed at room temperature even in solution. The coordination to the oxygen from nitrate bridge can however not be detected at room temperature due to the high thermal motion of the complexes.

3.8 THERMAL PROPERTIES

3.8.1 Polarising Microscopy

The dendrimeric copper (II) complexes were investigated under a polarising microscope POM, equipped with a hot stage. The complexes are crystalline at room temperature and show birefringence which is preserved upon heating above the melting point. This indicates the ordered character of the fluid phase. The observed optical textures are mostly small-sized and non-specific, and do not allow an unambiguous identification of the mesophase. Nevertheless in some cases a pseudofocal conic texture was detected, being a distinctive feature of columnar phases, cf. Fig. 3.35. The mesophases are strongly viscoelastic, flow slowly under mechanical shearing or pressure and readily contract when the exerted forces are withdrawn. This behaviour is found in columnar phases of different compounds ^[42, 188]. The complexes decompose before isotropisation, except for the complexes with very low copper loadings. These last ones have a clearing temperature below the decomposition temperature.

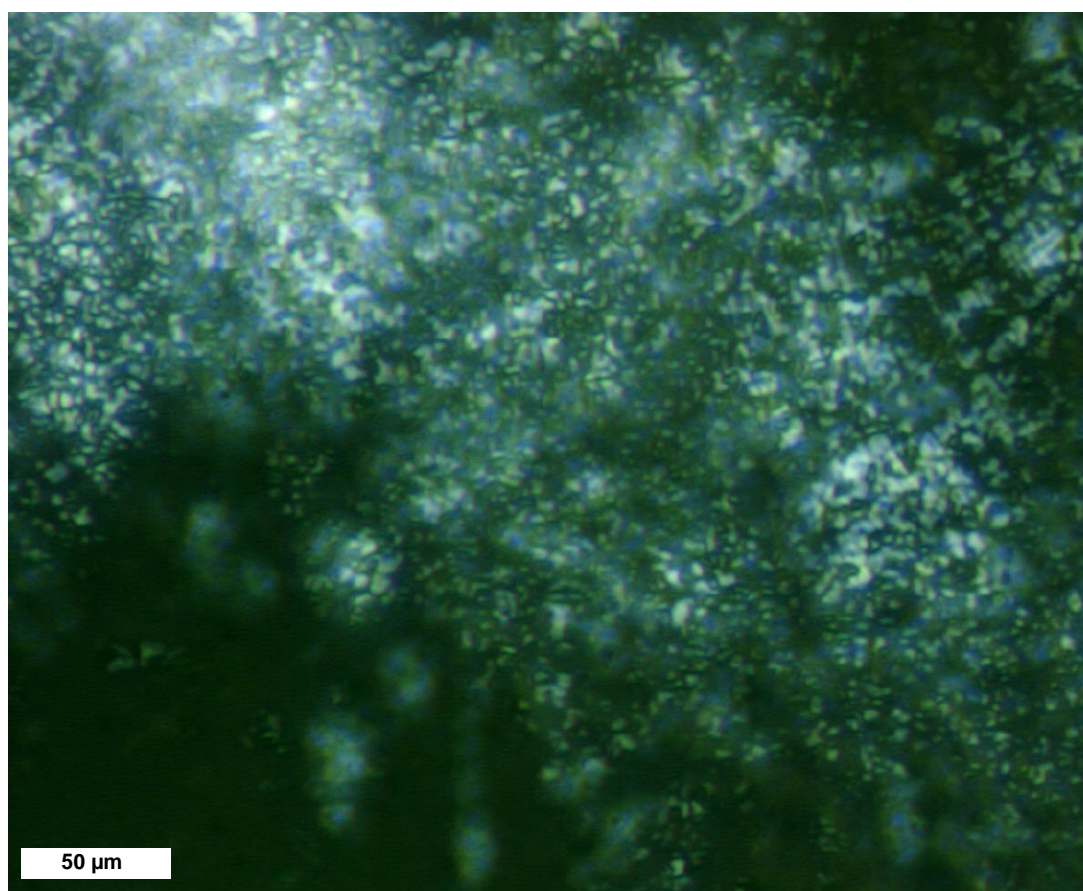


Fig. 3.35: *Broken, pseudo focal conic texture of the 3rd generation complex C3.2(7.9) in the undercooled columnar hexagonal mesophase at 82°C under polarisation microscope.*

3.8.2 Thermal Analysis

The decomposition temperatures of the complexes were determined in air by means of thermogravimetric analysis, TGA. The decomposition temperature was defined as the onset temperature (heating rate $10\text{K}\cdot\text{min}^{-1}$) at which the weight curve deviates 5% from the baseline. In some cases, a small step (ca. 0.5% weight loss) is observed before the main weight drop. This step could be associated with the loss of small molecules, e.g. water molecules, which, despite careful lyophilisation, could still be enclosed in the highly polar dendrimeric scaffold. As an example the thermograms of some 2nd generation complexes of different loadings are presented in Fig. 3.36.

It can be seen from the TGA curves that the copper complexes are, with respect to the dendrimeric ligands, thermally less stable. The decomposition temperature decreases in general with the copper content n , per ligand. In spite of their lower stability, the complexes exhibit broader liquid crystalline ranges than the free ligands, cf. 3.8.2.1, Fig. 3.39.

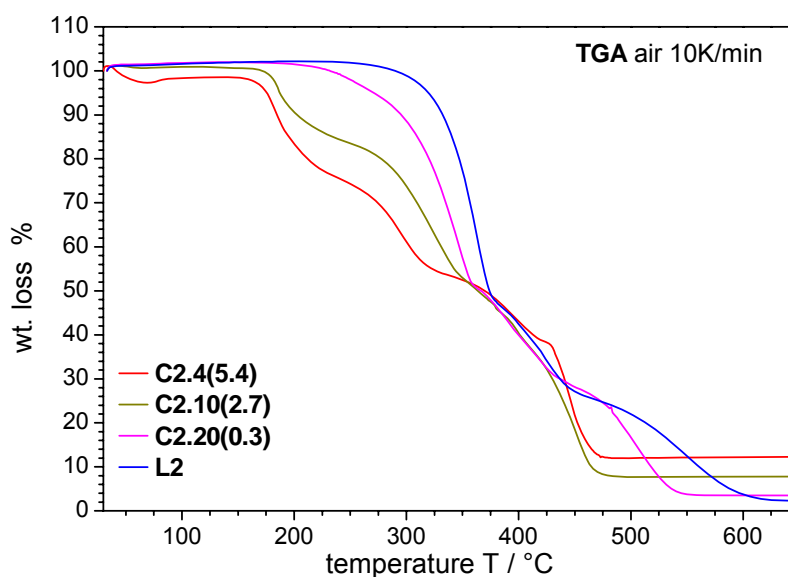
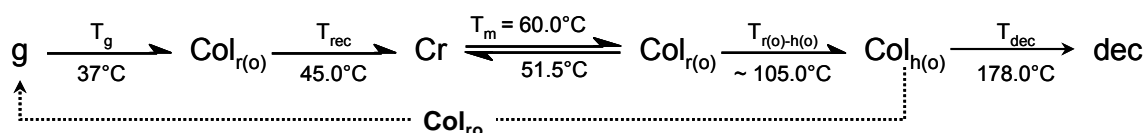


Fig. 3.36: TGA thermograms of selected 2nd generation copper(II) complexes, C2.4(5.4), C2.10(2.7), C2.20(0.3) with varying copper loading and the 2nd generation ligand L2.

Differential scanning calorimetry, DSC, allows a precise determination of the transition temperatures which are in good agreement with those observed by means of polarising microscopy. The established phase transitions will be the basis for X-ray diffractometry that can identify the structure of the mesomorphic arrangement. The data from X-ray diffractometry will be discussed in detail in the next chapter. However, to clarify the DSC findings, some of the X-ray results are presented next.

The thermal behaviour of the complexes follows a general sequence, cf. Scheme 3.5, which is shown for the complex **C2.4(5.4)** as a typical example for the general behaviour. Upon heating, after a glass transition followed by a recrystallisation process, the complex melts into an ordered rectangular columnar mesophase $\text{Col}_{\text{r(o)}}$. At still higher temperatures, an ordered hexagonal columnar mesophase $\text{Col}_{\text{h(o)}}$ develops from the $\text{Col}_{\text{r(o)}}$ phase and persists until the thermal decomposition of the molecule. On cooling from the $\text{Col}_{\text{h(o)}}$ phase, the sample transforms partially and very slowly in the $\text{Col}_{\text{r(o)}}$ phase which below the glass transition temperature T_g , freezes into a $\text{Col}_{\text{r(o)}}$ / $\text{Col}_{\text{h(o)}}$ glass. As for most of the other complexes, the $\text{Col}_{\text{h(o)}}$ - $\text{Col}_{\text{r(o)}}$ transition on cooling is better detectable on annealing the sample, as revealed by the X-ray measurements. So, without annealing, no complete transition into the $\text{Col}_{\text{r(o)}}$ phase occurs. Therefore at room temperature a $\text{Col}_{\text{r(o)}}$ / $\text{Col}_{\text{h(o)}}$ mixture is frozen into the glassy state. On heating again from the glassy state with its mixture of $\text{Col}_{\text{r(o)}}$ / $\text{Col}_{\text{h(o)}}$ phases, the $\text{Col}_{\text{r(o)}}$ phase is thermodynamically favoured over the $\text{Col}_{\text{h(o)}}$ phase and so further formed until the crystalline phase recrystallises above $T_{\text{rec}} = 45^\circ\text{C}$.



Scheme 3.5: General phase transition sequence shown with the 2nd generation complex **C2.4(5.4)** as a typical example.

The DSC thermogram of the complex **C2.4(5.4)** is presented exemplarily in Fig. 3.37. The transition from the $\text{Col}_{\text{r(o)}}$ into the $\text{Col}_{\text{h(o)}}$ phase is not well detectable in DSC. For some complexes, at the most, a very broad and weak peak around 90°C - 110°C is observed. As the rearrangement of the molecules in the transition from the rectangular to the hexagonal lattice is relatively small, not very much energy input should be required for the change, and an accordingly small peak in DSC would be expected. If moreover, the kinetics of the transition is very slow compared to the time scale of the measurement, the peak should be broad; both aspects together would explain the absence of well indicated peaks in the DSC. No textural change was observed under polarising microscope either. However, the transitions were verified by measuring X-ray diffractograms of this complex as a function of temperature in steps of 10°C . From X-ray data, a transition temperature of $\sim 105^\circ\text{C}$ was estimated for **C2.4(5.4)**. The temperatures of the $\text{Col}_{\text{r(o)}}$ - $\text{Col}_{\text{h(o)}}$ transitions for the rest of the complexes are also obtained from X-ray measurements. Complexes of the 1st and 5th generation as well as 2nd generation complexes with very low copper loading exhibit some particularities, which will be discussed separately.

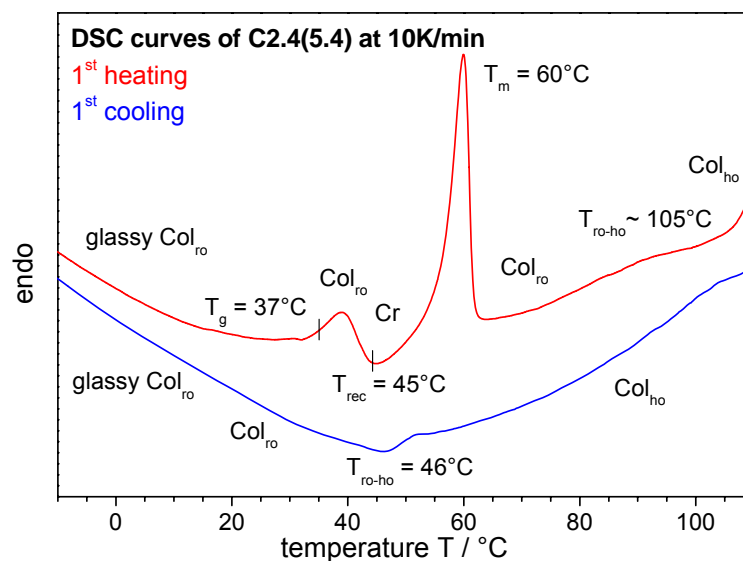


Fig. 3.37: DSC thermogram of the 2nd generation complex **C2.4(5.4)**. Heating over the transition $Col_{r(o)}$ to $Col_{h(o)}$. Heating rate $\pm 10K \cdot min^{-1}$.

3.8.2.1 Series of Highest Loading: Thermal Properties

The influence of the ligand size, i.e. dendrimer generation, on the transition temperatures and type of mesophase is investigated. To this end, the highest loaded complexes of 1st to 5th generations, prepared according to the general synthetic procedure, are compared ^[i]. The thermal data for the THF series are summarised in Fig. 3.38 and Table 3.11, those of the γ -Butyrolactone/ $CHCl_3$ series in Table 3.13.

After synthesis and purification, the five generations exhibit partially crystalline phases at room temperature. Other metal complexes of the same dendrimeric ligands with other metals have been found to show crystalline or amorphous phases at room temperature depending on the metal. So, Co(II), Fe(II) and Fe(III) complexes are crystalline solids at room temperature whereas Cr(III) complexes are amorphous, glassy solids ^[188, 194]. At around $50 \pm 10^\circ C$ all compounds melt into a liquid crystalline phase. The melting points slightly decrease with increasing generation, as already described for the dendrimeric ligands ^[188] and other dendrimers ^[197] and in contrast to the standard behaviour of linear polymers ^[102, 175, 197]. The melting enthalpies increase with the generation, they are smaller than those of the reference ligands. The molar enthalpies ΔH_m , were calculated with the molecular weights estimated from elementary analyse, cf. 3.2, Table 3.2. The molar enthalpies ΔH_m , represent average values due to two factors: the dendrimeric

^[i] **C1.4(1.5)** is the highest loaded complex of the 1st generation exhibiting a mixture of the two coordination types, N_2O_3 and NO_4 observed by EPR for the PPI copper(II) complexes, cf. 3.7.3. Complexes of higher generation exhibit always mixed coordinations, therefore **C1.4(1.5)** is presented here for comparison. Higher loaded 1st generation complexes, showing only one coordination type, are presented separately, cf. 3.8.2.3.

ligands, especially those of the higher generations, are not really monodisperse ^[188], and the complexes are polydisperse with respect to their copper contents. The enthalpy values are furthermore not always accurate, even in some cases can not be given, because the glass transition and the melting point are often partially overlapped and it is impossible to decouple the contribution of each one.

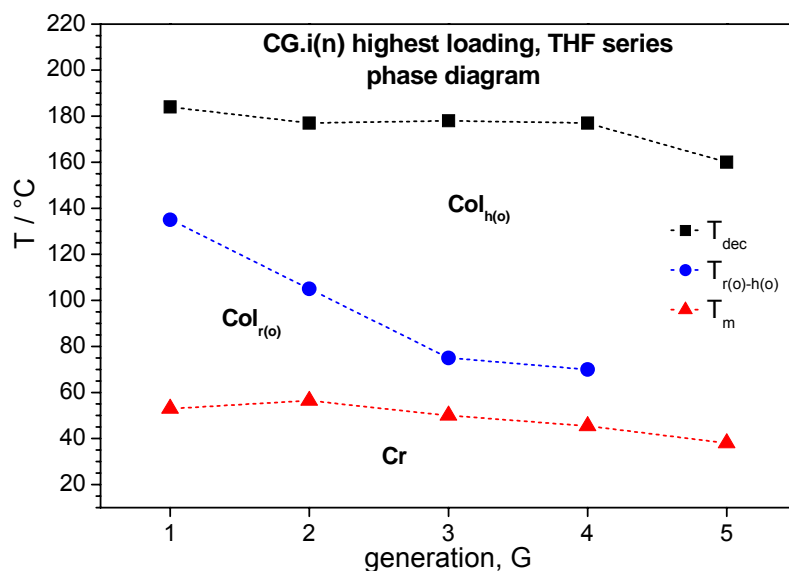


Fig. 3.38: Thermal behaviour of the highest loaded copper(II) complexes of the THF series in dependence on the generation G . Plotted complexes: **C1.4(1.5)**, **C2.3(6.0)**, **C3.1(12.0)**, **C4.1(24.2)** and **C5.1(45.9)**.

Table 3.11: Transition temperatures (°C), molar ΔH_m (kJ·mol⁻¹) and measured ΔH_w (J·g⁻¹) enthalpies, mesophases and decomposition temperatures of the copper(II) complexes of the THF series, highest loading.

CG.i(n)	LG	g	T_g	Cr	T_m ΔH_m (ΔH_w)	Col _{r(o)}	$T_{r(o)-h(o)}$	Col _{h(o)}	T_{dec}
C1.4(1.5)	L1	•	48	•	53.0 44.2 (17.7) ^a	•	~ 135	•	184
C2.3(6.0)	L2	•	43	•	56.5 41.8 (6.9) ^a	•	~ 105	•	177
C3.1(12.0)	L3	•	43	•	50.0 60.6 (4.8) ^a	•	~ 75	•	178
C4.1(24.2)	L4	•	20 ^b	•	45.5 291.5 (11.9) ^a	•	~ 70	•	177
C5.1(44.9)	L5	•	17 ^b	•	38.0 382.0 (8.1) ^a			•	160

CG.i(n): copper(II) complex **i** of the **G** generation ligand (**LG**) with copper(II) loading **n**.
g: glassy state, T_g : glass transition, **Cr**: crystalline phase, T_m : melting point, $T_{r(o)-h(o)}$: transition from the ordered rectangular Columnar **Col_{r(o)}** into the ordered hexagonal columnar **Col_{h(o)}** mesophase, T_{dec} : decomposition temperature;
d: disordered **o**: ordered mesophase, []: monotrope phase.

T_g , T_m , T_c , ΔH_w from DSC (1st run, 10 K·min⁻¹); T_{ro-ho} from X-ray; T_{dec} from TGA (air, 10 K·min⁻¹).

a) T_g and T_m partially overlapped thus the ΔH_w is not accurate, b) 2nd heating.

The strongest dependence on the generation is observed for the transition temperature between the two columnar phases and consequently for the width of the rectangular phase: for the smallest generation the $\text{Col}_{\text{r(o)}}$ to $\text{Col}_{\text{h(o)}}$ takes place at around 135°C and decreases to approx. 70°C for the 4th generation. No columnar rectangular mesophase was observed at all for the 5th generation and the 5th generation complex melts directly into the hexagonal phase. This columnar polymorphism, well known in different discotic molecules [44, 45, 52] and columnar metal complexes [43, 46, 47, 50] has also been described for dendrimers [49, 159, 164]. In case of dendrimers [164], the transition between the two columnar phases could not be detected with DSC either. The copper(II) complexes decompose at $170 \pm 10^\circ\text{C}$, before reaching the isotropic phase. A similar thermal behaviour has been observed for chromium complexes of the same dendrimeric ligands [188]

A diagram comparing the thermal behaviour of the complexes (THF series) with the ligands of the same generation is presented in Fig. 3.39. The thermal data of the ligands are summarized in Table 3.12.

Table 3.12: Transition temperatures ($^\circ\text{C}$), molar ΔH_m ($\text{kJ}\cdot\text{mol}^{-1}$) and measured ΔH_w ($\text{J}\cdot\text{g}^{-1}$) enthalpies, mesophases and decomposition temperatures of the the dendrimeric PPI ligands **L1-L5**.

LG	g	T _g	Cr	T _m	ΔH_m (ΔH_w)	Mesophase	T _c	ΔH_m (ΔH_w)	I	T _{dec}
L1	●	32	●	112.0	105.9 (53.4)	M	[62.5]	5.8 (2.9)	●	313
L2	●	33	●	99.5	189.7 (46.2)	Col _{h(d)}	[91.5]	6.8 (1.7)	●	310
L3	●	20	●	74.5	109.3 ^a (13.1)	Col _{h(d)}	115.0	10.9 ^a (1.3)	●	305
L4	●	20	●	62.0	53.9 ^a (3.2)	Col _{h(d)}	123.5	61.4 ^a (3.6)	●	293
L5	●	22				[Cub _s] ^b Col _{h(d)}	[75.0] 102.0	^b 131.9 ^a (3.9)	●	275

LG: PPI ligand of the **G** generation. **g**: glassy state, **T_g**: glass transition, **Cr**: crystalline phase, **T_m**: melting point, **M**: mesophase could not be identified by X-ray diffractometry, **Col_{h(d)}**: disordered hexagonal columnar mesophase, **Cub_s**: cubic spheroidic phase, **T_c**: clearing point, **I**: isotrope melt, **T_{dec}**: decomposition temperature; []: monotrope phase. **T_g**, **T_m**, **T_c**, ΔH_w from DSC (1st run, 10 K·min⁻¹); **T_{dec}** from TGA (air, 10 K·min⁻¹).

a) ΔH_m for the dendrimers of 3rd-5th generations are calculated with the molar mass of the perfectly built dendrimers. Since higher generations present increasing number of defects [188], the given ΔH_m represent only approximate values, b) monotrope regarding the Col_h phase, not detectable by means of DSC.

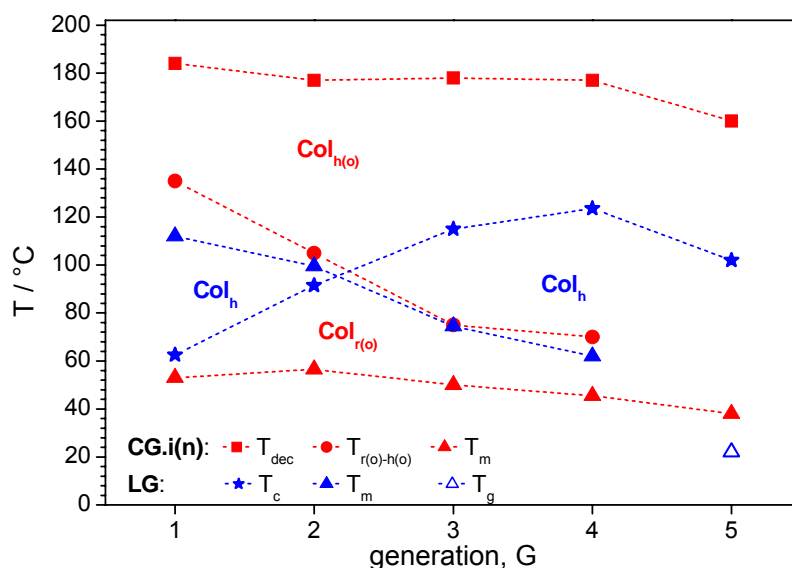


Fig. 3.39: Ranges of liquid crystallinity of the highest loaded dendrimeric copper complexes of each generation (THF series), compared with those of the dendrimeric ligands. For clarity, only the transitions which are significant for the mesophase range are depicted. Plotted complexes **C1.4(1.5)**, **C2.3(6.0)**, **C3.1(12.0)**, **C4.1(24.2)** and **C5.1(45.9)** and ligands **L1** - **L5**.

Table 3.13: Transition temperatures ($^{\circ}\text{C}$), molar ΔH_m ($\text{kJ}\cdot\text{mol}^{-1}$) and measured ΔH_w ($\text{J}\cdot\text{g}^{-1}$) enthalpies, mesophases and decomposition temperatures of the copper(II) complexes of the γ -butyrolactone/ CHCl_3 series, highest loading.

CG.i(n)	LG	g	T_g	Cr	T_m ΔH_m (ΔH_w)	$\text{Col}_{r(o)}$	$T_{r(o)-h(o)}$	$\text{Col}_{h(o)}$	T_{dec}
C1.7(1.0)b	L1	•		•	125.0 196.1 (79.4)	•	~ 135	•	183
C2.2(6.3)	L2	•	54	•	60.0 89.2 (14.5)	•	~ 100	•	180
C3.2(7.9)	L3	•	34 ^a	•	44.5 212.0 (19.8) ^b	•	~ 70	•	150

CG.i(n): copper(II) complex **i** of the **G** generation ligand (**LG**) with copper(II) loading **n**, **b**: blue complex. **ser**: synthesis via, **s**: variation in the reaction stoichiometry, **wo**: washing out with different solvents. **g**: glassy state, T_g : glass transition, **Cr**: crystalline phase, T_m : melting point, $T_{r(o)-h(o)}$: transition from the ordered rectangular columnar $\text{Col}_{r(o)}$ into the ordered hexagonal columnar $\text{Col}_{h(o)}$ mesophase, T_{dec} : decomposition temperature; **d**: disordered **o**: ordered mesophase, []: monotrope phase.

T_g , T_m , T_c , ΔH_w from DSC (1st run, 10 $\text{K}\cdot\text{min}^{-1}$); T_{ro-ho} from X-ray T_{dec} from TGA (air, 10 $\text{K}\cdot\text{min}^{-1}$). a) 2nd heating, b) T_g and T_m partially overlapped thus the ΔH_w is not accurate.

Compared to those of the THF series, the transition temperatures of the γ -Butyrolactone/ CHCl_3 series complexes are substantially the same, cf. Table 3.13. Differences are found for the 1st generation, since in the γ -butyrolactone/ CHCl_3 series no “mixed” complex was obtained. Only complex with coordination N_2O_3 , the blue complex **C1.7(1.0)b** could be isolated. The transition temperatures of this complex are homolo-

gous to those of the blue complex of the THF series **C1.2(1.9)b**, cf. 3.8.2.3. The thermal behaviour of the complexes is thus independent of the synthetic procedure. Consequently, solvent molecules from the reaction or working-up media do not take part, or at least not in a significant extent, in the composition of the complex.

The mesomorphic properties of the complexes are on the one hand determined through those of the dendrimeric ligands. In the ligands, the mean driving force causing liquid crystallinity is the microphase segregation between the polar inner core of poly(propylene imine) and the apolar outer sphere of the alkoxybenzamides as could be shown by *Lattermann et al.* ^[102, 136] They found that neither association nor anisometry play a significant role in the formation of the mesophases of these dendrimers. On the other hand, the coordination with copper together with the protonation of the tertiary amine groups, are also able to tune the mesogenic properties of the dendrimer. The influence of protonation is due to two factors as shown for poly(ethylene imine) dendrimers ^[136]: the quaternization of the dendritic amine centers reduces their flexibility, favouring the formation of mesophases and the resulting coulombic forces can furthermore stabilise the mesophase through formation of supramolecular interactions.

The three major differences to the ligands are (cf. Fig. 3.39):

- i. a new phase, the Col_{r(o)} phase, has been induced.
- ii. the mesophase ranges of the complexes are broader than those of the ligands
- iii. the 1st and 2nd generation ligands that exhibit monotropic columnar hexagonal mesophases became enantiotropic through the complexation.

3.8.2.2 Series of Lower Copper Loading: Thermal Properties of the 2nd Generation Complexes

The influence of the copper loading on the thermal properties of the complex for a given generation is discussed in this chapter. Dendrimers of the 2nd generation were chosen for this purpose. The highest copper loading was achieved following the general synthetic and working-up procedures described in 3.1.2. Lower copper contents were achieved with two methods as described before (cf. 3.1.3.1):

- i. variations in the stoichiometry of the reaction,
- ii. selective washing out of copper from end or crude products by treatment with solvents of different polarities.

Fig. 3.40 displays the thermal behaviour of the 2nd generation copper(II) complexes, prepared according to the methods referred above, in a kind of “phase diagram” being the copper loading, n , the variable. The transitions at loading 0 correspond to those of

the pure ligand. Transition temperatures and mesophases are summarized in Table 3.14 and Table 3.15. It can be observed that regardless the reaction media (THF or γ -butyrolactone/ CHCl_3) or the way (i or ii) the copper loadings were accomplished, for a certain copper content the transition temperatures are essentially the same. We can distinguish three regions in the phase diagrams depending on the copper loading n :

$n < 1$

Lowest loaded homologues exhibit melting temperatures similar to that of the ligand. They exhibit $\text{Col}_{\text{h(d)}}$ mesophases as the pure ligand and clear before decomposition. Unlike the ligand, all the complexes exhibit enantiotropic mesophases. Surprisingly already such low loadings as 0.3, i.e. only one dendrimer per three being complexed with a copper centre, is able to turn the mesophase into an enantiotropic one. The protonation of the tertiary amines, which according to elemental analysis cf. 3.2 occurs already at very low copper loadings, contributes presumably to this effect.

$n = 1$

A copper content of about one Cu(II) per dendrimer marks an inflection point in the behaviour of the complexes: the melting point decreases noticeably to ca. 50°C and the broad Col_{h} mesophase is observed up to 200°C. No clearing point is observed anymore and the mesophase is preserved till the decomposition temperature. The stability of the complex diminishes abruptly compared to the pure ligand and lower loaded ($n < 1$) complexes.

$n > 1$

Further increasing of the copper content, results in the appearance of a $\text{Col}_{\text{r(o)}}$ phase below the hexagonal one at $n = 1.3$. At the same time, the up to now disordered columnar hexagonal mesophase $\text{Col}_{\text{h(d)}}$, becomes ordered $\text{Col}_{\text{h(o)}}$. The transition from $\text{Col}_{\text{r(o)}}$ to the $\text{Col}_{\text{h(o)}}$ occurs at ca. 105°C according to X-ray. Structural considerations concerning the ordered phases are discussed in the next section. The rest of the transition temperatures remain in the regime initiated at the copper loading of 1. Variations with still higher copper loadings are only minor.

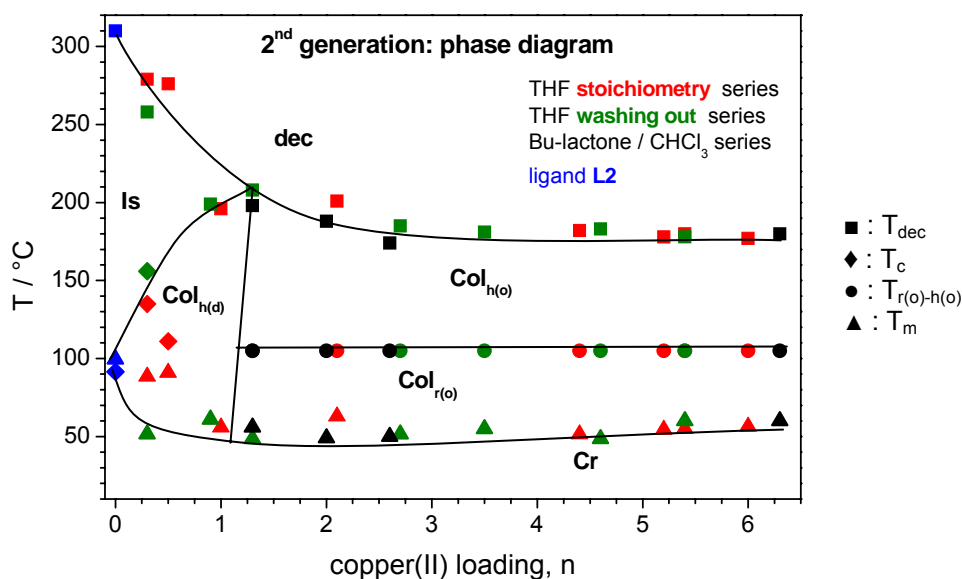


Fig. 3.40: Thermal behaviour of the 2nd generation copper(II) complexes of the THF and γ -butyrolactone- CHCl_3 series, in dependence on the copper loading. **Cr**: crystalline phase, **Col_{h(d)}**: disordered hexagonal columnar mesophase, **Col_{h(o)}**: ordered columnar mesophase, **Col_{r(o)}**: ordered rectangular mesophase, **I**: isotropic melt, **dec**: decomposition. Plotted complexes of Table 3.14 and Table 3.15.

Table 3.14: Transition temperatures ($^{\circ}\text{C}$), molar ΔH_m ($\text{kJ}\cdot\text{mol}^{-1}$) and measured ΔH_w ($\text{J}\cdot\text{g}^{-1}$) enthalpies, mesophases and decomposition temperatures of the 2nd generation copper(II) complexes of the γ -butyrolactone- CHCl_3 series at different copper loadings.

C2.i(n) / L2	ser	g	T_g	Cr	T_m ΔH_m (ΔH_w)	Col _{r(o)}	$T_{r(o)-h(o)}$	Col _h	T_c ΔH_m (ΔH_w)	I	T_{dec}
C2.2(6.3)	s	•	50	•	60 89.2 (14.5)	•	~ 105	• o			180
C2.11(2.6)	wo	•		•	50.0 88.6 (17.4) ^a	•	~ 105	• o			174
C2.13(2.0)	wo	•	46 ^b	•	49.0 94.4 (19.2) ^a	•	~ 105	• o			188
C2.15(1.3)	wo	•	50	•	56 99.6 (20.9)	•	~ 105	• o			198
L2	-	•	33	•	99.5 189.7(46.2)			• d	[91.5] 6.8(1.7)	•	310

C2.i(n): copper(II) complex **i** of the 2nd generation ligand (**L2**) with copper(II) loading **n**. **ser**: synthesis via, **s**: variation in the reaction stoichiometry, **wo**: washing out with different solvents. **g**: glassy state, T_g : glass transition, **Cr**: crystalline phase, T_m : melting point, $T_{r(o)-h(o)}$: transition from the ordered rectangular columnar **Col_{r(o)}** into the ordered hexagonal columnar **Col_{h(o)}** mesophase, T_c : clearing point, **I**: isotrope melt, T_{dec} : decomposition temperature; **d**: disordered **o**: ordered mesophase, []: monotropic phase. T_g , T_m , T_c , ΔH_w from DSC (1st run, 10 K·min⁻¹); T_{ro-ho} from X-ray T_{dec} from TGA (air, 10 K·min⁻¹)
a) T_g and T_m partially overlapped thus the ΔH_w is not accurate, b) 2nd heating.

Table 3.15: Transition temperatures ($^{\circ}\text{C}$), molar ΔH_m ($\text{kJ}\cdot\text{mol}^{-1}$) and measured ΔH_w ($\text{J}\cdot\text{g}^{-1}$) enthalpies, mesophases and decomposition temperatures of the 2nd generation copper(II) complexes of the THF series at different copper loadings.

C2.i(n) / L2	ser	g	T _g	Cr	T _m $\Delta H_m(\Delta H_w)$	Col _{r(o)}	T _{r(o)-h(o)}	Col _h	T _c $\Delta H_m(\Delta H_w)$	I	T _{dec}
C2.3(6.0)	s	•	43	•	56.5 41.8 (6.9) ^a	•	~ 105	• o			177
C2.4(5.4)	wo	•	37	•	60.0 94.6 (16.2)	•	~ 105	• o			178
C2.5(5.4)	s	•	45	•	55.0 56.2 (9.5) ^a	•	~ 105	• o			180
C2.6(5.2)	s	•	47	•	54.5 48.7 (8.5) ^a	•	~ 105	• o			178
C2.7(4.6)	wo	•	60 ^b	•	48.5 85.3 (15.8)	•	~ 105	• o			183
C2.8(4.4)	s	•	40	•	51.5 49.1 (8.7) ^a	•	~ 105	• o			182
C2.9(3.5)	wo	•	42	•	55.0 30.9 (5.8)	•	~ 105	• o			181
C2.10(2.7)	wo	•	35 ^b	•	51.5 49.5 (9.8) ^a	•	~ 105	• o			185
C2.12(2.1)	s	•	46	•	63.0 16.8 (3.6) ^a	•	~ 105	• o			201
C2.14(1.3)	wo	•	40	•	48.5 - ^a	•	~ 105	• o			208
C2.16(1.0)	s	•	34	•	56.0 - ^a			• d			196
C2.17(0.3)	s	•	53	•	88.5 79.8 (18.5)			• d	135.0 ^c	•	279
C2.18(0.9)	wo	•	41	•	61.0 34.7 (7.4) ^a			• d	125 ^c -		199
C2.19(0.5)	s	•	50	•	91.0 82.9(19.3)			• d	111.0 18.6 (4.3)	•	276
C2.20(0.3)	wo	•	24 ^b	•	51.5 79.9(18.1) ^a			• d	156 ^c -		258
L2		•	33	•	99.5 189.7(46.2)			• d	[91.5] 6.8 (1.7)	•	310

C2.i(n): copper(II) complex i of the 2nd generation ligand (L2) with copper(II) loading n. ser: synthesis via, s: variation in the reaction stoichiometry, wo: washing out with different solvents. g: glassy state, T_g: glass transition, Cr: crystalline phase, T_m: melting point, T_{r(o)-h(o)}: transition from the ordered rectangular columnar Col_{r(o)} into the ordered hexagonal columnar Col_{h(o)} mesophase, T_c: clearing point, I: isotrope melt, T_{dec}: decomposition temperature; d: disordered o: ordered mesophase, []: monotropic phase.

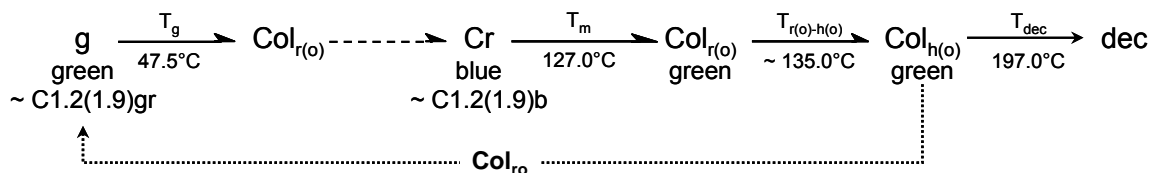
T_g, T_m, T_c, ΔH_w from DSC (1st run, 10 K·min⁻¹), T_{ro-ho} from X-ray, T_{dec} (TGA air, 10 K·min⁻¹).

a) T_g and T_m partially overlapped thus the ΔH_w is not accurate, b) 2nd heating, c) from POM.

3.8.2.3 Series of Lower Copper Loading: Thermal Properties of the 1st Generation Complexes

Besides the 1st generation complex **C1.4(1.5)**, where the two coordination types (N₂O₃ and NO₄) found for the dendrimeric copper(II) complexes occur (cf. 3.7.3), 1st generation complexes exhibiting one only coordination type have been isolated and characterised. These complexes are the blue complex **C1.2(1.9)b** (coordination N₂O₃) and the green complex **C1.2(1.9)gr** (coordination NO₄) in the THF series.

Special features have been found for complexes exhibiting only one type of coordination. Thus, thermochromism, i.e. change of colour with temperature variations, occurs. Below its melting point, **C1.2(1.9)b** exists as a crystalline blue powder. During melting ($T_m = 127^\circ\text{C}$), the compound turns into a liquid crystalline green modification, **C1.2(1.9)gr**. In the melt, **C1.2(1.9)gr** exhibits an ordered rectangular columnar (Col_{r(o)}) mesophase over a very narrow range of temperature (127 – 135°C) before developing the ordered hexagonal columnar (Col_{h(o)}) phase at ~ 135°C. The recovery of the rectangular phase takes place very slowly over several days at room temperature. Some evidences of crystallisation into the blue crystalline phase were found by means of X-ray measurements, even though neither a recrystallisation was detected in DSC nor blue colour was observed. The thermochromism seems therefore to be reversible over a long time scale. The phase sequence proposed for **C1.2(1.9)b** and **C1.2(1.9)gr** is depicted in Scheme 3.6:



Scheme 3.6: Phase transition sequence shown by the thermochromic 1st generation complexes **C1.2(1.9)b** and **C1.2(1.9)gr**.: slow transition -
-----: very slow transition.

The analogues of the γ -butyrolactone/CHCl₃ series (complexes **C1.7(1.0)b** and **C1.7(1.0)gr**) exhibit similar behaviour. The thermal properties of all 1st generation copper(II) complexes together with those of the 1st generation dendrimeric ligand (L1) are summarized in Table 3.16 and Fig. 3.41. Unlike the dendrimeric ligand, which only exhibits a monotropic mesophase below the melting point, the liquid crystalline 1st generation copper(II) complexes show enantiotropic mesomorphism over a broader range than the ligand.

Table 3.16: Transition temperatures ($^{\circ}\text{C}$), molar ΔH_m ($\text{kJ}\cdot\text{mol}^{-1}$) and measured ΔH_w ($\text{J}\cdot\text{g}^{-1}$) enthalpies, mesophases and decomposition temperatures of the 1st generation copper(II) complexes.

C1.i(n) / L1	g	T _g	Cr	T _m $\Delta H_m(\Delta H_w)$	Col _{r(o)}	T _{r(o)-h(o)}	Col _{h(o)}	T _c $\Delta H_m(\Delta H_w)$	I	T _{dec}
C1.2(1.9)b			•	127.0 206.6 (84.6)	•	~ 135	•			197
C1.2(1.9)gr	•	48	(•)		•	~ 135	•			196
C1.4(1.5)	•	49	•	53.0 44.2 (17.7)	•	~ 135	•			184
C1.7(1.0)b			•	125.0 196.1 (79.4)	•	~ 135	•			189
C1.7(1.0)gr	•	48	(•)		•	~ 135	•			a
L1	•	33	•	112.0 105.9 (53.4)	• M			[62.5] 5.8 (2.9)	•	313

C1.i(n): copper(II) complex **i** of the 1st generation ligand (**L1**) with copper(II) loading **n**, **b**: blue complex, **gr**: green complex. **ser**: synthesis via, **s**: variation in the reaction stoichiometry, **wo**: washing out with different solvents. **g**: glassy state, **T_g**: glass transition, **Cr**: crystalline phase, (•): no recrystallisation observed under DSC **T_m**: melting point, **T_{r(o)-h(o)}**: transition from the ordered rectangular columnar **Col_{r(o)}** into the ordered hexagonal columnar **Col_{h(o)}** mesophase, **T_c**: clearing point, **I**: isotrope melt, **T_{dec}**: decomposition temperature; **d**: disordered **o**: ordered mesophase, **M**: mesophase could not be identified by X-ray diffractometry, []: monotropic phase. **T_g**, **T_m**, **T_c**, ΔH_w from DSC (1st run, 10 K·min⁻¹); **T_{r(o)-h(o)}** from X-ray **T_{dec}** (TGA air, 10 K·min⁻¹) a) not determined.

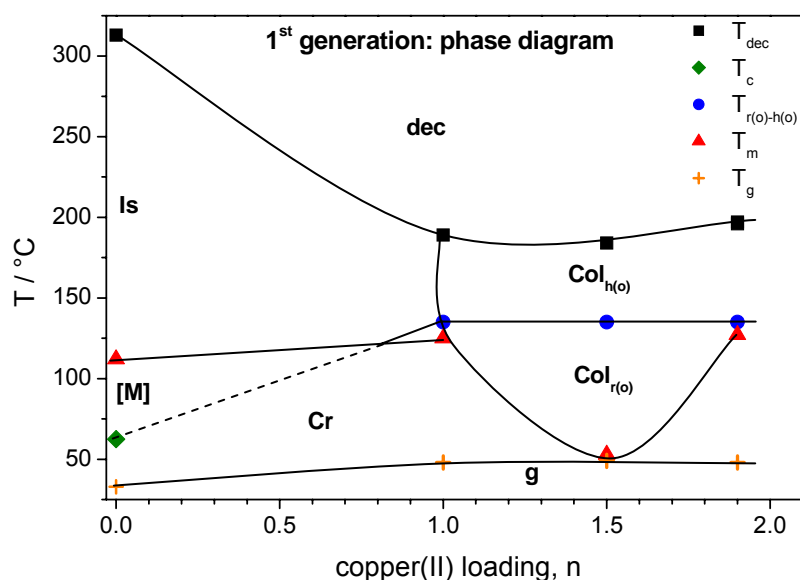


Fig. 3.41: Thermal behaviour of the 1st generation copper(II) complexes of the THF and γ -butyrolactone- CHCl_3 series, in dependence on the copper loading. **Cr**: crystalline phase, **[M]**: monotropic non-determined mesophase, **Col_{h(d)}**: disordered hexagonal columnar mesophase, **Col_{h(o)}**: ordered columnar mesophase, **Col_{r(o)}**: ordered rectangular mesophase, **I**: isotropic melt, **dec**: decomposition. Plotted complexes of Table 3.16.

Thermochromism has been described for many organic and inorganic compounds, both with low molecular weight and polymers ^[320]. It can be caused by modifications in the crystalline structure, molecular rearrangements, transition between two different stereoisomers etc.. Furthermore, in metal complexes thermochromism may occur by changes in the complex geometry, changes in the number or kind of ligands in the metal coordination sphere of the metal or through switching between low- and high-spin states (spin cross over, SCO).

Colour changing has also been observed in liquid crystals. It is intrinsic to the cholesteric mesophases: the variation of the pitch length of their helical structure with the temperature results in changes in the wavelength of the reflected light. True thermochromism has also been reported in metallomesogens ^[28, 31, 37, 46, 59, 321-328]. *Bruce et al* ^[325] observed a blue shift in the absorption bands of iridium(I) complexes by melting into the mesophase (N or Sm). The blue shift was attributed to the breaking down of the stacked structure of the crystalline state into discrete molecular species at the melting point.

The first description of thermochromism in complexes exhibiting ordered columnar hexagonal mesophases (Col_{h(o)}) was published by *Ohta et al* ^[323] in 1991. They observed a progressive blue shift in the absorption spectra of nickel(II) complexes on heating the mesophase up to the clearing point. The shift to higher energy was attributed to an increase of the intracolumnar distance with the temperature until the columns disintegrate into discrete molecules on reaching the clearing point. A similar behaviour was observed for a palladium(II) complex ^[324] on melting into a columnar mesophase. The disc-like palladium complexes are tightly stacked into columns in the crystalline phase. With increasing temperature the intracolumnar distance increases and the columns arrange into a hexagonal lattice, both causing this mesomorphic thermochromism.

By analogy to the aforementioned mechanisms, loosening of the highly ordered crystalline structure of the blue complex **C1.2(1.9)b** at the melting point (127°C) could be responsible for the observed colour change to green. On the other hand, according to the EPR results cf. 3.7, the blue and green complex exhibit different coordinations around the copper(II). The blue complex corresponds to a CuN₂O₃ coordination whereas the green one shows a CuNO₄ one. Thus, different spatial or geometrical environments of the copper centres in blue and green forms could also be responsible of the temperature dependent absorptions of these complexes. Unfortunately, UV-vis spectroscopy can not give further information concerning the blue complex **C1.2(1.9)b** since it is not possible to prepare a solution or film of it, avoiding the transformation into the green modification **C1.2(1.9)gr** cf. 3.6. Presumably, both effects (structure variation by melting in the mesophase and variation in the coordination sphere) are linked together.

EPR analysis of the higher generations copper complexes reveals the existence of blue forms in all the generations. There, the blue form coexists intradendrimerically with other coordinations and the isolation of a “pure blue complex” of higher generation is not possible. A similar situation is found for complex **C1.4(1.5)**. This explains, why in these “mixed” dendrimeric complexes the thermochromic behaviour has not been observed.

3.8.2.4 Thermal Properties of the Tetrafluoroborate Copper(II) Complex

In the previous chapter it was shown, that the solvent media has no influence on the resulting complexes. In order to determine the influence of the anion in the outgoing copper salt on the mesomorphic behaviour of the complexes, two 2nd generation copper(II) complexes were prepared from copper(II) tetrafluoroborate. Tetrafluoroborate is known as a non-coordinating anion. The characteristic thermal data are summarized in Table 3.17, the glass transition and melting point overlap partially therefore the enthalpy could not be determined. For comparison copper nitrate complexes of the same generation and loading are also presented. The copper complexes from tetrafluoroborate are glasses at room temperature and exhibit exclusively an enantiotropic columnar hexagonal mesophase up to the thermal decomposition, cf. 3.9.1.3. This occurs slowly but start already at very low temperatures. Compared to nitrate complexes of similar loading, tetrafluoroborate complexes exhibit higher melting points (ca. 5 – 8°C), i.e their mesophases are narrower. Since in tetrafluoroborate complexes have no possibility of protonation during the synthesis occur, and known the influence of the protonation in the broadening of mesophases, the higher melting points and in consequence the smaller mesophase regions of the tetrafluoroborate complexes are presumably due to the absence of protonation.

Table 3.17: Transition temperatures ($^{\circ}\text{C}$), molar ΔH_m ($\text{kJ}\cdot\text{mol}^{-1}$) and measured ΔH_w ($\text{J}\cdot\text{g}^{-1}$) enthalpies, mesophases and decomposition temperatures of the 2nd generation copper(II) complexes prepared from $\text{Cu}(\text{BF}_4)_2\cdot 4\text{H}_2\text{O}$ compared to those from $\text{Cu}(\text{NO}_3)_2\cdot 3\text{H}_2\text{O}$ of similar loading.

C2.i(n) / L2 anion	g	T _g	Cr	T _m $\Delta H_m(\Delta H_w)$	Col _{r(o)}	T _{r(o)-h(o)}	Col _h	T _c $\Delta H_m(\Delta H_w)$	I	T _{dec}
C2.7(4.6) NO ₃ ⁻	•	60 ^a	•	48.5 85.3 (15.8)	•	~ 105	• o			183
C2.8(4.4) NO ₃ ⁻	•	40	•	51.5 49.1 (8.7) ^b	•	~ 105	• o			182
C2.21(4.0) BF ₄ ⁻	•	48	•	56.0 19.6 (3.2)			• d			90
C2.22(2.9) BF ₄ ⁻	•	50	•	58.5 23.0 (3.9)			• d			109
C2.10(2.7) NO ₃ ⁻	•	35 ^a	•	51.5 49.5 (9.8) ^b	•	~ 105	• o			185
C2.12(2.6) NO ₃ ⁻	•	46	•	50.0 88.6 (17.4) ^b	•	~ 105	• o			174
L2 -	•	33	•	99.5 189.7 (46.2)			• d	[91.5] 6.8(1.7)	•	310

C2.i(n): copper(II) complex **i** of the 2nd generation ligand (**L2**) with copper(II) loading **n**.
ser: synthesis via, **s**: variation in the reaction stoichiometry, **wo**: washing out with different solvents.
g: glassy state, **T_g**: glass transition, **Cr**: crystalline phase, **T_m**: melting point, **T_{r(o)-h(o)}**: transition from the ordered rectangular columnar **Col_{r(o)}** into the ordered hexagonal columnar **Col_{h(o)}** mesophase, **T_c**: clearing point, **I**: isotrope melt, **T_{dec}**: decomposition temperature; **d**: disordered **o**: ordered mesophase, []: monotrope phase.
T_g, **T_m**, **T_c**, ΔH_w from DSC (1st run, 10 K·min⁻¹); **T_{ro-ho}** from X-ray **T_{dec}** (TGA air, 10 K·min⁻¹). a) 2nd heating, b) **T_g** and **T_m** partially overlapped thus the ΔH_w is not accurate.

3.8.2.5 Conclusions

All the copper (II)-complexes are thermotropic liquid crystalline. The complexes exhibit broader mesophase ranges than their ligands. This is consequence not only of the coordination of copper but also of the protonation of the amine groups in the dendrimer core subsequent to complexation.

3.9 X-RAY DIFFRACTOMETRY

The structure of the mesophases was determined by temperature-dependent X-ray diffractometry. Non-oriented powder samples of the dendrimeric copper(II)-complexes were examined with a Guinier goniometer in the angle region $\theta = 0.30^\circ - 15.0^\circ$.

Temperature dependent X-ray measurements were performed in steps of 10°C for each generation. The sequential X-ray measurements do not only allow the determination of the phase structures but also complement the calorimetric analysis. If the transition between the two mesophases was not observable with the calorimetric method because of its slow kinetics compared with respect to the time scale of the DSC measurements, cf. 3.8.2, X-ray reveals nevertheless the morphology. For complexes of the 2nd generation, where a broad series of copper loadings is available, temperature dependent measurements were performed only for selected samples in order to estimate the phase transition temperature of additional mesophases. For the rest of the complexes, the temperature was extrapolated.

Mesophases formed by slow cooling from the isotropic liquid state, grow into larger domains and give rise to narrower and more intensive reflections in their diffractograms. Since most of the copper(II) complexes decompose before isotropisation, it was not possible to heat above the clearing point prior to measurement. The samples were heated up to the desired mesophase, kept at this temperature for some minutes and were cooled to 65°C before measuring. According to the observations of DSC, the lower temperature mesophases recover very slowly (over several days, even weeks) from the higher temperature mesophase after cooling. Therefore, it may be possible to measure both mesophases at the same temperature: the lower-temperature thermodynamically stable mesophase and the higher-temperature metastable supercooled mesophase.

Representative diffractograms of the complexes prepared from copper nitrate trihydrate are shown as e.g. for the 2nd generation complex **C2.4(5.4)**, as depicted in Fig. 3.42a, b. In the small-angle region of the diffractograms, a set of sharp diffraction maxima are observed, whereas in the wide-angle region, both a broad maximum at $\theta \sim 10^\circ$ and two narrow reflections at $\theta = 6.40^\circ$ and $\theta = 12.85^\circ$, the second order of the precedent, are found. The broad halo at $\theta \sim 10^\circ$ ($d \sim 4.4 \text{ \AA}$) corresponds to the liquid-like short range order of the melted alkyl chains and confirms the liquid crystalline nature of the phases. The sharp reflections in the small-angle region of the pattern clearly show a columnar rectangular structure at lower temperatures (here 65°C) and at the higher temperatures (here 110°C) a hexagonal columnar one. The sharp diffraction maxima in the wide-angle range $\theta = 6.40^\circ$ ($d = 6.9 \text{ \AA}$) and $\theta = 12.85^\circ$ ($d = 3.5 \text{ \AA}$), present in both

mesophases, could either evidence an intra-columnar order along the columns or an impurity, present in the sample despite careful working-up procedure.

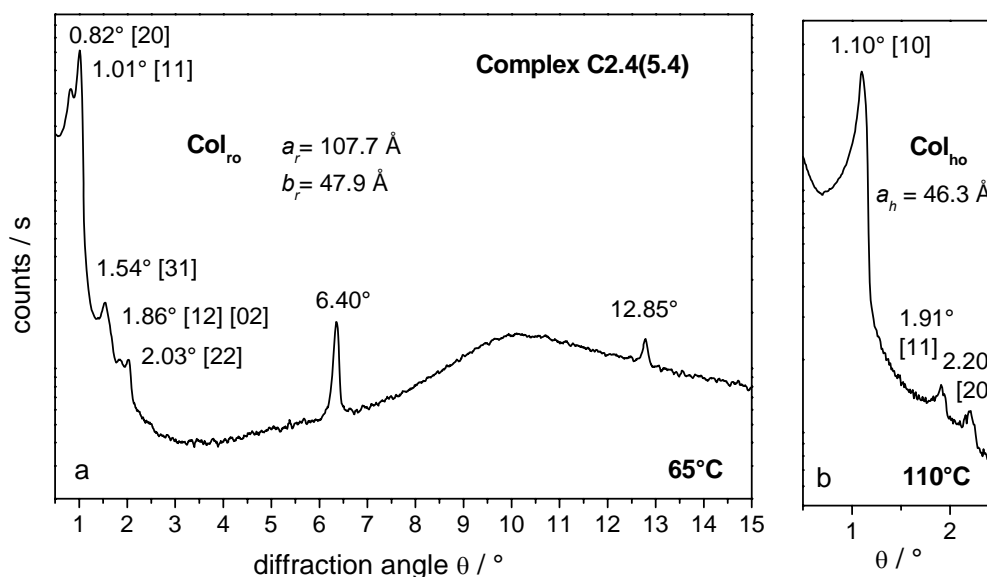


Fig. 3.42: *Diffraction patterns of the 2nd generation complex C2.4(5.4). a) Small and wide-angle region in the rectangular columnar mesophase Col_{r(o)} at 65°C. b) Small-angle region in the hexagonal columnar mesophase Col_{h(o)} at 110°C. Attributed to the peaks: the θ values in ° and the Miller indexes $[hk]$*

The small angle region of the diffractograms, i.e. the structure of the two columnar phases and the influence of generation and copper loading on the type and range of the mesophase is considered first. The origin of the reflections in the wide angle region of the diffractograms and the feasibility of an ordered columnar phase will be discussed next.

3.9.1 Small-Angle Region

The liquid crystalline behaviour and mesophase structures of high loaded poly(propylene imine) complexes can be explained by the 2nd generation complex **C2.4(5.4)** as an example. Diffractograms of **C2.4(5.4)** at different temperatures, cf. Fig. 3.43 enlighten the standard phase sequence.

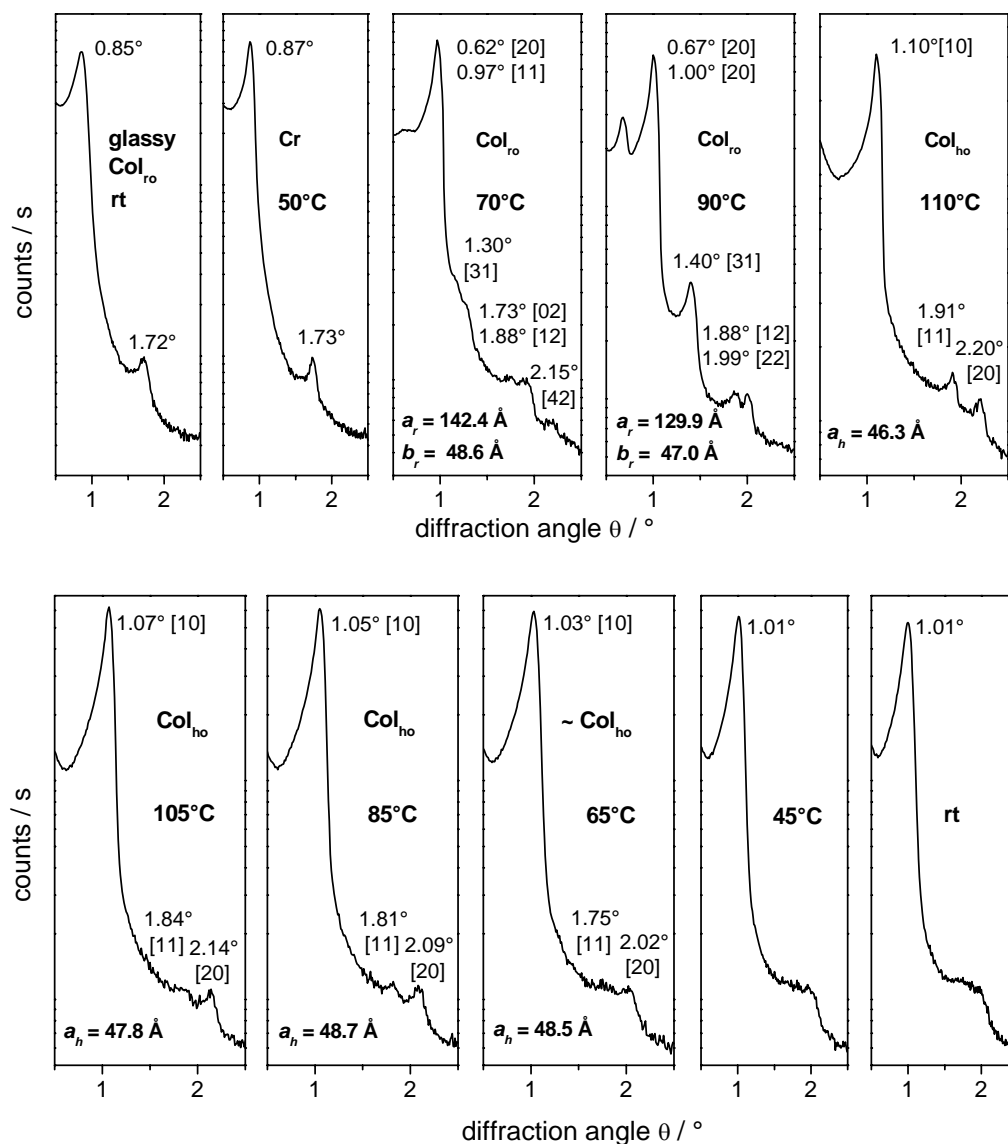


Fig. 3.43: Temperature dependent diffractograms of the 2nd generation complex **C2.4(5.4)**. Upper part (heating): glassy, partially crystalline state (rt and 50°C), Col_{r(o)} (70°C and 90°C) and Col_{h(o)} (110°C). Lower part (cooling): only the Col_{h(o)} mesophase is observed up to 65°C where probably a mixture of Col_{h(o)} and Col_{r(o)} exists. Attributed to the peaks: the θ values in ° and the Miller indexes [hk].

At room temperature, the complex is partially crystalline as indicated by the sharp reflections observed over the whole θ -range, as shown as an example in Fig. 3.44. According to the DSC observations cf. chapter 3.8.2.1, and Scheme 3.5, after its glass transition at ca. 37°C, the complex undergoes a recrystallisation at ca. 45°C, whereby the reflections sharpen and become more intensive. As shown in detail from $0.5^\circ \leq \theta \leq 2.5^\circ$, in Fig. 3.43 above the melting point at 60°C, the complex organises into a mesophase, which is fully developed at around 90°C. At 110°C a new pattern, symptomatic of a different mesophase, is observed.

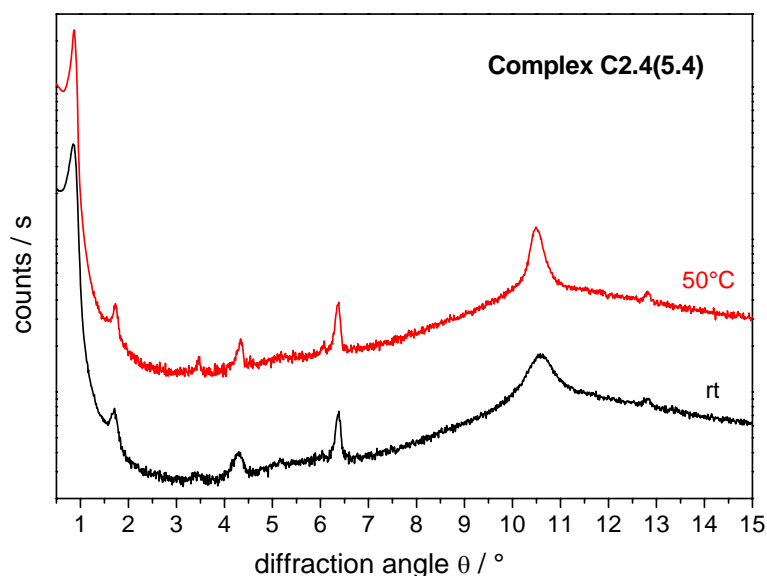


Fig. 3.44: Diffractogram of the 2nd generation complex **C2.4(5.4)** at rt and 50°C below the melting point ($T_m = 60^\circ\text{C}$).

The sharp reflections of the mesophase at high temperature, at 110°C: $\theta_1 = 1.10^\circ$, $\theta_2 = 1.91^\circ$, $\theta_3 = 2.20^\circ$, correspond to reciprocal lattice distances: 40.1, 23.1 and 20.1 Å respectively. The observed distance ratio, $1:1/\sqrt{3}:2$, is characteristic of a hexagonal columnar mesophase Col_h . The reflections can therefore be indicated with the Miller indexes [10], [11] and [20]. The hexagonal lattice is described by the lattice constant a_h (inter-columnar distance), calculated from the measured reciprocal distances and the assigned Miller indexes (cf. 6.5). For **C2.4(5.4)** at 110°C: $a_h = 46.3$ Å. Table 3.18 summarises the measured (obs.) and calculated (calcd.) diffraction angles θ and corresponding spacings d as well as the Miller indexes hk for **C2.4(5.4)** in the hexagonal columnar mesophase at 110°C.

Table 3.18: Lattice parameter a_h and detailed indexation of complex **C2.4(5.4)** in the hexagonal columnar mesophase at 110°C.

	$T_{\text{meas}} / ^\circ\text{C}$	$\theta_{\text{obs}} / ^\circ$	$d_{\text{obs}} / \text{\AA}$	hk	$\theta_{\text{calcd}} / ^\circ$	$d_{\text{calcd}} / \text{\AA}$	$a_h / \text{\AA}$
C2.4(5.4)	110	1.10	40.14	10	1.10	40.11	46.3
		1.91	23.12	11	1.91	23.16	
		2.20	20.07	20	2.20	20.05	

T_{meas} : measurement temperature, measured diffraction angle θ_{obs} and corresponding spacing d_{obs} , hk : Miller indexes, θ_{calcd} and d_{calcd} calculated from hexagonal lattice parameter a_h .

The stacking in the columnar phase can be random or periodic to give rise to disordered ($\text{Col}_{h(d)}$) or ordered ($\text{Col}_{h(o)}$) hexagonal arrangements respectively. The periodic stacking distance (intra-columnar distance) is equal c . cf. 1.1.3. The area of the stacking unit is in any case perpendicular to the column axis.

From simple geometrical and molecular values, it is possible to calculate the number of molecules of dendrimeric copper(II) complex per hexagonal unit cell N_h . From the volume of an elemental hexagonal cell, V_h , and the volume occupied by a single molecule $V_{complex}$ it follows:

$$N_h = \frac{V_h}{V_{complex}} \quad Eq. 3.9$$

The volume of the hexagonal cell is defined by the cell geometry. The area of the two-dimensional hexagonal arrangement S_h is:

$$S_h = a_h^2 \sin 60 \quad Eq. 3.10$$

Assuming that the sharp reflection $\theta = 6.40^\circ$ ($d = 6.9 \text{ \AA}$) in the wide angle region is indicative of intra-columnar ordering (see discussion in the next section 3.9.2), the distance between slices in a column is in average $6.9 \text{ \AA} = c$, which is considered as the height of the hexagonal cell. Therefore the volume of the hexagonal cell is described by:

$$V_h = a_h^2 c \sin 60 \quad Eq. 3.11$$

The volume of a copper(II) complex molecule can be determined from the density ρ , assuming that $\rho \sim 1 \text{ g}\cdot\text{cm}^{-3}$ and the molecular mass of the complex:

$$V_{complex} = \frac{M_{complex}}{\rho \cdot N_A} \quad Eq. 3.12$$

where N_A is the Avogadro's number. The molar mass of a copper(II) complex is estimated from its elemental analysis as indicated in 3.2.

The calculations for complex **C2.4(5.4)**, ($M_{complex} = 5840$, cf. 3.2) in the hexagonal mesophase at 110°C are presented in Table 3.19. The volume of the hexagonal unit cell V_h and the calculated volume for a **C2.4(5.4)** molecule $V_{complex}$, are quite near. According to Eq. 3.9, approximately one dendrimer complex molecule (exactly $N_h = 1.3$) occupies the hexagonal unit cell which is verified by the hexagonal geometry. Therefore, the lattice parameter a_h is a measure of the average diameter of the dendrimeric copper(II) complex in the mesophase. The area of the unit cell S_h can be approximated to the cross section of a column in the hexagonal phase.

Table 3.19: Number of complex molecules per hexagonal unit cell N_h , and cross section S_h , of a column in the hexagonal mesophase at 110°C for complex **C2.4(5.4)**.

M_{complex}	a_h	c	$V_h = a_h^2 c \sin 60$	$V_{\text{complex}} = \frac{M_{\text{complex}}}{\rho \cdot N_A}$	$N_h = \frac{V_h}{V_{\text{complex}}}$	$S_h = a_h^2 \sin 60$
	/ Å	/ Å	/ Å ³	/ Å ³		/ Å ²
5840	46.3	6.9	12810	9698	1.3	1857

$\rho \sim 1 \text{ g} \cdot \text{cm}^{-3}$ and $N_A = 6.022 \cdot 10^{23}$, V_{complex} : volume of a 2nd generation dendrimeric copper(II) complex molecule, V_h : volume of the hexagonal unit cell.

Molecular modelling of isolated ligand molecules in the gas phase ^[188] indicate that the dendrimer can adopt a cylindrical shape, where the polar poly(propylene imine) core is surrounded by the apolar alkyl chains. The description is consistent with the observed hexagonal arrangement for the ligands, being more accurately described as columns of poly(propylene imine) cores in an alkyl chain continuum. The appearance of mesomorphism is after all a direct result of this segregation of polar and apolar parts. This model fits well with the hexagonal mesophase exhibited by the copper(II) complexes of the same ligands too. According to elemental analysis cf. 3.2 and to the spectroscopic investigations (FTIR cf. 3.5.3 and ESR cf. 3.7.2) of the copper(II) complexes, which show the coordination of copper to the amide groups at the outer part of the inner protonated poly(propylene imine) core, the copper centres are thus located in the interface between the columns and peripheral alkyl chains of the matrix. Chromium(III), cobalt(II) and iron (II) and (III) complexes of the same dendrimers exhibit as well hexagonal columnar mesophases ^[188, 194].

Coming back to the temperature dependence, the complexes exhibit on cooling, large hysteresis to return into the low temperature phase and remain in the metastable hexagonal arrangement until room temperature as shown in Fig. 3.43. The hexagonal lattice constant a , is slightly temperature dependent as indicated by the shift in the reflections observed at different temperatures.

The mesophase at lower temperatures is indexed as a rectangular one. The observed reflections at 90°C, $\theta = 0.68^\circ$, 1.00° , 1.40° , 1.88° , and 1.99° , can be indexed either as [20], [11], [31], **[12]** and [22] respectively or as [20], [11], [31], **[02]** and [22]. In the first case, the mesophase would exhibit a p2mg symmetry (reflection condition $h = 2n$ (even number) for reflections of the $h0$ type). In the second one a c2mm symmetry (reflection conditions: $h+k = 2n$ for reflections hk , $h = 2n$, for $h0$ and $k = 2n$ for $0k$) ^[i].

^[i] “p2mg” and “c2mm” are the current Hermann-Mauguin notations recommended in the “International Tables for Crystallography B” for the two-dimensional space groups. “p2mg” is equivalent to the previously used “pmg”; likewise, “c2mm” is equivalent to “cmm”. Alternative notation based on the eighty plane space groups are “P2/a” for “p2mg” and “C2/m” for “c2mm”.

A schematic representation of the two possible rectangular mesophases is presented in Fig. 3.45.

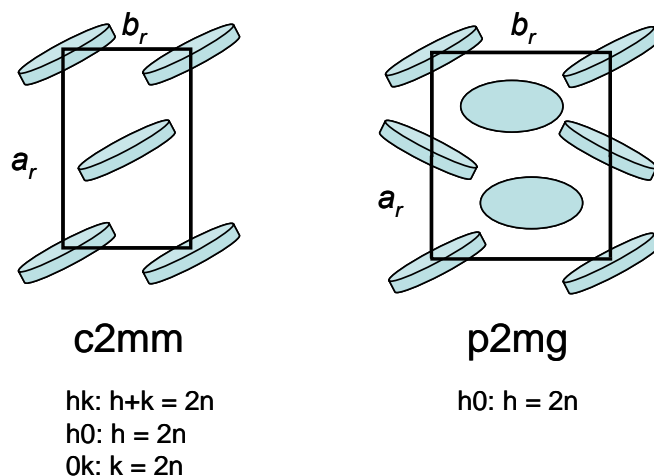


Fig. 3.45: Schematic representation of c2mg and p2mg rectangular mesophases. The sections are perpendicular to the column axes. Rectangular lattice parameters are indicated by solid lines. Reflection conditions below the figure drawings.

The lattice parameters a_r and b_r , determined with the indexation of the reflection at 1.88° as [12] ($a_r = 129.9 \text{ \AA}$ and $b_r = 47.0 \text{ \AA}$), are very close to those determined with the indexation [02] ($a_r = 129.9 \text{ \AA}$ and $b_r = 46.8 \text{ \AA}$). Therefore no criterion to elucidate of the symmetry type can be obtained herefrom. In Table 3.20, the observed and calculated diffraction angles and corresponding spacings (θ_{obs} , d_{obs} , θ_{calcd} , d_{calcd}) and Miller indexes hk according to both a p2mg and a c2mm symmetry are given.

Table 3.20: Detailed indexation of complex C2.4(5.4) in the rectangular columnar mesophase at 90°C

C2.4(5.4)	$T_{meas} / ^\circ\text{C}$	$\theta_{obs} / ^\circ$	$d_{obs} / \text{\AA}$	hk	$\theta_{calcd} / ^\circ$	$d_{calcd} / \text{\AA}$	$a_r / \text{\AA}$	$b_r / \text{\AA}$
p2mg	90	0.68	64.92	20	0.68	64.92	129.9	47.0
		1.00	44.15	11	1.00	44.19		
		1.40	31.54	31	1.39	31.84		
		1.88	23.49	12	1.91	23.12		
		1.99	22.19	22	2.00	22.09		
c2mg	90	0.68	64.92	20	0.68	64.92	129.9	46.8
		1.00	44.15	11	1.00	44.02		
		1.40	31.54	31	1.39	31.77		
		1.88	23.49	02	1.89	23.40		
		1.99	22.19	22	2.01	22.01		

T_{meas} : measurement temperature measured diffraction angle θ_{obs} and corresponding spacing d_{obs} ,
hk: Miller indexes, θ_{calcd} and d_{calcd} calculated from rectangular lattice parameters a_r , b_r .

The number of molecules per rectangular unit cell can be calculated in analogy to that for the hexagonal mesophase, cf. Eq. 3.9 and Eq 3.12, being now V_r :

$$V_r = a_r b_r c \quad \text{Eq. 3.13}$$

For the rectangular mesophase at 90°C, the calculations of the volume of the rectangular unit cell V_r , the volume of a molecule of complex **C2.4(5.4)**, number of molecules of **C2.4(5.4)** in the rectangular cell N_r , and cross sections of a column in the rectangular mesophase for each p2mg and c2mm symmetries are presented in Table 3.21. It follows, according to Eq. 3.9 (adapted for rectangular phases, i.e. $N_r = V_r / V_{\text{complex}}$), that one unit cell is approximately occupied by four molecules of dendrimeric complex (exactly 4.3). This supports strongly the p2mg symmetry where 4 molecules occupy the unit cell. Aggregation or dimer formation, which could justify the high number of molecules per unit cell is not likely to occur at the rectangular phase since only one molecule covers the column section in the hexagonal phase.

In addition, the calculated area per column assuming a c2mm symmetry ($S_r(\text{c2mm}) = 3040 \text{ \AA}^2$) is much bigger than the area of the columns in the hexagonal phase ($S_h = 2054 \text{ \AA}^2$, cf. Eq. 3.10) at a similar temperature (85°C, $a_h = 48.7 \text{ \AA}$). Assuming that in the rectangular mesophase the column slices are tilted relative to the column axes, a larger area of the columns in the rectangular phase compared to the cross section in the hexagonal is senseless. The projection of the tilted slices in the rectangular phase must be smaller than the flat molecule in the hexagonal mesophase. However, the calculated cross section per column for a p2mg symmetry [$S_r(\text{p2mg}) = 1526 \text{ \AA}^2$] is smaller than the hexagonal as expected for inclined molecules. Furthermore, all the generations and copper loadings can be indexed as p2mg, and not all as c2mm. Since we deal with homologue compounds, the same symmetry is expected to appear in all series. In conclusion, the overall analysis suggests a p2mg symmetry for the rectangular mesophase.

Table 3.21: Number of complex molecules per rectangular unit cell N_r and cross section S_r of a column in the rectangular mesophase at 90°C **C2.4(5.4)**

	M_{complex}	$a_r b_r$	c	$V_r = a_r b_r c$	$V_{\text{complex}} = \frac{M_{\text{complex}}}{\rho \cdot N_A}$	$N_r = \frac{V_r}{V_{\text{complex}}}$	S_r
		/ \AA	/ \AA	/ \AA^3	/ \AA^3		/ \AA^2
p2mg	5840	129.9 47.0	6.9	42127	9698	4.3	1526 ($a_r b_r / 4$)
c2mm	5840	129.9 46.8	6.9	41947	9698	4.3	3040 ($a_r b_r / 2$)

$\rho \sim 1 \text{ g} \cdot \text{cm}^{-3}$ and $N_A = 6.022 \cdot 10^{23}$, V_{complex} : volume of a 2nd generation dendrimeric copper(II) complex molecule, V_r : volume of the rectangular unit cell.

The dendrimeric copper-complexes exhibit therefore columnar polymorphism: a rectangular columnar phase and a hexagonal columnar one are shown above a partially crystalline phase, cf. Scheme 3.5. A lot of examples of columnar polymorphism from rectangular to hexagonal are described in the literature for dendrimers^[49, 159, 164]. In most of the cases no detailed analysis of the mesophase structure is given. Only one example of transition from a rectangular phase with $c2mm$ symmetry into a hexagonal one (symmetry $p6mm$) is reported for a 3rd generation PAMAM derivative. For discotic molecules as triphenylenes or triphenylen derivatives or different disc-like metal complexes, transitions from a rectangular columnar mesophase with $c2mm$ ^[49] or $p2gg$ ^[45, 47, 48, 50] symmetry to the hexagonal one are found often in the literature. Less but significant examples are found for the transition from $p2mg$ ^[46] into the hexagonal pahse.

The interpretation of the transition between a hexagonal columnar mesophase and a $p2mg$ rectangular one is presented in Fig. 3.46. On the left is depicted the molecular organisation of the $p2mg$ mesophase. The molecules are either asymmetrically built or the cylindrical shape is tilted with regard to the column axes. This arrangement allows a compact packing in the rectangular mesophase. The hexagonal packing is defined by the hexagonal lattice parameter a_h . The hexagonal lattice can equivalently be described by a pseudo-rectangular “supra-unit cell” defined by $2a_h$ and b_h , $b_h = a_h 3^{1/2}$. At the transition between the two columnar mesophases, the molecules lose either their asymmetrical shape or their tilt. The b_r parameter of the rectangular lattice expands up to almost its double and the a_r parameter contract around 70% of its value to reach $2a_h$ as indicated in Fig. 3.46.

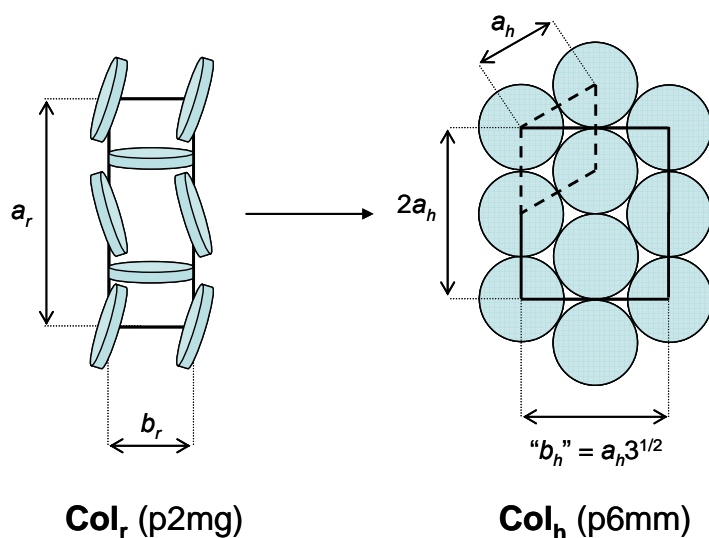


Fig. 3.46: Transition from a rectangular columnar ($p2mg$) to a hexagonal columnar ($p6mm$) mesophase. Solid line indicates the rectangular parameters and dashed line the hexagonal one.

The rectangular mesophase is novel for metal complexes of the 3,4-decyloxybenzoyl-functionalized poly(propylene imine) dendrimers. Beside the 1st generation of a Fe(III) complex, which exhibit an oblique mesophase ^[188, 194] and the 2nd generation of Cr(III), where it could not be distinguished between an oblique or a rectangular mesophase, all the complexes prepared so far (Cr(III), Co(II), Fe(II) and Fe(III) ^[188, 194]) exhibit hexagonal mesophases. Other copper(II) complexes of poly(propylene imine), where the coordination of copper takes place at the salicyl groups in the periphery of the poly(propylene imine), show smectic C phases and no columnar ones. Columnar polymorphism, has also not been reported for these or other poly(propylene imine) derivatives or their metal complexes. Liquid crystalline poly(propylene imine) derivatives usually exhibit smectic ^[175, 179] or columnar hexagonal ^[179] mesophases. Exceptionally, only when a mesogenic unit is laterally attached to the periphery of the dendrimer, a nematic ^[179] phase has been achieved. Finally only one example of a rectangular columnar mesophase (p2gg) has been found in the literature for a trisubstituted benzoic acid ammonium salt of a 1st generation poly(propylene imine) dendrimer, an “ionic” analogue of the **L1** ligand ^[192].

After clarifying the standard pattern followed by most of the dendrimeric copper(II) complexes, it was studied, how the size, i.e. the generation, and the copper loading tune the mesophase type and mesophase structure. For discussion in this chapter, only the lattice parameters of each mesophase are presented; the complete indexing of all the complexes, at each mesophase and temperature, is compiled in the compound register II: X-ray evaluation of mesophases 6.5, at the end of the experimental section.

3.9.1.1 Influence of the Generation on the Mesophase. Series of Highest Loading

As described above for the model compound **C2.4(5.4)**, the maximum loaded copper(II) dendrimeric complexes of generations one to four exhibit columnar polymorphism: a p2mg rectangular columnar mesophase at low temperatures and a p6mm hexagonal columnar mesophase above the rectangular. The 5th generation complex exhibits only a columnar hexagonal one. The hexagonal and rectangular lattice parameters of the maximum loaded complexes of the series prepared by the general procedure for complexation in THF are presented in Table 3.22 and depicted in Fig. 3.47; for comparison the hexagonal lattice parameters of the ligands are included too. The series in γ -butyrolactone/CHCl₃ follow the same tendency of those in THF.

The calculated hexagonal parameters a_h grow linearly with the generation. The volume expansion of the hexagonal lattice with increasing generation is much bigger in the complexes than in the ligand, showing the expansion of the dendrimeric framework which can be stretched due to the charges of the metal centres and the simultaneous protonation of the polyamine core, keeping anyway its cylindrical shape and hexagonal arrangement, cf. Fig. 3.47a. The 5th generation dendrimeric ligand (**L5**) which, under the same measurement conditions of the complex, exhibits a monotropic cubic spheroidic phase (Cub_s) becomes hexagonal through the complexation process.

Table 3.22: Rectangular and hexagonal lattice parameters of the copper(II) complexes of the THF series of maximal loading and starting dendrimeric ligands.

Compound	$T_{\text{anneal}} / ^\circ\text{C}$	$T_{\text{meas}} / ^\circ\text{C}$	M	lattice parameter		$N_{h/r}$	$S_{h/r} / \text{\AA}^2$
				a_h	a_r $b_r / \text{\AA}$		
L1	I	65	[M]	-			
C1.4(1.5)	160	65	Col _{h(o)}	$a_h = 43.6$		2.7	1646
	100	65	Col _{r(o)}		$a_r = 122.2$ $b_r = 54.1$	11.0	601
L2	I	65	[Col _{h(d)}]	$a_h = 43.8$			
C2.3(6.0)	135	65	Col _{h(o)}	$a_h = 45.5$		1.2	1793
	100	65	Col _{r(o)}		$a_r = 133.8$ $b_r = 49.0$	4.3	1535
L3	I	65	Col _{h(d)}	$a_h = 45.7$			
C3.1(12.0)	100	65	Col _{h(o)}	$a_h = 53.7$		0.8	2497
	Rt	65	Col _{r(o)}		$a_r = 113.2$ $b_r = 52.0$	1.9	3039
L4	I	65	Col _{h(d)}	$a_h = 47.1$			
C4.1(24.2)	100	65	Col _{h(o)}	$a_h = 58.3$		0.5	2944
	85	65	Col _{r(o)}		$a_r = 101.2$ $b_r = 69.1$	1.2	5897
L5	I	65	Cub _s	$a_c = 75.2$			
C5.1(45.9)	100	65	Col _{h(o)}	$a_h = 59.4$		0.3	3056

T_{anneal} : annealing temperature, T_{meas} : measurement temperature, **M**: mesophase, not identified, []: monotropic mesophase, **I**: isotropic melt, $N_{h/r}$: calcd. number of molecules per hexagonal or rectangular unit cell, $S_{h/r}$: cross section per column in the hexagonal or rectangular lattice.

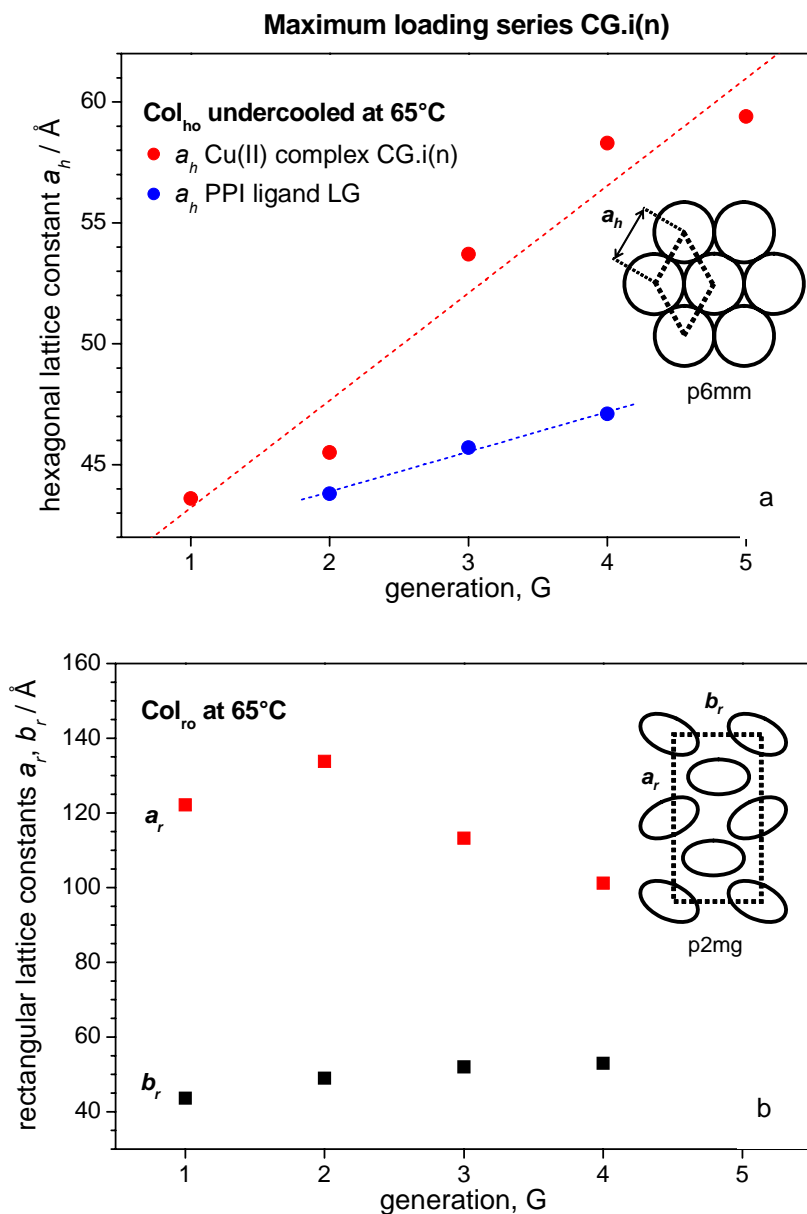


Fig. 3.47: Hexagonal a_h and rectangular a_r, b_r lattice parameters of the copper(II) complexes **CG.i(n)** of the THF series of maximum loading (n). a) hexagonal parameters a_h for each generation g ; •: copper(II) complexes **CG.i(n)**, •: dendrimeric ligands **L1-5**; b) rectangular lattice parameters a_r (■) and b_r (■). In both graphics depicted complexes **C1.4(1.5)**, **C2.3(6.0)**, **C3.1(12.0)**, **C4.1(24.2)** and **C5.1(45.9)**.

The synthesis in γ -butyrolactone/ CHCl_3 under standard conditions lead to complexes less loaded than those of the THF series. Therefore the highest loaded complexes of the γ -butyrolactone/ CHCl_3 series for a given generation, exhibit in general smaller hexagonal (a_h) and rectangular parameters (a_r, b_r) than the highest loaded complexes of the THF series. The lattice parameters and mesophases of the γ -butyrolactone/ CHCl_3 series are summarised in Table 3.23.

Table 3.23: Rectangular and hexagonal lattice parameters of the copper(II) complexes of the γ -butyrolactone/ CHCl_3 series of maximal loading and starting dendrimeric ligands.

Compound	$T_{\text{anneal}} / ^\circ\text{C}$	$T_{\text{meas}} / ^\circ\text{C}$	M	lattice parameter $a_h / a_r, b_r / \text{\AA}$	$N_{h/r}$	$S_{h/r} / \text{\AA}^2$
L1	I	65	[M]	-		
C1.7(1.0)b	135	65	$\text{Col}_{h(o)}$	$a_h = 43.2$	2.7	1616
L2	I	65	$[\text{Col}_{h(d)}]$	$a_h = 43.8$		
C2.2(6.3)	135	65	$\text{Col}_{h(o)}$	$a_h = 46.8$	1.3	1817
	100	65	$\text{Col}_{r(o)}$	$a_r = 126.1$ $b_r = 47.5$	4.0	1481
L3	I	65	$\text{Col}_{h(d)}$	$a_h = 45.7$		
C3.2(7.9)	100	65	$\text{Col}_{h(o)}$	$a_h = 52.8$	0.9	2414
	85	65	$\text{Col}_{r(o)}$	$a_r = 97.5$ $b_r = 54.8$	2.1	2577

T_{anneal} : annealing temperature, T_{meas} : measurement temperature, M: mesophase, not identified, []: monotropic mesophase, I: isotropic melt, $N_{h/r}$: calcd. number of molecules per hexagonal or rectangular unit cell, $S_{h/r}$: cross section per column in the hexagonal or rectangular lattice.

In the low-temperature mesophase, the 1st and 2nd generation exhibit clear diffractograms with multiple reflections, which can easily rectangularly indexed, cf. Fig. 3.48a, b and Table 6.5. As for **C2.5(5.4)** a p2mg symmetry was attributed. The diffractograms of 3rd and 4th generations, Fig. 3.48c, d, are less pronounced. They can be undoubtedly ascribed as rectangular, but the number of reflections is smaller and the resolution poorer compared to the lower generations. This hinders the direct determination of the symmetry group. Temperature dependent measurements show that with increasing generation the temperature range of the existence of the rectangular phase decreases. Furthermore the coexistence of both rectangular and hexagonal mesophases along some tens of degrees is observed, cf. Fig. 3.48d. This can be easily understood considering the unusual slow kinetics of the transition from the rectangular to the hexagonal phase. In consequence, there is a risk of error in the elucidation of the reflections which correspond to each phase and therefore in the indexing and determination of lattice parameters. The mesophases were indexed in analogy to the 1st and 2nd generations, i.e. a p2mg symmetry for 3rd and 4th generations was assumed. The evolution of the rectangular lattice parameters with the generation is presented in Fig. 3.47b. The rectangular lattice parameter a_r changes only slightly with increasing generation, whereas for b_r the change is more pronounced.

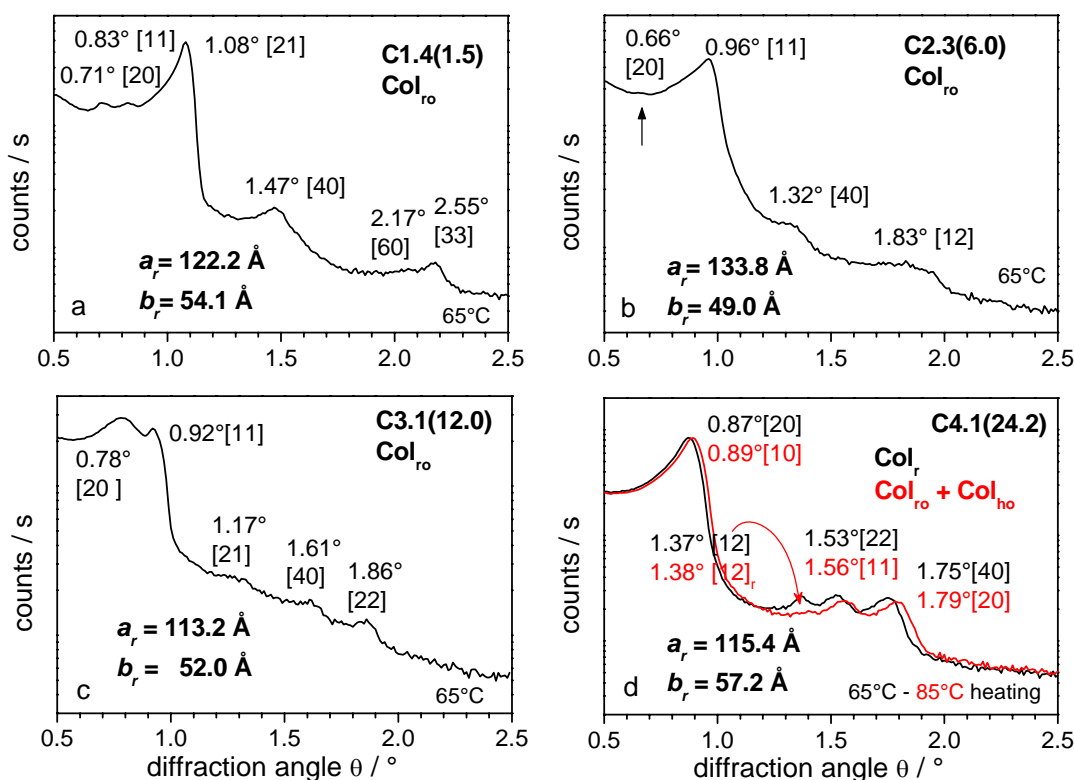


Fig. 3.48: Diffractograms of dendrimeric copper(II) complexes from 1st to 4th generation in their Col_r phases at 65°C. a) 1st generation **C1.4(1.5)**, b) 2nd generation **C2.3(6.0)**, c) 3rd generation **C3.1(12.0)** and d) 4th generation **C4.1(39.2)**, here additionally the diffractograms at 85°C with a mixture of Col_h and Col_r phases is shown. Attributed to the peaks: the θ values in ° and the Miller indexes [hk].

It has been shown that the 1st generation complexes exhibit a very particular behaviour: under special working-up procedure, it is possible to separate two types of copper coordination: blue and green complexes. Both have been identified by means of EPR (see 3.7), and the working-up procedures used for isolation are discussed in section 3.1.3.2. The X-ray analysis of the 1st generation presented so far, corresponds to a 1st generation complex in which a mixture of both coordination kinds is present, as is the case for the higher generations to which **C1.4(1.5)** was compared. Now we present the special features of the 1st generation complexes exhibiting only one coordination type, i.e. the blue complex **C1.2(1.9)b** (coordination N₂O₃) and the green one **C1.2(1.9)gr**, (coordination NO₅). Both exhibit thermochromism: blue up to the melting point, green in the liquid crystalline phase, cf. Scheme 3.6. **C1.2(1.9)b** exhibits a pale blue colour and is highly crystalline showing a high melting point at 127°C cf. Fig. 3.49a and Scheme 3.6. Above the melting point, the complex exhibits a green colour and displays an ordered Col_{r(o)} mesophase in a very narrow range developing steadily into the hexagonal one, as shown in Fig. 3.49b where reflections of a rectangular mesophase together with a hexagonal were recorded. All attempts to record an isolated rectangular phase failed. After quick cooling to 65°C the hexagonal columnar mesophase is presented in Fig. 3.49c.

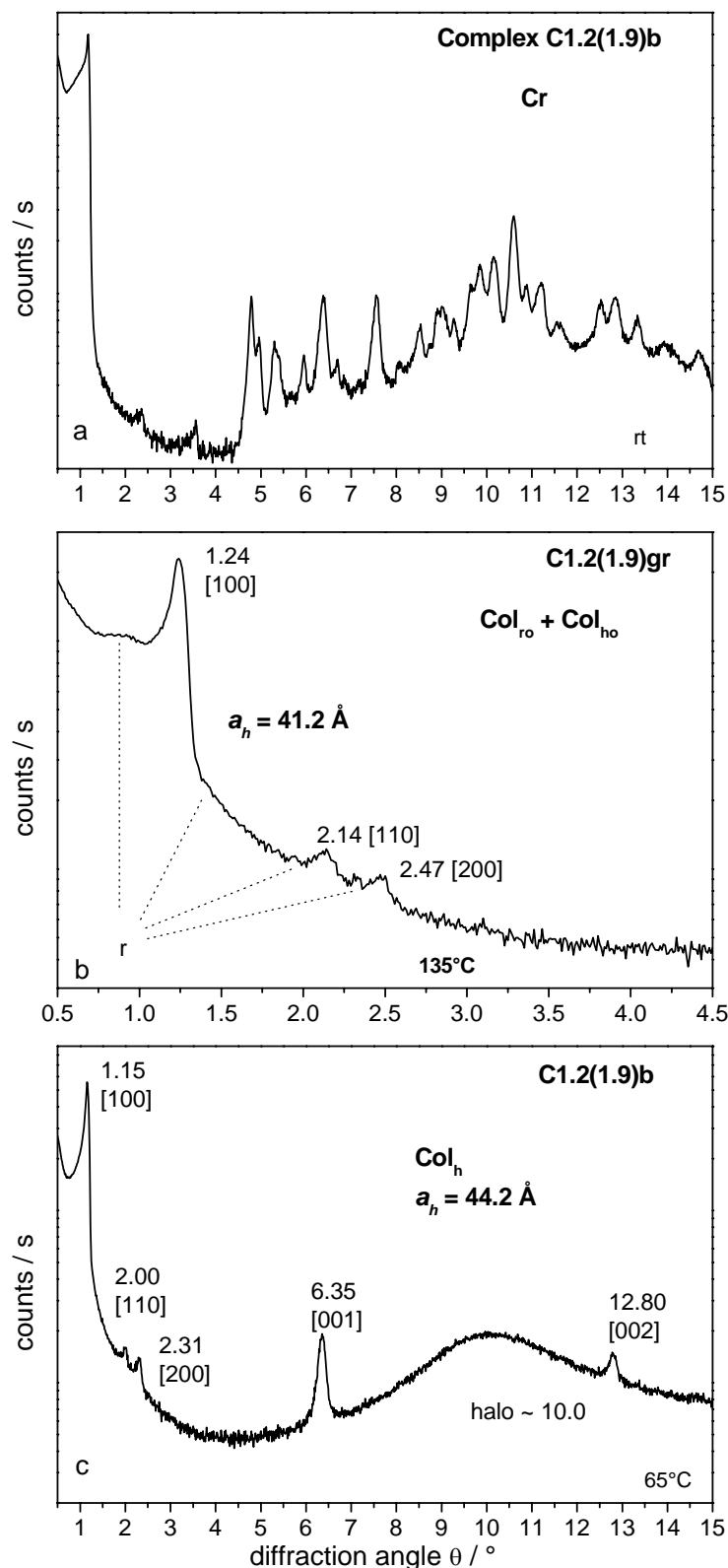


Fig. 3.49: Diffractograms of the 1st generation complexes **C1.2(1.9)b** at a) 65°C and **C2.1(1.9)gr** at b) 135°C in the transition from columnar rectangular to hexagonal columnar mesophase, and c) in a completely developed hexagonal columnar mesophase at 65°C after cooling. Attributed to the peaks: the θ -values in $^\circ$ and the Miller indexes $[hk]$.

3.9.1.2 Influence of the Copper Loading on the Mesophase. 2nd Generation Complexes of Different Loadings

All 2nd generation copper(II) complexes **C2.i(n)**, exhibit an enantiotropic hexagonal columnar mesophase. Complexes loaded with $n > 1$, exhibit a columnar rectangular mesophase below the hexagonal. The lattice parameters of the hexagonal and rectangular mesophases of both THF and γ -butyrolactone/ CHCl_3 series are presented in Table 3.24, Table 3.25 and Table 3.26 respectively. The hexagonal parameter of the 2nd generation dendrimeric ligand is given for comparison.

Table 3.24: Hexagonal lattice parameters a_h of the 2nd generation copper(II) complexes **C2.i(n)** at 65°C.

C2.i(n) L2	Series	T_{anneal}	T_{meas}	M	lattice parameter $a_h / \text{\AA}$	N_h	S_h / \AA^2
C2.3(6.0)	s	135	65	Col _{h(o)}	45.5	1.2	1809
C2.4(5.4)	wo	135	65	Col _{h(o)}	48.4	1.4	2029
C2.5(5.4)	s	135	65	Col _{h(o)}	47.5	1.4	1954
C2.6(5.2)	s	135	65	Col _{h(o)}	47.4	1.4	1946
C2.7(4.6)	wo	135	65	Col _{h(o)}	47.7	1.5	1970
C2.8(4.4)	s	135	65	Col _{h(o)}	48.4	1.5	2029
C2.9(3.5)	wo	135	65	Col _{h(o)}	48.3	1.6	2020
C2.10(2.7)	wo	135	65	Col _{h(o)}	47.8	1.6	1979
C2.12(2.1)	s	135	65	Col _{h(o)}	47.7	1.5	1970
C2.16(1.0)	s	100	65	Col _{h(d)}	49.4	1.2	2113
C2.18(0.9)	wo	100	65	Col _{h(d)}	47.9	1.1	1987
C2.19(0.5)	s	100	65	Col _{h(d)}	48.5	1.3	2037
C2.17(0.3)	s	100	65	Col _{h(d)}	44.6	1.0	1723
C2.20(0.3)	wo	100	65	Col _{h(d)}	45.5	1.1	1793
L2		Is	65	Col _{h(d)}	43.8	1.1	1661

Ser: series procedure used to achieve the different loadings. **s:** variations in the stoichiometry and **wo:** washing out **T_{anneal}:** annealing temperature (°C), **T_{meas}:** measurement temperature (°C), **M:** mesophase. All the samples were heated up to 135°C ($n > 1$) or 100°C ($n \leq 1$), cooled down to 65°C and measured. **N_h:** calcd. number of dendrimeric complexes per hexagonal unit cell, **S_h:** surface of a column in the hexagonal phase, $S_h = a^2 \sin 60$.

Table 3.25: Rectangular lattice parameters a_r and b_r of the 2nd generation copper(II) complexes of the THF series **C2.i(n)** at 65°C.

C2.i(n)	Ser	T_{anneal} / °C	T_{meas} / °C	M	lattice parameter a_r, b_r / Å	N_r	S_r / Å²
C2.3(6.0)	s	100	65	Col _{r(o)}	$a_r = 133.8$ $b_r = 49.0$	4.5	1458
C2.4(5.4)	wo	100	65	Col _{r(o)}	$a_r = 107.7$ $b_r = 47.9$	3.7	1405
C2.5(5.4)	s	100	65	Col _{r(o)}	$a_r = 126.1$ $b_r = 49.1$	4.3	1424
C2.6(5.2)	s	100	65	Col _{r(o)}	$a_r = 117.0$ $b_r = 47.6$	4.0	1380
C2.7(4.6)	wo	100	65	Col _{r(o)}	$a_r = 120.1$ $b_r = 48.5$	4.5	1300
C2.9(3.5)	wo	100	65	Col _{r(o)}	$a_r = 120.0$ $b_r = 49.1$	4.6	1284
C2.10(2.7)	wo	100	65	Col _{r(o)}	$a_r = 113.2$ $b_r = 48.2$	4.5	1214
C2.12(2.1)	s	100	65	Col _{r(o)}	$a_r = 107.0$ $b_r = 45.0$	3.8	1284

ser: synthesis via, **s**: variation in the reaction stoichiometry, **wo**: washing out with different solvents. **T_{anneal}**: annealing temp., **T_{meas}**: measurement temp., **M**: mesophase. **N_r**: calcd. number of dendrimer molecules per rectangular unit cell, **S_r**: surface of a column in the Col_{r(o)} phase (p2mg symmetry) $S_r = a \cdot b/4$

Table 3.26: Rectangular and hexagonal lattice parameters of the 2nd generation of the copper(II) complexes of the γ -butyrolactone/CHCl₃ series at 65°C.

C2.i(n) L2	T_{anneal} / °C	T_{meas} / °C	M	lattice parameter $a_h / a_r, b_r$ / Å	N_{r/h}	S_{r/h} / Å²
C2.2(6.3)	100	65	Col _{r(o)}	$a_r = 126.1$ $b_r = 47.5$	4.0	1481
	135	65	Col _{h(o)}	$a_h = 46.8$	1.3	1897
C2.11(2.6)	100	65	Col _{r(o)}	$a_r = 100.3$ $b_r = 48.9$	4.6	1225
	135	65	Col _{h(o)}	$a_h = 50.4$	1.8	2200
C2.13(2.0)	100	65	Col _{r(o)}	$a_r = 108.4$ $b_r = 48.7$	4.5	1184
	135	65	Col _{h(o)}	$a_h = 51.8$	2.0	2324
C2.15(1.3)	100	65	Col _{r(o)}	$a_r = 98.1$ $b_r = 49.1$	4.2	1147
	135	65	Col _{h(o)}	$a_h = 51.2$	2.0	2270
L2	I	65	Col _{h(d)}	$a_h = 43.8$	1.1	1661

T_{anneal}: annealing temp., **T_{meas}**: measurement temp., **M**: mesophase. **N_{r/h}**: calcd. number of dendrimer molecules per rectangular/hexagonal unit cell, **S**: surface of a column in the mesophase $S_h = a^2 \sin 60$ (hexagonal) $S_r = a \cdot b/4$ (rectangular, p2mg symmetry)

The complete indexing of all the complexes, at each mesophase and temperature, is summarised in the compound register II: X-ray evaluation of mesophases, cf. 6.5, at the end of the experimental section.

For both series, dendrimers loaded with up to one copper centre $n \leq 1$, do not exhibit sharp reflections in the wide-angle region, therefore an intracolumnar ordering in the hexagonal phase of these low loaded complexes is excluded. Complexes with $n > 1$ exhibit in contrast two sharp reflections in the halo. They are indicative of intra-columnar order along the columns in the hexagonal phase, i.e. $\text{Col}_{h(o)}$ phases, as discussed in the next section 3.9.2.

In order to calculate the number of dendrimeric molecules per hexagonal unit cell N_h , the periodic distance given by the halo ($\theta \sim 10^\circ$ i.e. $d \sim 4.4 \text{ \AA}$) is considered as the mean intracolumnar distance for complexes with $n \leq 1$. The distance indicated by the first of the sharp reflections in the halo ($\theta = 6.4^\circ$ [001] $d = 6.9 \text{ \AA}$) is taken as the intracolumnar distance c for complexes with $n > 1$. As result, one dendrimeric complex fills the unit cell in the columnar phase in average.

Fig. 3.50 and Fig. 3.51 illustrate the variation of the hexagonal and rectangular lattice parameters with the copper loading n .

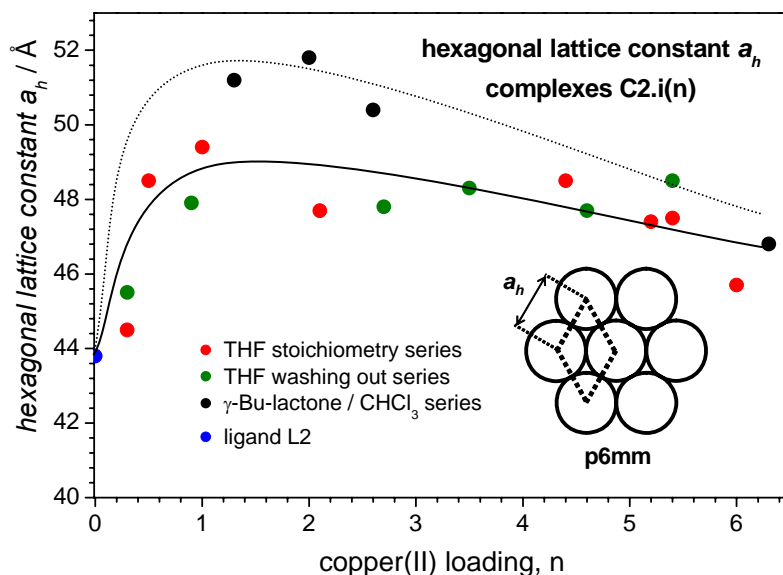


Fig. 3.50: Hexagonal lattice parameter a_h of the columnar mesophases of the 2nd generation copper(II) dendrimeric complexes **C2.i(n)**, fit to the points (— THF, --- γ -Bu-lactone) to guide the eye.

The coordination of copper by the dendrimer and its protonation result in an increase of the hexagonal lattice parameter a_h compared to that of the dendrimeric ligand, cf. Fig. 3.50. The incorporation of small amounts of copper such as one copper centre

per dendrimeric ligand causes a stretching of around 6 Å in the dendrimer scaffold. Further coordination of copper does not lead to further enlargement of the lattice parameter, but to a slight decrease of it. This phenomenon could be explained by the increased bridging behaviour of the nitrate groups (cf. 3.7.3, 3.9.2.1) to form dimeric and polymeric structures, which in the intradendrimeric case should lead to a contraction of the dendrimeric core. Surprisingly, complexes of the γ -butyrolactone/ CHCl_3 series exhibit larger hexagonal parameters than those of the THF series of similar loadings. No significant difference between complexes of both series with similar copper loadings, not either in the protonation, has been found in the behaviour of the complexes so far which could explain this anomaly.

C2.i(n) dendrimers with copper loadings $n > 1$ show columnar polymorphism. They exhibit a rectangular mesophase $\text{Col}_{\text{r(o)}}$ below the hexagonal $\text{Col}_{\text{h(o)}}$. Both are of the ordered type as indicated by the presence of sharp reflections in the halo region, cf. Fig. 3.42. Rectangular lattice parameters are depicted in Fig. 3.51. The rectangular lattice parameter a_r increases noticeably with the copper loading n , while the parameter b_r varies only slightly. The lattice parameter b_r is of the same order of magnitude as the hexagonal intercolumnar distance a_h . No differences are observed between parameters of complexes of THF or γ -butyrolactone/ CHCl_3 series.

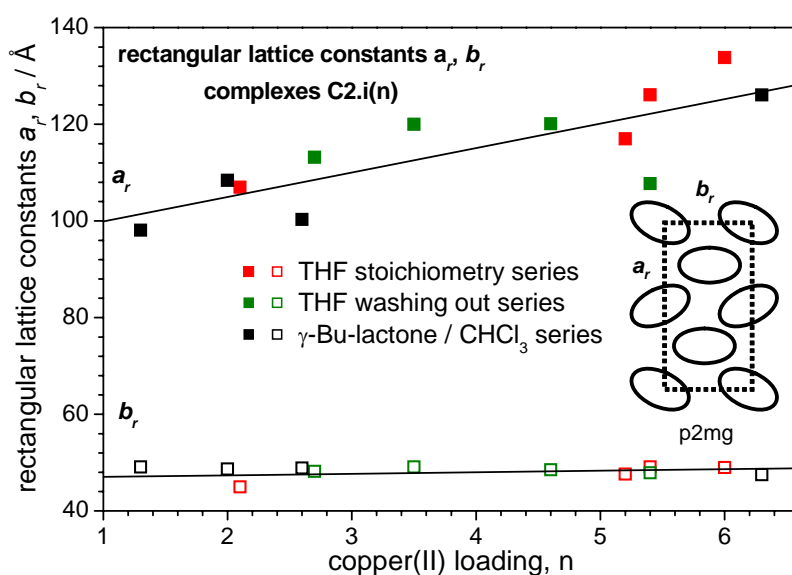


Fig. 3.51: Rectangular lattice parameters a_r and b_r of the columnar mesophases of the 2nd generation copper(II) dendrimeric complexes **C2.i(n)** with $n > 1$.

According to the indexation, number of molecules and surface per column, **C2.i(n)** complexes with $6.3 \geq n > 4.6$, exhibit a p2mg rectangular mesophase. The indexation of complexes with $1.0 < n \leq 4.6$ is not so clear, because the diffractograms are not so well resolved and for the lowest loadings of this range, the rectangular columnar mesophase

seems to coexist with the hexagonal one. As a consequence the indexing is not so reliable and the calculated lattice parameters should be taken with care. Coming back to the discussion of a possible $c2mm$ space group of the $Col_{r(o)}$ phase (cf. Fig. 3.45), Fig. 3.52 shows that the surface of the rectangular unit cell with $c2mm$ symmetry $S_r(c2mm) = a_r \cdot b_r/2$ is larger than that of a hexagonal cell $S_h = a_h^2 \sin 60$, even for complexes of the series which showed unusual large hexagonal lattice parameters. In consequence, the $p2mg$ symmetry with $S_r(p2mg) = a_r \cdot b_r/4$ is most probable.

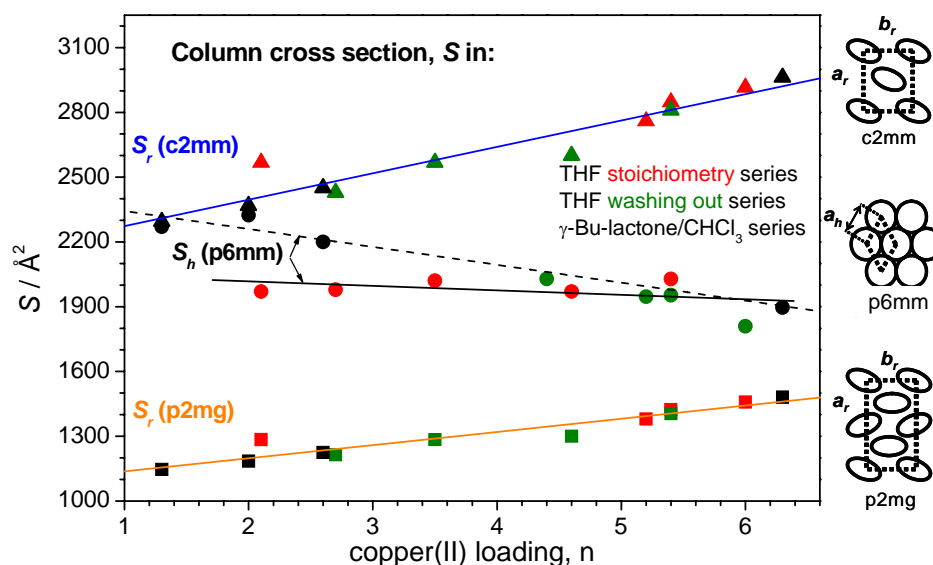


Fig. 3.52: Areas per column in the hexagonal S_h ($p62/m2/m$) and rectangular $S_r(c2mm)$, $S_r(p2mg)$ mesophases of the 2nd generation copper(II) dendrimeric complexes.

3.9.1.3 X-ray Analysis of the 2nd Generation Copper(II) Complex from Tetrafluoroborate C2.21(4.0)

The 2nd generation copper(II) complex prepared from the copper(II) tetrafluoroborate hydrate salt, **C2.21(4.0)**, exhibits solely a disordered columnar hexagonal mesophase, $Col_{h(d)}$, as presented in Fig. 3.53. A better developed mesophase is observed at 85°C, Fig. 3.53b. The parameters and lattice constants are given in Table 3.27. Under the same annealing conditions as the nitrate complexes, the lattice parameters of the tetrafluoroborate, 49.5 Å, is slightly larger than those analogues exhibiting similar loadings (48.1 Å for **C2.8(4.4)** and 48.3 Å **C2.9(3.5)**). Since the copper contents are similar, the difference could rely on the role of the tetrafluoroborate anion compared with respect to nitrate. The contraction of the dendrimer by nitrate groups (cf. 3.5, 3.7) does not occur with tetrafluoroborate. Very remarkable is the absence of reflections in the wide angle region. In the next section 3.9.2 the role of the anion in the formation of ordered columnar mesophases will be discussed.

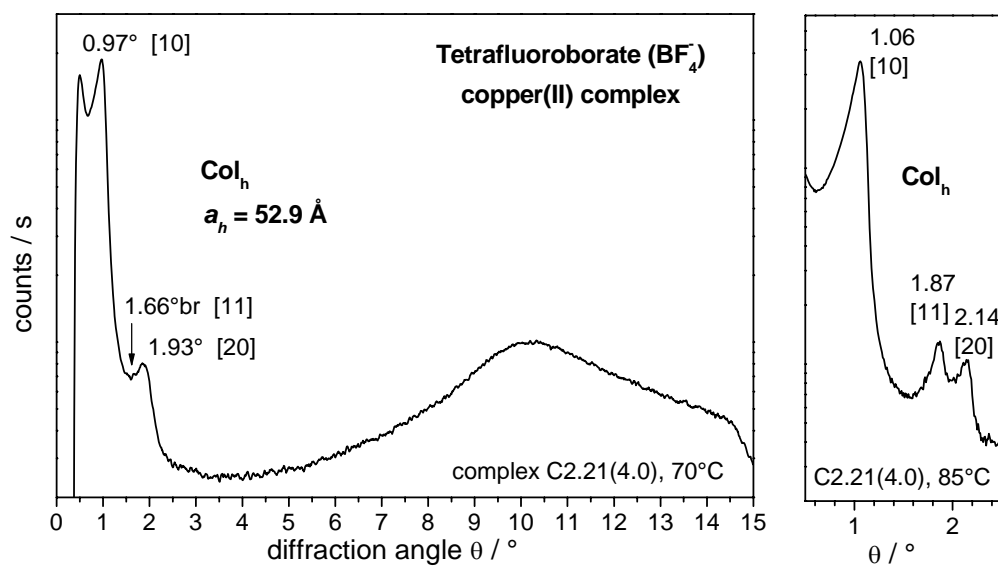


Fig. 3.53: X-ray diffractogram of the 2nd generation copper(II) complex from tetrafluoroborate **C2.21(4.0)** in the Col_h phase at 70°C. Attributed to the peaks: the θ -values in $^\circ$ and the Miller indexes $[hk]$.

Table 3.27: Hexagonal lattice parameter a_h of the 2nd generation dendrimeric copper(II) tetrafluoroborate complex

Compound	T_{anneal}	T_{meas}	$Col_{h(d)}$	lattice parameter $a_h / \text{\AA}$
C2.21(4.0)	100	70	●	52.9
	rt	85	●	47.7
L2	I	65	●	43.8

T_{anneal} : annealing temperature($^\circ\text{C}$), T_{meas} : measurement temperature ($^\circ\text{C}$), **M**: mesophase, **I**: isotrope melt.

3.9.2 Wide-Angle Region

In the wide-angle region of the mesophase diffractograms of the dendrimeric copper complexes prepared with copper nitrate trihydrate, we observe a halo at $\theta \sim 10^\circ$ and additionally one or two narrow reflections at $\theta = 6.40^\circ$ and $\theta = 12.85^\circ$. The halo at $\theta \sim 10^\circ$ ($d \sim 4.4$ Å) corresponds to the liquid-like short range order of the melted alkoxy chains and confirms the liquid crystalline nature of the phase. The sharp diffraction maxima in the wide-angle range with $\theta = 6.40^\circ$ ($d = 6.9$ Å) and $\theta = 12.85^\circ$ ($d = 3.5$ Å, the second order of the former), allow two interpretations which will be discussed in the following. The reflections are either:

- i. indication of intracolumnar order along the columns in the mesophase, i.e. occurrence of $\text{Col}_{\text{r(o)}}$ and/or $\text{Col}_{\text{h(o)}}$ phases, as defined until now.
- ii. or reflections of possible crystalline impurities still present in the sample despite careful working-up procedure.

3.9.2.1 Ordered Columnar Mesophases

The sharp reflection in the wide-angle region of the diffractograms, $\theta = 6.40^\circ$ ($d = 6.9$ Å), is observed in both the rectangular and the hexagonal columnar mesophases in every generation. It appears above a certain copper content, e.g. for the 2nd generation from a copper loading $n \geq 1.3$ (around the 20% of the maximal copper loading achieved by this generation). The second reflection at the double θ -value, $\theta = 12.85^\circ$ ($d = 3.5$ Å) is observed at the maximum loadings in higher generations and at $n \geq 4.4$ for the 2nd generation. The intensity of the reflections tends to increase with increasing copper(II) content as can be seen in Fig.3.54 for the 2nd generation. The intensity of a reflection is quantitative estimated through the area under this reflection. A cross-correlation coefficient, ρ , was calculated for the area of the peaks at 6.4° and the copper loading, n , in the final product, according to Eq. 3.14^[329].

$$\rho = \frac{\langle A \cdot n \rangle - \langle A \rangle \langle n \rangle}{\sqrt{(\langle A^2 \rangle - \langle A \rangle^2)(\langle n^2 \rangle - \langle n \rangle^2)}} \quad \text{Eq. 3.14}$$

A stands for the area under the reflection at $\theta = 6.40^\circ$ which was determined by a Lorentzian fit of this peak. The copper loading in the final products is denoted by n as usual, and $\langle \rangle$ indicates the arithmetic mean value. Two fully correlated variables, i.e. variables related by a linear dependence, result in a cross-correlation coefficient $\rho = 1$, non correlated variables in $\rho = 0$ and variables with an inverse dependence show a negative coefficient $\rho < 0$. For the area under $\theta = 6.40^\circ$ and the copper loading in the

complex n , the obtained cross-correlation coefficient was $\rho = 0.73$, i.e. the area of the reflection at $\theta = 6.40^\circ$ exhibit a fairly good linear dependence on the copper loading. On the other hand, very little and inverse correlation ($\rho = -0.21$) between the area under the diffraction peak $\theta = 6.40^\circ$ at and the excess of copper nitrate trihydrate, m , used in the synthesis (cf. 3.1.3.1) was found. Especially this last correlation argues for the absence of impurities.

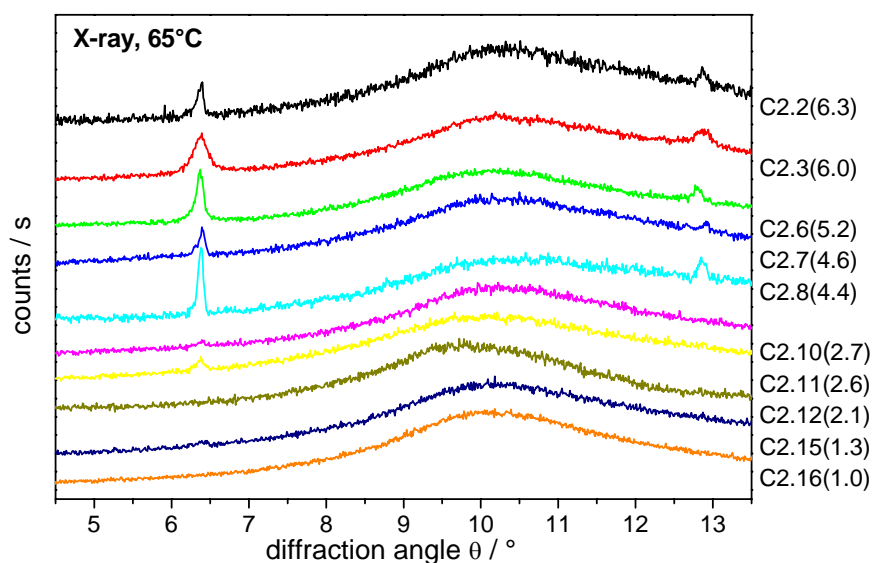


Fig. 3.54: Relative intensity of the diffraction maxima at $\theta = 6.40^\circ$ and $\theta = 12.85^\circ$ in dependence on the copper loading n for selected 2nd generation copper complexes **C2.i(n)**. Diffractograms normalised taking the halo at ca. 10° as reference.

The diffraction peak at $\theta = 6.40^\circ$ ($d = 6.9 \text{ \AA}$) is already present in the diffractograms of the samples in their partially crystalline state (cf. 3.8, Scheme 3.5) at room temperature. Its relative intensity (defined as $(I/I_{\max}) \cdot 100$, related to the most intense reflection in the pattern, I_{\max} considered by convention 100%) increases by a factor of two on the transition into the mesophase, cf. Fig. 3.55. This could be indicative of an enhancement of the intracolumnar ordering and supports strongly the model of an ordered columnar mesophase. The same amount of e.g. inorganic impurity would not cause a more intensive peak. Unfortunately, because the complexes decompose before isotropisation, it is not possible to record their diffractograms in the isotropic melt, to check, whether the wide angle peaks are still present. Here, sharp reflections, belonging to a $\text{Col}_{h(o)}$ phase should disappear, whereas reflections from impurities should be still observable.

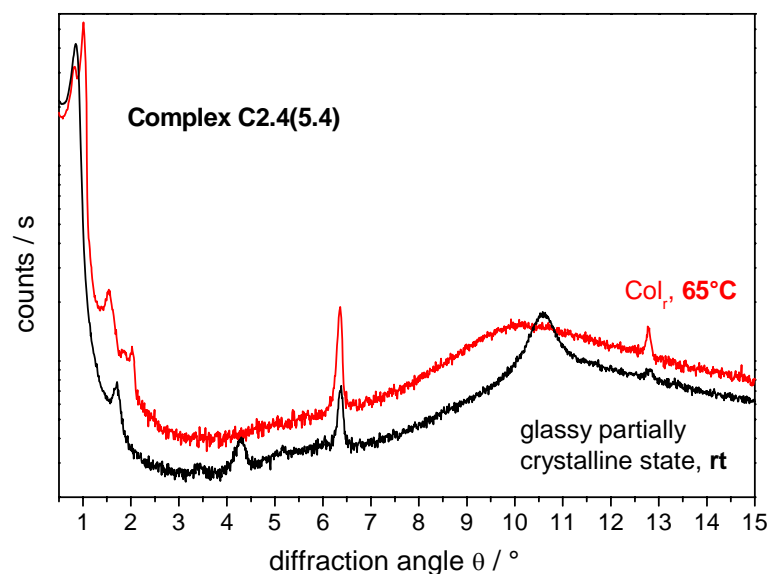


Fig. 3.55: Guinier diffractograms of the complex **C2.4(5.4)**.

A further strong argument in favour of an ordered columnar phase is the dimeric structure of the copper complexes revealed by EPR^[206], cf. 3.7.3. At very low temperatures, an antiferromagnetic coupling was observed in both the blue and green complexes **C1.2(1.9)b** and **C1.2(1.9)gr**. It was deduced that a nitrate group in a μ -1,3 bridging mode should be responsible for the spin exchange between the pairs of copper centres. The nitrate group, which is present at any temperature, would give rise to dimeric structures (**C1.2(1.9)b**) or polymeric chains (**C1.2(1.9)gr**), as indicated in Fig. 3.31 and 3.32. The EPR-estimated copper to copper distance of 6.92 Å coincides well with the distance revealed by X-ray diffraction 6.9 Å.

And further on, as mentioned in the previous section (cf. 3.9.1.3 Fig. 3.53), the copper complex from tetrafluoroborate exhibits exclusively a columnar hexagonal mesophase. No reflection at $\theta = 6.40^\circ$ was observed. The absence of this reflection indicates the lack of order along the columns. Again, this supports the role of the nitrate anion as bridging ligand in the regular stacking of the dendrimer complexes in the columns, and makes improbable the responsibility of impurities.

Ordered columnar mesophases, $\text{Col}_{\text{h(o)}}$ and $\text{Col}_{\text{r(o)}}$ (cf. 1.1.3) in the range of 3 - 11 Å intracolumnar distance, have been reported in the literature since end of the 1970s^[5, 15, 28, 29, 40, 43, 44, 46, 47, 50, 52, 149, 180, 188, 328, 330-333]. Metal centres are often involved in the formation of the intracolumnar ordering^[31, 42]. Columnar mesophases with more than one stacking distance have been also reported^[41, 47, 50, 334]. In our case, both values of ($d = 6.9$ Å and $d = 3.5$ Å) lie within the limits described in the literature. As significant for intracolumnar ordering, the reflection at $\theta = 6.0^\circ$ ($d = 6.9$ Å) would be indexed as [001] and its second order reflection at $\theta = 12.85^\circ$ ($d = 3.5$ Å) as [002]. The main objection for

an ordered columnar mesophase is the sharpness of the reflections, which is more characteristic of a crystalline peak. To exclude impurities as the cause of for the sharp wide angle reflections, the possible inorganic impurities have nevertheless been investigated.

3.9.2.2 Possible Inorganic Impurities in the Dendrimeric Copper(II) Complexes

The complexation conditions without dendrimeric ligand were checked in a blank reaction, cf. 3.1.2.1. The gravimetric analysis of the blank reaction, shows that inorganic impurities could be present in *not more* than 0.05 wt. % together with the dendrimeric copper(II) complexes. WAXS analysis ($5^\circ < 2\theta < 60^\circ$) at room temperature of the green residue of the blank reaction, presented in Fig. 3.56, reveal that it is a mixture of copper nitrate hemipentahydrate, $\text{Cu}(\text{NO}_3)_2 \cdot 2.5\text{H}_2\text{O}$ ^[220], similar to our starting copper salt, $\text{Cu}(\text{NO}_3)_2 \cdot 3\text{H}_2\text{O}$, and basic copper nitrate $\text{Cu}_2(\text{NO}_3)(\text{OH})_3$ ^[221, 222].

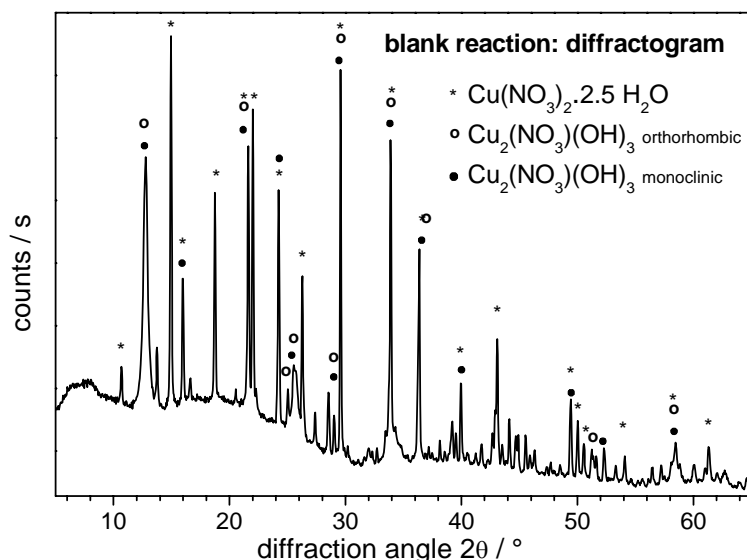


Fig. 3.56: Diffractogram at rt. of the green residue resulting from the blank reaction in THF. Coincidences with reflections of $\text{Cu}(\text{NO}_3)_2 \cdot 2.5\text{H}_2\text{O}$ or $\text{Cu}_2(\text{NO}_3)(\text{OH})_3$ are indicated according to the legend ^[220, 221].

These two species, $\text{Cu}(\text{NO}_3)_2 \cdot 3\text{H}_2\text{O}$ and $\text{Cu}_2(\text{NO}_3)(\text{OH})_3$, are therefore, even in a very low extent, the most likely inorganic candidates to be present in the end product. Less plausible, other copper(II) species are considered too. In overview, the studied species comprise:

- i. copper nitrate trihydrate, $\text{Cu}(\text{NO}_3)_2 \cdot 3\text{H}_2\text{O}$
- ii. cupric oxide, CuO
- iii. basic copper carbonate, $\text{Cu}_2(\text{CO}_3)(\text{OH})_2$
- iv. copper carbonate, CuCO_3

- v. hexaaquacopper(II) dinitrate, $[\text{Cu}(\text{H}_2\text{O})_6](\text{NO}_3)_2$
- vi. THF copper(II) solvate, $\text{Cu}(\text{THF})_n(\text{NO}_3)_2$
- vii. copper hydroxide, $\text{Cu}(\text{OH})_2$
- viii. basic copper nitrate, $\text{Cu}_2(\text{NO}_3)(\text{OH})_3$

Copper nitrate trihydrate, $\text{Cu}(\text{NO}_3)_2 \cdot 3\text{H}_2\text{O}$, **copper(II) oxide**, CuO , and **basic copper carbonate**, $\text{Cu}_2(\text{CO}_3)(\text{OH})_2$, have been investigated by X-ray. No significant coincidences with the sharp reflections of the complexes at $\theta = 6.40^\circ$ ($d = 6.9 \text{ \AA}$) and $\theta = 12.85^\circ$ ($d = 3.5 \text{ \AA}$) in the dendrimeric copper complexes were found, cf. Fig. 3.57. EPR investigations of $\text{Cu}(\text{NO}_3)_2 \cdot 3\text{H}_2\text{O}$ ^[206] excluded too its presence together with the dendrimers.

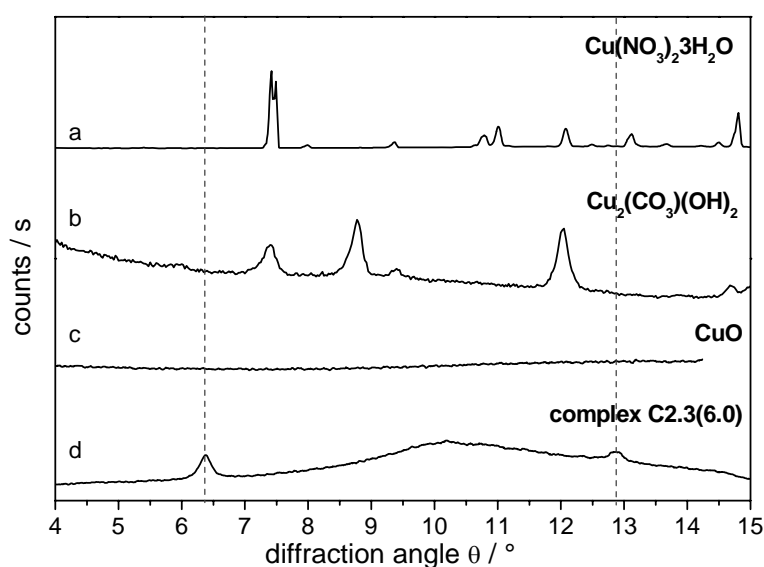


Fig. 3.57: Diffraction patterns of a: $\text{Cu}(\text{NO}_3)_2 \cdot 3\text{H}_2\text{O}$, b: $\text{Cu}_2(\text{CO}_3)(\text{OH})_2$, c: CuO , (no diffraction peaks found in this range) and d: complex **C2.3(6.0)**. a, c, d Guinier diffractograms at 65°C , b WAXS diffractogram at rt.

The presence of **copper(II) carbonate**, CuCO_3 , together with the dendrimeric copper complexes is not very likely, because it is not stable and evolution to the more stable basic carbonate form $\text{Cu}_2\text{CO}_3(\text{OH})_2$ would be favoured ^[335]. In any case, the neutral carbonate does not exhibit any reflection at $\theta = 6.40^\circ$ or $\theta = 12.85^\circ$ and therefore can not be the species responsible for the sharp reflections in the diffractograms of the dendrimeric complexes ^[336].

From EPR results, the formation of an **hexaaquacopper (II) complex** bridged through one of its six water ligands and a nitrate group to dendrimer-coordinated copper centres was deduced for complexes exposed to a water atmosphere (cf. 3.7.3.3) ^[206]. Here, in analogy, an inorganic hexaaquacopper(II) dinitrate, $[\text{Cu}(\text{H}_2\text{O})_6](\text{NO}_3)_2$, could be assumed. However a hexaaquacopper(II) dinitrate does not contribute to reflections in

the wide angle region of the diffractograms because it exhibits no diffraction maxima at $\theta = 6.40^\circ$ or $\theta = 12.85^\circ$ [315, 337].

Elemental analysis of the precipitate of the THF solution of $\text{Cu}(\text{NO}_3)_2 \cdot 3\text{H}_2\text{O}$ during the preparation of the stock solution, reveals a carbon content of 0.37%. The low carbon percentage rules out the possibility of a **copper THF solvate**, $\text{Cu}(\text{THF})_n(\text{NO}_3)_2$. The formation of a complex consisting exclusively of copper and THF molecules is not very plausible, because it would require the presence of more voluminous anions than nitrate, such as hexachloroantimonate, SbCl_6 to stabilise the copper solvate as described in the literature [338].

Copper hydroxide, $\text{Cu}(\text{OH})_2$ has been described in the literature to be formed by dissolving copper nitrate trihydrate in THF [339, 340], and could be therefore present as impurity in our complexes. X-ray diffractograms of commercial $\text{Cu}(\text{OH})_2$ were measured under the same experimental conditions than the mesophases of the dendrimeric copper complexes, see Fig. 3.58.

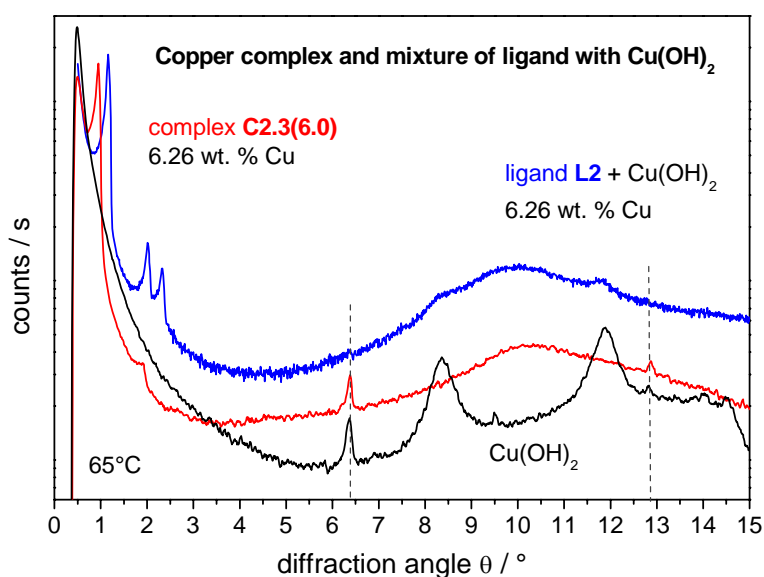


Fig. 3.58: Copper hydroxide as possible impurity in the dendrimeric copper-complexes. Physical mixture of **L2** and $\text{Cu}(\text{OH})_2$ in the Cu wt. % ratio found in **C2.3(6.0)**. Diffractograms recorded at 65°C in the $\text{Col}_{r(o)}$ mesophase of **C2.3(6.0)** and the Col_h mesophase of **L2**.

We observe diffraction peaks at $\theta = 6.40^\circ$ ($d = 6.9 \text{ \AA}$) and $\theta = 12.85^\circ$ ($d = 3.5 \text{ \AA}$), reflections at the same angles that appear in the diffractograms of the dendrimeric complexes. Nevertheless, further peaks significantly more intense than the former, were recorded at $\theta = 8.4^\circ$ ($d = 5.3 \text{ \AA}$) and $\theta = 11.9^\circ$ ($d = 3.7 \text{ \AA}$). If copper hydroxide is present together with the dendrimeric copper complexes as impurity, its diffraction maxima should be detectable in the complex diffractogram. To check this, the dendrimeric ligand **L2** was mixed with $\text{Cu}(\text{OH})_2$ in the same weight ratio as copper(II)

is present in **C2.3(6.0)**, crushed to fine powder, and a diffractogram of the mixture was recorded, cf. Fig. 3.58, blue line. As expected only the most intense reflections $\theta = 8.4^\circ$ and $\theta = 11.9^\circ$ are observed. Therefore the copper hydroxide, can not be responsible for the reflections at $\theta = 6.40^\circ$ and $\theta = 12.85^\circ$ in our samples.

The formation of *basic copper nitrate*, $\text{Cu}_2(\text{NO}_3)(\text{OH})_3$ also formulated as $\text{Cu}(\text{NO}_3)_2 \cdot 3\text{Cu}(\text{OH})_2$, has been observed under the complexation conditions of copper(II) by dendrimers, cf. section 3.1.2.1 and Fig. 3.56. Basic copper nitrate exhibits three sharp reflections at $\theta = 6.39^\circ$ ($d = 6.9 \text{ \AA}$), $\theta = 10.79^\circ$ ($d = 4.1 \text{ \AA}$), and $\theta = 12.88^\circ$ ($d = 3.5 \text{ \AA}$), relative intensities 100%, 7% and 45% respectively in the wide angle region of $5^\circ < \theta < 15^\circ$ in both its orthorhombic (gerhardite) ^[341] and monoclinic (rouaite) ^[221, 222] modifications. The reflections at $\theta = 6.40^\circ$ ($d = 6.9 \text{ \AA}$) and $\theta = 12.88^\circ$ ($d = 3.5 \text{ \AA}$) coincide with those observed by us in the diffractograms of the dendrimeric copper complexes as shown in Fig. 3.59. It constitutes therefore the one only potential inorganic salt to be present with the dendrimeric complexes, even if in no more than a 0.05 wt. %.

Basic copper nitrate powder was prepared by us according to the procedure described in Gmelin ^[223]. The bluish-green powder was x-rayed in a Guinier camera and its structure was confirmed by comparison with the literature data ^[221, 222, 341]. In order to check how the presence of free basic copper nitrate $\text{Cu}_2(\text{NO}_3)(\text{OH})_3$ would affect the diffractograms of the complexes, the pure dendrimeric ligand was mechanically mixed with the basic copper nitrate powder in the same weight ratio as copper(II) is present in the complex **C2.3(6.0)**, and a diffractogram of the mixture was recorded, cf. Fig. 3.59. We observe that the reflections at $\theta = 6.40^\circ$ and $\theta = 12.85^\circ$ in the mixture are much stronger than those of the complex **C2.3(6.0)**. The reflection at $\theta = 12.81^\circ$ in the mixture is furthermore shifted to around 0.07° to lower values with respect to the complex and the free $\text{Cu}_2(\text{NO}_3)(\text{OH})_3$. Finally, in the small-angle region ($\theta \leq 3^\circ$), mixture and complex exhibit different reflection patterns; the reflections of the complex at $\theta = 0.96^\circ$ appear at smaller angles, i.e. at larger distances, than those of the ligand in the mixture at $\theta = 1.14^\circ$. Therefore, free basic copper nitrate can not be responsible to a considerable extent for the peaks at $\theta = 6.40^\circ$ and $\theta = 12.85^\circ$ in the dendrimeric copper complex **C2.3(6.0)**.

Furthermore, the reflections at $\theta = 6.40^\circ$ and $\theta = 12.85^\circ$ are much less intense in samples evacuated and sealed under heating for e.g. synchrotron investigations ^[342]. After the measurement, if the capillary is exposed to a saturated water atmosphere for several hours and measured again, the intensity of the diffraction peak does not increase, excluding thus water as responsible for this phenomenon. During the evacuation and sealing process only a liquid or gaseous species could have been removed.

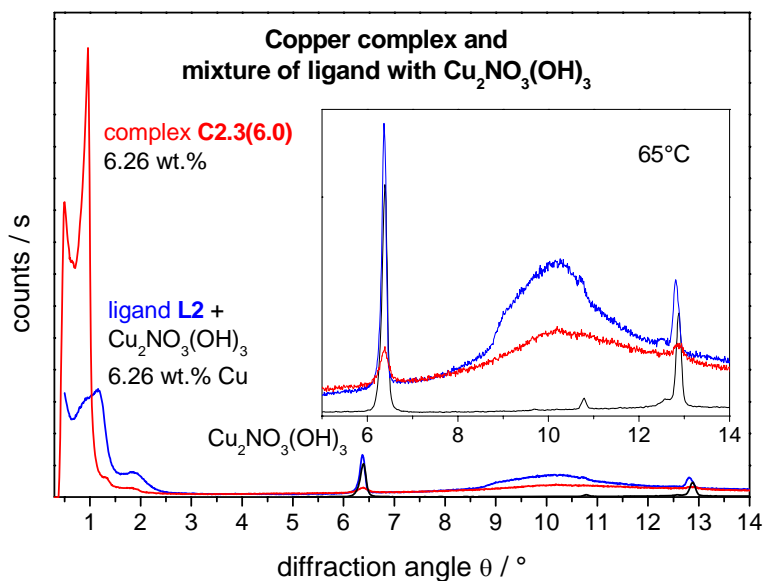
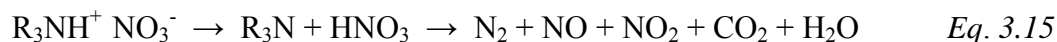


Fig. 3.59: Basic copper nitrate as possible impurity in the complex **C2.3(6.0)**, $\text{Cu}_2\text{NO}_3(\text{OH})_3$ and physical mixture **L2** + $\text{Cu}_2\text{NO}_3(\text{OH})_3$ in the Cu wt. % ratio found in the complex **C2.3(6.0)**. Diffractograms recorded at 65°C in the $\text{Col}_{r(o)}$ mesophase of **C2.3(6.0)** and the Col_h mesophase of **L2**.

A sublimation of the presumed impurity, $\text{Cu}_2\text{NO}_3(\text{OH})_3$, does not seem likely to happen and no bibliographic support for it was found either. The decomposition of $\text{Cu}_2\text{NO}_3(\text{OH})_3$ occurs at higher temperature (240°C^[343]) than the decomposition temperature of the copper complexes, i.e. for most of the complexes at approximately 180°C. Therefore, decomposition of $\text{Cu}_2\text{NO}_3(\text{OH})_3$ can not justify the lowering of the intensity of the reflections in the wide angle either. We have earlier postulated (cf. 3.2, 3.5.3.3, 3.8) that the dendrimer complexes, are organic ammonium nitrate salts, i.e. the tertiary amine groups of the poly(propylene imine) core are protonated. Low molecular alkylammonium nitrate salts undergo, with increasing temperature, a transformation involving proton transfer prior to the ultimate decomposition^[344, 345] as indicated in Eq. 3.15:



As a result, nitric acid or nitrous gases are developed, which can be easily removed in vacuum. A similar mechanism can be assumed for the dendrimeric ammonium nitrate salts. The fraction of removed nitrate is not any more able to bridge copper centres and since these bridges are responsible for the reflections in the wide angle, the intensity of these reflections decrease. In consequence, the reflections in the wide angle region of the diffractograms must only be caused by the ordered structure of the nitrate bridged dendrimeric copper complexes and are not due to any crystalline inorganic impurity.

No crystalline structure was observed in TEM images of the 2nd generation complexes loaded with 6 or less copper centres per dendrimeric ligand (complex **C2.3(6.0)**, cf. Fig.

3.60). In order to check from which limit impurities would appear in TEM one expressly “overloaded” complex, **C2.1(7.3)**, was prepared. Already with $n = 7.3$ (Cu:L2), crystallites (up to 60 nm large) and Moiré structures appeared in TEM as shown in Fig. 3.60a, b (in circles).

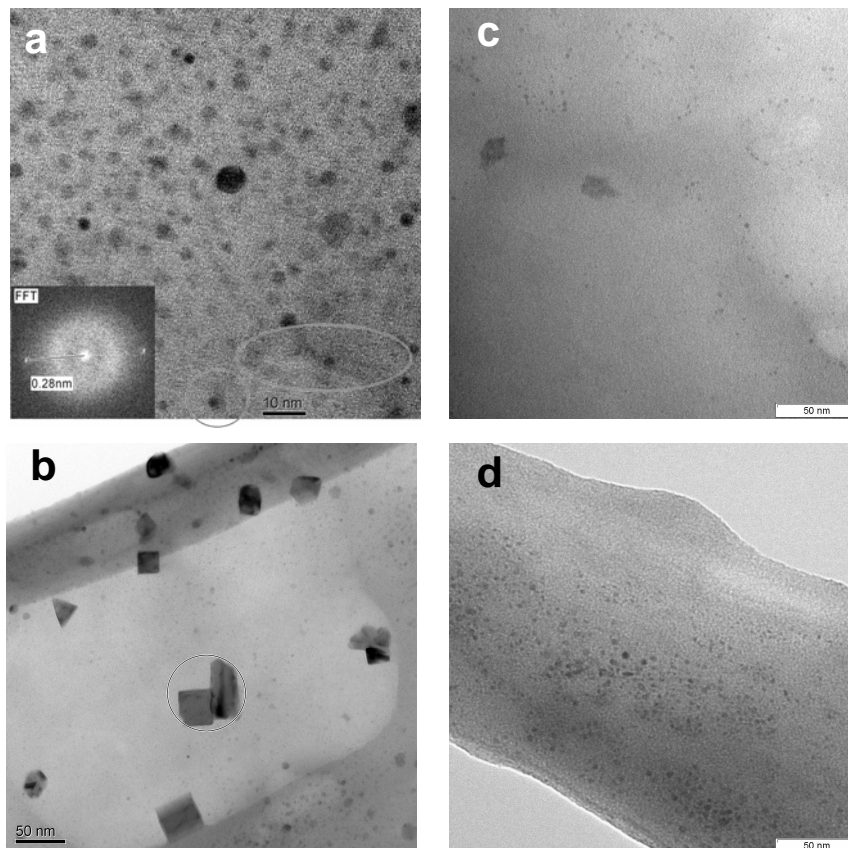


Fig. 3.60: TEM images of the complexes **C2.1(7.3)**, **C2.3(6.0)** and **C2.4(5.4)**. a) complex **C2.1(7.3)**, usual appearance of the dendrimeric copper complexes (smaller spots). Moiré patterns observed down-right. b) **C2.1(7.3)**, appearance of big crystallites. c) complex **C2.3(6.0)**, and d) complex **C2.4(5.4)**.

3.9.2.3 Conclusions

In summary, all the copper (II)-complexes were found to feature one or more thermotropic liquid crystalline phase. The columnar hexagonal mesophases, found in the pure ligands, reappear in the copper(II) complexes. Up to the 4th generation, a columnar rectangular mesophase (p2mg) is induced additionally below the hexagonal on exceeding a certain copper content. The columnar mesophases exhibit additional sharp reflections in the wide angle region of the diffractograms for complexes with metal loadings higher than one copper centre per dendrimeric ligand. We can exclude the presence of any inorganic copper salt other than the basic copper nitrate as impurity together with the dendrimeric copper-complexes which could be responsible for these reflections. The basic copper nitrate, even though exhibiting spacings similar to the observed intra-

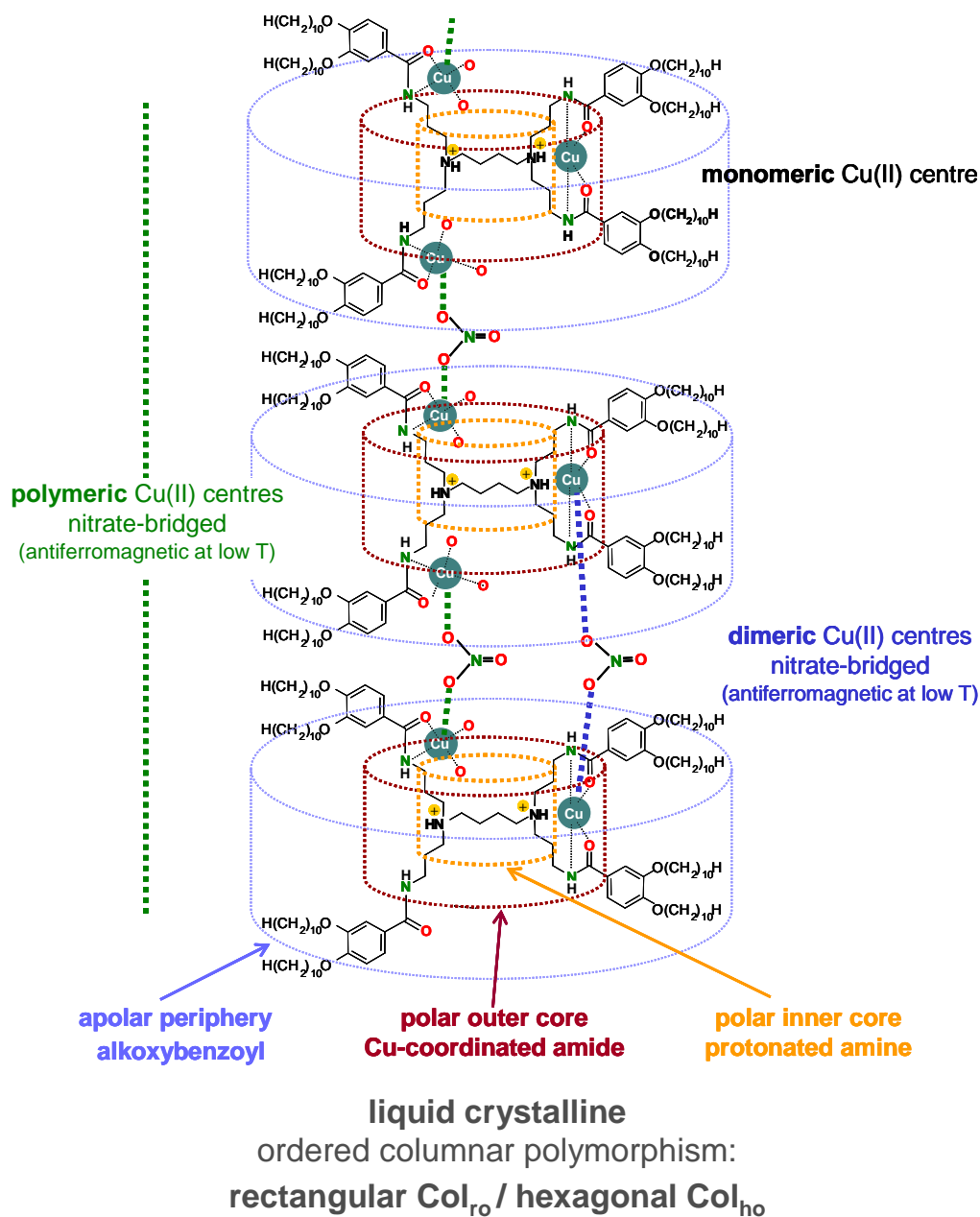
columnar distance, can not be responsible for the sharp reflections in the wide angle region. Firstly, the mixture of the ligand with the basic copper nitrate exhibit diffractograms, different from the complex. Secondly, the wide-angle reflections are reduced by simple evacuation of the X-ray samples under mild heating. Under those conditions the basic copper nitrate neither sublimates nor decomposes. Therefore, these sharp reflexes correspond actually to highly ordered columnar mesophases with stacking distances d of approx. 6.9 Å. We assume that the nitric acid, arising from the partial decomposition of the copper nitrate trihydrate during the preparation, causes on one hand the protonation of the tertiary amine groups in the inner core of the poly(propylene imine) and on the other the coordination of coppers centres belonging to different dendrimers in a μ -1,3 bridging mode. In this way, the ordered stacking of the dendrimer units along the columns in the mesophases is achieved. This result is in accordance with the high degree of orientation and the antiferromagnetic coupling of the copper centres, ~ 6.9 Å from each other, observed by EPR.

3.10 PROPOSAL OF A MODEL FOR THE PPI COPPER(II) COMPLEXES

According to the findings gained in the previous sections a scheme, which summarises in one graphical model all structural features and complexation possibilities of copper(II) by the PPI dendrimeric ligands is proposed in Scheme 3.7:

- i. The tertiary amines in the PPI core are protonated. The nitric acid, developed as a consequence of the partial decomposition of the starting copper salt $\text{Cu}(\text{NO}_3)_2 \cdot 3\text{H}_2\text{O}$, is responsible for the protonation cf. 3.1.2.1. As a result, the tertiary amines, though being in principle good ligands for copper, are not available for the complexation of copper, cf. 3.2, 3.5.3.3.
- ii. The amide groups coordinate copper(II), cf. 3.5.3.1. Therefore copper centres are located in the outer part of the PPI core.
- iii. Nitrate is clearly involved in complexing copper(II). Evidences for the presence of bidentate nitrates and -to a less extent- monodentate nitrates are found cf. 3.5.3.2. The bidentate nitrate seems to coordinate in a μ -1,3-bridging mode, although chelating nitrate could also be present.
- iv. The dendrimeric copper complexes consist of mixtures of two kinds of copper coordination involving the amide moiety: N_2O_3 and NO_4 , cf. 3.7.3. N_2O_3 consists of copper centres in a pseudotetrahedral N_2O_2 environment bridged to a similar copper centre by a nitrate group through the oxygen atoms, cf. 3.7.2.4, leading to dimer formation. NO_4 consists of copper centres in a NO_3 environment, cf. 3.7.2.4, with a further nitrate bridging group in apical position. The nitrates bridge further copper centres with the same environment giving rise to polymeric structures, cf. 3.7.3.
- v. The nitrate bridges are responsible for the antiferromagnetic exchange between the copper spins at low temperatures and for the high degree of orientation of the copper complexes in a magnetic field, cf. 3.7.3.
- vi. The copper complexes are liquid crystalline in a broader range than the dendrimeric ligands. The broader mesophases are due to both the protonation of the polyamine core and the coordination to copper(II), cf. 3.8.2.1. The complexes present columnar polymorphism: $p2mg$ rectangular mesophase at lower temperatures and a $p6mm$ hexagonal at higher temperatures cf. 3.9.1. The columnar phases are ordered, the bridging nitrates are responsible for this intracolumnar ordering, cf. 3.9.2.

Detected structures for complexed copper(II) centres



Scheme 3.7: Concluding model for the liquid crystalline PPI dendrimeric copper(II) complexes exemplified by means of several units of the 1st generation. For simplicity only the donor atoms and not all the donor ligands are depicted. Note that it is a schematic planar representation which does not describe the real conformation of the dendrimers

4 SUMMARY

This work focuses on the synthesis and characterisation of new liquid crystalline, polynuclear copper(II) complexes of poly(propylene imine) (PPI) dendrimers from 1st to 5th generation. The dendrimeric ligands, 3,4-decyloxybenzoyl-functionalized poly(propylene imine) derivatives (abbrev. **LG**, where G stands for generation), are amphiphilic dendrimers with a polar polyamine interior surrounded by an apolar alkoxy shell and benzamide units in between. The incompatibility of the polar and apolar parts leads to nanophase segregation of these two segments. As a consequence, the PPI dendrimers organise into columnar (hexagonal) mesophases. These PPI derivatives offer in principle a defined number of coordination sites, i. e. tertiary amine and amide groups in the inner and outer part of the dendrimer scaffold, respectively. In addition, the number of coordination sites increases with the generation. Both amine and amide moieties are good ligands for copper(II) complexation. Copper(II) is a paramagnetic cation with one unpaired electron. The presence of multiple paramagnetic metal centres close to each other may lead to materials with cooperative magnetic properties. The organisation in liquid crystalline phases should assist this behaviour.

Polynuclear copper(II) complexes of 1st to 5th generation dendrimers were prepared by coordination of copper(II) to the corresponding ligands. Light green powders were obtained. The prepared complexes are abbreviated as **CG.i(n)**, where C stands for dendrimeric complex and i is a running index. The average number of copper centres per dendrimer, the copper loading, is denoted by *n*. The maximum loadings reached for generations 1st to 5th are: 1.9, 6.3, 12.0, 24.2 and 45.9 respectively. In order to investigate the influence of the copper loading on the properties of the resulting complexes, a series of 2nd generation complexes, covering the whole range of copper loadings (0.3 to 6.3), has been prepared by varying either the stoichiometry of the reaction or the working-up procedure.

Two series of syntheses in different reaction media, in THF and in a binary (1:1 v:v) mixture of γ -butyrolactone and chloroform, have been carried out. The properties of the complexes for a given generation and copper loading are the same irrespective of the reaction media. This indicates that the solvents do not take part in the complexation as further ligands. However, the complexation and isolation in the THF series is easier and leads to higher loading, and was therefore chosen as standard.

For the complexation, the copper was used as its nitrate trihydrate $\text{Cu}(\text{NO}_3)_2 \cdot 3\text{H}_2\text{O}$. Under the reaction conditions the copper nitrate trihydrate partially decomposes into basic copper nitrate, $\text{Cu}_2(\text{NO}_3)(\text{OH})_3$, and nitric acid.



The decomposition is evidenced by the X-ray diffractograms of a blank reaction reproducing the complexation conditions without dendrimer LG. Gravimetric analysis of the blank reaction and elemental analysis of the complexes indicate that only traces of basic copper nitrate per dendrimeric ligand (≤ 0.05 and ≤ 0.001 wt. %, respectively) are present in the copper complex. Nitric acid, however, takes part in the composition of almost every complex as indicated by the N and O contents. These are high compared to those necessary for the electroneutrality of the copper centres. As a result, the protonation of the tertiary amines is assumed. This statement is supported by FTIR spectroscopic analysis. An immediate consequence of the protonation of the tertiary amines in the dendrimer core is that these groups can not take part in the coordination of copper.

Since the nitrate itself can coordinate copper through one, two, or three of its oxygen atoms, a further copper complex from a non-coordinating anion, the tetrafluoroborate ($\text{Cu}(\text{BF}_4)_2 \cdot 4\text{H}_2\text{O}$), was prepared to study the influence of the anion on the complex properties. The lack of reproducibility of the synthesis with the tetrafluoroborate salt and a possible reduction of copper(II) to copper(I) under the reaction conditions argued against its use for the preparation of the copper complexes.

The 1st generation complexes (from copper nitrate trihydrate) can be separated in two types of complexes: „blue“ and „green“. These complexes can be selectively prepared and are furthermore related to each other. The blue complex heated over its melting point converts into the green one, i.e. a thermochromic equilibrium occurs, which is reversible over a long time scale. The individual structures have been studied by EPR spectroscopy, which has furthermore shown the coexistence of both types of complexes within the dendrimers of the higher generations.

MALDI-ToF-MS has been successfully used to characterise the copper complexes of the 1st to 3rd generations. The individual copper complex species, corresponding to a dendrimeric ligand with different copper loadings, have been detected. However, these observations are only qualitative. The ionisation paths of the dendrimeric copper(II) complexes involve the reduction of copper(II) to copper(I) and/or deprotonation in order to yield monovalent cationic species. Therefore high loaded complexes are more difficult to be detected and their relative intensities in the MS-spectra are smaller.

TEM has allowed the imaging of the dendrimeric copper(II) complexes giving direct evidence of the complexation. Particles with circular structures (projection of spherical

or cylindrical morphologies) have been observed. The mean particle diameter is a function of the generation: 2.14 nm for the 2nd up to 3.04 nm for the 5th generation. The particle size distributions are relatively monodisperse. According to estimations from X-ray experiments, these sizes correspond roughly to the dimensions of the dendrimeric polar core (tertiary amine scaffold and amidobenzoyl groups in the outer part), where the coordination of copper takes place. EELS spectroscopy has been also performed and confirms the presence of copper.

Spectroscopic analysis revealed the amide groups as the coordinating groups of copper(II). FTIR spectroscopy gives evidence of the coexistence of N- and O-amido copper coordination in the complexes. Bands characteristic of quaternary ammonium salts are observed in the spectra of the complexes. This supports the protonation of the tertiary amine groups as suggested by elemental analysis and excludes the tertiary amines as complexation site for copper in the dendrimers. Evidences of copper-coordinated nitrate (mainly bidentate, probably as bridge between two copper centres) as well as to a lower extent monodentate nitrate have been also observed. FTIR did not indicate the presence of free $\text{Cu}(\text{NO}_3)_2 \cdot 3\text{H}_2\text{O}$ or $\text{Cu}_2(\text{NO}_3)(\text{OH})_3$. The results obtained by FTIR are further supported by the absorption spectra of the complexes in the UV-Vis range, which suggest the participation of the amide moiety and the nitrate groups in the coordination of copper.

EPR, electron paramagnetic resonance, spectroscopy of the dendrimeric copper(II)-complexes was carried out by Dr. N. E. Domracheva, Kazan Physical-Technical Institute, Russian Academy of Science in cooperation with the Universität Bayreuth. It allowed the determination of the structure and geometry of the different copper(II) coordination sites in the dendrimers. Low loaded copper complexes exhibit isolated (monomeric) copper centres with a N_2O_2 coordination of both carbonyl oxygen and amido nitrogen atoms in an approximately square planar environment. In higher loaded complexes, a mixture of two coordinations is present. Isolation of complexes exhibiting exclusively a single coordination is only possible for the 1st generation ("blue" and "green" complexes). At low temperatures an antiferromagnetic exchange has been observed ($\theta = -11.4$ K for the "blue" complex and $\theta = -11.9$ K for the "green" complex). A nitrate group bridging two copper centres in a μ -1,3- bridging mode is responsible for this exchange. The estimated nitrate bridged copper to copper distance is 6.92 Å. The nitrate bridge gives rise to highly ordered dimeric (for "blue" complexes) or polymeric (for "green" complexes) structures. The copper(II) in the blue complexes exhibit a N_2O_3 coordination. It consists of a pseudotetrahedral N_2O_2 environment with an additional oxygen atom from the nitrate bridge in apical position. The copper(II) in the green complexes exhibit a NO_4 coordination: one nitrogen and one oxygen atom, belonging to amido moieties, and three nitrato oxygens, one of them belonging to the nitrato bridge.

These structures are already present at room temperature as indicated by the unusual high degree of order of the “green” complex observed at room temperature even in solution. The coordination to the oxygen from nitrate bridge however can not be detected at room temperature due to the high thermal motion of the complexes. Thus, for the 1st generation “blue” complexes a pseudotetrahedral N₂O₂ coordination (amido nitrogen and amido carbonyl) is detected at room temperature. For the 1st generation “green” complexes a NO₃ coordination (amido nitrogen, one amido oxygen and two further oxygen atoms probably from nitrate). In addition, the copper centres are isolated and only a dipole-dipole interaction without spin exchange is observed with increasing copper loading.

All investigated copper (II)-complexes are liquid crystalline. Their mesophase ranges are broader than those of the dendrimeric ligands. The complexation of copper(II) together with the protonation of the tertiary amine groups in the dendrimer core contribute to the formation of the mesophases. The PPI copper complexes exhibit one or more thermotropic columnar phases. The segregation of the polar core and the apolar alkoxy terminal chains in different domains is responsible for the appearance of mesophases, as is the case for the ligands. The PPI copper(II) complexes exhibit a hexagonal columnar (p6mm symmetry) mesophase. Moreover, for complexes up to the 4th generation a columnar rectangular mesophase (probably with a p2mg symmetry) is induced below the hexagonal mesophase, if a certain copper content is exceeded. In X-ray measurements on the complexes additional sharp reflections in the wide angle region of the diffractograms were observed at $\theta = 6.4^\circ$ (6.9 Å) and $\theta = 12.8^\circ$ (3.5 Å). Any possible inorganic impurity other than the basic copper nitrate can be excluded by X-ray analysis as origin for those reflections. The basic copper nitrate, even though exhibiting spacings similar to the observed intracolumnar distances, can not be responsible for the sharp reflections in the wide angle region. These reflections are reduced by simple evacuation of the X-ray samples under mild heating conditions under which the basic copper nitrate neither sublimates nor decomposes. Therefore these sharp reflexes correspond actually to highly ordered columnar mesophases with stacking distances of approx. 6.9 Å. The distance is in agreement with that estimated from EPR analysis for two copper centres bridged by a nitrate group. Hence, it is assumed that the nitrate coordinated copper centres, belonging to different dendrimers in a μ -1,3 bridging mode, causes the ordered stacking of the dendrimer units along the columns in the mesophases.

To summarise, it has been shown in this thesis that the coordination of paramagnetic copper(II) centres by liquid crystalline PPI dendrimers leads to the formation of polynuclear amido copper(II) complexes exhibiting highly ordered columnar (rectangular, p2mg, and hexagonal, p6mm) mesophases and antiferromagnetic properties at low temperatures. The copper salt chosen for complexation, Cu(NO₃)₂·3H₂O, plays a central

role for the properties of the resulting complexes. First, its partial decomposition leads to the protonation of the PPI amine core contributing thereby to the broadening of the mesophase range. Second, the nitrate is a further ligand of copper giving rise to ordered, nitrate bridged copper dimers or polymers, which allow the spin exchange of copper centres (antiferromagnetism) at low temperatures.

A graphical summary of the findings of this work is presented in Scheme 3.7 on page 156.

5 ZUSAMMENFASSUNG

Diese Dissertation beschreibt die Synthese und Charakterisierung neuer flüssigkristalliner, polynuklearer Kupfer(II)-Komplexe aus Poly(propylenimin) (PPI) Dendrimeren der 1. bis 5. Generation. Die Dendrimerliganden, 3,4-Didecyloxybenzoyl-substituierte Poly(propylenimin) Derivate (abgek. **LG**, wobei L für Ligand und G für Generation steht), sind amphiphile Dendrimere mit einem apolaren Polyamin-Kern, der von einer apolaren Alkoxy-Hülle umgeben ist; Benzamideinheiten befinden sich im Zwischenbereich. Die Unverträglichkeit der polaren und apolaren Segmente führt zur Nanophasensegregation der beiden Bereiche. Als Folge organisieren die PPI-Dendrimere in kolumnar hexagonalen Mesophasen. Diese PPI-Derivate weisen eine definierte Anzahl an Koordinationsstellen auf: tertiäre Amin- und Amid-Gruppen in den inneren und äußeren Bereichen des Dendrimerkerns. Außerdem gibt es eine zunehmende Anzahl an Koordinationsstellen mit zunehmender Generation. Sowohl die Amin- als auch die Amid-Gruppen sind prinzipiell gute Liganden für die Kupferkomplexierung. Kupfer(II) ist ein paramagnetisches Kation mit einem ungepaarten Elektron. Die Anwesenheit mehrerer nahe beieinander liegender paramagnetischer Metallzentren, wie es in einem Dendrimer der Fall ist, kann zu Materialien mit kooperativen magnetischen Eigenschaften führen. Die Organisation in flüssigkristalline Phasen sollte dieses Verhalten unterstützen.

Polynukleare Kupfer(II)-Komplexe der 1. bis 5. Generation wurden durch Koordination von Kupfer(II) durch die entsprechenden Liganden hergestellt und ergaben hellgrüne Pulver. Diese Komplexe werden mit **CG.i(n)** bezeichnet, wobei C für den dendrimeren Komplex ("complex" auf Englisch) steht und i einen laufenden Index darstellt. Der Mittelwert der Anzahl an Kupferatomen pro Dendrimer, die so genannte Kupferbeladung, wird als n bezeichnet. Die maximalen Beladungen, die für die Generationen 1 bis 5 erreicht wurden, sind 1.9, 6.3, 12.0, 24.2 bzw. 45.9 Kupferzentren. Um den Einfluss der Kupferbeladung auf die Eigenschaften der Komplexe zu untersuchen, wurde eine Reihe von Komplexen der 2. Generation synthetisiert, indem entweder die Stöchiometrie der Reaktion oder die Aufarbeitung verändert wurden. Diese Serie deckte den gesamten Bereich der Kupferbeladungen von 0.3 bis 6.3 Kupferzentren pro Dendrimer ab.

Zwei Synthesen in verschiedenen Lösungsmitteln, THF und eine binäre 1:1 Volumen-Mischung aus γ -Butyrolacton und Chloroform, wurden durchgeführt. Die Eigenschaften

der Komplexe für eine bestimmte Generation und Kupferbeladung sind unabhängig vom Lösungsmittel. Dies deutet darauf hin, dass das Lösungsmittel als weiterer Ligand an der Komplexbildung nicht teilnimmt. Da jedoch die Komplexbildung und Isolierung in der THF-Reihe leichter ist und zu einer höheren Kupferbeladung führt, wurde diese als Standard gewählt.

Für die Komplexbildung wurde Kupfernitrattrihydrat, $\text{Cu}(\text{NO}_3)_2 \cdot 3\text{H}_2\text{O}$, eingesetzt. Unter den Reaktionsbedingungen zersetzt sich das Kupfernitrattrihydrat teilweise in basisches Kupfernitrat, $\text{Cu}_2(\text{NO}_3)(\text{OH})_3$, und Salpetersäure:



Einen starken Hinweis auf die Zersetzung liefern Röntgendiffraktogramme am Produkt einer Blindreaktion unter Komplexbildungsbedingungen ohne Dendrimer **LG**. Die gravimetrische Analyse des Blindversuchs und die Elementaranalyse der Komplexe deuten auf die Anwesenheit von nur Spuren von basischem Kupfernitrat pro dendrimerelem Ligand im Kupferkomplex hin (≤ 0.05 bzw. ≤ 0.001 Gew. %). Die Salpetersäure muss jedoch Teil der Zusammensetzung von fast jedem Komplex sein, was durch die mit Elementaranalyse gemessenen N- und O-Gehalte gezeigt wird. Diese sind hoch, verglichen mit denjenigen Gehalten, die für die Elektroneutralität der Kupferzentren nötig wären. Daher wird angenommen, dass die tertiären Amine protoniert sind. Dies wird auch unterstützt von Ergebnissen der FTIR-Spektroskopie. Als unmittelbare Konsequenz der Protonierung der tertiären Amine im Dendrimerkern können diese Gruppen nicht an der Koordinierung von Kupfer beteiligt sein.

Da das Nitrat Kupfer durch ein, zwei oder drei seiner Sauerstoffatome koordinieren kann, wurde ein weiterer Kupferkomplex aus einem nicht-koordinierenden Anion, Tetrafluoroborat ($\text{Cu}(\text{BF}_4)_2 \cdot 4\text{H}_2\text{O}$), hergestellt, um den Einfluss des Anions auf die Komplexeigenschaften zu untersuchen. Jedoch ist zum einen die Synthese mit dem Tetrafluoroborat-Salz nicht reproduzierbar, und zum anderen wird Kupfer(II) unter den Reaktionsbedingungen möglicherweise zu Kupfer(I) reduziert. Beides sprach gegen die weitere Benutzung von Tetrafluoroborat-Salz zur Synthese der Kupferkomplexe.

Die Komplexe der 1. Generation (aus Kupfernitrattrihydrat) können in „blaue“ und „grüne“ Komplexe getrennt werden. Diese können gezielt präpariert werden und stehen in Beziehung zueinander. Wenn der blaue Komplex über seinen Schmelzpunkt erhitzt wird, wandelt er sich in den grünen um, d.h. ein thermochromes Gleichgewicht tritt auf, das reversibel über einen langen Zeitraum ist. Die einzelnen Strukturen wurden mittels EPR Spektroskopie untersucht, die außerdem die Koexistenz beider Klassen von Komplexen innerhalb der Dendrimere der höheren Generationen zeigen.

MALDI-ToF-MS wurde zur Charakterisierung der Kupferkomplexe der 1. bis 3. Generation eingesetzt. Die einzelnen Spezies von Kupferkomplexen wurden detektiert, die dendrimeren Liganden mit unterschiedlichen Kupferbeladungen entsprechen. Allerdings sind diese Beobachtungen nur qualitativer Natur. Die Ionisierung der dendrimeren Kupfer(II)-Komplexe erfolgt über die Reduktion von Kupfer(II) zu Kupfer(I) und/oder Deprotonierung, um die monovalenten, kationischen Spezies zu erhalten. Daher können hoch beladene Komplexe schwieriger detektiert werden und ihre relativen Intensitäten in den MS-Spektren sind kleiner.

TEM erlaubt die Abbildung der dendrimeren Kupfer(II)-Komplexe und liefert einen direkten Beweis der Komplexierung. Es wurden kreisförmige Strukturen (Projektion sphärischer oder zylindrischer Morphologien) beobachtet. Der mittlere Durchmesser dieser Strukturen hängt von der Generation ab und beträgt 2.14 nm für die 2. und bis zu 3.04 nm für die 5. Generation. Aufgrund von Abschätzungen aus Röntgenexperimenten kann geschlossen werden, dass diese Teilchengrößen ungefähr den Ausdehnungen des dendrimeren, polaren Kerns (tertiäres Amin-Gerüst und Amidobenzoyl-Gruppe in der äußeren Schale) entsprechen, wo die Koordinierung von Kupfer stattfindet. Die Verteilungen der Teilchengrößen sind relativ monodispers. EELS-Spektroskopie wurde ebenfalls durchgeführt und bestätigt die Anwesenheit von Kupfer.

Spektroskopische Analysen zeigen, dass die Amide die Koordinierungsgruppen von Kupfer(II) sind. Die Ergebnisse der FTIR-Spektroskopie deuten auf eine Koexistenz von N- und O-Amido Kupferkoordinierung in den Komplexen hin. In den Spektren der Komplexe wurden charakteristische Banden von quaternären Ammoniumsalzen identifiziert. Dies unterstützt die Interpretation der Ergebnisse der Elementaranalyse, die eine Protonierung der tertiären Amingruppen implizieren, und schließt die tertiären Amine als Komplexierungsgruppen für Kupfer in den Dendrimeren aus. Außerdem wurden Hinweise auf Kupfer-koordiniertes Nitrat (hauptsächlich zweizählig, vermutlich als Brücke zwischen zwei Kupferzentren) und in geringerem Umfang einzähliges Nitrat gefunden. Die FTIR-Messungen deuten nicht auf die Anwesenheit von freiem $\text{Cu}(\text{NO}_3)_2 \cdot 3\text{H}_2\text{O}$ oder $\text{Cu}_2(\text{NO}_3)(\text{OH})_3$ hin. Weiterhin deuten auch die Resultate der UV-Vis Spektroskopie darauf hin, dass die Amid- und Nitratgruppen an der Kupferkoordinierung teilnehmen.

ESR-Spektroskopie der dendrimeren Kupfer(II)-Komplexe wurde von *Dr. N. E. Domracheva, Kazan Physical-Technical Institute, Russian Academy of Science* in Zusammenarbeit mit der *Universität Bayreuth* durchgeführt. Dadurch konnte die Struktur und Geometrie der verschiedenen Stellen der Kupfer(II)-Koordinierung in den Dendrimeren bestimmt werden. Niedrig beladene Kupferkomplexe weisen isolierte (monomerische) Kupferzentren auf mit einer N_2O_2 -Koordinierung sowohl des Carbonyl-Sauerstoffs als auch des Amido-Stickstoffatoms in einer ungefähr quadratisch

planaren Umgebung. In höher beladenen Komplexen liegt eine Mischung aus zwei Koordinierungen vor, die isoliert in den „blauen“ und „grünen“ Komplexen der 1. Generation vorhanden sind. Bei tiefen Temperaturen wurde eine antiferromagnetische Austauschwechselwirkung nachgewiesen ($\theta = -11.4$ K für die „blauen“ und $\theta = -11.9$ K für die „grünen“ Komplexe). Eine Nitratgruppe, die zwei Kupferzentren durch eine μ_4 -1,3-Brücke verbindet, ist für diese Austauschwechselwirkung verantwortlich. Der Abstand zweier verbrückter Kupferzentren wurde zu 6.92 \AA abgeschätzt. Die Nitratbrücke führt zu hoch geordneten dimerischen (für „blaue“ Komplexe) oder polymerischen Strukturen (für „grüne“ Komplexe). Das Kupfer(II) in den „blauen“ Komplexen weist eine N_2O_3 Koordinierung auf. Diese besteht aus einer pseudo-tetraedrischen N_2O_2 -Umgebung mit einem zusätzlichen Sauerstoffatom der Nitratbrücke in apikaler Position. Das Kupfer(II) der „grünen“ Komplexe besitzt eine NO_4 Koordinierung: ein Stickstoff- und ein Sauerstoffatom gehören zu den Amido-Gruppen, und drei Nitrato-Sauerstoffatome, wobei eines davon zur Nitrato-Brücke gehört. Diese Strukturen sind bereits bei Raumtemperatur vorhanden, was aus der außergewöhnlich hohen Ordnung der „grünen“ Komplexe in Lösung folgt. Die Koordinierung zum Sauerstoff von den Nitrat-Brücken kann jedoch bei Raumtemperatur wegen der starken thermischen Bewegung der Komplexe nicht beobachtet werden. Daher wird für die „blauen“ Komplexe der ersten Generation eine pseudo-tetraedrische N_2O_2 Koordinierung (Amido-Stickstoff und Amido-Carbonyl) bei Raumtemperatur detektiert. Die „grünen“ Komplexe der ersten Generation weisen eine NO_3 Koordinierung auf (Amido-Stickstoff, ein Amido-Sauerstoff und zwei weitere Sauerstoffatome vermutlich vom Nitrat). Außerdem sind die Kupferzentren isoliert und nur eine Dipol-Dipol-Wechselwirkung ohne Spinaustausch wird für zunehmende Kupferbeladung beobachtet.

Alle untersuchten Kupfer(II)-Komplexe zeigen flüssigkristalline Eigenschaften. Die Bereiche ihrer Mesophasen sind breiter als die der dendrimeren Liganden. Die Komplexierung von Kupfer(II) zusammen mit der Protonierung der tertiären Amin-Gruppen im Dendrimerkern trägt zur Bildung der Mesophasen bei. Die PPI-Kupferkomplexe weisen eine oder mehrere thermotrope kolumnare Phasen auf. Die Segregation des polaren Kerns und der apolaren Alkoxy-Endgruppen in unterschiedliche Domänen ist für das Auftreten der Mesophasen verantwortlich (genau wie bei den Liganden). Die PPI-Kupfer(II)-Komplexe besitzen eine hexagonal kolumnare Mesophase mit $p6mm$ Symmetrie. Weiterhin wird für Komplexe bis zur 4. Generation eine rechtwinklig kolumnare Mesophase unterhalb der hexagonalen beobachtet, wenn ein bestimmter Kupfergehalt überschritten wird. In Röntgenuntersuchungen an den Komplexen wurden zusätzliche scharfe Reflexe im Weitwinkelbereich bei $\theta = 6.4^\circ$ (6.9 \AA) und $\theta = 12.8^\circ$ (3.5 \AA) beobachtet. Als Ursache dieser Reflexe konnten mögliche anorganische Verunreinigungen, außer basisches Kupfernitrat, mit Hilfe der Röntgenmessungen ausgeschlossen werden. Das basische Kupfernitrat ist ebenfalls nicht ver-

antwortlich für die scharfen Reflexe im Weitwinkelbereich, obwohl diese Abstände besitzen, die vergleichbar mit den intra-kolumnaren Abständen sind. Die Intensität der Reflexe von basischem Kupfernitrat können verringert werden, indem die Probe evakuiert und leicht erhitzt wird, wobei das basische Kupfernitrat unter diesen Bedingungen weder sublimiert noch sich zersetzt. Daher entsprechen diese Reflexe tatsächlich hoch geordneten kolumnaren Mesophasen mit intra-kolumnaren Abständen von ca. 6.9 Å. Dies stimmt gut mit dem Wert überein, der aus den EPR Messungen für zwei Nitrat-verbrückte Kupferzentren bestimmt wurde. Aus diesem Grund wird angenommen, dass die Nitrat-Koordinierung zwischen Kupferzentren (μ -1,3 Brücken) in verschiedenen Dendrimern die intra-kolumnare Ordnung in den kolumnaren Mesophasen verursacht.

Zusammenfassend wurde in dieser Arbeit gezeigt, dass die Koordinierung von paramagnetischen Kupfer(II)-Komplexen durch flüssigkristalline PPI-Dendrimere zur Bildung von polynuklearen Amido Kupfer(II)-Komplexen führt, die hoch geordnete kolumnare (rechtwinklige, $p2mg$, bzw. hexagonale, $p6mm$) Mesophase und antiferromagnetische Eigenschaften bei tiefen Temperaturen aufweisen. Eine zentrale Rolle für die Eigenschaften der Komplexe spielt das Kupfersalz, $Cu(NO_3)_2 \cdot 3H_2O$, das für die Komplexbildung gewählt wurde. Erstens folgt aus dessen teilweiser Zersetzung die Protonierung des PPI-Amin-Kerns, was auch zur Verbreiterung der Bereiche der Mesophasen beiträgt. Zweitens ist das Nitrat ein weiterer Ligand für Kupfer, was zu geordneten Nitrat-verbrückten Kupfer-Dimeren oder -Polymeren und damit zum Spin-Austausch der Kupferzentren (Antiferromagnetismus) führt.

Eine graphische Zusammenfassung der Ergebnisse dieser Arbeit ist in Schema 3.7 auf Seite 156 gezeigt.

6 EXPERIMENTAL SECTION

6.1 MATERIALS

Amine-terminated poly(propylene imine) dendrimers (4, 8, 16, 32 and 64 terminal groups; 1,4-diaminobutane core) from 1st to 5th generation were purchased from *Aldrich* and used as received. 1-Bromodecane (*Fluka*, 97% G.C.), ethyl 3,4-dihydroxybenzoate (*Avocado*, 97%) and N-hydroxysuccinimide (*Aldrich*, 98%) were used to prepare the N-hydroxysuccinimidoyl-activated ester of 3,4-decyloxybenzoic acid used for the amidation of the commercial dendrimers. N,N'-bis(3,4-decyloxybenzoyl)-1,4-diaminobutane, also indicated L0, "zero" generation, had been prepared and was kindly provided by A. Facher.

High purity copper(II) nitrate trihydrate, $\text{Cu}(\text{NO}_3)_2 \cdot 3\text{H}_2\text{O}$; copper(II) tetrafluoroborate hydrate 19-22 % Cu(II), $\text{Cu}(\text{BF}_4)_2 \cdot x\text{H}_2\text{O}$ $x \sim 4$; copper(II) hydroxide, $\text{Cu}(\text{OH})_2$; tetrabutylammonium bromide TBAB, $(\text{C}_4\text{H}_9)_4\text{NBr}$; sodium borohydride, NaBH_4 ; copper(II) oxide, CuO and copper(I) oxide, Cu_2O , were purchased from *Fluka* and *Aldrich* and used as received.

Technical grade solvents were dried and purified as follows: tetrahydrofuran THF, was refluxed over potassium hydroxide, then over metallic potassium and finally fractionated distilled. Chloroform, dichloromethane and toluene were distilled from calcium hydride. Acetone was refluxed over anhydrous sodium sulfate. γ -Butyrolactone (> 99% *Aldrich*), was distilled under reduced pressure at 35°C (~ 0.02 mbar). All of them were stored under argon over dried molecular sieves (4 Å). Benzene (*Fluka*) and acetonitrile (*Riedel de Haën*) were purchased at puriss. p.a. grade and kept over dried molecular sieves; ethyl acetate (*Fluka*, puriss.) was provided in a sealed flask over molecular sieves.

Inert atmosphere was maintained by argon (5.0), which was further dried by subsequently passing a column with molecular sieves (3 Å) and a second one with potassium-coated aluminium oxide powder.

Filtrations were performed through P4 (nominal pore size 10 - 16 μm) *Schott Duran*[®] filter funnels and microfiltrations through disposable hydrophobic Rotilabo[®]-syringe filters (tetrafluoroethylene membrane, nominal pore size 0.45 μm and 0.20 μm) from *Carl-Roth*.

6.2 ANALYTICAL METHODS

6.2.1 Molecular Composition Determination: Elemental Analysis, EA

Elemental analysis of carbon, hydrogen and nitrogen, were carried out at the *Mikroanalytisches Labor I. Beetz*, Kronach, Germany whereas copper content was determined by atomic spectroscopic methods at the *Mikroanalytisches Labor E. Pascher*, Remagen, Germany. The percentage of oxygen was not determined but calculated as the difference between 100% and the measured elements.

6.2.2 Molecular Weight Determination: MALDI-ToF-MS

Positive-ion MALDI-TOF mass spectra were recorded on a *Bruker Reflex III* mass spectrometer operating in both reflector and linear modes and 20 kV acceleration voltage. Ions were generated by a nitrogen laser emitting at 337 nm. The measured molecular weights were based on an external calibration with a peptide (*Bruker 20 61 95*) and a protein (*Bruker 20 63 55*) mixture.

Umbelliferone (7-hydroxycoumarin) 99% (*Aldrich*) was used as matrix for N,N'-bis(3,4-decyloxybenzoyl)-1,4-diaminobutane and 1st and 2nd generation copper(II) complexes. THAP (2',4',6' -Trihydroxyacetophenone monohydrate) 98% (*Aldrich*) was chosen for the complexes of the 3rd generation. THF solutions of the matrix (20 mg·ml⁻¹) and dendrimer (10 mg·ml⁻¹) were prepared and mixed to give a matrix to analyte mass ratio of 8:1 for the samples with umbelliferone and 4:1 in case of THAP. Some µl of the mixed solution were deposited onto the stainless steel sample stage and allowed to air dry. No salt was added.

The reflector mode enabled the isotopic resolution of the complexes up to the 2nd generation and the given masses correspond to the maxima of the isotope distribution of each peak. The average molecular weights are quoted for the spectra recorded in linear mode. In case of ambiguity in the peak assignment of the masses, the isotopic distribution of the proposed structure was simulated and compared with the measured isotopic distribution. For an identification of the masses with their structures cf. 3.3, Table 3.6.

6.2.3 Spectroscopic Methods

6.2.3.1 Fourier Transform Infrared Spectroscopy, FTIR

Fourier transform infrared spectra at room temperature were recorded in absorbance mode using a *BioRad Digilab FTS-40 FTIR* spectrometer in the range from 4000 - 400 cm^{-1} ; 32 scans were averaged for each spectrum, the resolution is 4 cm^{-1} . Silicon wafers were used as substrates. A thin film of the sample from dichloromethane solution was coated onto them and measured under nitrogen.

6.2.3.2 Ultraviolet-Visible Spectroscopy, UV-Vis

Absorption spectra in the ultraviolet-visible range (200 - 900 nm) were acquired on a two beam *Hitachi U-3000 UV-Spectrometer*. Standard scanning rates were 300 or 600 nm/min and the spectral resolution was 0.5 or 1.0 nm, respectively. Measurements were carried out in CHCl_3 and CH_2Cl_2 solutions ($c \sim 0.2 - 0.02 \text{ mg}\cdot\text{ml}^{-1}$), placed in quartz cuvettes (path length 1 cm) or films from CH_2Cl_2 or toluene solutions onto quartz microscopy slides (1 mm).

6.2.3.3 Electron Paramagnetic Resonance Spectroscopy, EPR

EPR spectroscopy, electron spin resonance spectroscopy, (ESR); was carried out by *Dr. N. E. Domracheva, Kazan Physical-Technical Institute, Russian Academy of Science* in cooperation with *Prof. Dr. M. Schwoerer and Dr. A. Mirea, Experimentalphysik II, Universität Bayreuth*.

X-band (9.7 GHz) EPR measurements were performed with a *CW EPR-200D Bruker* spectrometer, equipped with a static *Oxford* cryostat (*CF 935*) and a home-made temperature controller ($T = 5 - 298 \text{ K}$). The magnetic field was frequency-modulated with 100 kHz, so that EPR spectra were recorded as first derivatives. At different temperatures, the microwave power was chosen such that saturation was avoided. Small differences in the microwave frequency of compared sample spectra were corrected by appropriately shifting the magnetic field. The accuracy of the reported magnetic parameters is $\Delta A = \pm 5 \cdot 10^{-4} \text{ cm}^{-1}$ (ca. $\pm 5 \text{ G}$), and $\Delta g = \pm 0.005$. The orientation of the copper(II) PPI dendrimeric complexes in an external magnetic field was investigated using an *EPR - 200D* spectrometer. The samples were kept in the resonator at room temperature in the presence of a high magnetic field ($B_0 = 8000 \text{ G}$) for 5 - 10 min and then rapidly cooled to low temperatures while maintaining that field. To investigate the angular dependencies in the EPR spectra, a home-made goniometer was used, which allowed the sample to be rotated in one plane.

The Q-band (34 GHz) EPR spectra were recorded on a *CW ESP-300 Bruker* spectrometer; the temperature was controlled by a dynamic *Oxford* cryostat (*CF 935*) using an *ITC 4 Oxford* controller. Simulations of the powder EPR spectra have been performed using the *WinSimfonia (Bruker)* software.

The EPR experiments were carried out on powder samples and solutions. The latter were prepared by dissolving the copper(II) dendrimeric complexes in a 1:1 mixture of toluene and chloroform ($C \sim 5 \text{ mg}\cdot\text{mL}^{-1}$).

6.2.4 Microscopy

6.2.4.1 Transmission Electron Microscopy, TEM

In cooperation with *Dr. M. Drechsler, Universität Bayreuth*; both electron microscope images and electron diffraction patterns of some selected samples were taken on a *Zeiss 922 OMEGA* transmission electron microscope operating at 200 kV and having a point-to-point resolution of down to 0.29 nm. Images were acquired using a *Gatan Ultrascan 1000* CCD camera and were processed with the software *DigitalMicrograph* from *Gatan*. The microscope was equipped with an in-column energy filter for the electron energy loss spectroscopy, EELS.

Additional measurements were performed by *Dr. M. Krekhova, Universität Bayreuth*, on a *Zeiss CEM 902* operating at 80 kV with a point-to-point resolution down to 0.5 nm.

A diluted solution of the sample in CHCl_3 was dropped onto a *Plano* copper grid (200 mesh) coated with a lacey-carbon film and left to dry in air.

The size distributions of the complexes and copper nanoparticles were determined by measuring the diameter of at least 50 randomly selected particles on micrographs; ellipsoidal particles were characterized by their largest diameter.

6.2.4.2 Polarized Light Microscopy, POM

Transmitted polarized light microscopy was performed on an inverted *Nikon Diaphot 300* microscope with objectives of different magnifications and numerical apertures (*Nikon M Plan SLWD 210/0 40x/0.40*, *20/0.35*, *10/0.21*). The microscope was equipped with a digital camera *Nikon DXM 1200* for recording images of the samples.

A hot stage for thermal microscopy *Mettler FP82HT*, with central processor *Mettler FP90*, allowed the controlled heating and cooling of the sample during the optical investigations.

6.2.5 Thermal Analysis

6.2.5.1 Thermogravimetric Analysis, TGA

Thermogravimetric analysis was performed on a *TGA/SDTA851* module from *Mettler Toledo* under air flow ($60 \text{ ml}\cdot\text{min}^{-1}$) over the temperature range from 30° to 650°C at a heating rate of $10 \text{ K}\cdot\text{min}^{-1}$. Samples (ca. 2 - 8 mg) were measured in aluminium oxide crucibles. Decomposition temperature, T_{dec} was defined as the onset temperature at which the weight curve deviates 5% from the base line.

6.2.5.2 Differential Scanning Calorimetry, DSC

Differential scanning calorimetry measurements were carried out with a *Perkin Elmer DSC 7* as well as a *Perkin Elmer Diamond* calorimeter. Unless otherwise specified, the heating and cooling rate was $10 \text{ K}\cdot\text{min}^{-1}$. Calibration was done with indium as reference material. 40 μl , aluminium pans, ca. 3 - 6 mg sample.

6.2.5.3 X-Ray Diffraction

Wide-angle X-ray diffraction, WAXS

Powder diffractograms in the angle region from 20° to 80° (2θ) were performed on a *Bruker-AXS D8 Advance* diffractometer ($\text{CuK}_{\alpha 1}$ -radiation, $\lambda = 1.541 \text{ \AA}$) in transmission mode.

Samples were placed between two Scotch adhesive films. The diffractogram of the empty film was subtracted from the sample diffractogram. Standard measurement conditions: step size 0.025° and 20 seconds step time, rt.

The powder diffractogram of the blank reaction, cf. 3.1.2.1, was taken by *Dr. W. Millius, Anorganische Chemie I, Universität Bayreuth*

Temperature dependent "Middle" angle diffraction, Guinier

X-ray analysis in the angle region of $\theta = 0.3^\circ - 15^\circ$ were carried out with a *Huber 600* Guinier goniometer equipped with a germanium monochromator *Huber 611*. An extra slit diaphragm reduces the broadening of the primary beam due to scattering in air. A home made furnace ($\Delta T = \pm 0.2 \text{ K}$) is integrated in the diffractometer and allows investigations at temperatures up to 250°C .

The copper anode *Fine Focus DX-Cu8x0.4-S* (1500 W, 60 kV) from Seifert was operated by a *Seifert ID 3003* X-ray generator. The specimen was irradiated with the $\text{K}_{\alpha 1}$ spectral line of copper, $\lambda = 1.541 \text{ \AA}$.

A *Huber 9900* detector system, a *Huber HTC 9634* temperature controller, and a *Huber SMC 9000* control unit were coordinated by means of the software *Gony* and complete the X-ray set-up. Additional diaphragm, beam stop system, furnace and control software *Gony*, were developed by *Dr. A. Schaz*, (née Eisenmann) ^[346].

Non-oriented powder samples were sealed in 1.0 mm diameter soda glass mark-tubes from *Hilgenberg* prior to the measurement. Standard diffractograms were collected in symmetric transmission arrangement of the camera with steps $\Delta\theta = 0.01^\circ$ and 20 seconds step time. In case of a low signal-to-noise ratio, the measured curves were smoothed by a five point adjacent averaging smoothing procedure.

6.3 PREPARATIVE METHODS

The compounds mentioned in this experimental part will be abbreviated with an identification code of the type “**LG**” or “**CGi(n)**”. L indicates PPI dendrimeric ligand and C a copper(II) dendrimeric complex. The generation of the dendrimer is given by the number G, and finally i is a consecutive index. The loading of the complex, i.e. the average number of copper centres per dendrimer is given in parenthesis by n.

6.3.1 Procedures for Copper(II) Nitrate Trihydrate Complexation with PPI Dendrimers.

Dendrimeric copper(II)-complexes from “zero” up to 5th generation were synthesised in solutions of both THF and a 1:1 v/v mixture of γ -butyrolactone and chloroform. Copper(II) was used as its nitrate trihydrate $\text{Cu}(\text{NO}_3)_2 \cdot 3\text{H}_2\text{O}$, for the complex formation. Additionally, a second generation dendrimeric copper(II)-complex from tetrafluoroborate hydrate $\text{Cu}(\text{BF}_4)_2 \cdot 4\text{H}_2\text{O}$ was prepared. All syntheses were carried out under an inert, moisture-free atmosphere of argon.

6.3.1.1 Series of Highest Copper(II) Loading

Complexation of copper(II) nitrate trihydrate in THF

General procedure of complexation in THF

The following general synthetic and working up procedures described in this section yield for generations 2 – 5 the highest copper loadings per dendrimer.

Copper(II) nitrate trihydrate stock solution: A stock solution of $\text{Cu}(\text{NO}_3)_2 \cdot 3\text{H}_2\text{O}$ (1.13 M) in absolute THF was prepared by dissolving copper(II) nitrate trihydrate in THF and stirring at room temperature for 5 hours. The slightly turbid dark blue solution was filtered through a 0.20 μm Rotilabo®-Teflon filter and kept under argon for further complexation experiments. The solution is stable for months.

General synthetic procedure of complexation: The dendrimeric ligand, LG, was dissolved in THF and added to an aliquot of the stock $\text{Cu}(\text{NO}_3)_2 \cdot 3\text{H}_2\text{O}$ solution (1 to 25 fold molar excess of copper(II) per nitrogen centre, see Table 6.1); whereas the reaction mixture darkened or turned into green depending on the excess of copper salt. It was stirred over night. Only for the first generation a copious precipitate was formed. At higher generations a reaction solution with a slight turbidity at the utmost could be observed.

General working up procedure: The solvent was carefully evaporated under reduced pressure and the dendrimeric copper(II) complex was extracted from the residue with chloroform. The chloroform solution was at first filtered through a P4 filter funnel and then through a 0.20 µm Teflon filter. The filtrate was concentrated in vacuum, subsequently dissolved in benzene, filtered again through a 0.200 µm mesh filter and lyophilized from that benzene solution. Light green powders were obtained.

Table 6.1: Standard reaction conditions for the complexation of $\text{Cu}(\text{NO}_3)_2 \cdot 3\text{H}_2\text{O}$ in THF.

Complex	C0.1(0.2)	C1.4(1.5)	C2.3(6.0)	C3.1(12.0)	C4.1(24.2)	C5.1(45.9)
Dendrimeric ligand	L0	L1	L2	L3	L4	L5
Molar excess Cu-N	25	25	1	10	10	10
Temperature	55°C	rt.	rt.	rt.	rt.	rt.
Time	o. n.	o. n.	o. n.	o. n.	o. n.	o. n.

Complexes and **C0.1(0.2)**, **C1.4(1.5)**, **C2.3(6.0)**, **C3.1(12.0)**, **C4.1(24.2)** and **C5.1(45.9)** were synthesised and worked up according to this general procedure (cf. 6.4, compounds register I), o.n.: over night.

Specific working-up procedure for 1st generation copper(II) complexes in THF

The synthesis was carried out according to the general synthetic procedure for complexation in THF (see section 6.3.1.1). Specific working up procedure:

- The intense turbid reaction mixture was kept for 6 hours at 2°C, whereas a copious precipitate appeared. It was subsequently filtered through a P4 (10 - 16 µm nominal pore size) filter. The collected powder was carefully washed with THF and allowed to dry in air. A light blue powder was obtained (complex **C1.2(1.9)b**, cf. 6.4, compounds register I).
- The copious precipitate from THF (see i) was divided into two portions. One portion was used as isolated; the second one was heated to 130°C for 30 minutes, whereas it turned dark green (complex **C1.2(1.9)gr**, cf. 6.4, compounds register I).
- 100 mg of **C1.2(1.9)b** were heated in 20 ml of a 1:1 v/v mixture of chloroform and toluene and was let to sedimentate in a narrow glass burette. After 24 h at room temperature a light blue precipitate appeared at the bottom and a blue suspension swam over the blue precipitate. The suspension was taken up with a syringe and then dried in air without further purification (complex **C1.2(1.0)b1**, cf. 6.4, compounds register I). The blue precipitate at the bottom, **C1.2(5.2)b2**, has been identified as inorganic by elemental analysis and was discarded.

Complexation of copper(II) nitrate trihydrate in γ -butyrolactone/ CHCl_3 **General procedure of complexation in γ -butyrolactone/ CHCl_3**

Copper(II) nitrate trihydrate stock solution: A stock solution of $\text{Cu}(\text{NO}_3)_2 \cdot 3\text{H}_2\text{O}$ ($9 \cdot 10^{-2}\text{M}$) in a 1:1 v/v γ -butyrolactone/ CHCl_3 mixture was prepared by adding copper(II) nitrate trihydrate to γ -butyrolactone; followed by the same volume of chloroform. Stirring at room temperature continued for 5 hours. The resulting slightly turbid dark blue solution was filtered through a $0.20\ \mu\text{m}$ Rotilabo[®]-Teflon filter and kept under argon for further complexation experiments. The solution is stable for months.

General synthetic procedure for complexation of 2nd to 5th generations: The dendrimeric ligand, LG, was dissolved in chloroform and added to an aliquot of the stock $\text{Cu}(\text{NO}_3)_2 \cdot 3\text{H}_2\text{O}$ solution in γ -butyrolactone/ CHCl_3 (11-12 fold molar excess of copper salt per nitrogen centre, see Table 6.2) whereas the colour of the reaction mixture turned into green. The mixture was stirred at room temperature over night.

General working up procedure: After evaporating the chloroform under reduced pressure; the γ -butyrolactone was distilled off at high vacuum ($3 \cdot 10^{-2}$ mbar, 35°C). The dendrimeric copper(II) complex was extracted from the residue with chloroform and filtered through a P4 filter funnel, and then consecutively through $0.45\ \mu\text{m}$ and $0.20\ \mu\text{m}$ Teflon filters. The filtrate was brought to dryness, subsequently dissolved in benzene, filtered through a $0.20\ \mu\text{m}$ filter and freeze- dried several times (see Table 6.2) in this solvent. Light green powders were obtained.

Complexes **C2.2(6.3)**, **C3.2(7.9)**, **C4.2(7.4)**, and **C5.2(44.9)** were prepared according to this general procedure (cf. 6.4 compounds register I).

Table 6.2: Standard reaction conditions for the complexation of $\text{Cu}(\text{NO}_3)_2 \cdot 3\text{H}_2\text{O}$ in γ -butyrolactone/ CHCl_3 .

Complex	C2.2(6.3)	C3.2(7.9)	C4.2(7.4)	C5.2(44.9)
Dendrimeric ligand	L2	L3	L4	L5
Molar excess Cu-N	11	12	12	12
Temperature	rt.	rt.	rt.	rt.
Time	o. n.	o. n.	o. n.	o. n.
Freeze - drying	1x	2x	4x	4x

o.n.: over night

Specific procedure for 1st generation copper(II) complexes in γ -butyrolactone/ CHCl_3

Synthetic procedure of complexation for the 1st generation: 200 mg (0.10 mmol) of the 1st generation dendrimeric ligand, were dissolved in 4 ml chloroform and added to 11 ml of a $\text{Cu}(\text{NO}_3)_2 \cdot 3\text{H}_2\text{O}$ solution (3.65 g, i.e. 15.13 mmol) in γ -butyrolactone (25 fold molar excess of copper salt per nitrogen centre), whereas the colour of the reaction mixture darkened and copious precipitate developed. The mixture was stirred at room temperature over night.

Specific working up procedure for the 1st generation: After evaporating the chloroform under reduced pressure, the intense precipitate was filtered through a P4 filter. It was washed with γ -butyrolactone, subsequently with benzene, and dried in air. A light blue powder was obtained.

Complex **C1.7(1.0)b** was prepared according to this specific procedure (cf. 6.4 compounds register I).

6.3.1.2 Series of Lower Copper(II) Loading***Complexation varying the stoichiometry of the reaction***

The synthesis was carried out in analogy to the general procedure for complexation in THF or γ -butyrolactone/ CHCl_3 , using Cu:N molar ratios, m, different than the ones indicated there, cf. 6.3.1.1. In the case of complex **C2.7(4.6)** a non metallic salt (TBAB 0.01% wt.) was supplementary added. The working up procedure was also the general one for the complexes synthesised in THF (see 6.3.1.1). The washing out procedure with acetone described below was the one followed for the complex prepared in γ -butyrolactone/ CHCl_3 .

- i. Standard working up procedure in THF (see 6.3.1.1). Complexes **C2.5(5.4)**, **C2.6(5.2)**, **C2.7(4.6)**, **C2.8(4.4)**, **C2.12(2.1)**, **C2.15(1.3)**, **C2.16(1.0)**, **C2.17(0.3)**, and **C2.19(0.5)** were prepared according to this variant, (see 6.4 compounds register I).
- ii. The copper(II) salt solution was used without previous filtration; the reaction mixture was either centrifugated and the sedimentate discarded or directly worked up. Complexes **C2.10(2.7)**, **C2.11(2.6)**, **C2.14(1.3)**, **C2.18(0.9)**, and **C2.20(0.3)** were synthesised according to this variant, (see 6.4 compounds register I).

Washing out a higher loaded complex

End products obtained according to the general synthetic procedures or crude complexes before working up were treated with different polar solvents in order to wash out selectively copper(II) ions from the complex. In all cases, the washed complexes were dried in reduced vacuum, dissolved in benzene, filtered through a 0.20 μm Teflon filter, and finally freeze-dried.

- i. *Washing of purified highly loaded complex*: some milligrams of the lyophilized complex were placed in a P4 filter funnel and washed with ethyl acetate (complex **C2.4(5.4)**) or acetone (complex **C2.9(3.5)**); see 6.4 compounds register I.
- ii. *Washing of crude highly loaded complex*: once the reaction volume was reduced on a rotary evaporator, the complex was precipitated with γ -butyrolactone (complex **C2.10(2.7)**) or acetonitrile (complex **C2.18(0.9)**). The precipitation was left to complete at 2°C over night, filtrated through a P4 filter funnel, and washed with a portion of the corresponding solvent. In the case of washing with water, the THF was completely evaporated under reduced pressure and the residue was extracted with water. The $\text{Cu}(\text{NO}_3)_2 \cdot 3\text{H}_2\text{O}$ solution was filtered from the residue (complexes **C2.14(1.3)** and **C2.20(0.3)**). The crude products after reaction in γ -butyrolactone/ CHCl_3 were washed with some millilitres of acetone (complexes **C2.11(2.6)**, **C2.13(2.0)**, and **C2.15(1.3)**); see 6.4 compounds register I.

6.3.2 Procedure for Copper(II) Tetrafluoroborate Hydrate Complexation with PPI Dendrimers

100 mg ($2.44 \cdot 10^{-2}$ mmol) of dendrimeric ligand of the 2nd generation dissolved in 2.7 ml THF were added to 3.3 ml solution of copper(II) tetrafluoroborate hydrate $\text{Cu}(\text{BF}_4)_2 \cdot x\text{H}_2\text{O}$ ($x \sim 4$) in the same solvent (11 fold molar excess of copper(II) per nitrogen centre). The reaction mixture was stirred at room temperature over night. After the solvent was evaporated under reduced pressure, the complex was extracted from the residue with benzene. The solution was concentrated in vacuum, filtered through a 0.20 μm Teflon filter, and freeze dried.

6.4 COMPOUNDS REGISTER I: SYNTHESIS AND CHARACTERIZATION

Together with the identification code defined in 6.3, i.e. **CG.i(n)**, in this section, a more descriptive notation is also given for clarity. The copper(II) complexes have been denoted as $LG \cdot a\text{Cu}(\text{NO}_3)_2 \cdot b\text{Cu}_2(\text{NO}_3)(\text{OH})_3 \cdot c\text{HNO}_3 \cdot d\text{H}_2\text{O}$ according to 3.2, with:

- LG: L describes the dendrimeric ligand, G identifies the generation, and
- *a* represents the moles of $\text{Cu}(\text{NO}_3)_2$ per dendrimer,
- *b* the moles of possible $\text{Cu}_2(\text{NO}_3)(\text{OH})_3$ per dendrimer,
- *c* the moles of HNO_3 per dendrimeric ligand, and finally
- *d* the moles of water molecules.

6.4.1 Dendrimeric Copper(II) Complexes from $\text{Cu}(\text{NO}_3)_2 \cdot 3\text{H}_2\text{O}$

6.4.1.1 Copper(II) Complex of the “Zero” Generation, **C0.1(n)**

C0.1(0.2)	L0·0.2Cu(NO₃)₂·4.8H₂O
Synthesis:	general procedure for complexation in THF
Starting materials:	0.10 g ($1.09 \cdot 10^{-4}$ mol) L0 1.31 g ($5.43 \cdot 10^{-3}$ mol) $\text{Cu}(\text{NO}_3)_2 \cdot 3\text{H}_2\text{O}$ 14.8 ml THF
Working up:	general for complexation in THF
Yield:	$62 \cdot 10^{-3}$ g, green powder
Characterisation:	
EA	$\text{C}_{58}\text{H}_{100}\text{N}_2\text{O}_6 \cdot 0.2\text{Cu}(\text{NO}_3)_2 \cdot 4.8\text{H}_2\text{O}$ found: Cu 1.49%, C 67.22%, H 10.12%, N 2.22% calcd.: Cu 1.12%, C 66.43%, H 10.53%, N 3.17%
MALDI-ToF-MS, m/z	$M_{\text{calcd.}}$ for L0Cu_x : $921.4 + 63.5 \cdot x$; $\text{L0} = \text{C}_{58}\text{H}_{100}\text{N}_2\text{O}_6$, $x = 0, 1, \dots$ M_{found} (ref.): 488.5 $[(\text{C}_{31}\text{H}_{55}\text{NO}_3)\text{-H}]^+$ (100%), 518.4 $[(\text{C}_{31}\text{H}_{55}\text{NO}_3)\text{Na}+6\text{H}]^+$, 551.4 $[(\text{C}_{31}\text{H}_{55}\text{NO}_3)\text{Cu-2H}]^+$, 921.8 $[\text{L0}]^+$, 944.8 $[\text{L0Na}]^+$, 983.8 $[\text{L0Cu-H}]^+$, 1038.8 $[(\text{C}_{27}\text{H}_{47}\text{NO}_3)(\text{C}_{31}\text{H}_{56}\text{N}_2\text{O}_3)\text{CuK-2H}]^+$, 1155.8 $[(\text{C}_{31}\text{H}_{56}\text{N}_2\text{O}_3)_2\text{Cu}_2\text{Na-4H}]^+$, 1509.3 $[\text{L0}(\text{C}_{31}\text{H}_{56}\text{N}_2\text{O}_3)\text{CuNa-4H}]^+$
FTIR, $\tilde{\nu}$ /cm⁻¹	3260, 3073, 2953, 2921, 2906 sh, 2869 sh, 2850, 1653, 1634, 1617, 1601, 1582, 1540, 1516, 1509, 1489, 1466, 1435, 1420, 1393, 1374, 1337 sh, 1318, 1277, 1262, 1227, 1194, 1152 sh, 1138, 1107, 1069, 1048, 1023, 988, 934, 913, 870, 816, 795, 768, 739, 722, 646, 610

6.4.1.2 Copper(II) Complexes of the 1st Generation, C1.i(n)

C1.2 (1.9)b	L1·1.9 Cu(NO ₃) ₂ ·1.5 HNO ₃
Synthesis:	general procedure for complexation in THF
Starting materials:	0.80 g (4.03·10 ⁻⁴ mol) L1 14.62 g (60.51·10 ⁻³ mol) Cu(NO ₃) ₂ ·3H ₂ O 74.7 ml THF
Working up:	specific for the 1 st generation in THF
Yield:	736·10 ⁻³ g, light blue powder
Characterisation:	
EA	C ₁₂₄ H ₂₁₆ N ₆ O ₁₂ ·1.9Cu(NO ₃) ₂ ·1.5HNO ₃ found: Cu 4.90%, C 61.00%, H 8.81%, N 6.27% calcd.: Cu 4.92%, C 61.01%, H 8.81%, N 6.14%
MALDI-ToF-MS, m/z	M _{calcd.} for L1Cu _x : 1983.1 + 63.5x; L1 = C ₁₂₄ H ₂₁₆ N ₆ O ₁₂ , x = 0, 1, ... M _{found} (ref.): 1983.2 [L1] ⁺ , 2005.2 [L1Na-H] ⁺ , 2021.2 [L1K-H] ⁺ , 2046.1 [L1Cu-H] ⁺ (100%), 2068.2 [L1CuNa-H] ⁺ , 2084.2 [L1CuK-2H] ⁺ , 2109.1 [L1Cu ₂ -H] ⁺ , 2130.9 [L1Cu ₂ Na-2H] ⁺ , 2145.2 [(C ₆₀ H ₁₀₅ N ₃ O ₆) ₂ Cu ₃ Na+2H] ⁺ , 2171.0 [L1Cu ₃ -3H] ⁺ , 2206.0 [(C ₆₀ H ₁₀₅ N ₃ O ₆)(C ₆₇ H ₁₂₁ N ₅ O ₆)Cu ₂ Na-H] ⁺ , 2236.0 [L1Cu ₄ -H] ⁺ , 2270.1 [L1Cu ₄ K-6H] ⁺ , 2298.0 [L1Cu ₅ -3H] ⁺ M _{found} (lin.): 1981.7 [L1-H] ⁺ (100%), 2003.6 [L1Na-2H] ⁺ , 2019.5 [L1K-3H] ⁺ , 2043.9 [L1Cu-3H] ⁺ , 2065.8 [L1CuNa-4H] ⁺ , 2083.6 [L1CuK-2H] ⁺ , 2107.4 [L1Cu ₂ -3H] ⁺ , 2142.7 [(C ₆₀ H ₁₀₅ N ₃ O ₆) ₂ Cu ₃ Na] ⁺ , 2170.1 [L1Cu ₃ -4H] ⁺ , 2205.0 [(C ₆₀ H ₁₀₅ N ₃ O ₆)(C ₆₇ H ₁₂₁ N ₅ O ₆)Cu ₂ Na-2H] ⁺ , 2234.9 [L1Cu ₄ -2H] ⁺ , 2268.8 [L1Cu ₄ K-7H] ⁺

C1.2(1.9)gr	L1·1.9Cu(NO ₃) ₂
Synthesis:	general procedure for complexation in THF
Working up:	specific for the 1 st generation in THF
Starting materials:	C1.2(1.9)b i.e. L1·1.9Cu(NO ₃) ₂ ·1.5HNO ₃
Yield:	quantitative, green powder
Characterisation:	
EA	C ₁₂₄ H ₂₁₆ N ₆ O ₁₂ ·1.9Cu(NO ₃) ₂ found: Cu 5.24%, C 64.28%, H 9.29%, N 4.73% calcd.: Cu 4.65%, C 63.78%, H 9.16%, N 5.36%
MALDI-ToF-MS, m/z	M _{calcd.} for L1Cu _x : 1983.1 + 63.5x; L1 = C ₁₂₄ H ₂₁₆ N ₆ O ₁₂ , x = 0, 1, ... M _{found} (ref.): 474.3 [(C ₃₀ H ₅₃ NO ₃)-H] ⁺ , 986.5 [(C ₆₀ H ₁₀₅ N ₃ O ₆)Na-H] ⁺ , 1531.7 [(C ₉₄ H ₁₆₅ N ₅ O ₉)Na-H] ⁺ , 1571.7 [(C ₉₄ H ₁₆₅ N ₅ O ₉)Cu-H] ⁺ , 1983.1 [L1] ⁺ , 2005.0 [L1Na-H] ⁺ , 2021.1 [L1K-H] ⁺ , 2029.9 [(C ₆₀ H ₁₀₅ N ₃ O ₆) ₂ CuK-2H] ⁺ , 2046.0 [L1Cu-H] ⁺ (100%), 2062.1 [(C ₆₀ H ₁₀₅ N ₃ O ₆) ₂ Cu ₂ +6H] ⁺ , 2068.1 [L1CuNa-2H] ⁺ , 2084.1 [L1CuK-2H] ⁺ , 2091.0 [(C ₆₀ H ₁₀₅ N ₃ O ₆) ₂ Cu ₂ K-4H] ⁺ , 2108.0 [L1Cu ₂ -2H] ⁺ , 2124.0 [(C ₆₀ H ₁₀₅ N ₃ O ₆)(C ₆₄ H ₁₁₄ N ₄ O ₆)Cu ₂ -3H] ⁺ , 2130.9 [L1Cu ₂ Na-2H] ⁺ , 2144.0 [(C ₆₀ H ₁₀₅ N ₃ O ₆) ₂ Cu ₃ Na+H] ⁺ , 2165.2 [(C ₆₀ H ₁₀₅ N ₃ O ₆)(C ₆₇ H ₁₂₁ N ₅ O ₆)CuK+6H] ⁺ , 2172.0 [L1Cu ₃ -2H] ⁺

	2206.9	$[(C_{60}H_{105}N_3O_6)(C_{67}H_{121}N_5O_6)Cu_2Na]^+$,	2509.3
		$[(C_{60}H_{105}N_3O_6)(C_{94}H_{165}N_5O_9)K-4H]^+$,	2580.4
		$[(C_{60}H_{105}N_3O_6)(C_{94}H_{165}N_5O_9)CuK+4H]^+$	
FTIR, $\tilde{\nu}$ /cm⁻¹	3548, 3343, 3035 sh, 2956 sh, 2921, 2871 sh, 2853, 2755, 2769, 2672, 2556 sh, 1717 sh, 1632, 1601, 1578, 1545, 1507, 1498, 1468, 1439 sh, 1428 sh, 1391, 1379, 1337 sh, 1316 sh, 1300, 1273, 1227, 1160, 1132, 1067, 1048, 1017, 994 sh, 949, 874, 824 sh, 810, 760, 722, 677, 646		
UV-Vis, λ/nm	Film 261.5, 290.5, 357.5		
UV-Vis,	CHCl ₃ , c = 1.90·10 ⁻¹ g·l ⁻¹		
λ_{max} /nm (ϵ /10³ cm²·g⁻¹)	266 (18311), 291 (11600)		

C1.4(1.5)		L1·1.5Cu(NO ₃) ₂ ·2.0HNO ₃ ·5.0H ₂ O	
Synthesis:	general procedure for complexation in THF		
Starting materials:	0.30 g (1.51·10 ⁻⁴ mol)	L1	
	5.48 g (22.69·10 ⁻³ mol)	Cu(NO ₃) ₂ ·3H ₂ O	
	28.0 ml	THF	
Working up:	general for complexation in THF		
Yield:	137·10 ⁻³ g, light green powder		
Characterisation:			
EA	C ₁₂₄ H ₂₁₆ N ₆ O ₁₂ ·1.5Cu(NO ₃) ₂ ·2.0HNO ₃ ·5.0H ₂ O found: Cu 3.87%, C 59.59%, H 9.07%, N 6.18% calcd.: Cu 3.84%, C 59.69%, H 9.05%, N 5.86%		
MALDI-ToF-MS, m/z	M _{calcd.} for L1Cu _x : 1983.1 + 63.5x; L1 = C ₁₂₄ H ₂₁₆ N ₆ O ₁₂ , x = 0, 1, ... M _{found} (ref.): 1983.5 [L1] ⁺ , 2005.5 [L1Na-H] ⁺ , 2021.4 [L1K-H] ⁺ , 2046.4 [L1Cu] ⁺ (100%), 2068.4 [L1CuNa-H] ⁺ , 2084.4 [L1CuK-H] ⁺ , 2108.3 [L1Cu ₂ -2H] ⁺ , 2171.3 [L1Cu ₃ -2H] ⁺		
FTIR, $\tilde{\nu}$ /cm ⁻¹	3344, 3084, 3058 sh, 2955, 2921, 2872, 2851, 2774, 2684, 2531, 1630, 1620sh, 1603, 1577, 1554, 1513, 1505, 1468, 1445 sh, 1424, 1391, 1379 sh, 1339 sh, 1310, 1276, 1228, 1154 sh, 1133, 1067, 1045, 1020, 989, 934, 869, 824, 810 sh, 760, 722, 644,		

C1.2(1.0)b1		L1·1.0Cu(NO ₃) ₂ ·1.1HNO ₃
Synthesis:	general procedure for complexation in THF	
Working up:	specific for the 1 st generation in THF	
	100·10 ⁻³ g	C1.2(1.9)b
	10 ml	CHCl ₃
	10 ml	toluene
Yield:	68·10 ⁻³ g, light blue powder	
Characterisation:		
EA	C ₁₂₄ H ₂₁₆ N ₆ O ₁₂ ·1.0Cu(NO ₃) ₂ ·1.1HNO ₃	
	found: Cu 2.75%, C 64.93%, H 9.54%, N 7.79%	
	calcd.: Cu 3.05%, C 65.55%, H 9.46%, N 5.37%	

MALDI-ToF-MS, m/z	$M_{\text{calcd.}}$ for $L1Cu_x$: $1983.1 + 63.5x$; $L1 = C_{124}H_{216}N_6O_{12}$, $x = 0, 1, \dots$ M_{found} (ref.): 1983.3 $[L1]^+$, 2005.3 $[L1Na-H]^+$, 2021.2 $[L1K-H]^+$, 2046.2 $[L1Cu]^+$ (100%), 2068.3 $[L1CuNa-H]^+$, 2084.3 $[L1CuK-H]^+$, 2092.1 $[(C_{60}H_{105}N_3O_6)_2Cu_2K-3H]^+$, 2108.2 $[L1Cu_2-2H]^+$, 2131.9 $[L1Cu_2Na-H]^+$, 2145.1 $[(C_{60}H_{105}N_3O_6)_2Cu_3Na+2H]^+$, 2171.1 $[L1Cu_3-3H]^+$, 2207.1 $[(C_{60}H_{105}N_3O_6)(C_{67}H_{121}N_5O_6)Cu_2Na]^+$, 2234.0 $[L1Cu_4-3H]^+$, 2270.1 $[L1Cu_4K-6H]^+$, 2299.3 $[L1Cu_5-2H]^+$ M_{found} (lin.): 1981.9 $[L1-H]^+$ (100%), 2004.1 $[L1Na-2H]^+$, 2021.1 $[L1K-H]^+$, 2045.0 $[L1Cu-2H]^+$, 2067.1 $[L1CuNa-3H]^+$, 2083.6 $[L1CuK-2H]^+$, 2108.3 $[L1Cu_2-2H]^+$, 2142.8 $[(C_{60}H_{105}N_3O_6)_2Cu_3Na]^+$, 2170.9 $[L1Cu_3-3H]^+$, 2206.2 $[(C_{60}H_{105}N_3O_6)(C_{67}H_{121}N_5O_6)Cu_2Na-H]^+$, 2232.3 $[L1Cu_4-5H]^+$, 2270.5 $[L1Cu_4K-6H]^+$	
C1.7(1.0)	$L1 \cdot 1.0Cu(NO_3)_2 \cdot 2.0HNO_3 \cdot 9.2H_2O$	
Synthesis:	specific for the 1 st generation in γ -butyrolactone/ $CHCl_3$	
Starting materials:	0.20 g ($1.01 \cdot 10^{-4}$ mol)	L1
	3.65 g ($15.13 \cdot 10^{-3}$ mol)	$Cu(NO_3)_2 \cdot 3H_2O$
	11.0 ml	γ -butyrolactone
	4.0 ml	$CHCl_3$
Working up:	specific for the 1 st generation in γ -butyrolactone/ $CHCl_3$	
Yield:	$162 \cdot 10^{-3}$ g, light blue powder	
Characterisation:		
EA	$C_{124}H_{216}N_6O_{12} \cdot 1.0Cu(NO_3)_2 \cdot 2.0HNO_3 \cdot 9.2H_2O$ found: Cu 2.59%, C 60.30%, H 8.83%, N 5.71% calcd.: Cu 2.57%, C 60.03%, H 9.44%, N 5.33%	
MALDI-ToF-MS, m/z	$M_{\text{calcd.}}$ for $L1Cu_x$: $1983.1 + 63.5x$; $L1 = C_{124}H_{216}N_6O_{12}$, $x = 0, 1, \dots$ M_{found} (ref.): 1983.8 $[L1]^+$ (100%), 1998.8 $[(C_{60}H_{105}N_3O_6)(C_{64}H_{114}N_4O_6)-H]^+$, 2005.8 $[L1Na]^+$, 2021.7 $[L1K]^+$, 2029.7 $[(C_{60}H_{105}N_3O_6)_2CuK-2H]^+$, 2046.7 $[L1Cu]^+$, 2061.7 $[(C_{60}H_{105}N_3O_6)_2Cu_2+6H]^+$, 2068.7 $[L1CuNa-H]^+$, 2084.7 $[L1CuK-H]^+$, 2108.6 $[L1Cu_2-2H]^+$, 2132.5 $[L1Cu_2Na-H]^+$, 2144.8 $[(C_{60}H_{105}N_3O_6)_2Cu_3Na-2H]^+$, 2172.6 $[L1Cu_3-H]^+$, 2206.7 $[(C_{60}H_{105}N_3O_6)(C_{67}H_{121}N_5O_6)Cu_2Na-H]^+$, 2269.6 $[L1Cu_4K-7H]^+$	

6.4.1.3 Copper(II) Complex of the 2nd Generation, C2.i(n)

C2.2(6.3)	$L2 \cdot 6.3Cu(NO_3)_2 \cdot 3.7HNO_3 \cdot 35.7H_2O$	
Synthesis:	general procedure for complexation in γ -butyrolactone / $CHCl_3$	
Starting materials:	0.10 g ($2.44 \cdot 10^{-5}$ mol)	L2
	0.88 g ($3.65 \cdot 10^{-3}$ mol)	$Cu(NO_3)_2 \cdot 3H_2O$
	20.0 ml	γ -butyrolactone
	25.0 ml	$CHCl_3$
Working up:	general for complexation in γ -butyrolactone / $CHCl_3$	

Yield: $124 \cdot 10^{-3}$ g, light green powder

Characterisation:

EA $C_{256}H_{448}N_{14}O_{24} \cdot 6.3Cu(NO_3)_2 \cdot 3.7HNO_3 \cdot 35.7H_2O$
found: Cu 6.53%, C 49.98%, H 7.95%, N 6.48%
calcd.: Cu 6.46%, C 49.43%, H 8.47%, N 6.51%

MALDI-ToF-MS, m/z $M_{\text{calcd.}}$ for $L2Cu_x$: $4106.4 + 63.5 \cdot x$; $L2 = C_{256}H_{448}N_{14}O_{24}$, $x = 0, 1, \dots$
 M_{found} (ref.): 4106.0 $[L2]^+$, 4127.9 $[L2Na-2H]^+$, 4168.9 $[L2Cu-H]^+$ (100%), 4231.8 $[L2Cu_2-2H]^+$, 4294.7 $[L2Cu_3-2H]^+$, 4356.6 $[L2Cu_4-4H]^+$, 4421.1 $[L2Cu_5-3H]^+$, 4484.5 $[L2Cu_6-3H]^+$

FTIR, $\tilde{\nu}$ /cm⁻¹ 3352, 3966, 2956, 2921, 2873 sh, 2851, 2765, 2732, 2668, 2618, 2502, 1635, 1622, 1602, 1576, 1559, 1540, 1514, 1506, 1489, 1469, 1459, 1394, 1379 sh, 1339 sh, 1311 sh, 1283, 1279, 1230, 1156 sh, 1132, 1109, 1068, 1040 sh, 1020, 989, 935, 877, 820 sh, 809, 797 sh, 758, 722, 646, 611

C2.3(6.0) L2·6.0Cu(NO₃)₂·5.1HNO₃·31.0H₂O

Synthesis: general procedure for complexation in THF

Starting materials: 0.06 g ($1.46 \cdot 10^{-5}$ mol) **L2**
0.04 g ($1.75 \cdot 10^{-4}$ mol) $Cu(NO_3)_2 \cdot 3H_2O$
1.75 ml THF

Working up: general for complexation in THF

Yield: $74 \cdot 10^{-3}$ g, light green powder

Characterisation:

EA $C_{256}H_{448}N_{14}O_{24} \cdot 6.0Cu(NO_3)_2 \cdot 5.1HNO_3 \cdot 31.0H_2O$
found: Cu 6.26%, C 50.76%, H 7.63%, N 7.00%
calcd.: Cu 6.24%, C 50.19%, H 8.33%, N 7.00%

MALDI-ToF-MS, m/z $M_{\text{calcd.}}$ for $L2Cu_x$: $4106.4 + 63.5 \cdot x$; $L2 = C_{256}H_{448}N_{14}O_{24}$, $x = 0, 1, \dots$
 M_{found} (ref.): 4106.0 $[L2]^+$, 4129.3 $[L2Na]^+$, 4169.5 $[L2Cu-H]^+$ (100%), 4190.8 $[L2CuNa-2H]^+$, 4232.4 $[L2Cu_2-H]^+$, 4293.4 $[L2Cu_3-4H]^+$

FTIR, $\tilde{\nu}$ /cm⁻¹ 3366, 3077, 2955, 2924, 2869 sh, 2854, 2655, 2610, 2502, 1653, 1636, 1621 sh, 1601, 1572, 1559, 1507, 1492 sh, 1469, 1443 sh, 1394, 1379 sh, 1337 sh, 1314 sh, 1289 sh, 1278, 1230, 1156 sh, 1135, 1050 sh, 1014, 989 sh, 940, 889, 874, 809, 759, 722, 667, 646

UV-Vis, $CHCl_3$, $c = 2.00 \cdot 10^{-1}$ g·l⁻¹
 λ_{max} /nm (ϵ /10³ cm²·g⁻¹) 266 (18175), 291 (13260)

C2.4(5.4) L2·5.4Cu(NO₃)₂·6.0HNO₃·18.8H₂O

Synthesis: general procedure for complexation in THF

Working up: washing out with ethyl acetate

Starting materials: $400 \cdot 10^{-3}$ g **C2.1(7.3)**
20 ml ethyl acetate

Yield: $362 \cdot 10^{-3}$ g, light green powder

Characterisation:	
EA	$C_{256}H_{448}N_{14}O_{24} \cdot 5.4Cu(NO_3)_2 \cdot 6.0HNO_3 \cdot 18.8H_2O$ found: Cu 5.90%, C 52.65%, H 8.06%, N 7.08% calcd.: Cu 5.86%, C 52.36%, H 8.43%, N 7.01%
FTIR, $\tilde{\nu}$ /cm⁻¹	3354, 3042 sh, 2954, 2923, 2969 sh, 2853, 1653, 1646, 1636, 1618, 1601, 1576, 1559, 1540, 1512 sh, 1497, 1489, 1472, 1466, 1457, 1437, 1395, 1387, 1375, 1339, 1312, 1296, 1275, 1225, 1156 sh, 1131, 1069, 1015, 967, 883, 816, 810, 758, 722, 668, 648
UV-Vis, λ_{max} /nm (ϵ /10³cm²·g⁻¹)	CH ₂ Cl ₂ , c = 1.10·10 ⁻¹ g·l ⁻¹ 232 (23809), 266 (15564), 293 (11645)
<hr/>	
C2.5(5.4)	L2·5.4Cu(NO₃)₂·3.5HNO₃·35.5H₂O
Synthesis:	complexation varying the stoichiometry
Starting materials:	0.05 g (1.22·10 ⁻⁵ mol) L2
	0.18 g (7.31·10 ⁻³ mol) Cu(NO ₃) ₂ ·3H ₂ O
	1.95 ml THF
Working up:	general for complexation in THF
Yield:	72·10 ⁻³ g, light green powder
 Characterisation:	
EA	$C_{256}H_{448}N_{14}O_{24} \cdot Cu(NO_3)_2 \cdot 3.5HNO_3 \cdot 35.5H_2O$ found: Cu 5.76%, C 51.98%, H 7.51%, N 6.07% calcd.: Cu 5.71%, C 50.98%, H 8.73%, N 6.23%
FTIR, $\tilde{\nu}$ /cm⁻¹	3365, 3052, 2955, 2924, 2869 sh, 2854, 2743, 2660, 2610, 2510, 1624 sh, 1601, 1574, 1559 sh, 1508, 1495 sh, 1469, 1393, 1379, 1337 sh, 1306 sh, 1293 sh, 1279, 1230, 1154 sh, 1135, 1057 sh, 1014, 940, 867, 818 sh, 808, 759, 721, 668, 645
<hr/>	
C2.6(5.2)	L2·5.2Cu(NO₃)₂·2.5HNO₃·28.0H₂O
Synthesis:	complexation varying the stoichiometry
Starting materials:	0.05 g (1.22·10 ⁻⁵ mol) L2
	0.08 g (3.65·10 ⁻⁴ mol) Cu(NO ₃) ₂ ·3H ₂ O
	1.62 ml THF
Working up:	general for complexation in THF
Yield:	70·10 ⁻³ g, light green powder
 Characterisation:	
EA	$C_{256}H_{448}N_{14}O_{24} \cdot 5.2Cu(NO_3)_2 \cdot 2.5HNO_3 \cdot 28.0H_2O$ found: Cu 5.77%, C 53.62%, H 8.27%, N 6.13% calcd.: Cu 5.72%, C 53.09%, H 8.81%, N 6.17%
MALDI-ToF-MS, m/z	M _{calcd.} for L2Cu _x : 4106.4 + 63.5·x; L2= C ₂₅₆ H ₄₄₈ N ₁₄ O ₂₄ , x = 0, 1, ... M _{found} (ref.): 4107.6 [L2+H] ⁺ , 4130.4 [L2Na+H] ⁺ , 4170.5 [L2Cu+H] ⁺ (100%), 4192.1 [L2CuNa-H] ⁺ , 4233.2 [L2Cu ₂] ⁺ , 4297.1 [L2Cu ₃] ⁺ , 4359.9 [L2Cu ₄] ⁺

FTIR, $\tilde{\nu}$ /cm⁻¹	3367, 3083, 2955, 2923, 2869 sh, 2853, 2684, 2628, 2514, 1640 sh, 1623 sh, 1600, 1572, 1552, 1511, 1493, 1485 sh, 1468, 1453 sh, 1435 sh, 1392, 1379, 1306 sh, 1276, 1230, 1156 sh, 1135, 1059 sh, 1015, 994 sh, 949, 874, 807, 759, 722, 647, 622	
C2.7(4.6)	L2·4.6Cu(NO₃)₂·0.1HNO₃·26.0H₂O	
Synthesis:	complexation varying the stoichiometry	
Starting materials:	0.10 g (2.44·10 ⁻⁵ mol)	L2
	0.88 g (3.65·10 ⁻³ mol)	Cu(NO ₃) ₂ ·3H ₂ O
	14.2 ml	THF
	1.27·10 ⁻³ g	TBAB
Working up:	general for complexation in THF	
Yield:	119·10 ⁻³ g, light green powder	
Characterisation:		
EA	C ₂₅₆ H ₄₄₈ N ₁₄ O ₂₄ ·Cu(NO ₃) ₂ ·0.1HNO ₃ ·26.0H ₂ O found: Cu 5.41%, C 56.93%, H 8.42%, N 5.86% calcd.: Cu 5.15%, C 56.50%, H 9.06%, N 5.97%	
MALDI-ToF-MS, m/z	M _{calcd.} for L2Cu _x : 4106.4 + 63.5·x; L2= C ₂₅₆ H ₄₄₈ N ₁₄ O ₂₄ , x = 0, 1, ... M _{found} (ref.): 4106.0 [L2] ⁺ , 4128.0 [L2Na-H] ⁺ , 4145.0 [L2K-H] ⁺ , 4169.0 [L2Cu-H] ⁺ (100%), 4191.0 [L2CuNa-2H] ⁺ , 4231.9 [L2Cu ₂ -2H] ⁺ , 4253.8 [L2Cu ₂ Na-3H] ⁺ , 4293.8 [L2Cu ₃ -3H] ⁺ , 4329.8 [(C ₁₂₆ H ₂₂₁ N ₇ O ₁₂) ₂ Cu ₄ Na] ⁺ , 4356.7 [L2Cu ₄ -4H] ⁺ , 4391.7 [(C ₁₂₆ H ₂₂₁ N ₇ O ₁₂) ₂ Cu ₅ Na-H] ⁺ , 4421.1 [L2Cu ₅ -3H] ⁺ , 4486.6 [L2Cu ₆ -H] ⁺	
FTIR, $\tilde{\nu}$ /cm⁻¹	3375, 3080, 2955, 2922, 2873, 2853, 2678, 2649, 2618 sh, 2504, 1621 sh, 1601, 1574, 1555, 1510, 1497 sh, 1469, 1443 sh, 1393, 1379, 1341 sh, 1310 sh, 1291 sh, 1278, 1230, 1154 sh, 1134, 1067, 1015, 997 sh, 936, 873, 816 sh, 808, 759, 722, 646	
UV-Vis,	CHCl ₃ , c = 4.40·10 ⁻² g·l ⁻¹	
λ_{\max} /nm (ϵ /10³cm²·g⁻¹)	266 (14727), 293 (10750)	

C2.8(4.4)		L2·4.4Cu(NO ₃) ₂ ·4.3HNO ₃ ·27.3H ₂ O
Synthesis:	complexation varying the stoichiometry	
Starting materials:	0.05 g (1.22·10 ⁻⁵ mol)	L2
	0.26 g (1.10·10 ⁻³ mol)	Cu(NO ₃) ₂ ·3H ₂ O
	2.27 ml	THF
Working up:	general for complexation in THF	
Yield:	78·10 ⁻³ g, light green powder	
Characterisation:		
EA	C ₂₅₆ H ₄₄₈ N ₁₄ O ₂₄ ·4.4Cu(NO ₃) ₂ ·4.3HNO ₃ ·27.3H ₂ O found: Cu 4.91%, C 54.47%, H 8.07%, N 6.53% calcd.: Cu 4.90%, C 53.87%, H 8.76%, N 6.61%	
MALDI-ToF-MS, m/z	M _{calcd.} for L2Cu _x : 4106.4 + 63.5·x; L2= C ₂₅₆ H ₄₄₈ N ₁₄ O ₂₄ , x = 0, 1, ... M _{found} (ref.): 4106.4 [L2] ⁺ , 4129.2 [L2Na] ⁺ , 4170.1 [L2Cu] ⁺	

FTIR, $\tilde{\nu}$ /cm ⁻¹	(100%), 4191.2 [L2CuNa-2H] ⁺ , 4232.9 [L2Cu ₂ -H] ⁺ , 4293.9 [L2Cu ₃ -3H] ⁺	
	3359, 3054, 2955, 2924, 2869 sh, 2854, 2761, 2684, 2633, 2522, 1655 sh, 1620 sh, 1601, 1573, 1552, 1510, 1493 sh, 1469, 1455sh, 1392, 1378, 1339 sh, 1304 sh, 1287 sh, 1276, 1230, 1154 sh, 1134, 1068, 1014, 992 sh, 945, 875, 820 sh, 808, 759, 722, 646, 621	
<hr/>		
C2.9(3.5)	L2·3.5Cu(NO ₃) ₂ ·6.0HNO ₃ ·10.3H ₂ O	
Synthesis:	general procedure for complexation in THF	
Working up:	washing out with acetone	
Starting materials:	400 ·10 ⁻³ g	C2.1(7.3)
	20 ml	acetone
Yield:	336·10 ⁻³ g, light green powder	
Characterisation:		
EA	C ₂₅₆ H ₄₄₈ N ₁₄ O ₂₄ ·3.5Cu(NO ₃) ₂ ·6.0HNO ₃ ·10.3H ₂ O found: Cu 4.15%, C 57.64%, H 8.54%, N 6.89% calcd.: Cu 4.17%, C 57.45%, H 8.93%, N 6.69%	
MALDI-ToF-MS, m/z	M _{calcd.} for L2Cu _x : 4106.4 + 63.5·x; L2= C ₂₅₆ H ₄₄₈ N ₁₄ O ₂₄ , x = 0, 1, ... M _{found} (ref.): 4106.2 [L2] ⁺ , 4129.1 [L2Na] ⁺ , 4169.1 [L2Cu-H] ⁺ (100%), 4191.0 [L2CuNa-2H] ⁺ , 4208.0 [L2CuK-H] ⁺ , 4231.0 [L2Cu ₂ -3H] ⁺ , 4294.9 [L2Cu ₃ -2H] ⁺ M _{found} (lin.): 4106.6 [L2] ⁺ , 4129.3 [L2Na] ⁺ , 4145.1 [L2K] ⁺ , 4153.1 [(C ₁₂₆ H ₂₂₁ N ₇ O ₁₂) ₂ CuK-2H] ⁺ , 4169.5 [L2Cu-H] ⁺ (100%), 4184.5 [(C ₁₂₆ H ₂₂₁ N ₇ O ₁₂) ₂ Cu ₂ +5H] ⁺ , 4192.1 [L2CuNa-H] ⁺ , 4208.2 [L2CuK-H] ⁺ , 4214.9 [(C ₁₂₆ H ₂₂₁ N ₇ O ₁₂) ₂ Cu ₂ K-4H] ⁺ , 4232.6 [L2Cu ₂ -H] ⁺ , 4255.1 [L2Cu ₂ Na-H] ⁺ , 4268.6 [L2Cu ₂ K-4H] ⁺ , 4295.3 [L2Cu ₃ -2H] ⁺ , 4330.5 [(C ₁₂₆ H ₂₂₁ N ₇ O ₁₂) ₂ Cu ₄ Na+H] ⁺ , 4358.2 [L2Cu ₄ -2H] ⁺	
FTIR, $\tilde{\nu}$ /cm ⁻¹	3329, 3019 sh, 2954, 2024, 2867 sh, 2853, 2740, 2668, 2626, 2524, 1657, 1640, 1632, 1622 sh, 1601, 1580, 1547, 1511, 1497, 1468, 1454 sh, 1424, 1391, 1379, 1331 sh, 1310, 1273, 1225, 1156 sh, 1132, 1067, 1040, 1017, 996 sh, 947, 878, 824, 812 sh, 760, 722, 646	
UV-Vis,	CH ₂ Cl ₂ , c = 1.80·10 ⁻¹ g·l ⁻¹	
λ_{\max} /nm (ϵ /10 ³ cm ² ·g ⁻¹)	233 (22222), 264 (17417), 291 (11639)	

C2.10(2.7)		L2·2.7Cu(NO₃)₂·6.0HNO₃·2.0H₂O
Synthesis:	complexation varying the stoichiometry	
Starting materials:	0.10 g (2.44·10 ⁻⁵ mol)	L2
	0.88 g (3.65·10 ⁻³ mol)	Cu(NO ₃) ₂ ·3H ₂ O
	12.5 ml	THF
Working up:	washing out with γ-butyrolactone	
Yield:	93·10 ⁻³ g, light green powder	
Characterisation:		
EA	C ₂₅₆ H ₄₄₈ N ₁₄ O ₂₄ ·2.7Cu(NO ₃) ₂ ·6.0HNO ₃ ·2.0H ₂ O	

	found: Cu 3.41%, C 60.94%, H 9.07%, N 6.81% calcd.: Cu 3.41%, C 60.97%, H 9.14%, N 6.66%
MALDI-ToF-MS, m/z	$M_{\text{calcd.}}$ for L2Cu_x : $4106.4 + 63.5 \cdot x$; $\text{L2} = \text{C}_{256}\text{H}_{448}\text{N}_{14}\text{O}_{24}$, $x = 0, 1, \dots$ M_{found} (ref.): 4105.3 $[\text{L2-H}]^+$, 4128.2 $[\text{L2Na-H}]^+$, 4168.2 $[\text{L2Cu-2H}]^+$ (100%), 4231.1 $[\text{L2Cu}_2\text{-2H}]^+$, 4294.0 $[\text{L2Cu}_3\text{-3H}]^+$, 4356.9 $[\text{L2Cu}_4\text{-4H}]^+$, 4420.7 $[\text{L2Cu}_5\text{-3H}]^+$, 4485.0 $[\text{L2Cu}_6\text{-3H}]^+$
FTIR, $\tilde{\nu}/\text{cm}^{-1}$	3351, 3045, 2955, 2923, 2869 sh, 2853, 2757, 2676, 2608 sh, 2516, 1650 sh, 1635, 1626 sh, 1602, 1577, 1559, 1543, 1508, 1491, 1468, 1460 sh, 1420, 1394, 1379, 1331 sh, 1304 sh, 1293 sh, 1275, 1227, 1158 sh, 1129, 1113, 1068, 1040 sh, 1016, 994 sh, 947sh, 875, 820, 809, 759, 722, 667, 648, 619
UV-Vis, $\lambda_{\text{max}}/\text{nm}$ ($\epsilon/10^3\text{cm}^2\cdot\text{g}^{-1}$)	CH_2Cl_2 , $c = 1.05 \cdot 10^{-1} \text{ g}\cdot\text{l}^{-1}$ 234 (14286), 263 (16762), 291 (10752)

C2.11(2.6)	$\text{L2}\cdot 2.6\text{Cu}(\text{NO}_3)_2\cdot 0.9\text{HNO}_3\cdot 25.3\text{H}_2\text{O}$
Synthesis:	complexation varying the stoichiometry
Starting materials:	0.20 g ($4.87 \cdot 10^{-5}$ mol) L2 4.1 g ($17.0 \cdot 10^{-3}$ mol) $\text{Cu}(\text{NO}_3)_2\cdot 3\text{H}_2\text{O}$ 15.0 ml γ -butyrolactone 4.5 ml CHCl_3
Working up:	washing out with acetone
Yield:	$140 \cdot 10^{-3}$ g, light green powder
Characterisation:	
EA	$\text{C}_{256}\text{H}_{448}\text{N}_{14}\text{O}_{24}\cdot 2.6\text{Cu}(\text{NO}_3)_2\cdot 0.9\text{HNO}_3\cdot 25.3\text{H}_2\text{O}$ found: Cu 3.23%, C 60.41%, H 9.02%, N 5.00% calcd.: Cu 3.22%, C 59.74%, H 9.78%, N 5.08%
FTIR, $\tilde{\nu}/\text{cm}^{-1}$	3340, 3064, 2954, 2921, 2871 sh, 2851, 2755, 2680, 2608, 2512, 1653, 1636, 1624, 1617, 1601, 1576, 1559, 1539, 1507, 1489, 1466, 1459, 1437, 1420, 1395, 1387, 1376, 1337, 1289 sh, 1275, 1227, 1150 sh, 1129 sh, 1109, 1073, 1044, 1019, 988, 934, 886 sh, 822, 810, 799 sh, 758, 722, 608

C2.12(2.1)	$\text{L2}\cdot 2.1\text{Cu}(\text{NO}_3)_2\cdot 2.5\text{HNO}_3$
Synthesis:	complexation varying the stoichiometry
Starting materials:	0.20 g ($4.87 \cdot 10^{-5}$ mol) L2 $23.5 \cdot 10^{-3}$ g ($9.74 \cdot 10^{-5}$ mol) $\text{Cu}(\text{NO}_3)_2\cdot 3\text{H}_2\text{O}$ 5.42 ml THF
Working up:	general for complexation in THF
Yield:	$183 \cdot 10^{-3}$ g, light green powder
Characterisation:	
EA	$\text{C}_{256}\text{H}_{448}\text{N}_{14}\text{O}_{24}\cdot 2.1\text{Cu}(\text{NO}_3)_2\cdot 2.5\text{HNO}_3$ found: Cu 2.80%, C 65.83%, H 9.62%, N 6.99% calcd.: Cu 2.88%, C 66.17%, H 9.75%, N 5.69%
MALDI-ToF-MS, m/z	$M_{\text{calcd.}}$ for L2Cu_x : $4106.4 + 63.5 \cdot x$; $\text{L2} = \text{C}_{256}\text{H}_{448}\text{N}_{14}\text{O}_{24}$, $x = 0, 1, \dots$

		M_{found} (ref.): 4107.1 [L2+H] ⁺ , 4128.7 [L2Na-H] ⁺ , 4144.8 [L2K-H] ⁺ , 4169.5 [L2Cu-H] ⁺ (100%), 4191.2 [L2CuNa-2H] ⁺ , 4232.3 [L2Cu ₂ -H] ⁺ , 4294.5 [L2Cu ₃ -3H] ⁺ M_{found} (lin.): 4106.4 [L2] ⁺ (100%), 4168.5 [L2Cu-H] ⁺ , 4231.2 [L2Cu ₂ -2H] ⁺ , 4269.0 [L2Cu ₂ K-4H] ⁺ , 4293.0 [L2Cu ₃ -4H] ⁺ , 4329.4 [(C ₁₂₆ H ₂₁₁ N ₇ O ₁₂) ₂ Cu ₄ Na] ⁺ FTIR, $\tilde{\nu}$ /cm ⁻¹ 3327, 3068 sh, 3023 sh, 2955, 2924, 2869 sh, 2854, 2763, 2676, 2618 sh, 2541, 1634, 1602, 1581, 1547, 1509, 1495 sh, 1468, 1459, 1410 sh, 1387 sh, 1379, 1337, 1312, 1272, 1224, 1152 sh, 1130, 1068, 1039, 1018, 991, 945 sh, 877, 825, 805, 761, 722, 646, 623
C2.13(2.0)		L2·2.0Cu(NO₃)₂·2.8HNO₃·15.4H₂O
Synthesis:	general procedure for complexation in γ -butyrolactone / CHCl ₃	
Starting materials:	0.10 g (2.44·10 ⁻⁵ mol)	L2
	0.88 g (3.65·10 ⁻³ mol)	Cu(NO ₃) ₂ ·3H ₂ O
	20.0 ml	γ -butyrolactone
	25.0 ml	CHCl ₃
Working up:	washing out with γ -butyrolactone	
Yield:	47·10 ⁻³ g, light green powder	
Characterisation:		
EA	C ₂₅₆ H ₄₄₈ N ₁₄ O ₂₄ ·2.0Cu(NO ₃) ₂ ·2.8HNO ₃ ·15.4H ₂ O found: Cu 2.54%, C 62.51%, H 9.37%, N 5.85% calcd.: Cu 2.54%, C 62.26%, H 9.61%, N 5.86%	
FTIR, $\tilde{\nu}$ /cm⁻¹	3337, 3077 sh, 3048, 2955, 2920, 2873 sh, 2851, 2753, 2753, 2655, 2622, 2514, 1653, 1635, 1628 sh, 1602, 1577, 1559, 1540, 1508, 1501 sh, 1489, 1467, 1456, 1437, 1420, 1395, 1387, 1379 sh, 1339, 1311, 1275, 1227, 1150 sh, 1130, 1113 sh, 1068, 1044, 1020, 989, 934, 872, 826, 818 sh, 795, 759, 741, 722, 669, 646, 610	
C2.14(1.3)		L2·1.3Cu(NO₃)₂·2.7HNO₃·4.6H₂O
Synthesis:	complexation varying the stoichiometry	
Starting materials:	0.06 g (1.46·10 ⁻⁵ mol)	L2
	0.53 g (2.19·10 ⁻³ mol)	Cu(NO ₃) ₂ ·3H ₂ O
	7.5 ml	THF
Working up:	washing out with water	
Yield:	45·10 ⁻³ g, green powder	
Characterisation:		
EA	C ₂₅₆ H ₄₄₈ N ₁₄ O ₂₄ ·1.3Cu(NO ₃) ₂ ·2.7HNO ₃ ·4.6H ₂ O found: Cu 1.76%, C 67.03%, H 9.69%, N 5.81% calcd.: Cu 1.77%, C 66.92%, H 9.90%, N 5.73%	
FTIR, $\tilde{\nu}$ /cm⁻¹	3328, 3069 sh, 3037 sh, 2955, 2924, 2869 sh, 2854, 1636, 1601, 1582, 1545, 1508, 1460 sh, 1468, 1441 sh, 1387 sh, 1378, 1337, 1312, 1270, 1225, 1154 sh, 1129, 1067 sh, 1038, 1019, 996, 941, 874, 812 sh, 803, 762, 722, 646	

UV-Vis, λ_{max} /nm	film 258, 289, 319 sh
--	--------------------------

C2.15(1.3)	L2·1.3Cu(NO₃)₂·2.8HNO₃·12.6H₂O
Synthesis:	complexation varying the stoichiometry
Starting materials:	0.05 g ($1.22 \cdot 10^{-5}$ mol) L2 0.21 g ($8.52 \cdot 10^{-4}$ mol) Cu(NO ₃) ₂ ·3H ₂ O 10.0 ml γ -butyrolactone 12.5 ml CHCl ₃
Working up:	washing out with acetone
Yield:	$48 \cdot 10^{-3}$ g, light green powder
Characterisation:	
EA	C ₂₅₆ H ₄₄₈ N ₁₄ O ₂₄ ·1.3Cu(NO ₃) ₂ ·2.8HNO ₃ ·12.6H ₂ O found: Cu 1.67%, C 64.51%, H 10.08%, N 5.29% calcd.: Cu 1.67%, C 64.39%, H 10.04%, N 5.23%
FTIR, $\tilde{\nu}$ /cm⁻¹	3327, 3033, 2955, 2922, 2852, 2751, 2668, 2606, 2524, 1646 sh, 1636, 1628, 1602, 1579, 1559, 1540, 1509, 1491, 1468, 1460 sh, 1437, 1420, 1387, 1333 sh, 1308, 1275, 1225, 1154 sh, 1131, 1105 sh, 1068, 1040, 1019, 989, 936, 875, 825, 801 sh, 760, 722, 646, 615

C2.16(1.0)	L2·1.0Cu(NO₃)₂·5.7HNO₃·3.7H₂O
Synthesis:	complexation varying the stoichiometry
Starting materials:	0.06 g ($1.46 \cdot 10^{-5}$ mol) L2 0.02 g ($8.77 \cdot 10^{-5}$ mol) Cu(NO ₃) ₂ ·3H ₂ O 1.68 ml THF
Working up:	general for complexation in THF
Yield:	$54 \cdot 10^{-3}$ g, light green powder
Characterisation:	
EA	C ₂₅₆ H ₄₄₈ N ₁₄ O ₂₄ ·1.0Cu(NO ₃) ₂ ·5.7HNO ₃ ·3.7H ₂ O found: Cu 1.33%, C 65.11%, H 9.49%, N 5.95% calcd.: Cu 1.33%, C 64.88%, H 9.80%, N 6.00%
MALDI-ToF-MS, m/z	M _{calcd.} for L2Cu _x : 4106.4 + 63.5·x; L2= C ₂₅₆ H ₄₄₈ N ₁₄ O ₂₄ , x = 0, 1, ... M _{found} (ref.): 4106.3 [L2] ⁺ (100%), 4128.2 [L2Na-H] ⁺ , 4169.9 [L2Cu] ⁺ , 4191.2 [L2CuNa-2H] ⁺ , 4208.2 [L2CuK-H] ⁺ , 4232.1 [L2Cu ₂ -H] ⁺
FTIR, $\tilde{\nu}$ /cm⁻¹	3330, 3073 sh, 3023, 2956, 2924, 2869 sh, 2854, 2767, 2655, 2626, 2514, 1636, 1602, 1580, 1545, 1508, 1468, 1426 sh, 1390, 1379, 1335, 1306, 1273, 1225, 1152 sh, 1131, 1063 sh, 1038, 1017, 992, 941, 874, 824, 810, 802 sh, 760, 722, 645, 612 sh

C2.17(0.3)		L2·0.3Cu(NO ₃) ₂
Synthesis:	complexation varying the stoichiometry	
Starting materials:	0.20 g (4.87·10 ⁻⁵ mol)	L2
	5.88·10 ⁻³ g (2.44·10 ⁻⁵ mol)	Cu(NO ₃) ₂ ·3H ₂ O
	5.35 ml	THF
Working up:	general for complexation in THF, CHCl ₃	
Yield:	130·10 ⁻³ g, light green powder	
Characterisation:		
EA	C ₂₅₆ H ₄₄₈ N ₁₄ O ₂₄ ·0.3Cu(NO ₃) ₂ ^[i] found: C 71.29%, H 10.59%, N 5.08%	
MALDI-ToF-MS, m/z	M _{calcd.} for L2Cu _x : 4106.4 + 63.5·x; L2= C ₂₅₆ H ₄₄₈ N ₁₄ O ₂₄ , x = 0, 1, ... M _{found} (ref.): 4108.0 [L2+2H] ⁺ , 4129.6 [L2Na] ⁺ (100%), 4169.3 [L2 ⁶³ Cu] ⁺ , 4192.0 [L2 ⁶³ CuNa] ⁺ , 4232.1 [L2 ⁶³ Cu ₂] ⁺	
FTIR, $\tilde{\nu}$ /cm ⁻¹	3322, 3075, 2954, 2924, 2869 sh, 2854, 2745, 2680, 2610, 2531, 1635, 1602, 1581, 1544, 1508, 1468, 1459, 1437, 1387 sh, 1379, 1331 sh, 1309, 1271, 1224, 1158, 1130, 1067, 1039, 1017, 991, 942, 879, 819, 802, 761, 722, 668, 646	
UV-Vis, λ_{\max} /nm	film 258, 289	

C2.18(0.9)		L2·0.9Cu(NO ₃) ₂ ·6.0HNO ₃ ·2.1H ₂ O
Synthesis:	complexation varying the stoichiometry	
Starting materials:	0.10 g (2.44·10 ⁻⁵ mol)	L2
	0.88 g (3.65·10 ⁻³ mol)	Cu(NO ₃) ₂ ·3H ₂ O
	12.5 ml	THF
Working up:	washing out with acetonitrile	
Yield:	95·10 ⁻³ g, light green powder	
Characterisation:		
EA	C ₂₅₆ H ₄₄₈ N ₁₄ O ₂₄ ·0.9Cu(NO ₃) ₂ ·6.0HNO ₃ ·2.1H ₂ O found: Cu 1.22%, C 65.54%, H 9.45%, N 6.87% calcd.: Cu 1.31%, C 65.71%, H 9.77%, N 6.13%	
MALDI-ToF-MS, m/z	M _{calcd.} for L2Cu _x : 4106.4 + 63.5·x; L2= C ₂₅₆ H ₄₄₈ N ₁₄ O ₂₄ , x = 0, 1, ... M _{found} (ref.): 4106.6 [L2] ⁺ , 4129.0 [L2Na] ⁺ (100%), 4144.8 [L2K-H] ⁺ , 4169.9 [L2Cu] ⁺ , 4191.8 [L2CuNa-H] ⁺ , 4207.9 [L2CuK-H] ⁺ , 4232.4 [L2Cu ₂ -H] ⁺ , 4254.8 [L2Cu ₂ Na-2H] ⁺	
FTIR, $\tilde{\nu}$ /cm ⁻¹	3325, 3012, 2955, 2924, 2870 sh, 2854, 2751, 2651, 2522, 1652, 1635, 1602, 1577, 1558, 1540, 1508, 1489, 1469, 1459 sh, 1437, 1419, 1388, 1378, 1333 sh, 1312, 1273, 1226, 1152 sh, 1132, 1065 sh, 1034 sh, 1017, 991, 876, 825, 762, 722, 668	
UV-Vis, λ_{\max} /nm (ϵ /10 ³ cm ² ·g ⁻¹)	CHCl ₃ , c = 2.40·10 ⁵ g·ml ⁻¹ 263 (18625), 292 (10667)	

^[i]Copper(II) loading (n) estimated from EPR

C2.19(0.5)		L2·0.5Cu(NO ₃) ₂ ·0.4HNO ₃ ·4.2H ₂ O
Synthesis:	complexation varying the stoichiometry	
Starting materials:	0.20 g (4.87·10 ⁻⁵ mol)	L2
	5.88·10 ⁻³ g (2.44·10 ⁻⁵ mol)	Cu(NO ₃) ₂ ·3H ₂ O
	5.35 ml	THF
Working up:	general for complexation in THF, CHCl ₃	
Yield:	220·10 ⁻³ g, light green powder	
Characterisation:		
EA	C ₂₅₆ H ₄₄₈ N ₁₄ O ₂₄ ·0.5Cu(NO ₃) ₂ ·0.4HNO ₃ ·4.2H ₂ O found: Cu 0.71 %, C 71.59%, H 10.56%, N 4.99% calcd.: Cu 0.73%, C 71.64%, H 10.54%, N 4.83%	
MALDI-ToF-MS, m/z	M _{calcd.} for L2Cu _x : 4106.4 + 63.5·x; L2= C ₂₅₆ H ₄₄₈ N ₁₄ O ₂₄ , x = 0, 1, ... M _{found} (ref.): 4107.5 [L2+H] ⁺ (100%), 4129.1 [L2Na] ⁺ , 4169.8 [L2Cu] ⁺ , 4192.0 [L2CuNa-H] ⁺ , 4232.6 [L2Cu ₂ -H] ⁺ M _{found} (lin.): 4105.9 [L2-H] ⁺ (100%), 4127.9 [L2Na-2H] ⁺ , 4168.4 [L2Cu-2H] ⁺ , 4192.5 [L2CuNa-H] ⁺ , 4233.6 [L2Cu ₂] ⁺ , 4269.7 [L2Cu ₂ K-3H] ⁺	
FTIR, $\tilde{\nu}$ /cm ⁻¹	3327, 3079, 2955, 2924, 2869 sh, 2854, 2817, 2742, 2691, 2618, 1653 sh, 1633, 1602, 1581, 1545, 1509, 1468, 1457 sh, 1435 sh, 1390 sh, 1379, 1331 sh, 1309, 1272, 1224, 1157, 1130, 1080 sh, 1069, 1018, 990, 955 sh, 880, 820, 805 sh, 762, 722, 647, 621	

C2.20(0.3)		L2·0.3Cu(NO ₃) ₂ ·2.5HNO ₃ ·5.8H ₂ O
Synthesis:	complexation varying the stoichiometry	
Starting materials:	0.10 g (2.44·10 ⁻⁵ mol)	L2
	0.88 g (3.65·10 ⁻³ mol)	Cu(NO ₃) ₂ ·3H ₂ O
	12.5 ml	THF
Working up:	washing out with water	
Yield:	96·10 ⁻³ g, green powder	
Characterisation:		
EA	C ₂₅₆ H ₄₄₈ N ₁₄ O ₂₄ ·0.3Cu(NO ₃) ₂ ·2.5HNO ₃ ·5.8H ₂ O found: Cu 0.47%, C 69.61%, H 10.25%, N 5.37% calcd.: Cu 0.43%, C 69.60%, H 10.30%, N 5.39%	
MALDI-ToF-MS, m/z	M _{calcd.} for L2Cu _x : 4106.4 + 63.5·x; L2= C ₂₅₆ H ₄₄₈ N ₁₄ O ₂₄ , x = 0, 1, ... M _{found} (ref.): 4107.2 [L2+H] ⁺ , 4128.7 [L2Na-H] ⁺ (100%), 4144.0 [L2K-2H] ⁺ , 4173.1 [L2Cu+3H] ⁺ , 4191.1 [L2CuNa-2H] ⁺ , 4234.1 [L2Cu ₂ +H] ⁺	
FTIR, $\tilde{\nu}$ /cm ⁻¹	3321, 3069 sh, 3039 sh, 2955, 2924, 2869, 2854, 2751, 2686, 2622, 2535, 1642 sh, 1636, 1602, 1577, 1558, 1540, 1508, 1468, 1457, 1435, 1419, 1387, 1378, 1337, 1309, 1272, 1223, 1158 sh, 1110, 1075 sh, 1040, 1017, 990, 877, 818, 761, 722, 645, 611	

6.4.1.4 Copper(II) complex of the 3rd generation, C3.i(n)

C3.1(12.0)	L3·12.0Cu(NO₃)₂·14HNO₃·59.6H₂O
Synthesis:	general procedure for complexation in THF
Starting materials:	0.10 g (1.20·10 ⁻⁵ mol) L3 0.87 g (3.59·10 ⁻³ mol) Cu(NO ₃) ₂ ·3H ₂ O 5.9 ml THF
Working up:	general for complexation in THF
Yield:	126·10 ⁻³ g, green powder
Characterisation:	
EA	C ₅₂₀ H ₉₁₂ N ₃₀ O ₄₈ ·12.0Cu(NO ₃) ₂ ·14HNO ₃ ·59.6H ₂ O found: Cu 6.03%, C 49.46%, H 7.83%, N 7.29% calcd.: Cu 6.04%, C 49.04%, H 8.19%, N 7.26%
MALDI-ToF-MS, m/z	M _{calcd.} for L3Cu _x : 8353.1 + 63.5·x; L3= C ₅₂₀ H ₉₁₂ N ₃₀ O ₄₈ , x = 0, 1, ... M _{found} (ref.): 8356.3 [L3+3H] ⁺ , 8417.1 [L3Cu-H] ⁺ (100%), 8479.5 [L3Cu ₂ -H] ⁺ , 8542.2 [L3Cu ₃ -2H] ⁺ , 8604.9 [L3Cu ₄ -2H] ⁺ , 8667.6 [L3Cu ₅ -3H] ⁺ , 8730.4 [L3Cu ₆ -4H] ⁺ , 8801.8 [L3Cu ₇ +3H] ⁺ , 8959.9 [L3Cu ₉ K-5H] ⁺
FTIR, $\tilde{\nu}$/cm⁻¹	3361, 3979, 2955, 2923, 2871 sh, 2854, 2687, 2620, 2540, 1653 sh, 1621 sh, 1601, 1573, 1556 sh, 1510, 1493 sh, 1468, 1450 sh, 1428 sh, 1393, 1379, 1306 sh, 1289 sh, 1278, 1230, 1161 sh, 1135, 1063 sh, 1016, 947, 870, 820 sh, 808, 759, 722, 646, 623

C3.2(7.9)	L3·7.9Cu(NO₃)₂·0.1Cu₂NO₃(OH)₃·14HNO₃·59.6H₂O
Synthesis:	general procedure for complexation in γ -butyrolactone / CHCl ₃
Starting materials:	0.10 g (1.20·10 ⁻⁵ mol) L3 1.01 g (4.19·10 ⁻³ mol) Cu(NO ₃) ₂ ·3H ₂ O 23.0 ml γ -butyrolactone 28.8 ml CHCl ₃
Working up:	general for complexation in γ -butyrolactone / CHCl ₃
Yield:	196·10 ⁻³ g, green powder
Characterisation:	
EA	C ₅₂₀ H ₉₁₂ N ₃₀ O ₄₈ ·7.9Cu(NO ₃) ₂ ·0.1Cu ₂ NO ₃ (OH) ₃ ·14HNO ₃ ·59.6H ₂ O found: Cu 4.67%, C 58.33%, H 9.08%, N 6.45% calcd.: Cu 4.67%, C 58.27%, H 8.98%, N 6.39%
FTIR, $\tilde{\nu}$/cm⁻¹	3352, 3067, 2955, 2924, 2869 sh, 2855, 2737, 2687, 2529, 1657, 1632, 1603, 1574, 1554, 1512, 1491, 1486, 1468, 1445 sh, 1395, 1393, 1378, 1336, 1302 sh, 1282, 1221, 1163, 1071, 1032 sh, 1016, 992 sh, 945 sh, 870, 809, 771, 760 sh, 723, 671, 642, 621

6.4.1.5 Copper(II) Complex of the 4th Generation, C4.i(n)

C4.1(24.2)	L4·24.2Cu(NO₃)₂·30HNO₃·55.5H₂O
Synthesis:	general procedure for complexation in THF
Starting materials:	0.10 g ($5.94 \cdot 10^{-6}$ mol) L4 0.93 g ($3.86 \cdot 10^{-3}$ mol) Cu(NO ₃) ₂ ·3H ₂ O 6.1 ml THF
Working up:	general for complexation in THF
Yield:	$128 \cdot 10^{-3}$ g, green powder
Characterisation:	
EA	C ₁₀₄₈ H ₁₈₄₀ N ₆₂ O ₉₆ ·24.2Cu(NO ₃) ₂ ·30HNO ₃ ·55.5H ₂ O found: Cu 6.28%, C 51.37%, H 8.06%, N 8.08% calcd.: Cu 6.32%, C 51.28%, H 8.23%, N 7.85%
FTIR, $\tilde{\nu}$ /cm⁻¹	3389, 3068, 2955, 2024, 2867 sh, 2854, 2693, 2618 sh, 2525 sh, 1657, 1640, 1630, 1620, 1601, 1572, 1551, 1511, 1503, 1493, 1486, 1469, 1453 sh, 1433 sh, 1391, 1383 sh, 1333 sh, 1304 sh, 1278, 1230, 1161 sh, 1135, 1061, 1017, 870, 808, 760, 723, 646, 621, 614

C4.2(7.4)	L4·7.4Cu(NO₃)₂·6.8HNO₃·58.5H₂O
Synthesis:	general procedure for complexation in γ -butyrolactone / CHCl ₃
Starting materials:	0.10 g ($5.94 \cdot 10^{-6}$ mol) L4 1.08 g ($4.45 \cdot 10^{-3}$ mol) Cu(NO ₃) ₂ ·3H ₂ O 24.1 ml γ -butyrolactone 30.2 ml CHCl ₃
Working up:	general for complexation in γ -butyrolactone / CHCl ₃
Yield:	$150 \cdot 10^{-3}$ g, green powder
Characterisation:	
EA	C ₁₀₄₈ H ₁₈₄₀ N ₆₂ O ₉₆ ·7.4Cu(NO ₃) ₂ ·6.8HNO ₃ ·58.5H ₂ O found: Cu 2.38%, C 63.45%, H 9.65%, N 5.60% calcd.: Cu 2.37%, C 63.09%, H 10.04%, N 5.63 %

6.4.1.6 Copper(II) Complex of the 5th Generation, C5.i(n)

C5.1(45.9)	L5·45.9Cu(NO₃)₂·18.2HNO₃·198.2H₂O
Synthesis:	general procedure for complexation in THF
Starting materials:	0.10 g ($2.96 \cdot 10^{-6}$ mol) L5 0.93 g ($3.84 \cdot 10^{-3}$ mol) Cu(NO ₃) ₂ ·3H ₂ O 6.1 ml THF
Working up:	general for complexation in THF
Yield:	$151 \cdot 10^{-3}$ g, green powder
Characterisation:	
EA	C ₂₁₀₄ H ₃₆₉₆ N ₁₂₆ O ₁₉₂ ·45.9Cu(NO ₃) ₂ ·18.2HNO ₃ ·198.2H ₂ O found: Cu 6.19%, C 53.59%, H 7.26%, N 6.63%

	calcd.: Cu 6.16%, C 52.65%, H 8.49%, N 6.82%	
FTIR , $\tilde{\nu}$ /cm ⁻¹	3361, 3074, 2955, 2924, 2969 sh, 2854, 2683, 2626 sh, 2524, 1638 sh, 1618, 1601, 1572, 1553, 1509, 1503, 1493, 1489, 1469, 1449 sh, 1391, 1378, 1339 sh, 1304 sh, 1293, 1279, 1231, 1158 sh, 1135, 1063 sh, 1015, 876, 808, 759, 722, 646, 622	
UV-Vis , λ_{max} /nm	film 262.0, 291.0, 327.5 sh	
UV-Vis , λ_{max} /nm (ϵ /10 ³ cm ² ·g ⁻¹)	CHCl ₃ , c = 2.20·10 ⁻¹ g·l ⁻¹ 264 (16527), 290 (12332)	
<hr/>		
C5.2(44.9)	L5·44.9Cu(NO₃)₂·102.9H₂O	
Synthesis:	general procedure for complexation in γ -butyrolactone / CHCl ₃	
Starting materials:	0.10 g (2.96·10 ⁻⁶ mol)	L5
	1.11 g (4.58·10 ⁻³ mol)	Cu(NO ₃) ₂ ·3H ₂ O
	24.8 ml	γ -butyrolactone
	31.0 ml	CHCl ₃
Working up:	general for complexation in γ -butyrolactone / CHCl ₃	
Yield:	54·10 ⁻³ g, green powder	
<hr/>		
Characterisation:		
EA	C ₂₁₀₄ H ₃₆₉₆ N ₁₂₆ O ₁₉₂ ·44.9Cu(NO ₃) ₂ ·102.9H ₂ O found: Cu 6.46%, C 57.22%, H 8.25%, N 5.99% calcd.: Cu 6.23%, C 56.55%, H 8.65%, N 6.60%	
FTIR , $\tilde{\nu}$ /cm ⁻¹	3351, 3087, 2955, 2924, 2870 sh, 2854, 2701, 2514 sh, 1656, 1640 sh, 1630, 1604, 1579, 1554, 1522, 15013 sh, 1505 sh, 1467, 1457, 1289 sh, 1433, 1391, 1380, 1337, 1302 sh, 1280, 1220, 1132, 1071, 1048, 1019, 992 sh, 869, 822, 811, 772, 760, 722, 668, 621	

6.4.2 Dendrimeric Copper(II) Complex from Cu(BF₄)₂·4H₂O

C2.21(4.0)		L2·4.0Cu(BF ₄) ₂
Synthesis:	Procedure for complexation of copper (II) tetrafluoroborate	
Starting materials:	0.10 g (2.44·10 ⁻⁵ mol)	L2
	1.13 g (3.65·10 ⁻³ mol)	Cu(BF ₄) ₂ ·4H ₂ O
	6.0 ml	THF
Working-up:	extraction with benzene	
Yield:	110·10 ⁻³ g, yellowish powder	
Characterisation:		
EA	C ₂₅₆ H ₄₄₈ N ₁₄ O ₂₄ ·4.0Cu(BF ₄) ₂	
	found: Cu 4.19%, C 50.24%, H 8.32%, N 3.18%	
	calcd.: Cu %, C %, H %, N %	
MALDI-ToF-MS, m/z	M _{calcd.} for L2Cu _x : 4106.4 + 63.5·x; L2=C ₂₅₆ H ₄₄₈ N ₁₄ O ₂₄ , x = 0, 1, ...	
	M _{found} (<i>ref.</i>): 4107.3 [L2+H] ⁺ , 4167.3 [L2Cu-3H] ⁺ (100%), 4230.6 [L2Cu ₂ -3H] ⁺ , 4294.5 [L2Cu ₃ -3H] ⁺ , 4357.9 [L2Cu ₄ -3H] ⁺ , 4419.0	

FTIR, $\tilde{\nu}$ /cm⁻¹	[L2Cu ₅ -5H] ⁺ 3502, 3402, 3171, 2955, 2923, 2871 sh, 2853, 1638 sh, 1619 sh, 1602, 1572, 1554, 1514, 1468, 1453 sh, 1426, 1393, 1378, 1343, 1331 sh, 1276, 1232, 11334, 1064, 1023 sh, 993 sh, 869, 817, 762, 722, 646, 621, 612 sh, 521	
C2.22(2.9)	L2·2.9Cu(BF₄)₂	
Synthesis:	Procedure for complexation of copper(II) tetrafluoroborate	
Starting materials:	0.10 g (2.44·10 ⁻⁵ mol)	L2
	1.13 g (3.65·10 ⁻³ mol)	Cu(BF ₄) ₂ ·4H ₂ O
	6.0 ml	THF
Working up:	extraction with benzene	
Yield:	136·10 ⁻³ g, light brown powder	
Characterisation:		
EA	C ₂₅₆ H ₄₄₈ N ₁₄ O ₂₄ ·2.9Cu(BF ₄) ₂ ·X found: Cu 3.15%, C 52.14%, H 8.23%, N 3.27% calcd.: Cu %, C %, H %, N %	
MALDI-ToF-MS, m/z	M _{calcd.} for L2Cu _x : 4106.4 + 63.5·x; L2=C ₂₅₆ H ₄₄₈ N ₁₄ O ₂₄ , x = 0, 1, ... M _{found} (ref.): 4107.9 [L2+2H] ⁺ , 4129.5 [L2Na] ⁺ , 4170.4 [L2Cu] ⁺ (100%), 4192.9 [L2CuNa] ⁺ , 4232.9 [L2Cu ₂ -H] ⁺ , 4295.8 [L2Cu ₃ -H] ⁺	
FTIR, $\tilde{\nu}$ /cm⁻¹	3534, 3418, 3166, 2955, 2922, 2872 sh, 2852, 1640 sh, 1621, 1602, 1575, 1554, 1513, 1468, 1445 sh, 1393, 1379, 1342, 1317, 1275, 1228, 1130, 1065, 1039 sh, 994 sh, 945 sh, 868, 818, 761, 722, 643, 612, 512	

6.5 COMPOUNDS REGISTER II: X-RAY EVALUATION OF MESOPHASES

Evaluation of the diffractograms: indexing of the mesophases and calculation of lattice parameters.

Periodic structures such as crystals and liquid crystals diffract X-ray radiation for certain incidence angles θ according to Bragg's law Eq. 6.1.

$$\lambda = 2d_{hkl} \cdot \sin \theta \quad \text{Eq. 6.1}$$

Each reflection θ corresponds to the diffraction of a set of planes (spacing or lattice distance d) of atoms or molecules within the periodic structure. These planes are defined by three integer numbers hkl Miller indexes; $1/h$, $1/k$, $1/l$ indicate the points at which the plane intersect the edges (a , b , c) of the unit cell. Each hkl plane can be equivalently defined by a vector normal to this plane: the diffraction vector \vec{r}_{hkl}^* . All the diffraction vectors define the so-called reciprocal lattice and are given by:

$$(\vec{r}_{hkl}^*) = (h\vec{a}^* + k\vec{b}^* + l\vec{c}^*) \quad \text{Eq. 6.2}$$

\vec{a}^* , \vec{b}^* and \vec{c}^* being the reciprocal lattice basic vectors, which in turn are defined as:

$$\vec{a}^* = \frac{(\vec{b} \wedge \vec{c})}{\vec{a} \cdot (\vec{b} \wedge \vec{c})} \quad \vec{b}^* = \frac{(\vec{c} \wedge \vec{a})}{\vec{b} \cdot (\vec{c} \wedge \vec{a})} \quad \vec{c}^* = \frac{(\vec{a} \wedge \vec{b})}{\vec{c} \cdot (\vec{a} \wedge \vec{b})} \quad \text{Eq. 6.3}$$

The lattice distance d_{hkl} and the diffraction vector \vec{r}_{hkl}^* are related to each other by:

$$d_{hkl} = \frac{1}{|\vec{r}_{hkl}^*|} \quad \text{Eq. 6.4}$$

which can be expressed as:

$$\frac{1}{d_{hkl}^2} = \frac{b^2 c^2 h^2 \sin^2 \alpha + a^2 c^2 k^2 \sin^2 \beta + a^2 b^2 l^2 \sin^2 \gamma + 2abc^2 hk(\cos \alpha \cos \beta - \cos \gamma) + 2ab^2 cl(\cos \alpha \cos \gamma - \cos \beta) + 2a^2 bcl(\cos \beta \cos \gamma - \cos \alpha)}{[a^2 b^2 c^2 (1 - \cos^2 \alpha - \cos^2 \beta - \cos^2 \gamma + 2 \cos \alpha \cos \beta \cos \gamma)]} \quad \text{Eq. 6.5}$$

Here, α, β, γ are the angles between each pair of edges in the unit cell. This equation Eq. 6.5 is simplified when the specific dependencies among edges and angles for each symmetry are considered.

For *hexagonal columnar* mesophases, Col_h, it is $a = b$, $\alpha = \beta = 90^\circ$, and $\gamma = 120^\circ$. It follows from Eq. 6.5 that for

$$2 \text{ dim} \quad \frac{1}{d_{hk0}} = \frac{1}{a_h} \sqrt{\frac{4}{3}(h^2 + k^2 + hk)} \quad a_h = d_{hk0} \sqrt{\frac{4}{3}(h^2 + k^2 + hk)} \quad \text{Eq. 6.6}$$

$$3 \text{ dim} \quad \frac{1}{d_{hkl}} = \sqrt{\frac{4}{3a_h^2}(h^2 + k^2 + hk) + \frac{l^2}{c^2}} \quad a_h \text{ as above,} \quad \text{Eq. 6.7}$$

$$c = l \cdot d_{00l}$$

The ratio between lattice distances is given by:

$$d_{100} : d_{110} : d_{200} = 1 : \frac{1}{\sqrt{3}} : \frac{1}{2} \quad \text{Eq. 6.8}$$

For *rectangular columnar* mesophases, Col_r, $a \neq b$, $\alpha = \beta = \gamma = 90^\circ$

$$2\text{-dim.} : \quad \frac{1}{d_{hk0}} = \sqrt{\frac{h^2}{a_r^2} + \frac{k^2}{b_r^2}} \quad a_r = h \cdot d_{h00} \quad \text{Eq. 6.9}$$

$$b_r = \frac{d_{hk0} \cdot a \cdot k}{\sqrt{a^2 - h^2 \cdot d_{hk0}^2}}$$

$$3\text{-dim.} : \quad \frac{1}{d_{hkl}} = \sqrt{\frac{h^2}{a_r^2} + \frac{k^2}{b_r^2} + \frac{l^2}{c^2}} \quad a_r, b_r \text{ as above,} \quad \text{Eq. 6.10}$$

$$c = l \cdot d_{00l}$$

The lattice distances d can be calculated from the measured reflections θ by means of Bragg's equation. The indexing, i.e. the ascription of the Miller indexes [hkl] to the diffraction planes, was accomplished by a trial-error procedure. For each symmetry, the lattice distances fulfill a fixed relationship. The experimental lattice distances were compared with those relationships and the best indexing was chosen. The lattice constant is then calculated with Eq. 6.6 and Eq. 6.7 for hexagonal phases and with Eq. 6.9 and Eq. 6.10 for rectangular phases.

With the lattice constants obtained in this way both lattice spacings and angles were re-calculated; the agreement with the experimental values certify the accuracy of the indexing. The lattice parameters quoted in this work correspond to the arithmetical mean value of those calculated for each d_{hkl} .

6.5.1 Series of Highest Loading: CG.i(n)

6.5.1.1 Columnar Hexagonal Mesophases

Table 6.3: Measured diffraction angles θ , indexing $[hk]$, found and calculated spacings d_{found} , d_{calcd} and hexagonal lattice parameter a_h for the THF series of highest loading in the hexagonal columnar mesophase $\text{Col}_{h(o)}$.

CG.i(n)	LG	T / °C	θ / °	hk	d_{found}	$d_{\text{calcd.}}$	a_h / Å
C1.4(1.5)	L1	65	1.17	10	37.73	37.78	43.6
			2.02	11	21.86	21.81	
			3.34	20	18.87	18.89	
C2.3(6.0)	L2	65	1.12	10	39.42	39.41	45.5
			1.95	11	22.64	22.76	
			2.23	20	19.80	19.71	
C3.1(12.0)	L3	65	0.94	10	46.97	46.52	53.7
			1.66	11	26.60	26.86	
			1.88	20	23.49	23.26	
C4.1(24.2)	L4	65	0.87	10	50.74	50.51	58.3
			1.52	11	29.05	29.16	
			1.75	20	25.23	25.25	
C5.1(45.9)	L5	65	0.86	10	51.33	59.43	59.4
			1.49	11	29.63	29.69	
			1.71	20	25.82	25.77	

Table 6.4: Measured diffraction angles θ , indexing $[hk]$, found and calculated spacings d_{found} , d_{calcd} and hexagonal lattice parameter a_h for the γ -butyrolactone/ CHCl_3 series of highest loading in the hexagonal columnar mesophase $\text{Col}_{h(o)}$.

CG.i(n)	LG	T / °C	θ / °	hk	d_{found}	$d_{\text{calcd.}}$	a_h / Å
C1.7(1.0)	L1	65	1.18	10	37.41	37.43	43.2
			2.05	11	21.54	21.61	
			2.35	20	18.79	18.72	
C2.2(6.3)	L2	65	1.09	10	40.50	40.56	46.8
			1.89	11	23.36	23.41	
			2.17	20	20.35	20.28	
C3.2(7.9)	L3	65	0.96	10	45.99	45.75	52.8
			1.68	11	26.28	26.42	
			1.93	20	22.88	22.88	

6.5.1.2 Columnar Rectangular Mesophases

Table 6.5: Measured diffraction angles θ , indexing $[hk]$, found and calculated spacings d_{found} , d_{calcd} and rectangular lattice parameter a_r , b_r , for the γ -THF series of highest loading in the rectangular columnar mesophase $\text{Col}_{r(o)}$.

CG.i(n)	LG	T / °C	θ / °	hk	d_{found}	d_{calcd}	a_r / Å	b_r / Å
C1.4(1.5)	L1	65	0.71	20	62.18	61.10	122.20	54.1
			0.83	01	53.19	54.12		
			1.08	21	40.88	40.51		
			1.47	40	30.03	30.55		
			2.17	60	20.35	20.37		
			2.55	23	17.32	17.30		
C2.3(6.0)	L2	65	0.66	20	66.89	66.89	133.8	49.0
			0.96	11	45.99	46.00		
			1.32	40	33.45	33.45		
			1.83	12	24.13	24.09		
			1.94	22	22.76	23.00		
			2.22	42	19.89	19.76		
C3.1(12.0)	L3	65	0.78	20	56.60	56.60	113.2	52.0
			0.92	11	47.99	47.23		
			1.17	21	37.73	38.28		
			1.61	40	27.42	28.30		
			1.86	22	23.74	23.62		
C4.1(24.2)	L4	65	0.87	20	50.74	50.60	101.2	69.1
			1.37	12	32.23	32.71		
			1.53	22	28.86	28.54		
			1.75	40	25.23	25.30		

Table 6.6: Measured diffraction angles θ , indexing $[hk]$, found and calculated spacings d_{found} , d_{calcd} and rectangular lattice parameter a_r , b_r , for the γ -butyrolactone/ CHCl_3 series of highest loading in the rectangular columnar mesophase $\text{Col}_{r(o)}$.

CG.i(n)	LG	T / °C	θ / °	hk	d_{found}	d_{calcd}	a_r / Å	b_r / Å
C2.2(6.3)	L2	65	0.70	20	63.07	63.07	126.1	47.5
			0.97	11	45.51	44.43		
			1.19	21	37.10	37.93		
			1.40	40	31.54	31.54		
			1.69	41	26.13	26.27		
			1.84	02	24.00	23.74		
			1.97	22	22.41	22.22		
			2.10	32	21.03	20.67		
			2.36	42	18.71	18.97		
C3.2(7.9)	L3	65	0.95	20	46.47	46.23	97.5	54.8
			1.68	12	26.28	26.28		
			1.92	40	23.00	23.12		

6.5.2 2nd Generation Series: C2.i(n)

6.5.2.1 Columnar Hexagonal Mesophases

Table 6.7: Measured diffraction angles θ , indexing $[hk]$, found and calculated spacings d_{found} , d_{calcd} and hexagonal lattice parameter a_h for the 2nd generation THF series in the hexagonal columnar mesophase $Col_{h(d)}$, $Col_{h(o)}$.

C2.i(n)	T / °C	θ / °	hk	d_{found}	$d_{\text{calcd.}}$	a_h / Å
C2.3(6.0)	65	1.12	10	39.42	39.41	45.5
		1.95	11	22.64	22.76	
		2.23	20	19.80	19.71	
C2.4(5.4)	65	1.05	10	42.05	42.04	48.5
		1.82	11	24.26	24.27	
		2.10	20	21.03	21.02	
C2.4(5.4)	85	1.05	10	42.05	42.18	48.7
		1.81	11	24.39	24.36	
		2.09	20	21.13	21.09	
C2.4(5.4)	105	1.07	10	41.26	41.36	47.8
		1.84	11	24.60	23.88	
		2.14	20	20.63	20.68	
C2.4(5.4)	110	1.10	10	40.14	40.11	46.3
		1.91	11	23.12	23.16	
		2.20	20	20.07	20.05	
C2.5(5.4)	65	1.08	10	40.88	41.10	47.5
		1.85	11	23.87	23.73	
		2.15	20	20.54	20.55	
C2.6(5.2)	65	1.08	10	40.88	41.05	47.4
		1.84	11	24.00	23.50	
		2.17	20	20.35	20.52	
C2.7(4.6)	65	1.07	10	41.26	41.28	47.7
		1.86	11	23.74	23.83	
		2.13	20	20.73	20.64	
C2.8(4.4)	65	1.06	10	41.65	41.92	48.4
		1.81	11	24.39	24.20	
		2.10	20	20.93	20.90	
C2.9(3.5)	65	1.06	10	41.65	41.84	48.3
		1.82	11	29.26	24.16	
		2.11	20	20.93	20.92	
C2.10(2.7)	65	1.07	10	41.26	41.43	47.8
		1.84	11	24.00	23.92	
		2.13	20	20.73	20.71	
C2.12(2.1)	65	1.07	10	41.26	41.29	47.7
		1.85	11	23.87	23.84	
		2.14	20	20.63	20.64	

C2.i(n)	T / °C	θ / °	hk	d_{found}	d_{calcd.}	a_h / Å
C2.16(1.0)	65	1.03	10	42.86	42.74	49.4
		1.80	11	24.53	24.68	
		2.06	20	21.43	21.37	
C2.17(0.3)	65	1.14	10	38.73	38.52	44.6
		1.99	11	22.19	22.24	
		2.29	20	19.20	19.26	
C2.18(0.9)	65	1.06	10	41.65	41.48	47.9
		1.85	11	23.87	23.95	
		2.13	20	20.74	20.74	
C2.19(0.5)	65	1.05	10	42.06	42.04	48.5
		1.82	11	24.26	24.27	
		2.10	20	21.03	21.02	
C2.20(0.3)	65	1.12	10	39.42	39.36	45.5
		1.94	11	22.76	22.73	
		2.25	20	19.63	19.68	

Table 6.8: Measured diffraction angles θ , indexing $[hk]$, found and calculated spacings d_{found} , d_{calcd} and hexagonal lattice parameter a_h for the 2nd generation γ -butyrolactone/ CHCl_3 series in the hexagonal columnar mesophase $\text{Col}_{h(o)}$.

C2.i(n)	T / °C	θ / °	hk	d_{found}	d_{calcd.}	a_h / Å
C2.2(6.3)	65	1.09	10	40.50	40.56	46.8
		1.89	11	23.36	23.41	
		2.17	20	20.35	20.28	
C2.11(2.6)	65	1.01	10	43.71	43.64	50.4
		1.75	11	25.23	25.19	
		2.03	20	21.75	21.82	
C2.13(2.0)	65	0.98	10	45.05	44.87	51.8
		1.71	11	25.82	25.90	
		1.97	20	22.41	22.43	
C2.15(1.3)	65	1.00	10	44.15	44.33	51.2
		1.72	11	25.67	25.59	
		1.99	20	22.19	22.16	

6.5.2.2 Columnar Rectangular Mesophases

Table 6.9: Measured diffraction angles θ , indexing $[hk]$, found and calculated spacings d_{found} , d_{calcd} and rectangular lattice parameter a_r , b_r , for the 2nd generation THF series in the rectangular columnar mesophase $\text{Col}_{r(o)}$.

C2.i(n)	T / °C	θ / °	hk	d_{found}	$d_{\text{calcd.}}$	a_r / Å	b_r / Å
C2.3(6.0)	65	0.66	20	66.89	66.89	133.8	49.0
		0.96	11	45.99	46.00		
		1.32	40	33.45	33.45		
		1.83	12	24.13	24.09		
		1.94	22	22.76	23.00		
		2.22	42	19.89	19.76		
C2.4(5.4)	65	0.82	20	53.84	53.84	107.7	47.9
		1.01	11	43.71	43.79		
		1.54	31	28.67	28.73		
		1.86	12	23.74	23.39		
		2.03	22	21.75	21.89		
C2.4(5.4)	70	0.62	20	71.21	71.21	142.4	48.6
		0.97	11	45.51	46.03		
		1.30	31	33.96	33.97		
		1.88	12	23.49	23.97		
		2.15	42	20.54	20.08		
C2.4(5.4)	90	0.68	20	64.91	64.92	129.9	46.8
		1.00	11	44.15	44.19		
		1.40	31	31.54	31.84		
		1.88	12	23.49	23.12		
		1.99	22	22.19	22.09		
C2.5(5.4)	65	0.70	20	63.07	63.07	126.1	49.1
		0.97	11	45.51	45.78		
		1.40	40	31.54	31.54		
		1.80	12	24.53	24.11		
		1.96	22	22.53	22.89		
C2.6(5.2)	65	0.76	20	58.09	58.48	117.0	47.6
		1.00	11	44.15	44.08		
		1.50	40	29.43	29.24		
		1.87	12	23.61	23.32		
		2.03	22	21.75	22.04		
C2.7(4.6)	65	0.96	11	45.99	49.95	120.1	48.5
		1.10	21	40.14	37.72		
		1.47	40	30.03	30.03		
		1.75	41	25.23	25.53		
		1.84	12	24.00	23.76		
		1.96	22	22.53	22.47		
C2.9(3.5)	65	0.97	11	45.51	45.43	130.0	49.1
		1.31	40	33.70	29.99		
		1.68	41	26.28	25.59		
		1.84	12	24.00	24.05		

C2.i(n)	T / °C	θ / °	hk	d _{found}	d _{calcd.}	a _r / Å	b _r / Å
C2.10(2.7)	65	0.78	20	56.60	56.60	113.2	48.2
		0.99	11	44.59	44.33		
		1.46	31	30.24	29.71		
		1.89	12	23.36	23.56		
		2.06	22	21.43	22.16		
		2.19	32	20.16	20.30		
C2.12(2.1)	65	1.06	11	41.65	41.51	107.0	45.0
		1.65	40	26.76	26.76		
		1.91	41	23.12	23.00		
		2.15	22	20.54	20.75		
		2.58	42	17.12	17.23		

Table 6.10: Measured diffraction angles θ , indexing $[hk]$, found and calculated spacings d_{found} , d_{calcd} and hexagonal lattice parameter a_r , b_r , for the 2nd generation γ -butyrolactone/ CHCl_3 series in the rectangular columnar mesophase $\text{Col}_{r(o)}$.

C2.i(n)	T / °C	θ / °	hk	d _{found}	d _{calcd.}	a _r / Å	b _r / Å
C2.2(6.3)	65	0.70	20	63.07	63.07	126.1	47.5
		0.97	11	45.51	44.43		
		1.19	21	37.10	37.93		
		1.40	40	31.54	31.54		
		1.69	41	26.13	26.27		
		1.84	02	24.00	23.74		
		1.97	22	22.41	22.22		
		2.10	32	21.03	20.67		
		2.36	42	18.71	18.97		
C2.11(2.6)	65	0.88	20	50.17	50.17	100.3	48.9
		1.00	11	44.15	43.93		
		1.76	40	25.09	25.09		
		2.02	22	21.86	21.97		
C2.13(2.0)	65	0.81	20	54.50	54.18	108.4	48.7
		0.98	11	45.05	44.43		
		1.54	31	28.67	29.01		
		1.84	12	24.00	23.76		
		1.98	22	22.30	22.21		
		2.05	50	21.54	21.67		
C2.15(1.3)	65	0.90	20	49.05	49.05	98.1	49.1
		1.00	11	44.15	43.88		
		1.27	21	35.60	34.69		
		1.62	31	27.25	27.21		
		1.83	12	24.13	23.80		
		2.02	41	21.86	21.94		

6.5.3 1st Generation Complexes C1.i(n)

Table 6.11: Measured diffraction angles θ , indexing $[hk]$, found and calculated spacings d_{found} , d_{calcd} and hexagonal lattice parameter a_h , for the 1st generation complexes of the THF series in the columnar hexagonal mesophase Col_h .

CG.i(n)	LG	T / °C	θ / °	hk	d_{found}	$d_{\text{calcd.}}$	a_h / Å
C1.2(1.9)b	L1	65	1.15	10	38.39	38.29	44.2
			2.00	11	22.08	22.11	
			2.31	20	19.12	19.14	
C1.2(1.9)b	L1	135	1.24	10	35.60	35.70	41.2
			2.14	11	20.63	20.61	
			2.47	20	17.88	17.85	

6.5.4 Complexes from $\text{Cu}(\text{BF}_4)_2 \cdot 4\text{H}_2\text{O}$

Table 6.12: Measured diffraction angles θ , indexing $[hk]$, found and calculated spacings d_{found} , d_{calcd} and hexagonal lattice parameter a_h , in the hexagonal columnar mesophase Col_h .

CG.i(n)	LG	T / °C	θ / °	hk	d_{found}	$d_{\text{calcd.}}$	a_h / Å
C2.21(4.0)	L2	70	0.97	10	45.51	45.78	52.9
			1.66	11	26.60	26.43	
			1.93	20	22.88	22.89	
C2.21(4.0)	L2	85	1.06	10	41.65	41.27	47.7
			1.87	11	23.61	23.83	
			2.14	20	20.63	20.64	
C2.22(2.9)	L2	70	0.99	10	44.59	45.18	51.5

7 REFERENCES

- [1] Demus, J. W. Goodby, Gray, Spiess, Vill, *Handbook of liquid crystals, Vol. 1. Fundamentals*, Wiley-VCH, Weinheim, **1998**.
- [2] P. J. Collins, M. Hird, *Introduction to Liquid Crystals Chemistry and Physics*, Taylor & Francis, **1997**.
- [3] H. Stegemeyer, *Liquid Crystals*, Steinkopff, Darmstadt, **1994**.
- [4] M. Sorai, T. Nakamura, S. Seki, *Pramana Suppl.* **1975**, *1*, 503.
- [5] J. Billard, J. C. Dubois, N. H. Tinh, A. Zann, *Nouveau Journal de Chimie* **1978**, *2*, 535.
- [6] S. Mery, D. Haristoy, J.-F. Nicoud, D. Guillon, S. Diele, H. Monobe, Y. Shimizu, *J. Mater. Chem.* **2002**, *12*, 37.
- [7] G. Pelzl, S. Diele, W. Weissflog, *Adv. Mater.* **1999**, *11*, 707.
- [8] H. Zimmermann, R. Poupko, Z. Luz, J. Billard, *Z. Naturforsch.* **1985**, *40a*, 149.
- [9] U. Beginn, G. Lattermann, *Mol. Cryst. Liq. Cryst.* **1994**, *241*, 215.
- [10] J. Malthete, N. H. Tinh, A. M. Levelut, *J. Chem. Soc., Chem. Commun.* **1986**, 1548.
- [11] P. E. Cladis, *Phys. Rev. Lett.* **1975**, *35*, 48.
- [12] R. Deschenaux, M. Schweissguth, A. M. Levelut, *Chem. Commun.* **1996**, 1275.
- [13] J. Malthete, N. H. Tinh, C. Destrade, *Liquid Crystals* **1993**, *13*, 171.
- [14] E. Alami, H. Levy, R. Zana, P. Weber, A. Skoulios, *Liquid Crystals* **1993**, *13*, 201.
- [15] K. Ohta, R. Higasi, M. Ikejima, I. Yamamoto, N. Kobayashi, *J. Mater. Chem.* **1998**, *8*, 1979.
- [16] U. Stebani, G. Lattermann, M. Wittenberg, R. Festag, J. H. Wendorff, *Adv. Mater.* **1994**, *6*, 572.
- [17] A. Facher, U. Stebani, G. Lattermann, S. Diele, M. Neundorf, *Liquid Crystals* **1998**, *25*, 441.
- [18] V. Percec, J. Heck, D. Tomazos, F. Falkenberg, H. Blackwell, G. Ungar, *J. Chem. Soc., Perkin Trans. 1* **1993**.
- [19] T. P. Russell, J. F. Rabolt, R. J. Twieg, R. L. Siemens, B. L. Farmer, *Macromolecules* **1986**, *19*, 1135.
- [20] C. Tschierske, *J. Mater. Chem.* **1998**, *8*, 1485.
- [21] A. M. Godquin Giroud, J. Billard, *Mol. Cryst. Liq. Cryst.* **1983**, *97*, 287.
- [22] W. Maier, A. Saupe, *Z. Naturforsch. A* **1960**, *15*, 287.
- [23] G. W. Gray, J. W. Goodby, *Smectic liquid crystals. Textures and structures.*, Hill, Glasgow, **1984**.
- [24] U. Stebani, G. Lattermann, M. Wittenberg, R. Festag, J. Wendorff, *Adv. Mater.* **1994**, *6*, 572.
- [25] K. Praefcke, D. Blunk, *Liquid Crystals* **1993**, *14*, 1181.
- [26] A. M. Levelut, *Journal de chimie physique* **1983**, *80*, 149.
- [27] A. M. Levelut, P. Oswald, A. Ghanem, J. Malthête, *J. Physique* **1984**, *45*, 745.
- [28] J. Vacus, P. Doppelt, J. Simon, G. Memetzidis, *J. Mater. Chem.* **1992**, *2*, 1065.
- [29] W. Wan, H. Monobe, Y. Tanaka, Y. Shimizu, *Liquid Crystals* **2003**, *30*, 571.

- [30] A. Schaz, G. Lattermann, *Liquid Crystals* **2005**, *32*, 407.
- [31] M. Serebyuk, A. B. Gaspar, V. Ksenofontov, S. Reiman, Y. G. Galyametdinov, W. Haase, E. Rentschler, P. Gülich, *Chem. Mater.* **2006**, *18*, 2513.
- [32] K. Ohta, H. Hasebe, H. Ema, M. Moriya, T. Fujimoto, I. Yamamoto, *Mol. Cryst. Liq. Cryst.* **1991**, *208*, 21.
- [33] K. Borisch, S. Diele, P. Goring, H. Müller, C. Tschierske, *Liquid Crystals* **1997**, *22*, 427.
- [34] M. Sepelj, A. Lesac, U. Baumeister, S. Diele, D. W. Bruce, Z. Hamersak, *Chem. Mater.* **2006**, *18*, 2050.
- [35] Y. Hendriks, J. Charvolin, *Liquid Crystals* **1992**, *11*, 677.
- [36] J. A. Schröter, C. Tschierske, M. Wittenberg, J. H. Wendorf, *Angew. Chem. Int. Ed. Engl.* **1997**, *36*, 1119.
- [37] J. J. Reczek, K. R. Villazor, V. Lynch, T. M. Swager, B. L. Iverson, *J. Am. Chem. Soc.* **2006**, *128*, 7995.
- [38] K. Hatsusaka, K. Ohta, I. Yamamoto, H. Shirai, *J. Mater. Chem.* **2000**, *11*, 423.
- [39] T. Komatsu, K. Ohta, T. Watanabe, H. Ikemoto, T. Fujimoto, I. Yamamoto, *J. Mater. Chem.* **1994**, *4*, 537.
- [40] C. Destrade, M. C. Mondon, J. Malthête, *Journal de Physique* **1979**, *3*, 17.
- [41] H. Miwa, N. Kobayashi, K. Ban, K. Ohta, *Bull. Chem. Soc. Jpn.* **1999**, *72*, 2719.
- [42] J. Barberá, R. Iglesias, J. L. Serrano, T. Sierra, M. R. de la Fuente, B. Palacios, M. A. Pérez-Jubindo, J. T. Vázquez, *J. Am. Chem. Soc.* **1998**, *120*, 2908.
- [43] J. Barberá, M. A. Esteruelas, A. M. Levelut, L. A. Oro, J. L. Serrano, E. Sola, *Inorg. Chem.* **1992**, *31*, 732.
- [44] C. Destrade, H. Gasparoux, P. Foucher, N. H. Tinh, J. Malthête, J. Jacques, *Journal de chimie physique* **1983**, *80*, 137.
- [45] C. R. Safinya, K. S. Liang, W. A. Varady, N. A. Clark, G. Andersson, *Physical Review Letters* **1984**, *53*, 1172.
- [46] K. Ohta, M. Ikejima, M. Moriya, H. Hasebe, I. Yamamoto, *J. Mater. Chem.* **1998**, *8*, 1971.
- [47] R. Naito, K. Ohta, H. Shirai, *Journal of Porphyrins and Phthalocyanines* **2001**, *5*.
- [48] R. Zniber, R. Achour, M. Z. Cherkaoui, B. Donnio, L. Gehringer, D. Guillon, *J. Mater. Chem.* **2002**, *12*, 2208.
- [49] J.-M. Rueff, J. Barberá, B. Donnio, D. Guillon, M. Marcos, J.-L. Serrano, *Macromolecules* **2003**, *36*, 8368.
- [50] F. Maeda, K. Hatsusaka, K. Ohta, M. Kimura, *J. Mater. Chem.* **2003**, *13*, 243.
- [51] A. C. Ribeiro, B. Heinrich, C. Cruz, N. H. Tinh, S. Diele, M. W. Schröder, D. Guillon, *Eur. Phys. J. E* **2003**, *10*, 143.
- [52] C. Destrade, P. Foucher, H. Gasparoux, N. H. Tinh, *Mol. Cryst. Liq. Cryst.* **1984**, *106*, 121.
- [53] S. Diele, *Current Opinion in Colloid and Interface Science* **2002**, *7*, 333–342.
- [54] D. Demus, L. Richter, *Textures of liquid crystals*, Chemie, Weinheim, **1978**.
- [55] C. Tschierske, G. Pelzl, S. Diele, *Angew. Chem.* **2004**, *116*, 6340.
- [56] J. L. Serrano, *Metallomesogens. Synthesis, Properties, and Applications.*, VCH, **1996**.
- [57] D. W. Bruce, E. Lalinde, P. Styring, D. A. Dunmur, P. M. Maitlis, *J. Chem. Soc. Chem. Commun.* **1986**, *8*, 581.

- [58] B. A. Gregg, M. A. Fox, A. J. Bard, *J. Am. Chem. Soc.* **1989**, *111*, 3024.
- [59] M. A. Esteruelas, L. A. Oro, E. Sola, M. B. Ros, J. L. Serrano, *J. Chem. Soc., Chem. Commun.* **1989**, 55.
- [60] E. Campillos, M. Marcos, J. L. Serrano, P. J. Alonso, *J. Mater. Chem.* **1991**, *1*, 197.
- [61] S. N. Poelsma, S. A. H., F. P. Fanizzi, P. M. Maitlis, *Liquid Crystals* **1994**, *16*, 675.
- [62] K. Ohta, S. Watanabe, T. Fujimoto, I. Yamamoto, *J. Chem. Soc. Chem. Commun.* **1989**, 1611.
- [63] K. Ohta, T. Watanabe, H. Hasebe, Y. Morizumi, T. Fujimoto, I. Yamamoto, D. Lelievre, J. Simon, *Mol. Cryst. Liq. Cryst.* **1991**, *196*, 13.
- [64] W. T. Ford, L. Sumner, W. Zhu, Y. H. Chang, P. J. Um, K. H. Choi, P. A. Heiney, N. C. Maliszewsky, *New J. Chem.* **1994**, *18*, 495.
- [65] P. G. de Gennes, *The Physics of Liquid Crystals*, Clarendon Press, Oxford, **1974**.
- [66] A. Liebmman, C. Mertesdorf, T. Plesniviy, H. Ringsdorf, J. H. Wendorf, *Angew. Chem. Int. Ed.* **1991**, *30*, 1375.
- [67] G. Lattermann, S. Schmidt, R. Kleppinger, J. H. Wendorf, *Adv. Mater.* **1992**, *4*, 30.
- [68] B. Xu, T. M. Swager, *J. Am. Chem. Soc.* **1993**, *115*, 1159.
- [69] D. Singer, A. Liebmman, K. Praefcke, J. H. Wendorf, *Liquid Crystals* **1993**, *14*, 785.
- [70] R. Deschenaux, J.-L. Marendaz, *J. Chem. Soc., Chem. Commun.* **1991**, 909.
- [71] V. Busico, D. Castaldo, M. Vacatello, *Mol. Cryst. Liq. Cryst.* **1981**, *78*, 221.
- [72] A. Skoulios, V. Luzzati, *Nature* **1959**, *183*, 1310.
- [73] P. Ekwall, *Colloid Polym. Sci.* **1988**, *266*, 1435.
- [74] M. Ibn-Elhaj, D. Guillon, A. Skoulios, A. M. Giroud-Godquin, P. Maldivi, *Liquid Crystals* **1992**, *11*, 731.
- [75] D. W. Bruce, D. A. Dunmur, P. M. Maitlis, J. M. Watkins, G. J. T. Tiddy, *Liquid Crystals* **1992**, *11*, 127.
- [76] N. V. Usoltseva, V. V. Bykova, *Mol. Cryst. Liq. Cryst.* **1992**, *215*, 89.
- [77] A. Donald, A. Windle, S. Hanna, *Liquid Crystalline Polymers*, 2nd ed., Cambridge University Press, **2006**.
- [78] H. Finkelmann, M. Happ, M. Portugall, H. Ringsdorf, *Makromol. Chem.* **1978**, *179*, 2541.
- [79] H. Finkelmann, H. J. Kock, G. Rehage, *Makromol. Chem. Rapid. Comm.* **1981**, *2*, 317.
- [80] H. Mori, Y. Itoh, Y. Nishiura, T. Nakamura, Y. Shinagawa, *Jpn. J. Appl. Phys. Part 1.* **1997**, *36*, 143.
- [81] R. Zentel, *Adv. Mater.* **1989**, *101*, 1437.
- [82] T. Kato, J. M. Fréchet, *Macromolecules* **1989**, *22*, 3818.
- [83] L. Cui, G. Lattermann, *Macromol. Chem. Phys.*, **2002**, *203*, 2432.
- [84] S. Kotani, K. Shiina, K. Sonogashira, *Appl. Organomet. Chem.* **1991**, *5*, 417.
- [85] A. K. Khandpur, *Macromolecules* **1995**, *28*, 8804.
- [86] J. M. Fréchet, D. A. Tomalia, in *Dendrimers and other dendritic polymers* (Eds.: J. M. Fréchet, D. A. Tomalia), Wiley, **2001**, pp. 3.
- [87] G. R. Newkome, C. N. Moorefield, F. Vögtle, *Dendrimers and Dendrons. Concepts, Syntheses, Applications.*, Wiley-VCH, **2001**.
- [88] E. Buhleier, W. Wehner, F. Vögtle, *Synthesis* **1978**, 155.

- [89] D. A. Tomalia, G. A. Baker, J. Dewald, M. Hall, G. Kallos, S. Martin, J. Roeck, J. Ryder, P. Smith, *Polym. J.* **1985**, *117*, 117.
- [90] C. J. Hawker, J. M. Fréchet, *J. Am. Chem. Soc.* **1990**, *112*, 7638.
- [91] C. J. Hawker, J. M. Fréchet, *J. Chem. Soc. Chem. Commun.* **1990**, 1010.
- [92] M. Ballauff, C. N. Likos, *Angew. Chem. Int. Ed.* **2004**, *43*, 2998.
- [93] A. W. Bosman, H. M. Janssen, E. W. Meijer, *Chem. Rev.* **1999**, *99*, 1665.
- [94] B. J. Bauer, E. J. Amis, in *Dendrimer and other dendritic polymers* (Eds.: J. M. Fréchet, D. A. Tomalia), Wiley, **2001**, pp. 255.
- [95] P. G. de Gennes, H. Hervet, *J. Phys. Lett. Fr.* **1983**, *44*, L351.
- [96] J. F. G. A. Jansen, E. M. M. de Brabander-van den Berg, E. W. Meijer, *Science* **1994**, *266*, 1226.
- [97] J. F. G. A. Jansen, E. W. Meijer, E. M. M. de Brabander-van den Berg, *J. Am. Chem. Soc.* **1995**, *117*, 4417.
- [98] R. L. Lescanec, M. Muthukumar, *Macromolecules* **1990**, *23*, 2280.
- [99] S. Rosenfeldt, N. Dingenouts, M. Ballauff, N. Werner, F. Vögtle, P. Lindner, *Macromolecules* **2002**, *36*, 8098.
- [100] P. Welch, M. Muthukumar, *Macromolecules* **1998**, *31*, 5892.
- [101] B. Donnio, J. Barberá, R. Gimenez, D. Guillon, M. Marcos, J. L. Serrano, *Macromolecules* **2002**, *35*, 370.
- [102] J. H. Cameron, A. Facher, G. Lattermann, S. Diele, *Adv. Mater.* **1997**, *9*, 398.
- [103] A. Topp, B. J. Bauer, T. J. Prosa, R. Scherrenberg, E. J. Amis, *Macromolecules* **1999**, *32*, 8923.
- [104] Y. Ribourdouille, G. D. Engel, M. Richard-Plouet, L. H. Gade, *Chem. Commun.* **2003**, 1228.
- [105] V. Balzani, P. Ceroni, S. Gestermann, C. Kaufmann, M. Gorka, F. Vögtle, *Chem. Commun.* **2000**, 853.
- [106] K. Tsuda, G. C. Dol, T. Gensch, J. Hofkens, L. Latterini, J. W. Weener, E. W. Meijer, F. C. De Schryver, *J. Am. Chem. Soc.* **2000**, *122*, 3445.
- [107] C. Wörner, R. Mülhaupt, *Angew. Chem. Int. Ed.* **1993**, *32*, 1306.
- [108] E. M. M. de Brabander-van den Berg, E. W. Meijer, *Angew. Chem. Int. Ed.* **1993**, *32*, 1308.
- [109] J. C. Hummelen, J. L. J. van Dongen, E. W. Meijer, *Chem. Eur. J.* **1997**, *3*, 1489.
- [110] M. H. P. van Genderen, M. H. A. P. Mak, E. M. M. de Brabander-van den Berg, E. W. Meijer, in *Dendrimers and other dendritic polymers* (Eds.: J. M. Fréchet, D. A. Tomalia), Wiley, **2001**.
- [111] G. J. M. Koper, M. H. P. van Genderen, C. Elissen-Roman, M. W. P. L. Baars, E. W. Meijer, M. Borkovec, *J. Am. Chem. Soc.* **1997**, *119*, 6512.
- [112] R. Scherrenberg, B. Coussens, P. van Vliet, G. Edouard, J. Brackman, E. de Brabander, K. Mortensen, *Macromolecules* **1998**, *31*, 456.
- [113] A. W. Bosman, A. P. H. J. Schenning, R. A. J. Janssen, E. W. Meijer, *Chem. Ber./Recueil* **1997**, *130*, 725.
- [114] D. Appelhans, H. Komber, R. Kirchner, J. Seidel, C.-F. Huang, D. Voigt, D. Kuckling, F.-C. Chang, B. Voit, *Macromol. Rapid. Commun.* **2005**, *26*, 586.
- [115] R. E. A. Dillon, D. F. Shriver, *Chem. Mater.* **2001**, *13*, 1369.
- [116] K. Vassilev, W. T. Ford, *Journal of Polymer Science: Part A: Polymer Chemistry* **1999**, *37*, 2727.

- [117] R. L. Sherman, E. Murugan, W. T. Ford, *Polymer Preprints* **2004**, *45*, 1003.
- [118] P. N. Floriano, C. O. Noble, J. M. Schoonmaker, E. D. Poliakoff, R. L. McCarley, *J. Am. Chem. Soc.* **2001**, *123*, 105454.
- [119] R. Velarde-Ortiz, G. Larsen, *Chem. Mater.* **2002**, *14*, 858.
- [120] M. Chai, A. K. Holly, M. L. Norton, *Polymer Preprints* **2003**, *44*, 296.
- [121] K. Esumi, R. Isono, T. Yoshimura, *Langmuir* **2004**, *20*, 237.
- [122] K. Esumi, in *Topics in Current Chemistry. Colloid Chemistry II*, Vol. 227 (Ed.: M. Antonietti), Springer Verlag, Berlin, Heidelberg, **2003**, pp. 31.
- [123] R. M. Crooks, B. I. Lemon, L. Sun, L. K. Yeung, M. Zhao in *Top. Curr. Chem. Dendrimers III, Design, Dimension, Function*, Vol. 212 (Ed.: F. Vögtle), Springer Verlag, **2001**, pp. 81.
- [124] J. J. J. M. Donners, R. Hoogenboom, A. P. H. J. Schenning, P. A. van Hal, R. J. M. Nolte, E. W. Meijer, N. A. J. M. Sommerdijk, *Langmuir* **2002**, *18*, 2571.
- [125] R. J. M. Klein Gebbink, A. W. Bosman, M. C. Feiters, E. W. Meijer, R. J. M. Nolte, *Chem. Eur. J.* **1999**, *5*, 65.
- [126] S. M. Cohen, S. Petoud, K. N. Raymond, *Chem. Eur. J.* **2001**, *7*, 272.
- [127] H. Kobayashi, S. Kawamoto, T. Saga, N. Sato, A. Hiraga, T. Ishimori, Y. Akita, M. H. Mamede, J. Konishi, K. Togashi, M. W. Brechbiel, *Magnetic Resonance in Medicine* **2001**, *46*, 795.
- [128] G. D. Engel, L. H. Gade, *Chem. Eur. J.* **2002**, *8*, 4319.
- [129] M. W. P. L. Baars, P. E. Froehling, E. W. Meijer, *Chem. Commun.* **1997**, 1959.
- [130] S. Stevelmans, J. C. M. van Hest, J. F. G. A. Jansen, D. A. F. J. van Boxtel, E. M. M. de Brabander-van den Berg, E. W. Meijer, *J. Am. Chem. Soc.* **1996**, *118*, 7398.
- [131] G. Larsen, E. Lotero, M. Marquez, *Chem. Mater.* **2000**, *12*, 1513.
- [132] J. J. J. M. Donners, B. R. Heywood, E. W. Meijer, R. J. M. Nolte, N. A. J. M. Sommerdijk, *Chem. Eur. J.* **2002**, *8*, 2561.
- [133] F. Vögtle, S. Gestermann, C. Kauffmann, P. Ceroni, V. Vicinelli, L. De Cola, V. Balzani, *J. Am. Chem. Soc.* **1999**, *121*, 12161.
- [134] F. Vögtle, M. Gorka, R. Hesse, P. Ceroni, M. Maestri, V. Balzani, *Photochem. Photobiol. Sci.* **2002**, *1*, 45.
- [135] F. Vögtle, S. Gestermann, C. Kauffmann, P. Ceroni, V. Vicinelli, V. Balzani, *J. Am. Chem. Soc.* **2000**, *122*, 10398.
- [136] U. Stebani, G. Lattermann, *Adv. Mater.* **1995**, *7*, 578.
- [137] U. Stebani, G. Lattermann, M. Wittenberg, J. H. Wendorff, *Angew. Chem. Int. Ed. Engl.* **1996**, *35*, 1858.
- [138] M. Krämer, N. Pérignon, R. Haag, J.-M. Marty, R. Thomann, N. Lauth-deViguerie, C. Mingotaud, *Macromolecules* **2005**, *38*, 8308.
- [139] R. Esfand, D. A. Tomalia, in *Dendrimers and Other Dendritic Polymers* (Eds.: J. M. Fréchet, D. A. Tomalia), Wiley, **2001**, pp. 587.
- [140] P. R. Dvornic, J. Hu, S. D. Reeves, M. J. Owen, *Silicon Chemistry* **2002**, *1*, 177.
- [141] P. R. Dvornic, *Journal of Polymer Science: Part A: Polymer Chemistry* **2006**, *44*, 2755.
- [142] M. S. Diallo, L. Balogh, A. Shafagati, J. H. Johnson Jr., W. A. Goddard III, D. A. Tomalia, *Environmental Science & Technology* **1999**, *33*, 820.
- [143] M. S. Diallo, S. Christie, P. Swaminathan, L. Balogh, X. Shi, W. Um, C. Papelis, W. A. Goddard, J. H. Johnson Jr., *Langmuir* **2004**, *20*, 2640.
- [144] L. Balogh, D. A. Tomalia, *J. Am. Chem. Soc.* **1998**, *120*, 7355.

- [145] M. Zhao, L. Sun, R. M. Crooks, *J. Am. Chem. Soc.* **1998**, *120*, 4877.
- [146] R. W. J. Scott, O. M. Wilson, R. M. Crooks, *J. Phys. Chem. B* **2005**, *109*, 692.
- [147] B. Donnio, S. Buathong, I. Bury, D. Guillon, *Chem. Soc. Rev.* **2007**, *36*, 1495.
- [148] J. Barberá, B. Donnio, L. Gehringer, D. Guillon, M. Marcos, A. Omenat, J. L. Serrano, *J. Mater. Chem.* **2005**, *15*, 4093.
- [149] D. J. Pesak, J. S. Moore, *Angew. Chem. Int. Ed. Engl.* **1997**, *36*, 1636.
- [150] H. Meier, M. Lehmann, *Angew. Chem. Int. Ed.* **1998**, *37*, 643.
- [151] V. Percec, P. Chu, M. Kawasumi, *Macromolecules* **1994**, *27*, 4441.
- [152] V. Percec, P. Chu, G. Ungar, J. Zhou, *J. Am. Chem. Soc.* **1995**, *117*, 11441.
- [153] J. Li, K. A. Crandall, P. Chu, V. Percec, R. G. Petscheck, C. Rosenblatt, *Macromolecules* **1996**, *29*, 7813.
- [154] S.-W. Hahn, Y.-K. Yun, J.-I. Jin, *Macromolecules* **1998**, *31*, 6417.
- [155] L. Gehringer, D. Guillon, B. Donnio, *Macromolecules* **2003**, *36*, 5593.
- [156] L. Gehringer, C. Bourgogne, D. Guillon, B. Donnio, *J. Am. Chem. Soc.* **2004**, *126*, 3856.
- [157] L. Gehringer, C. Bourgogne, D. Guillon, B. Donnio, *J. Mater. Chem.* **2005**, *15*, 1696.
- [158] S. A. Ponomarenko, E. A. Rebrov, N. I. Boiko, A. M. Muzafarov, V. P. Shibaev, *Polym. Sci. Ser. A+* **1998**, *40*, 763.
- [159] R. M. Richardson, S. A. Ponomarenko, N. I. Boiko, V. P. Shibaev, *Liquid Crystals* **1999**, *26*, 101.
- [160] H. Frey, C. Lach, K. Lorenz, *Adv. Mater.* **1998**, *10*, 279.
- [161] H. Frey, K. Lorenz, D. Hölter, R. Mülhaupt, *Polymer Preprints* **1996**, *37*, 758.
- [162] K. Lorenz, D. Hölter, B. Stühn, R. Mülhaupt, H. Frey, *Adv. Mater.* **1996**, *8*, 414.
- [163] I. M. Saez, J. W. Goodby, *Liquid Crystals* **1999**, *26*, 1101.
- [164] I. M. Saez, J. W. Goodby, R. M. Richardson, *Chem. Eur. J.* **2001**, *7*, 2758.
- [165] I. M. Saez, J. W. Goodby, *J. Mater. Chem.* **2005**, *26*, 26.
- [166] R. Elsässer, G. H. Mehl, J. W. Goodby, M. Veith, *Angew. Chem. Int. Ed.* **2001**, *40*, 2688.
- [167] R. Elsässer, J. W. Goodby, G. H. Mehl, D. Rodriguez-Martín, R. M. Richardson, D. J. Photinos, M. Veith, *Mol. Cryst. Liq. Cryst.* **2003**, *402*, 1.
- [168] K. Lorenz, H. Frey, B. Stühn, R. Mülhaupt, *Macromolecules* **1997**, *30*, 6860.
- [169] B.-K. Cho, A. Jain, S. Mahajan, H. Ow, S. M. Gruner, U. Wiesner, *J. Am. Chem. Soc.* **2004**, *126*, 4070.
- [170] V. Percec, M. N. Holerca, S. Uchida, W.-D. Cho, G. Ungar, Y. Lee, D. J. P. Yeardley, *Chem. Eur. J.* **2002**, *8*, 1106.
- [171] V. Percec, W.-D. Cho, G. Ungar, D. J. P. Yeardley, *J. Am. Chem. Soc.* **2001**, *123*, 1302.
- [172] V. Percec, T. K. Bera, M. Glodde, Q. Fu, V. S. K. Balagurusamy, P. A. Heiney, *Chem. Eur. J.* **2003**, *9*, 921.
- [173] V. Percec, C. M. Mitchell, W.-D. Cho, S. Uchida, M. Glodde, G. Ungar, X. Zeng, Y. Liu, V. S. K. Balagurusamy, P. A. Heiney, *J. Am. Chem. Soc.* **2004**, *126*, 6078.
- [174] R. Deschenaux, E. Serrano, A. M. Levelut, *Chem. Commun.* **1997**, 1577.
- [175] M. W. P. L. Baars, S. H. M. Söntjens, H. M. Fischer, H. W. I. Peerlings, E. W. Meijer, *Chem. Eur. J.* **1998**, *4*, 2456.
- [176] J. Barberá, M. Marcos, J. L. Serrano, *Chem. Eur. J.* **1999**, *5*, 1834.
- [177] O. Haba, K.-I. Okuyama, H. Osawa, K. Yonetake, *Liquid Crystals* **2005**, *32*, 633.

- [178] M. Marcos, R. Gimenez, J. L. Serrano, B. Donnio, B. Heinrich, D. Guillon, *Chem. Eur. J.* **2001**, *7*, 1006.
- [179] J. Barberá, B. Donnio, R. Gimenez, D. Guillon, M. Marcos, A. Omenat, J. L. Serrano, *J. Mater. Chem.* **2001**, *11*, 2808.
- [180] M. D. McKenna, J. Barberá, M. Marcos, J. L. Serrano, *J. Am. Chem. Soc.* **2005**, *127*, 619.
- [181] J. Barberá, G. R., M. Marcos, J. L. Serrano, *Liquid Crystals* **2002**, *29*, 309.
- [182] L. Pastor, J. Barberá, M. McKenna, M. Marcos, R. Martín-Rapún, J. L. Serrano, G. R. Luckhurst, A. Mainal, *Macromolecules* **2004**, *37*, 9386.
- [183] R. Martín-Rapún, M. Marcos, A. Omenat, J. L. Serrano, G. R. Luckhurst, A. Mainal, *Chem. Mater.* **2004**, *166*, 4969.
- [184] R. Alcalá, R. Gimenez, L. Oriol, M. Pinol, J. L. Serrano, B. Villacampa, A. I. Vinuales, *Chem. Mater.* **2007**, *19*, 235.
- [185] M. Marcos, R. Martín-Rapún, J. L. Serrano, A. Sánchez-Ferrer, *Macromol. Rapid Commun.* **2005**, *26*, 1604.
- [186] J.-M. Rueff, J. Barberá, M. Marcos, A. Omenat, R. Martín-Rapún, B. Donnio, D. Guillon, J. L. Serrano, *Chem. Mater.* **2006**, *18*, 249.
- [187] U. Stebani, PhD Thesis, Universität Bayreuth **1995**.
- [188] A. Facher, PhD Thesis, Universität Bayreuth, **2000**.
- [189] N. V. Usol'tseva, G. Lattermann, A. Facher, V. Bykova, A. Smirnova, M. S. Gruzdev, *Mol. Cryst. Liq. Cryst.* **2004**, *400*, 29.
- [190] R. Martín-Rapún, M. Marcos, A. Omenat, J. Barberá, P. Romero, J. L. Serrano, *J. Am. Chem. Soc.* **2005**, *127*, 7397.
- [191] R. Martín-Rapún, M. Marcos, A. Omenat, J. L. Serrano, E. Taffin de Givenchy, F. Guittard, *Liquid Crystals* **2007**, *34*, 395.
- [192] M. Marcos, R. Martín-Rapún, A. Omenat, J. Barberá, J. L. Serrano, *Chem. Mater.* **2006**, *18*, 1206.
- [193] D. Tsiourvas, K. Stathopoulou, Z. Sideratou, C. M. Paleos, *Macromolecules* **2002**, *35*, 1746.
- [194] M. Gruzdev, Thesis thesis, Ivanovo State University (Ivanovo, Russian Federation), **2006**.
- [195] M. S. Gruzdev, N. V. Usol'seva, L. Torre-Lorente, G. Lattermann, N. E. Domracheva, *Liquid crystals and their applying* **2006**, *4*, 89.
- [196] M. S. Gruzdev, N. V. Usol'tseva, L. Torre-Lorente, G. Lattermann, *Izvestiya Vysshikh Uchebnykh Zavedenii, Khimiya i Khimicheskaya Tekhnologiya* **2006**, *49*, 36.
- [197] J. Barberá, M. Marcos, A. Omenat, J.-L. Serrano, J. I. Martinez, P. J. Alonso, *Liquid Crystals* **2000**, *27*, 255.
- [198] D. G. Kurt, M. Higuchi, *Soft. Matter.* **2006**, *2*, 915.
- [199] S. Förster, M. Antonietti, *Adv. Mater.* **1998**, *10*, 195.
- [200] J. S. Miller, *Adv. Mater.* **2002**, *14*, 1105.
- [201] R. Werner, K. Falk, S. Ostrovsky, W. Haase, *Macromol. Chem. Phys.*, **2001**, *202*, 2813.
- [202] K. Binnemans, K. Lodewyckx, B. Donnio, D. Guillon, *Chem. Eur. J.* **2002**, *8*, 1101.
- [203] K. Binnemans, Y. G. Galyametdinov, R. Van Deun, D. W. Bruce, S. R. Collinson, A. P. Polishchuk, I. Bikchantaev, W. Haase, A. W. Prosvirin, L. Tinchurina, I. Litvinov, A. Gubajdullin, A. Rakhmatullin, K. Uytterhoeven, L. Van Meervelt, *J. Am. Chem. Soc.* **2000**, *122*, 4335.

- [204] in *Encyclopedia of inorganic chemistry* (Ed.: R. B. King), Wiley, Chichester, **1994**.
- [205] N. Domracheva, A. Mirea, M. Schwoerer, L. Torre-Lorente, G. Lattermann, *ChemPhysChem*. **2005**, *6*, 110.
- [206] N. Domracheva, A. Mirea, M. Schwoerer, L. Torre-Lorente, G. Lattermann, *ChemPhysChem*. **2006**, *7*, 2567.
- [207] R. J. Anderson, P. H. Hagback, P. J. Steel, *Inorganica Chimica Acta* **1999**, *284*, 273.
- [208] Y. Li, Y.-H. Lai, K. F. Mok, M. G. B. Drew, *Inorganica Chimica Acta* **1998**, 221.
- [209] C. Kimblin, V. J. Murphy, T. Hascall, B. M. Bridgewater, J. B. Bonanno, G. Parkin, *Inorg. Chem.* **2000**, *39*, 967.
- [210] B. Duffin, *Acta Cryst.* **1968**, *B24*, 396.
- [211] K. Kurdziel, T. Glowiak, J. Jezierska, *J. Chem. Soc., Dalton Trans.* **2000**, 1095.
- [212] F. B. Hulsbergen, R. W. M. ten Hoedt, G. C. Verschoor, J. Reedijk, A. L. Spek, *J. Chem. Soc. Dalton Trans.* **1983**, 539.
- [213] G. Aromí, P. Gamez, O. Roubeau, H. Kooijman, A. L. Spek, W. L. Driessen, J. Reedijk, *Angew. Chem.* **2002**, *114*, 1216.
- [214] C. Janiak, L. Uehlin, H.-P. Wu, P. Klüfers, H. Piotrowski, T. G. Scharmann, *J. Chem. Soc. Dalton Trans.* **1999**, 3121.
- [215] T. Otieno, S. J. Rettig, R. C. Thompson, J. Trotter, *Inorg. Chem.* **1995**, *34*, 1718.
- [216] G. De Munno, G. Bruno, *Acta Cryst.* **1984**, *C40*, 2030.
- [217] W. L. Driessen, J. Reedijk, *Inorg. Syn.* **1992**, *29*, 111.
- [218] A. N. Chebotarev, M. V. Shestakova, T. M. Shcherbakova, *Russian Journal of Coordination Chemistry* **2002**, *28*, 131.
- [219] C. Hemmert, M. Renz, H. Gornitzka, B. Meunier, *J. Chem. Soc., Dalton Trans.* **1999**, 3989–3994.
- [220] J. Garaj, *Acta Chem. Scand.* **1968**, *22*, 1710.
- [221] H. Effenberger, *Z. Kristallogr.* **1983**, *165*, 127.
- [222] N. Guillou, M. Louer, D. Louer, *Journal of Solid State Chemistry* **1994**, *109*, 307.
- [223] Gmelins, *Handbuch der Anorganische Chemie. Kupfer. Teil B. Lieferung 1*, **1958**.
- [224] J. Ghose, A. Kanungo, *Journal of Thermal Analysis and Calorimetry* **1981**, *20*, 459.
- [225] L. Zhou, D. H. Russel, M. Zhao, R. M. Crooks, *Macromolecules* **2001**, *34*, 3567.
- [226] A. Rether, M. Schuster, *Reactive & Functional Polymers* **2003**, *57*, 13.
- [227] M. Chai, Y. Niu, W. J. Youngs, P. L. Rinaldi, *J. Am. Chem. Soc.* **2001**, *123*, 4670.
- [228] C.-Y. Su, S. Liao, M. Wanner, J. Fiedler, C. Zhang, B.-S. Kang, W. Kaim, *Dalton Trans.* **2003**, 189.
- [229] J. Foley, Kennefick, D., Phelan, D., et al, *J. Chem. Soc. Dalton Trans.* **1983**, *21*, 2333.
- [230] W. L. Driessen, R. A. G. de Graaf, W. G. R. W. G. R. Wiesmeijer, *Acta Crystallogr., Sect. C* **1987**, *43*, 2319.
- [231] S. S. Wang, J. M. Boncella, K. A. Abboud, *Acta Crystallogr., Sect. C* **1997**, *53*, 436.
- [232] I. M. Verrosi, F. Zanolli, *Inorg. Chim. Acta* **1985**, *105*, 13.
- [233] A. Daubinet, Rhodes University (Grahamstown, South Africa), **2001**.
- [234] E. Gutierrez-Rios, *Química Inorgánica*, Reverté, **1991**.
- [235] J.-W. Weener, J. L. J. van Dongen, E. W. Meijer, *J. Am. Chem. Soc.* **1999**, *121*, 10346.
- [236] D. Tsiourvas, T. Felekis, Z. Sideratou, C. M. Paleos, *Liquid Crystals* **2004**, *31*, 739.

- [237] G. Montaudo, M. S. Montaudo, F. Samperi, in *Mass Spectrometry of Polymers* (Ed.: G. L. R. P. Montaudo), CRC Press, **2002**, pp. 419.
- [238] D. Suckau, A. Resemann, M. Schuerenberg, P. Hufnagel, J. Franzen, A. Holle, *Anal. Bioanal. Chem.* **2003**, 376.
- [239] S. J. Shields, B. K. Bluhm, D. H. Russell, *International Journal of Mass Spectrometry* **1999**, 182/183, 185.
- [240] C. K. L. Wong, T.-W. D. Chan, *Rapid Communications in Mass Spectrometry* **1997**, 11, 513.
- [241] C. F. Llenes, R. M. O'Malley, *Rapid Communications in Mass Spectrometry* **1992**, 6, 564.
- [242] J. Zhang, V. Frankevich, R. Knochenmuss, S. D. Friess, R. Zenobi, *J. Am. Chem. Soc. Mass. Spectrom.* **2003**, 14, 42.
- [243] H. Neubert, K. A. Knights, Y. R. de Miguel, D. A. Cowan, *Macromolecules* **2003**, 36, 8297.
- [244] L. M. Mallis, D. H. Russell, *International Journal of Mass Spectrometry and Ion Processes* **1987**, 78, 147.
- [245] T. Yalcin, D. C. Schriemer, L. Li, *J. Am. Soc. Mass. Spectrom.* **1997**, 8, 1220.
- [246] S. Bouchonnet, Y. Hoppilliard, G. Ohanessian, *Journal of Mass Spectrometry* **1995**, 30, 172.
- [247] D. Chescocoe, P. J. Goodhew, *The operation of the transmission electron microscope*, Oxford University Press, **1984**.
- [248] R. M. Silverstein, F. X. Webster, D. J. Kiemle, *Spectrometric identification of organic compounds*, 7th ed., Wiley, **2005**.
- [249] C. Jubert, A. Mohamadou, C. Gérard, S. Brandes, A. Tabard, J.-P. Barbier, *Dalton Trans.* **2002**, 2660.
- [250] E. Pretsch, P. Bühlmann, C. Affolter, M. Badertscher, *Spektroskopische Daten zur Strukturaufklärung organischer Verbindungen*, 4th ed., Springer, **2001**.
- [251] V. Romanova, V. Begishev, V. Karmanov, A. Kondyurin, M. F. Maitz, *J. Raman Spectrosc.* **2002**, 33, 769.
- [252] K. Nakanashi, T. Goto, M. Ohasi, *Bull. Chem. Soc. Jpn.* **1957**, 30, 403.
- [253] J. T. Braunholtz, E. A. V. Ebsworth, F. G. Mann, N. Sheppard, *J. Chem. Soc.* **1958**, 2780.
- [254] V. Manríquez, M. Campos-Vallette, N. Lara, N. González-Tejeda, O. Wittke, G. Díaz, S. Diez, R. Munoz, L. Kriskovic, *Journal of Chemical Crystallography* **1996**, 26, 15.
- [255] A. C. Stergiou, S. Papastephanou, C. Tsiamis, *Polyhedron* **1994**, 13, 2285/2290.
- [256] M. Shakir, K. S. Islam, A. K. Mohamed, N. Jahan, *Transition Met. Chem.* **1997**, 22, 189.
- [257] L. Antolini, L. Menabue, *Transition Met. Chem.* **1981**, 6, 377.
- [258] K. Nakamoto, *Infrared and Raman spectra of inorganic and coordination compounds*, 4th 1st print ed., Wiley-Interscience, **1986**.
- [259] H. Sigel, R. B. Martin, *Chem. Rev.* **1982**, 82, 385.
- [260] M. W. A. Steenland, I. Dierck, G. G. Herman, B. Devreese, W. Lippens, J. Van Beeumen, A. M. Goeminne, *J. Chem. Soc., Dalton Trans.* **1997**, 3637.
- [261] M. Casolaro, M. Chelli, M. Ginanneschi, F. Laschi, L. Messori, M. Muniz-Miranda, A. M. Papini, T. Kowalik-Jankowska, H. Kozłowski, *Journal of Inorganic Biochemistry* **2002**, 89, 181.

- [262] G. E. Jackson, L. Mkhonta-Gama, A. Voyé, M. Kelly, *Journal of Inorganic Biochemistry* **2000**, 79, 147.
- [263] A. F. Xie, D. L. Tao, Z. B. Zhang, Y. Z. Xu, Y. J. Wu, T. D. Hu, B. Y. Gu, J. G. Wu, G. Z. Yang, D. F. Xu, *Journal of Molecular Structure* **2002**, 613, 67.
- [264] P. Dunn, G. F. Sansom, *Journal of Applied Polymer Science* **1969**, 13, 1657.
- [265] M. Shakir, S. P. Varkey, *Polyhedron* **1995**, 14, 1117.
- [266] N. Adhikari, S. Chaudhuri, R. J. Butcher, N. Saha, *Polyhedron* **1999**, 18, 1323.
- [267] H. L. Conley Jr., R. B. Martin, *J. Phys. Chem.* **1965**, 69, 2914.
- [268] M. J. Bew, B. J. Hathaway, R. J. Fereday, *J. Chem. Soc. Dalton Trans.* **1972**, 1229.
- [269] N. F. Curtis, Y. M. Curtis, *Inorg. Chem.* **1965**, 4, 804.
- [270] N. Gupta, R. Gupta, S. Chandra, S. S. Bawa, *Spectrochimica Acta Part A* **2005**, 61, 1175.
- [271] M. Bellichi Ferrari, G. Fava Gasparri, C. Pelizzi, P. Tarasconi, *Acta Cryst.* **1986**, C42, 1148.
- [272] J. R. Ferraro, A. Walker, *The Journal of Chemical Physics* **1965**, 42, 1273.
- [273] H. Baranska, A. Labudzinska, J. Terpinski, *Laser Raman Spectrometry. Analytical Applications.*, Ellis Horwood Limited; John Wiley & Sons; PWN-Polish Scientific Publishers, **1987**.
- [274] J. R. Ferraro, A. Walker, *The Journal of Chemical Physics* **1965**, 42, 1278.
- [275] J. P. Malval, R. Lapouyade, *Helvetica Chimica Acta* **2001**, 84, 2439
- [276] S. Das, G. P. Muthukumaragopal, S. Pal, S. Pal, *New J. Chem.* **2003**, 27, 1102.
- [277] S. Pal, J. Pushparaju, N. R. Sangeetha, S. Pal, *Transition Met. Chem.* **2000**, 25, 529.
- [278] M. B. Inoue, E. F. Velazquez, F. Medrano, K. L. Ochoa, J. C. Galvez, M. Inoue, Q. Fernando, *Inorg. Chem.* **1998**, 37, 4070.
- [279] A. Carlington, A. D. Mc Lachlan, *Introduction to Magnetic Resonance. With applicaitons to chemistry and chemical physics.*, Chapman and Hall, London, **1979**.
- [280] J. E. Wertz, J. R. Bolton, *Electron spin resonance. Elementary theory and practical applications*, McGraw-Hill, Düsseldorf, **1972**.
- [281] C. P. Schlichter, *Principles of magnetic resonance*, Springer, Berlin, **1990**.
- [282] N. E. Domracheva, Physical-Technical Institute, Russian Academy of Science, Kazan, Russia, **2004**, personal communication.
- [283] M. F. Ottaviani, S. Bossmann, N. J. Turro, D. A. Tomalia, *J. Am. Chem. Soc.* **1994**, 116, 661.
- [284] I. G. Bikchantaev, Y. G. Galyametdinov, I. V. Ovchinnikov, *Zh. Strukt. Khim.* **1987**, 28, 61.
- [285] N. N. Tikhomirova, K. I. Zamaraev, *Zh. Strukt. Khim.* **1963.**, 4, 224 –230.
- [286] U. Sakaguchi, A. W. Addison, *J. Chem. Soc. Dalton Trans.* **1979**, 1, 600.
- [287] M. Symons, *Chemical and Biochemical Aspects of Electron-Spin Resonance Spectroscopy*, Halsted Press, Wiley, New York,, **1978**.
- [288] H. Yokoi, A. W. Addison, *Inorg. Chem.* **1977**, 16, 1341.
- [289] G. M. Larin, V. A. Kolosov, G. V. Panova, N. K. Vikulova, *Zh. Neorg. Khim* **1974**, 19, 1873.
- [290] Y. V. Rakitin, R. D. Kasumov, G. V. Panova, I. M. Turovets, V. T. Kalinnikov, *Izv. Akad. Nauk SSSR Ser. Khim.* **1981**, 2, 427.

- [291] Y. V. Rakitin, R. D. Kasumov, G. V. Panova, I. M. Turovets, V. T. Kalinnikov, *Zh. Neorg. Khim.* **1981**, 26, 659–663.
- [292] G. M. Larin, V. A. Kolosov, G. V. Panova, N. K. Vikulova, *Izv. Akad. Nauk SSSR Ser. Khim.* **1974**, 8, 1881–1884.
- [293] G. M. Larin, V. A. Kolosov, G. V. Panova, N. K. Vikulova, *Zh. Neorg. Khim.* **1973**, 18, 2868–2869.
- [294] R. Kubo, T. Tomita, *J. Phys. Soc. Jap.* **1954**, 9, 888–919.
- [295] P. W. Anderson, P. R. Weiss, *Rev. Mod. Phys.* **1953**, 25, 269
- [296] R. X. Timerov, *Dokl. Akad. Nauk SSSR* **1962**, 142, 870.
- [297] I. V. Ovchinnikov, V. N. Konstantinov, *Radiospectroscopy of Condensed Matter*, Nauka, Moscow, **1990**.
- [298] V. N. Konstantinov, I. V. Ovchinnikov, N. E. Domracheva, *Zh. Strukt. Khim.* **1984**, 25, 19–27.
- [299] G. D. Smith, B. B. Garrett, S. L. Holt, R. E. Barden, *J. Phys. Chem.* **1976**, 80, 1708–1713.
- [300] C. Kallay, K. Varnagy, I. Sovago, D. Sanna, G. Micera, *J. Chem. Soc. Dalton. Trans.* **2002**, 92–98.
- [301] N. E. Domracheva, I. Ovchinnikov, A. N. Turanov, V. N. Konstantinov, *J. Magn. Magn. Mater.* **2004**, 269, 385–392.
- [302] N. E. Domracheva, S. A. Luchkina, I. V. Ovchinnikov, *Koord. Khim.* **1995**, 21, 24–29.
- [303] N. E. Domracheva, S. A. Luchkina, I. V. Ovchinnikov, *Zh. Neorg. Khim.* **1986**, 31, 106–110.
- [304] N. E. Domracheva, V. N. Konstantinov, S. A. Luchkina, I. V. Ovchinnikov, *Koord. Khim.* **1985**, 11, 503–509.
- [305] V. F. Anufrienko, A. A. Shklyayev, *Dokl. Akad. Nauk SSSR* **1970**, 191, 107
- [306] V. F. Anufrienko, A. A. Shklyayev, *Dokl. Akad. Nauk SSSR* **1971**, 196, 844
- [307] A. A. Shklyayev, V. F. Anufrienko, E. I. Berus, Y. N. Molin, *Dokl. Akad. Nauk SSSR* **1972**, 207, 138
- [308] P. W. Atkins, M. C. R. Symons, *The Structure of Inorganic Radicals: an Application of Electron Spin Resonance to the Study of Molecular Structure.*, Elsevier, Amsterdam-London-New York, **1967**.
- [309] R. Prins, P. J. Birker, J. G. Haasnoot, G. C. Verschoor, J. Reedijk, *Inorg. Chem.* **1985**, 24, 4128.
- [310] R. Feyerherm, *J. Magn. Magn. Mater.* **2003**, 256, 328.
- [311] B. J. Kraft, H. J. Eppley, J. C. Huffman, J. M. Zalski, *J. Am. Chem. Soc.* **2002**, 124, 272
- [312] W. B. Lewis, M. Alei, L. O. Morgan, *J. Chem. Phys.* **1966**, 44, 2409.
- [313] Y.-Y. H. Chao, D. R. D. R. Kearns, *J. Phys. Chem.* **1977**, 81, 666.
- [314] A. Pöppl, L. Kevan, *J. Phys. Chem.* **1996**, 100, 3387.
- [315] R. Zibaseresht, R. M. Hartshorn, *Acta Cryst. Sect E* **2006**, 62, i19.
- [316] M. F. Ottaviani, F. Montalti, N. J. Turro, D. A. Tomalia, *J. Phys. Chem. B.* **1997**, 101, 158.
- [317] D. Zhou, R. W. Kreilick, *J. Phys. Chem.* **1993**, 97, 9304.
- [318] B. Morosin, *Acta Cryst.* **1970**, B26, 1203.
- [319] Y. Ajiro, N. S. Vander Ven, S. A. Friedberg, *Proc. Int. Conf. Low Temp. Phys. 13th* **1974**, 2, 380.

- [320] C. G. Granqvist, *Critical Reviews in Solid State and Materials Sciences* **1990**, *16*, 291.
- [321] F. Shvartsman, V. Krongauz, *Nature* **1984**, *309*, 608.
- [322] F. P. Shvartsman, V. A. Krongauz, *J. Phys. Chem.* **1984**, *88*, 6448.
- [323] K. Ohta, H. Hasebe, M. Moriya, T. Fujimoto, I. Yamamoto, *J. Mater. Chem.* **1991**, *1*, 831.
- [324] K. Ohta, M. Moriya, M. Ikejima, H. Hasebe, T. Fujimoto, I. Yamamoto, *Bull. Chem. Soc. Jpn.* **1993**, *66*, 3559.
- [325] D. W. Bruce, D. A. Dunmur, M. A. Esteruelas, S. E. Hunt, R. Le Lagadec, P. M. Maitlis, J. R. Marsden, E. Sola, J. M. Stacey, *J. Mater. Chem.* **1991**, *1*, 251.
- [326] B. A. Gregg, M. A. Fox, A. J. Bard, *J. Phys. Chem.* **1989**, *93*, 4227.
- [327] L.-K. Chau, E. J. Osburn, N. R. Armstrong, D. F. O'Brien, B. A. Parkinson, *Langmuir* **1994**, *10*, 351.
- [328] R. Gimenez, A. Elduque, J. L. López, J. Barberá, E. Cavero, I. Lantero, L. A. Oro, J. L. Serrano, *Inorg. Chem.* **2006**, *45*, 10363.
- [329] G. Lehmann, *Statistik*, Verlag S. Roderer, Regensburg, **2000**.
- [330] C. Destrade, N. H. Tinh, H. Gasparoux, J. Malthête, A. M. Levelut, *Mol. Cryst. Liq. Cryst.* **1981**, *71*, 111.
- [331] C. Destrade, J. Malthete, Nguyen Huu Tinh, H. Gasparoux, *Phys. Lett.* **1980**, *78*, 82.
- [332] C. Destrade, H. Gasparoux, A. Babeau, N. H. Tinh, M. J., *Mol. Cryst. Liq. Cryst.* **1981**, *67*, 37.
- [333] M. Suárez, J.-M. Lehn, S. C. Zimmerman, A. Skoulios, B. Heinrich, *J. Am. Chem. Soc.* **1998**, *120*, 9526.
- [334] H. Kobayashi, R. Higashi, K. Ishii, K. Hatsusaka, K. Ohta, *Bull. Chem. Soc. Jpn.* **1999**, *72*, 1263.
- [335] H. Seidel, K. Viswanathan, W. Johannes, H. Ehrhardt, *Z. anorg. allg. Chem.* **1974**, *410*, 138.
- [336] J. Xu, D. Xue, *J. Phys. Chem. B* **2005**, *109*, 17157.
- [337] R. M. Hartshorn, University of Canterbury, Christchurch, New Zealand, **2006**, personal communication.
- [338] W. L. Driessen, M. den Heijer, *Inorganica Chimica Acta* **1979**, *33*, 261.
- [339] S. Amaral, M. M. Turnbull, *Journal of Chemical Crystallography* **2002**, *32*, 11.
- [340] M. M. Turnbull, Clark University, Worcester, USA, **2006**, personal communication.
- [341] Data Base WinXPOW version PKS_2.01 from STOE & cie. PDF 14-687.
- [342] G. Ungar, University of Sheffield, Sheffield, UK, **2007**, personal communication.
- [343] H. Hayashi, M. J. Hudson, *J. Mater. Chem.* **1995**, *5*, 115.
- [344] S. R. Jain, M. V. Rao, *Propellants and Explosives* **1978**, *3*, 83.
- [345] G. Singh, I. P. Singh Kapoor, S. M. Mannan, J. Kaur, *J. Hazard. Mater. A* **2000**, *79*, 1.
- [346] A. Eisenmann, PhD Thesis, Universität Bayreuth, **2001**.

Acknowledgements

I would like to express my sincere gratitude to:

Professor Dr. H.-W. Schmidt for the possibility to work in his chair and for providing an excellently equipped work place. I would like to thank him sincerely for his support.

Dr. G. Lattermann my supervisor, for giving me the opportunity to work in his group and offering an interesting multidisciplinary topic. I very much appreciate his commitment, readiness for discussions, careful and thorough analysis, and his enthusiasm for science.

Dr. N. E. Domracheva, Kazan Physical-Technical Institute, Russian Academy of Science, Dr. A. Mirea and Prof. Dr. M. Schwoerer, Experimentalphysik II, Universität Bayreuth for performing the EPR measurements of the dendrimeric copper(II)-complexes. The fruitful cooperation resulted in important findings for this work.

Prof. Dr. G. Ungar, Department of Engineering Materials, University of Sheffield for some synchrotron measurements and interesting discussions. Dr. W. Millius, and Dr. R. Mariychuk Anorganische Chemie I, for recording one of the X-ray diffractograms and for letting me access to their inorganic data base. Dr. M. Drechsler, and Dr. M. Krekhova for the TEM images and EELS spectroscopy of the complexes. Dr. M. Bäte for the first MALDI-ToF-MS measurements and for introducing me to this technique.

Dr. C. Erdelen for reading this manuscript and his invaluable help with the format. I thank him for his unconditional support, disinterested help and encouragement in the difficult moments along these years.

My lab colleagues, Dr. A. Schaz (né Eisenmann), Dr. L. Cui, Dr. O. Lafuente, Dr. S. Belyaev, Dr. A. Smirnova, Dr. M. Krekhova, Dr. M. Gruzdev, Andreas Timme and Dominic Kaufmann for their helpfulness and friendly work atmosphere we had. I am grateful to Dr. O. Lafuente and Dr. A. Schaz for introducing me to the X-ray diffractometry and for the useful discussions on this topic.

Prof. Dr. J. L. Serrano, Universidad de Zaragoza, who gave me the opportunity to take part in the Erasmus Program with the Universität Bayreuth, opening indirectly the way to the PhD in this university.

All the “bayreuther” friends for the memorable time we have spent together in Bayreuth. R. Hildner for his unfailing support and encouragement, his constructive comments and for the unforgettable time he has devoted me. And my family, for their confidence, their inexhaustible patience, their generosity and their encouragement which have made possible the completion of this thesis.

Erklärung

Hiermit erkläre ich, dass ich die Arbeit selbständig verfasst und keine anderen als die von mir angegebenen Quellen und Hilfsmittel benutzt habe.

Ferner erkläre ich, dass ich anderweitig mit oder ohne Erfolg nicht versucht habe, diese Dissertation einzureichen. Ich habe keine gleichartige Doktorprüfung an einer anderen Hochschule endgültig nicht bestanden.

Bayreuth, 02. Januar 2008

Laura Torre Lorente

